TÉCNICO LISBOA

UNIVERSIDADE DE LISBOA

INSTITUTO SUPERIOR TÉCNICO

Engineering Extracellular Vesicles from Mesenchymal Stromal Cells with RNA-interference-expressing Minicircles towards a novel Anti-Angiogenic Therapy

Cristiana da Silva Ulpiano

Supervisors: Doctor Gabriel António Amaro Monteiro

Doctor Cláudia Alexandra Martins Lobato da Silva

Thesis approved in public session to obtain the PhD Degree in Biotechnology and Biosciences

Jury final classification: **Pass with Distinction**

2024

UNIVERSIDADE DE LISBOA
INSTITUTO SUPERIOR TÉCNICO

Engineering Extracellular Vesicles from Mesenchymal Stromal Cells with RNA-interference-expressing Minicircles towards a novel Anti-Angiogenic Therapy

Cristiana da Silva Ulpiano

Supervisors: Doctor Gabriel António Amaro Monteiro
Doctor Cláudia Alexandra Martins Lobato da Silva

Thesis approved in public session to obtain the PhD Degree in
Biotechnology and Biosciences

Jury final classification: **Pass with Distinction**

Jury

Chairperson: Doctor Arsénio do Carmo Sales Mendes Fialho, Instituto Superior Técnico, Universidade de Lisboa

Members of the committee:

Doctor Duarte Miguel de França Teixeira dos Prazeres, Instituto Superior Técnico, Universidade de Lisboa

Doctor Gabriela Araújo da Silva, NOVA Medical School, Universidade Nova de Lisboa

Doctor Gabriel António Amaro Monteiro, Instituto Superior Técnico, Universidade de Lisboa

Doctor Maria Margarida de Carvalho Negrão Serra, iBET/ITQB-NOVA - Instituto de Tecnologia Química e Biológica António Xavier

Doctor Nuno Filipe Santos Bernardes, Instituto Superior Técnico, Universidade de Lisboa

Funding Institution - Fundação para a Ciência e a Tecnologia

2024

RESUMO

Além de participar na angiogénese fisiológica, o fator de crescimento endotelial vascular (VEGF) contribui para condições relacionados com angiogénese excessiva. Estratégias com RNA de interferência (RNAi) demonstram resultados promissores na modulação angiogénica. Vetores de expressão que codificam short hairpin RNAs (shRNAs) são usados como efetores de RNAi, e os minicírculos (MC) são vetores vantajosos. Vesículas extracelulares (EVs) surgem como sistemas de entrega de ácidos nucleicos devido ao seu potencial inato para entregar carga funcional e ultrapassar barreiras biológicas, e as células mesenquimais estromais (MSCs) têm sido exploradas como fonte produtora de EVs.

Este trabalho visou desenvolver uma terapia génica anti-angiogénica à base de MCs que expressam shRNA (MC-shRNA) que silenciam reguladores do VEGF, utilizando MSC-EVs como sistema de entrega, estando dividido em três etapas.

Na primeira etapa, foram desenvolvidos MC-shRNA que inibem o VEGF-A e o seu recetor (VEGFR2). Após produção e purificação dos MCs superenrolados, experiências de transfeção demonstraram que MC-shVEGF induziu uma supressão máxima de ~78%, e MC-shVEGFR2 de ~56% em células de cancro da mama e células endoteliais, respetivamente.

Na segunda etapa, estabelecemos uma plataforma para produção de MSC-EVs. A combinação de meio cultura sem soro e componentes xenogénicos suplementado com lisado plaquetário humano (hPL) desprovido de EVs e reatores de tanque agitado, permitiu a produção contínua de EVs. Após o isolamento, esta plataforma proporcionou MSC-EVs com características bioquímicas/biofísicas aceites em números clinicamente relevantes.

Na terceira etapa, as MSC-EVs foram modificadas pelo carregamento direto dos MCs. MSC-EVs foram carregadas com MC anti-GFP por incubação passiva, microporação, sonicação e utilizando um reagente de transfeção. Os resultados demonstraram eficiências de carregamento baixas (<7%), não sendo observada uma diminuição na intensidade de fluorescência após a entrega das EV-MC a células GFP+.

Globalmente, este trabalho fornece perspetivas relevantes sobre MSC-EVs como sistema de entrega, demonstra o potencial dos MC-shRNA como abordagem terapêutica não viral para angiogénese excessiva e a plataforma de produção de MSC-EVs estabelecida representa um passo importante no estudo generalizado de terapias com EVs.

Palavras-chave: Minicírculos; RNA de interferência; Vesículas Extracelulares; Células Mesenquimais Estromais; Terapia anti-angiogénica.

ABSTRACT

Besides participating in physiological angiogenesis, vascular endothelial growth factor (VEGF) contributes to excessive angiogenesis-related disorders. RNA interference (RNAi)-based strategies have shown promising results in modulating angiogenesis. Expression vectors encoding short-hairpin RNAs (shRNAs) are used as alternative RNAi effectors, and minicircles (MC) are a favourable expressing system. Extracellular vesicles (EVs) emerge as delivery systems for nucleic acids due to their innate potential to deliver functional cargo and cross biological barriers. Due to their intrinsic therapeutic benefits and efficient ex vivo expansion capacity, mesenchymal stromal cells (MSCs) are widely explored as EV producers.

This work aimed to develop an anti-angiogenic gene-based therapy using shRNA-expressing MCs targeting VEGF regulatory players and MSC-EVs as a delivery system, being divided into three stages.

In the first stage, the shRNA-expressing MCs targeting VEGF-A and its receptor (VEGFR2) were developed. After large-scale production and purification of the supercoiled MCs, transfection experiments showed that 4 days after microporation MC-shVEGF induced a knockdown of ~78% and MC-shVEGFR2 a knockdown of ~56% in human breast cancer cells and umbilical vein endothelial cells, respectively.

In the second stage, we established a platform for manufacturing MSC-EVs. Combining serum-/xeno(geneic)-free exosome-depleted human platelet lysate (hPL)-supplemented medium and a stirred-tank reactor, the system sustained a 3-day continuous EV production. When combined with scalable EV isolation, this platform yielded MSC-EVs with accepted biochemical/biophysical characteristics, at clinically relevant numbers.

In the third stage, MSC-EVs were engineered by directly loading the MCs. GFP-targeting MC loading was tested by passive incubation, microporation, sonication and using a transfection reagent. The results showed that low loading efficiencies (<7%) were obtained and no significant decrease in fluorescent intensity after EV-MC delivery to GFP+cells was observed.

Overall, this work provided important insights regarding MSC-EVs as delivery systems. Moreover, it demonstrated the potential of MC-derived RNAi systems as a non-viral therapeutic approach for excessive angiogenesis. Lastly, the MSC-EV manufacturing platform established herein constitutes an important step towards making MSC-EV-based therapies widely available in clinical settings.

Keywords: Minicircles; RNA interference; Extracellular Vesicles; Mesenchymal Stromal Cells; Anti-Angiogenic Therapy.

ACKNOWLEDGEMENTS

I would like to express my deepest gratitude to my supervisors, Professor Gabriel Monteiro and Professor Cláudia Lobato, for their invaluable expertise, encouragement, and guidance throughout my research journey. I am truly thankful for the opportunity to work on a challenging and forefront project under their mentorship. Their continuous efforts to push me outside my comfort zone and encourage independence while providing unwavering problem-solving support have been instrumental in my development. Your mentorship has not only fostered my resilience, adaptability, and critical thinking as a researcher but has also profoundly shaped my personal growth.

I sincerely acknowledge Professor Isabel Sá-Correia for her pivotal role as the Coordinator of the BIOTECnico Doctoral Program - Biotechnology and Biosciences (IST-UL) and for giving me the opportunity to pursue my PhD. I extend my gratitude to Professor Arsénio M. Fialho, currently responsible for this doctoral program.

I would also like to express my appreciation to Professor Joaquim Sampaio Cabral as Coordinator of the Institute for Bioengineering and Biosciences (iBB), who provided the indispensable infrastructure for conducting the experimental work of this thesis. I am equally grateful to the current Head of iBB, Professor Mário N. Berberan-Santos.

I would also like to acknowledge “Fundação para a Ciência e Tecnologia” for funding my PhD scholarship PD/BD/150336/2019.

Special gratitude goes to all the collaborators, whose contributions allowed me to enrich my research: Professor José Paulo Farinha (CQE-IST) for allowing me to use the NTA equipment which was crucial for the development of my PhD work; Professor Fábio Fernandes for helping me with the fluorescence-related experiments and William Milligan and co-workers (AventaCell BiomedicalCorp.) for providing essential reagents. I would also like to acknowledge Doctor Nuno Bernardes and Professor Miguel Prazeres for their scientific input as members of my PhD Thesis Advisory Committee (CAT). I am sincerely thankful to Ana Fernandes-Platzgummer for her efforts in solving many lab-related problems and her continuous availability and assistance throughout my doctoral studies especially concerning cell culture and EV manufacturing.

To former and current lab colleagues from SCERG and BERG, a warm thank you for the excellent working environment. I am truly grateful to Cláudia Alves (original teacher), Sara Rosa (downstream sensei), Rita Silva (purification queen), Ricardo Silva (EV-purification expert), Marília Silva (electroporation boss), Miguel Fuzeta (MSC-EV mentor), Isabel Doutor (conference buddy and apprentice), William Salvador (bioreactor companion), and many others who supported me along the way, contributing to the successful completion of my PhD, whether through practical assistance in the lab, insightful discussions, or emotional support. It has been a pleasure sharing these years with you. A special thanks to my friend and “PhD program twin” Jorge João, for the companionship, shared experiences, and mutual support and encouragement throughout our doctoral studies - we will finish this together! To André Branco, my office-sharing

colleague and friend, whose positivity, support, and willingness to listen during challenging times have made a profound difference in my PhD journey. To Teresa Mendes, who joined our research team during the final stage of my PhD and quickly became not only a valued colleague but also a cherished friend and my "work bestie."

I am incredibly thankful to my dear friends from childhood, university, and swim team for their continued support and for always reminding me to embrace life beyond my PhD. Your friendship and encouragement have been a source of joy and balance during this quest, and I cherish all the moments we have shared.

I am immensely grateful to my wonderful family, especially my parents, António and Cristina, my sister Joana, and my life partner Hugo, for their unconditional love, support and understanding. You have not only shown me the beauty of life's simplicity but have also been my constant source of strength and reassurance. Thank you for believing in me – I could not have done this without you! 🌻

TABLE OF CONTENTS

LIST OF TABLES

LIST OF FIGURES

LIST OF ABBREVIATIONS

5-FC - 5-fluorocytosine

A/A - antibiotic-antimycotic

AAV - adeno-associated virus

AD - Alzheimer’s disease

AEC - anion-exchange chromatography

Ago - argonaute

Akt - protein kinase B

ALIX - ALG-2-interacting protein X

AMD - age-related macular degeneration

Ang-2 - angiopoietin-2

ApoBD - apoptotic bodies

AR - androgen receptor

ASO - antisense oligonucleotide

AT- adipose tissue

ATP - adenosine triphosphate

BBB - blood-brain barrier

BGH - bovine growth hormone

BM - bone marrow

CD - Crohn's disease

CDNs - cell-derived nanovesicles

CD-UPRT - cytosine deaminase fused to uracil phosphoribosyltransferase

CF - cystic fibrosis

CFU-F - colony forming unit - fibroblasts

CHIKV - Chikungunya virus

CM - conditioned medium

CMV - cytomegalovirus

CNS - central nervous system

CPP - cell-penetrating peptides

CTGF - connective tissue growth factor

cTnI - cardiac troponin I

Cur - curcumin

CV - column volumes

DARPin - designed ankyrin repeat protein

DC - dendritic cells

DCW - dry cell weight

DDS - drug delivery systems

DMEM - Dulbecco’s modified Eagles’ medium

DMPE - phospholipid 1,2-dimyristoyl-sn-glycero-3-phosphoethanolamine

DOPE - dioleylphosphatidylethanolamine

DOX - doxorubicin

DP - dental pulp

DPN - diabetic peripheral neuropathy

DR - diabetic retinopathy

DSPE - 1,2-distearoyl-sn-glycero-3-phosphoethanolamine

dsRNA – double-stranded RNA

DSS - dextran sulfate sodium

EC - endothelial cells

ECM - extracellular matrix

EGF - epidermal growth factor

EGFR - epidermal growth factor receptor

ELISA - enzyme-linked immunosorbent assay

EMA - European Medicines Agency

ESCRT - endosomal sorting complex required for transport

EV - extracellular vesicle

Exo - exosome

FBS - fetal bovine serum

FDA - Food and Drug Administration

FGF - fibroblast growth factor

GAPDH - glyceraldehyde 3-phosphate dehydrogenase

GEMP - gemcitabine monophosphate

GFP - green fluorescent protein

GMP - good manufacturing practices

GPI - glycosyl-phosphatidylinositol

GSC - glioma stem cells

GvHD - graft-versus-host disease

HD - Huntington’s disease

HEK - human embryonic kidney

HER2 - human epidermal growth factor receptor 2

HGF - hepatocyte growth factor

HIF- hypoxia-inducible factor

HoFH - homozygous familial hypercholesterolemia

hPL - human platelet lysate

HSP - heat shock proteins

HuR - human antigen R

HUVEC - human umbilical vein endothelial cell

IBD - inflammatory bowel disease

IFN-γ - interferon-gamma

IGF - insulin-like Growth Factor

IL - interleukin

ILVs - intraluminal vesicles

IMTP - ischemic myocardium-targeting peptide

iPSC - induced pluripotent stem cells

ISEV - International Society for Extracellular Vesicles

Lamps - lysosomal-associated membrane proteins

lcnR - long non-coding RNAs

LDL - low-density lipoprotein

LDLR - low-density lipoprotein receptor

MC - minicircles

MCS -multiple cloning sites

MHC - major histocompatibility complex

MI - myocardial infarction

miRNA – micro RNA

MMP - matrix metalloprotease

MP - miniplasmid

MRS - multimer resolution sites

MS - multiple sclerosis

MSC - mesenchymal stromal cells

MSC(AT) - adipose tissue-derived mesenchymal stromal cells

MSC(M) - bone marrow-derived mesenchymal stromal cells

MSC(WJ) - Wharton's jelly derived mesenchymal stromal cells

MSC-EVs - mesenchymal stromal cells derived-extracellular vesicles

MV - microvesicle

MVB - multivesicular body

MWCO - molecular weight cut-off

NCTD - norcantharidin

NHS - succinyl-N-hydroxy-succinimidyl

NPs - nanoparticles

NRP - neuropilin

nt – nucleotide

OA - osteoarthritis

oc - open-circular

OP - osteoporosis

OXA - oxaliplatin

PBMC - peripheral blood mononuclear cells

PDAC - pancreatic ductal adenocarcinoma

PDGF - platelet-derived growth factor

PD-L1 - programmed cell death-ligand 1

pDNA – plasmid DNA

PEDF - pigment epithelium-derived factor

PEG - polyethylene glycol

PEI - polyethyleneimine

PlGF - placental growth factor

PLK-1 - serine/threonine-protein kinase

PP - parental plasmid

Ppy - polypyrrole

PTEN - phosphatase and tensin homolog

PTX - paclitaxel

RA – rheumatoid arthritis

RBC - red blood cells

RBD - RNA binding domains

RBP - RNA-binding proteins

RISC - RNA-induced silencing complex

RNAi - RNA interference

RNAse – ribonuclease

RT-qPCR - quantitative real-time polymerase chain reaction

RVG - rabies viral glycoprotein

S/XF - serum-/xeno(geneic)-free

sc - supercoiled

SCI - Spinal cord injury

SEC - size-exclusion chromatography

SHN - schnurri-3 protein

shRNA - short harpin RNA

siRNA - small interference RNA

SM - synovial membrane

SPION - superparamagnetic iron oxide nanoparticles

STR - stirred-tank reactor

TAMEL - targeted and modular extracellular vesicles loading

Tf - transferrin

TFF - tangential flow filtration

TGF-β - transforming growth factor-beta

TKI - tyrosine kinase inhibitor

TNF-α - tumour necrosis factor-alpha

TRAIL - tumour necrosis factor-related apoptosis-inducing ligand

TSG101 - tumour susceptibility gene 101

TXL - taxol

UC – ultracentrifugation

UF - ultrafiltration

VEGF - vascular endothelial growth factor

VEGFR - vascular endothelial growth factor receptor

WJ - Wharton's jelly

εPL - ε-polylysine

Chapter I.

GENERAL INTRODUCTION

The contents of this chapter were partially based on the following publication:

Ulpiano, C., da Silva, C.L., Monteiro, G.A. Bioengineered Mesenchymal-Stromal-Cell-Derived Extracellular Vesicles as an Improved Drug Delivery System: Methods and Applications. Biomedicines, 2023, 11(4):1231. DOI: 10.3390/biomedicines11041231.

I.1. Angiogenesis

Vasculogenesis consists of the *de novo* formation of blood vessels from mesoderm-derived endothelial progenitor cells. During embryonic development, these endothelial precursors, also referred to as angioblasts, cluster and differentiate into endothelial cells (EC) leading to the formation of capillary tubes with lumens that with continued growth, merge and form early vascular plexuses. In parallel, extraembryonic vasculogenesis occurs in the yolk sac, where mesoderm precursor cells (hemangioblasts) aggregate into blood islands composed of endothelial precursors located at the periphery that will form the walls of vessels, and hematopoietic stem cells located interiorly that will give rise to primitive blood cells [1,2]. In adult vasculature, these precursors reside as endothelial colony-forming cells and have the potential to home to ischemic tissues and contribute to vascularization [3]. The remodelling and expansion of this initial network is achieved by a process called angiogenesis, which is generally defined as the growth or formation of new blood vessels from the pre-existing vasculature. In normal physiology, angiogenesis is essential for organ development, reproductive system in females and tissue repair in healthy adults [1,2,4,5]. This process is closely regulated by the balance between angiogenic activators and inhibitors in the extracellular environment of EC, being modulated by numerous pathological and physiological stimuli, such as hypoxia and inflammation [4,6]. Pro-angiogenic factors are secreted by various cell types including EC, fibroblasts, smooth muscle cells, platelets, inflammatory cells, and cancer cells [4]. The local concentration of factors can be influenced by physiological or pathologic responses to injury, chronic inflammation, or cancer [4]. Some well-known angiogenic growth factors and cytokines are vascular endothelial growth factor (VEGF), fibroblast growth factor (FGF), tumour necrosis factor-alpha (TNF-α), transforming growth factor-beta (TGF-β), and angiopoietin-2 (Ang-2) [4]. Generally, the process begins with the enzymatic degradation of the capillary basement membrane, resulting in the dissociation of the mural cells (e.g. pericytes and smooth muscle cells) and liberation of the EC. EC proliferate and migrate towards the angiogenic stimulus through the guidance of the specialized endothelial “tip cell” that sprouts through the extracellular matrix (ECM), aided by filopodia. This cell is followed by stalk cells which are responsible for the elongation of the sprout and formation of the lumen of the primitive vessel. Then, the tip cells from adjacent sprouts fuse leading to the formation of a continuous lumen through which blood can perfuse. Lastly, vessel stabilisation and maturation occur by the ECM deposit and the recruitment of mural cells, after which EC resume their quiescent state [1,2,5]. Alternatively, vascular growth can be accomplished by insertion of a transcapillary pillar followed by expansion of its diameter consequently causing a longitudinal splitting of the original vessel with a single lumen into 2 vessels, a process referred to as intussusceptive angiogenesis [1,2].

I.1.1. Angiogenesis-dependent diseases

In pathological angiogenesis, there is an imbalance between angiogenesis stimulators and inhibitors caused by excessive or sustained release of pro-angiogenic factors that ultimately lead to abnormal development of vasculature. Besides the well-known disorders - cancer, blinding retinopathy, arthritis, and psoriasis - numerous other disorders are characterized by excessive vessel growth including inflammatory, allergic, infectious, traumatic, metabolic or hormonal diseases (**Table I.1**) [6,7].

Table I.1 – Diseases that include excessive angiogenesis as part of the pathology. Reproduced from [6]

Specific organ	Diseases
Multi-organs abnormality	Cancer - infectious diseases - autoimmune disorders
Blood vessels abnormality	Vascular malformations - DiGeorge syndrome - Hereditary haemorrhagic telangiectasia - cavernous haemangioma – atherosclerosis - transplant arteriopathy
Adipose tissue abnormality	Obesity - Weight loss by angiogenesis inhibitors
Skin abnormality	Psoriasis – warts - allergic dermatitis - scar keloids - pyogenic granulomas - blistering disease - Kaposi sarcoma in AIDS patients
Eye abnormality	Persistent hyperplastic vitreous syndrome - diabetic retinopathy-retinopathy of prematurity - choroidal neovascularization
Lung abnormality	Primary pulmonary hypertension - asthma - nasal polyps
Intestines abnormality	Inflammatory bowel and periodontal disease – ascites - peritoneal adhesions
Reproductive system abnormality	Endometriosis - uterine bleeding - ovarian cysts - ovarian hyperstimulation
Bone and joints abnormality	Arthritis - synovitis – osteomyelitis - osteophyte formation

For example, in cancers, angiogenesis is essential not only for providing oxygen and nutrients to growing tumours but also for tumour metabolic deregulation and dissemination. Tumour vessels are characterized by having an excessive tortuosity, larger lumens, hyperpermeability and uncontrolled sprouting and remodelling. These abnormalities contribute to the resistance of tumour cells to common therapies, and thus tumour angiogenesis is considered one of the cancer hallmarks and an important target in cancer therapy [8].

Another angiogenesis-related disease is diabetic retinopathy (DR) that is a microvascular complication of diabetes and the leading cause of blindness among adults globally. In early stages the disease is characterized by microaneurysms, retinal haemorrhages and capillary occlusion, which cause retinal ischaemia. When advanced, DR can evolve into a proliferative stage in which the strong ischaemia-mediated angiogenic stimuli can result in an uncontrolled growth of blood vessels on the retina that can cause vitreous haemorrhage and tractional retinal detachment. At any stage of DR the increased vascular permeability and leakage of proteins and lipids into the extracellular space can cause diabetic macular edema. Inflammation and angiogenesis inhibition are current therapeutic options in DR [9].

Similarly, one of the early pathological features in chronic, non-infectious arthritis, such as rheumatoid arthritis (RA), is angiogenesis. In response to inflammatory stimuli, immune imbalance, and hypoxia, RA synovial tissue macrophages and fibroblasts produce pro-inflammatory cytokines that can modulate the different stages of angiogenesis. In turn, new vasculature facilitates the infiltration of leukocytes into the joints and provide oxygen and nutrients for the proliferating synovial tissue which leads to synovial hyperplasia and progressive bone and cartilage destruction. In contrast, the prevention of joint neovascularization can alleviate synovitis and pannus formation [10].

I.1.2. Vascular endothelial growth factor (VEGF) as an anti-angiogenic therapy target

VEGF plays a central role in angiogenesis, stimulating EC mitogenesis, migration, sprouting and tube formation. VEGF also potentiates vascular permeability, which precedes and accompanies angiogenesis [4,11,12]. VEGF family currently comprises six members: VEGF-A, VEGF-B, VEGF-C, VEGF-D, VEGF-E and placental growth factor (PlGF) [11,13]. These growth factors bind and activate three major types of tyrosine kinase receptors - vascular endothelial growth factor receptors (VEGFR1-3) (**Figure I.1**). The co-receptors, Neuropilin (NRP)-1 and NRP-2 bind to VEGFRs to potentiate their action. VEGF-A is the prominent regulator of blood vessel growth, whereas VEGF-C/D play a role in lymphatic angiogenesis. PlGF stimulates its own angiogenic signalling pathway while also potentiating VEGF-A action by activating a crosstalk between VEGFR1 and VEGFR2. Although with no role in angiogenesis, VEGF-B plays a part in cell survival. VEGF-E is a viral-expressed member that leads to highly vascularised skin lesions (**Figure I.1**) [11,13].

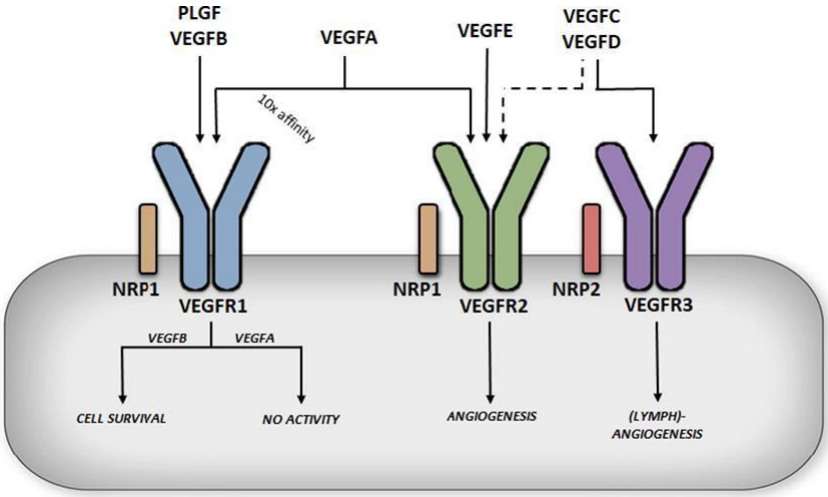

Figure I.1- Vascular endothelial growth factor (VEGF) family of growth factors and their receptors. The members bind to distinct receptors and exert different functions. Neuropilin (NRP)-1 and 2 function as co-receptors for VEGF. Reproduced from [13].

The human VEGF-A gene is organized in eight exons separated by seven introns, that by alternative splicing through exons 6 and 7, generates several protein isoforms named according to the amino acid number of the human synthesized protein (**Figure I.2**) [14,15]. Each exon encodes specific domains of the growth factor, and all isoforms contain exons 1–4 and exon 8. The selection exon 8 splice site results in two isoform groups, the pro-angiogenic (VEGF-Axxx) family and the anti-angiogenic (VEGF-Axxxb) family, whose activity allows receptor binding but impairs signal transduction. Exons 6 and 7 encode heparin-binding domains, responsible for the differences in the diffusibility and ECM affinity of the isoforms (**Figure I.2**) [14,15]. Even though the mechanisms regulating the levels of the different VEGF-A isoforms remain unknown, most cells appear to preferentially express VEGF-A_{165}, VEGF-A_{121} and VEGF-A_{189} [15].

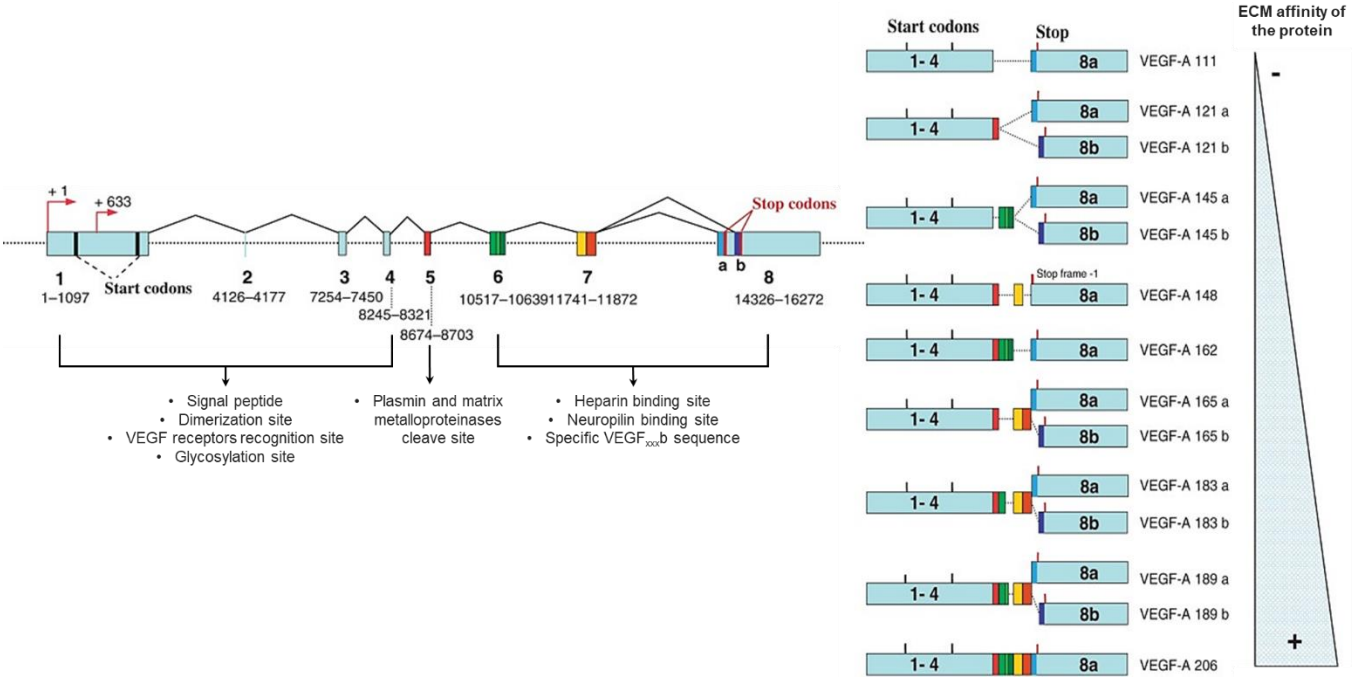

Figure I.2 - Structure of human VEGF-A gene exons and the protein isoforms generated by alternative splicing. The specific domains encoded by each exon are described. All isoforms contain exons 1–4 and exon 8, in which splice site determines its activity: pro-angiogenic (VEGF-Axxx) or anti-angiogenic (VEGF-Axxxb). Exons 6 and 7 encode heparin-binding domains being responsible for the differences in the diffusibility and ECM affinity of the isoforms. Adapted from [14,15].

VEGF-A exerts its biological effect through interaction with two VEGF-specific receptor tyrosine kinases, VEGF receptor 1 (VEGFR1) (Flt-1) and VEGF receptor 2 (VEGFR2) (KDR/Flk-1) (**Figure I.1**) that are strongly expressed on EC [11,12,16]. Interestingly, although VEGFR1 has a high affinity for VEGF-A, its tyrosine kinase activity is approximately 10-fold weaker than that of VEGFR2 [16]. VEGFR2 is considered the primary signal transducer during angiogenesis mediating several cellular functions though the activation of multiple downstream pathways, namely cell migration through the SHB-FAK-paxillin and NCK-p38-MAPKAPK2/3 pathways, cell permeability and proliferation by mediating the PLCγ-PKC, then eNOS-NO or MEK-ERK pathways, respectively [17] (**Figure I.3**). Hypoxia inducible factor (HIF) is the central transcription factor induced during hypoxia (i.e. low oxygen tension compared to atmospheric air, 21% O_2).

HIF regulates several hundred genes, mediating angiogenesis, metabolic reprogramming and inflammation, and VEGF is one of the primary target genes. Once activated, the transcriptional complex of HIF binds to hypoxia response elements in the promoter region of the VEGF-A gene to enhance its transcriptional expression [18] (**Figure I.3**). Cooperating with hypoxia, the paracrine action of several factors also upregulate VEGF-mRNA expression and secretion into the microenvironment, including epidermal growth factor (EGF), TGF-α and β, insulin-like growth factor (IGF), FGF and platelet-derived growth factor (PDGF) and inflammatory cytokines Interleukin (IL) - 1α and IL-6 [11].

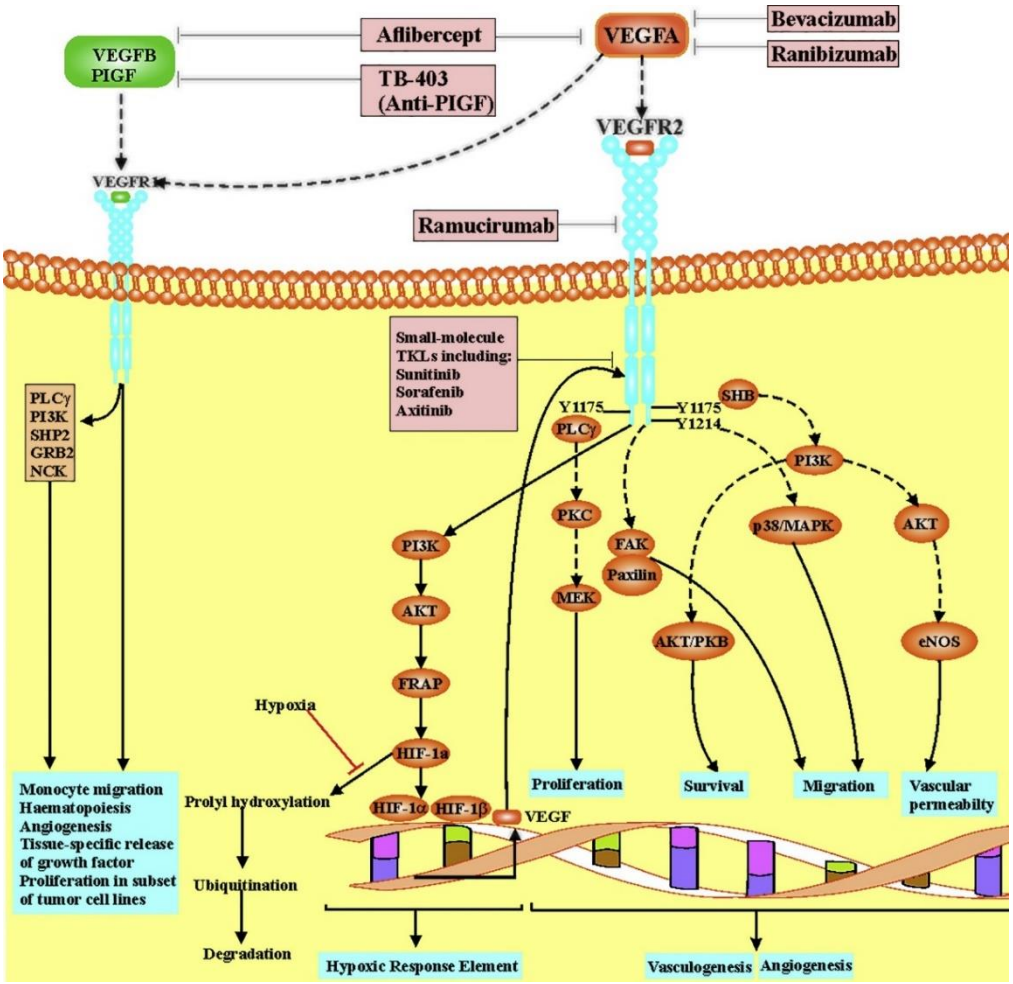

Figure I.3 - VEGF/VEGFR2 mediate several signalling pathways during angiogenesis, that induce cell survival, proliferation, migration and permeability. Hypoxia inducible factor (HIF) activates a signalling pathway that up-regulates VEGF expression, under hypoxic conditions. Several anti-angiogenic drugs are designed to prevent angiogenesis by inhibiting the VEGF–VEGFR system, including therapeutics antibodies and small molecules (depicted in pink boxes). Adapted from [6].

Besides actively participating in physiological angiogenesis, VEGF has a pathological role in many disorders including malignant, ocular such as age-related macular degeneration (AMD) and DR, and inflammatory conditions, such as RA and psoriasis [19–24]. The Food and Drug

Administration (FDA) has approved a spectrum of drugs designed to prevent angiogenesis by inhibiting VEGF or its receptors. Among these are anti-VEGF monoclonal antibodies Bevacizumab and Ranibizumab, anti-VEGFR2 monoclonal antibody Ramucirumab, human recombinant fusion protein Aflibercept that acts as a decoy receptor by binding to VEGF-A, VEGF-B, and PlGF, small-molecule Tyrosine Kinase Inhibitors (TKI) Sunitinib and Sorafenib, and RNA aptamer Pegaptanib, an oligonucleotide with high-affinity binding to $VEGF_{165}$ [6,25] (**Figure I.3**).

For instance, Bevacizumab combined with chemotherapy has been used as a first line treatment for various malignancies including metastatic colorectal cancer, glioblastoma, non-squamous non–small cell lung cancer, renal cell carcinoma and hepatocellular carcinoma [26]. Although the exact mechanism behind these synergistic effects remains unclear, anti-VEGF/VEGFR therapies induce morphologic normalisation of tumour vasculature, improving blood flow and cytotoxic drugs penetration. In fact, with anti-angiogenic treatment, immature blood vessels are pruned, and vessel tortuosity and leakage decrease, alleviating interstitial pressure and edema in cancer patients and improving the surviving blood vessel functionality [27].

Alternatively, ranibizumab and aflibercept have been used as standard treatments for AMD and DR [28,29]. Moreover, Pegaptanib, the first therapeutic aptamer in clinical use, was approved by the FDA to treat AMD [30].

Other classes of therapeutic agents are being investigated as novel and promising anti-angiogenic therapies including gene therapy, RNA interference (RNAi) therapy, and Chimeric antigen receptors (CAR)-T cell therapy [6].

I.2. RNA interference (RNAi) therapeutics

RNA interference (RNAi) is a biological mechanism by which small ~20–30 nucleotide (nt) double-stranded RNA (dsRNA) effectors and their associated proteins induce sequence-specific silencing of complementary target mRNAs by endonucleolytic cleavage or translational repression [31]. RNAi was initially discovered in 1993 by Lee and colleagues in *Caenorhabditis elegans* genome, in which the gene *lin-4* encoded two ~22 nt non-coding RNAs - later named microRNA (miRNA) - that contain sequences complementary to lin-14 mRNA which regulate lin-14 translation via RNA-RNA interaction [32]. Over time, it was discovered that miRNAs are widely distributed in the human genome encoding more than 2,300 mature miRNAs with a wide variety of biological and molecular functions essential in diverse developmental, cellular, and physiological processes [33,34]. An alternative class of small dsRNAs are small interfering RNAs (siRNAs) that although initially thought to have exogenous origin (ancestral viruses and other parasitic RNAs), can also be generated from endogenous genomic sources, such as transposable elements and pseudogenes [35]. siRNAs act not only as defenders of genome integrity in response to foreign or invasive nucleic acids but also as regulators of gene expression associated with specific biological processes [35,36]. In 2001, a landmark study by Elbashir and colleagues established the fundamentals of siRNA structure and RNAi mechanisms and effectively employed chemically synthesized siRNAs for sequence-specific target gene silencing

[37]. Since then, siRNAs have been extensively applied in loss-of-function studies and biomedical research in hopes of developing siRNA-based therapies for a variety of disorders including cancers and virus infections [31,38]. siRNA effectors can also originate from short-hairpin RNA (shRNA) precursors encoded in expression vectors after RNAi machinery processing, achieving similar functional outcomes [39,40].

I.2.1. Biogenesis and action of RNAi effectors

Despite their differences, miRNAs and siRNAs have similarities in their biogenesis and mechanisms of action (**Figure I.4**) [41].

Briefly, the biogenesis of mature miRNAs is initiated by transcription of the encoding genes by RNA polymerase II (Pol II). The transcripts are referred to as primary miRNAs (pri-miRNAs) and consist of >1,000 nt long, capped and polyadenylated stem-loop structures with incomplete double-stranded character, that can be single or clustered. The pri-miRNAs are cropped by the microprocessor complex composed of the ribonuclease (RNase) III Drosha and DiGeorge syndrome critical region 8 (DGCR8), a protein containing two double-stranded RNA-binding domains (RBDs), into double-stranded hairpin structure precursor miRNAs (pre-miRNAs) of 60–100 nucleotides [31,42].

Alternatively, artificially introduced sequences encoding the shRNA are conventionally transcribed by RNA polymerase III (Pol III), originating 50-70 nt long stem-loop structures consisting of a 19- to 29-nt region of complementary double-strand RNA separated by an unpaired loop and a dinucleotide 3' overhang [39,40].

The resulting hairpin precursors are subsequently transported to the cytoplasm by Exportin 5 and RanGTP transport facilitators [43].

In the cytoplasm, the precursors shRNA and pre-miRNAs are processed by RNase III-related endonuclease Dicer that after association with the double-stranded Tat–RNA-binding protein (TRBP) or Protein kinase RNA activator (PACT), to remove the harpin loop and form the mature miRNA/siRNAs duplexes composed by 19- to 25-nt double-stranded sequence with 2-nt 3′-overhangs. Similarly, long, perfectly base-paired dsRNA precursors are also recognized and cleaved by Dicer resulting in mature siRNA duplexes [44,45].

Afterwards, the Dicer-RNA complex provides a platform for Argonaute (Ago) protein recruitment and RNA-induced silencing complex (RISC) assembly. RISC loading is coincident with strand selection, in which the passenger strand (sense strand) is cleaved and discarded, while the guide strand (antisense strand) remains within the complex [46]. The effector complex performs cellular surveillance, silencing target single-stranded-mRNA sequences with complementarity to its bound guide strand [31,38].

In the siRNA-mediated pathway, the complementary binding of the siRNA guide strand activates Ago 2 which cleaves the target mRNA at a single site ~ 10 nts from the 5′ end between of guide strand, leading the subsequent exonuclease-mediated degradation of the fragments. In contrast, in the miRNA-mediated pathway Ago 2 is not activated, due to partially complementary base pairing between mRNA and miRNA. Depending on the different binding sites and degree of

complementarity, silencing can occur by translation repression or degradation induced by deadenylation, decapping or exonuclease activity, and in rare cases of high complementarity, by endonucleolytic cleavage similar to as for siRNAs [31,38].

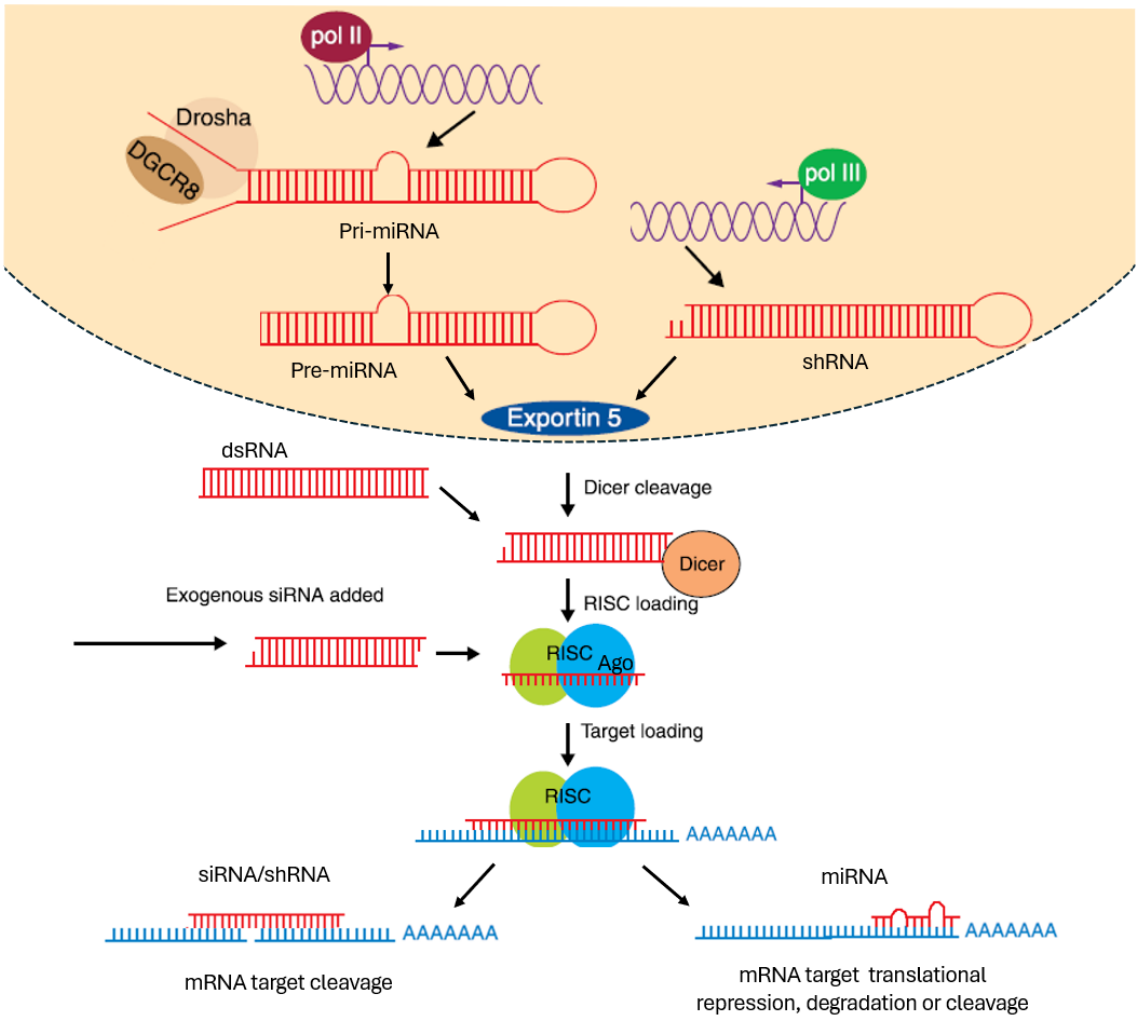

Figure I.4 - Schematic representation of biogenesis and gene silencing mechanisms miRNA and siRNA pathways. miRNAs are transcribed by RNA polymerase II (pol II) as primary miRNA (pri-miRNAs) and after Drosha processing result in double-stranded hairpin structure precursor miRNAs (pre-miRNAs) with incomplete complementarity character. Short-hairpin RNAs (shRNAs) are originated from RNA polymerase III (pol III) and are complementary double-strand structures separated by an unpaired loop. Both precursors are transported to the cytoplasm and recognized by Dicer that originated mature miRNA/siRNAs duplexes composed by 19- to 25-nt double-stranded sequence with 2-nt 3′-overhangs. Endogenous or exogenous dsRNAs are also processed by Dicer into siRNAs. After Argonaute (Ago) protein recruitment and RNA-induced silencing complex (RISC) assembly, the passenger strand is eliminated and the complex targets mRNAs with complementarity to the guide strand. The full complementary binding between the guide strand of siRNA and target mRNA leads to the cleavage of mRNA, while partially complementary binding generated by miRNA recognition can induce different post-transcriptional silencing mechanisms. Adapted from [41].

I.2.2. siRNA as therapeutic agents

Since the first demonstration of the potential of siRNA therapeutics by Song and colleagues, in which the injection of siRNAs targeting Fas expression protected mice from autoimmune hepatitis [47], drug development has advanced rapidly, and several siRNA-based drugs have been reported approved by the FDA or are currently on phase III clinical trials (**Table I.2**).

Table I.2 – Summary of siRNA-based drugs approved by the FDA and siRNA-based drugs candidates in phase III clinical trials. Adapted from [48].

Drug / Trade Name	siRNA Carrier	Disease / Target organ	Targeting Gene	Updated Status
Patisiran/ Onpattro	Lipid nanoparticles	Hereditary transthyretin mediated (hATTR) amyloidosis / Liver	transthyretin (TTR)	FDA approval (August 10, 2018)
Givosiran/ Givlaari	GalNAc-conjugation	Acute hepatic porphyria (AHP) / Liver	aminolevulinate synthase 1 (ALAS1)	FDA approval (November 20, 2019)
Lumasiran/ Oxlumo	GalNAc-conjugation	Primary hyperoxaluria type 1 (PH1) / Liver	hydroxy acid oxidase 1 (HAO1)	FDA approval (November 23, 2020)
Inclisiran/ Leqvio	GalNAc-conjugation	heterozygous familial hypercholesterolemia or clinical atherosclerotic cardiovascular disease / Liver	proprotein convertase subtilisin/ kexin type 9 (PCSK9)	FDA approval (December 21, 2021)
Vutrisiran/ amvuttra	GalNAc-conjugation	Hereditary transthyretin mediated (hATTR) amyloidosis / Liver	transthyretin (TTR)	FDA approval (June 13, 2022)
Nedosiran/ Rivfloza (DCR-PHXC)	GalNAc-conjugation	Primary hyperoxaluria type 1 (PH1) / Liver	lactate dehydrogenase A (LDH)	FDA approval (October 2, 2023)
ARO-APOC3	GalNAc-conjugation	Familial chylomicronemia syndrome / Liver	apolipoprotein C3 (APOC3)	Phase III, recruiting (NCT05089084)
Fitusiran (ALN-AT3SC)	GalNAc-conjugation	Haemophilia A and B and rare blood disorders / Liver	antithrombin (SERPINC1)	Phase III, completed (NCT03549871)
Teprasiran (QPI-1002)	None	Acute kidney injury following cardiac surgery / Kidney	tumour suppressor protein (p57)	Phase III, terminated (NCT03510897)
Cosdosiran (QPI-1007)	None	Acute Nonarteritic Anterior Ischemic Optic Neuropathy (NAION) / Eye	caspase 2 (CASP2)	Phase II/III, terminated (NCT02341560)
Tivanisiran (SYL1001)	None	Dry eye disease with Sjogren syndrome / Eye	capsaicin receptor (TRPV1)	Phase III, completed (NCT03108664)
Bevasiranib	None	Neovascular AMD / Eye	vascular endothelial growth factor (VEGF)	Phase III, terminated (NCT00499590)

siRNAs have the advantage of executing their function by complete Watson–Crick base pairing with mRNA, whereas small molecule and monoclonal antibody drugs rely on the recognition of often complex spatial configurations of target proteins [49]. Moreover, siRNA-mediated post-transcriptional silencing prevents target protein translation, and a single siRNA molecule can mediate the degradation of multiple mRNA molecules, making it a very efficient and specific therapeutic modality [49,50]. Despite the potential, siRNAs face limitations related with their poor stability and rapid degradation in physiological conditions, inability to cross cellular membranes, rapid clearance and innate immune activation which hampers their therapeutic efficacy [51,52]. Therefore, advanced research is focused on enhancing siRNA stability and minimizing immunological responses and off-target effects by introducing chemical modification to the backbone and nucleotides of siRNAs [53]. Moreover, extensive research is focused on developing nanocarriers to facilitate its deliver by improving physicochemical and biopharmaceutical properties of siRNA. These include lipidic, polymeric, and inorganic nanocarriers, like micelles, liposomes, dendrimers and gold nanoparticles [51,52]. In the last few decades, the potential of extracellular vesicles (EVs) has been explored as natural drug delivery systems (DDS) (further detailed in Section I.3.3) including for RNA delivery, demonstrating promising effects in pre-clinical studies for cancer, central nervous system disorders, COVID-19, and other diseases [54].

I.2.3. Short-hairpin RNA (shRNA) expression systems

As aforementioned, an alternative approach to delivering siRNA sequences is through expression systems that encode shRNAs, which are double-stranded stem-looped RNAs that after transcription are exported to the cytosol and processed by endogenous enzyme Dicer into functional siRNA duplexes [39,40]. Such expression systems are based on plasmids or viral vectors that typically encode sequences composed of complementary 19-22 nt sense and antisense segments of the target gene separated by a 6-11-nt spacer, allowing the transcript to fold back on itself forming a shRNA, analogous to natural miRNAs [55,56]. Traditionally, the shRNA sequence is expressed from Pol III promoters, such as U6 and H1 promoters, since they have a well-defined transcription start and end points producing a shorter, more predictable transcript. However, several studies have identified that Pol II transcripts represents an effective approach to express shRNA sequences adapted into a pri-miRNA-like structure [56].

Since the study developed by Brummelkamp and colleagues, in which a powerful new tool to stably suppress gene expression in mammalian cells using a retroviral expression system was first described [57], viral vectors have been the most employed approach when developing in shRNA-expressing systems. Among others, retroviruses, lentiviruses, adenoviruses, adeno-associated viruses (AAV), herpesviruses, have proven to efficiently silence gene expression [58–62]. In the case of retroviruses and lentiviruses, stable long-term shRNA expression can be accomplished, which can be beneficial for certain medical disorders. However, there is a risk of toxicity from over-saturation of RNAi machinery thus limiting the dosage of shRNA to stay below

the threshold of competitive inhibition of the endogenous miRNA biogenesis machinery is relevant [63]. Other favourable characteristics of viral vectors are their high gene transfer efficiency, ability to protect their genetic cargo from degradation and their capability to cross cellular barriers [64]. For example, systemic delivery of recombinant AAV vectors expressing shRNA against the androgen receptor (AR), a key factor in prostate cancer progression, eliminated prostate cancer xenografts in nude mice within 10 days by successfully inducing AR gene silencing *in vivo* [65]. However, the clinical application of viral vectors is still hampered by safety concerns related to potential immunogenicity and latent pathogenic effects, poor targeting potential, and high costs [64]. Plasmids are safer, more easily manipulated and manufactured at a lower cost and have more extended shelf-life [66], being a promising alternative to deliver shRNAs for sustained therapeutic gene silencing [67–69]. For instance, Zhang and colleagues developed a plasmid encoding a shRNA targeting human EGF receptor that, aided by liposomes with receptor-specific targeting ligands, caused a reduction in the target oncogenic gene expression and an increase of brain-tumour-bearing mice survival time by 88% after weekly intravenous administration [70]. In a different context, plasmid-based shRNAs targeting Chikungunya virus (CHIKV) E1 and nsP1 capsid genes were tested as an antiviral therapeutic strategy. The shRNA-expressing plasmids demonstrated effective long-lasting inhibition effects against CHIKV replication in a murine model, allowing 100% survival of the mice up to 15 days, in contrast to non-treated and scrambled-treated mice which showed complete mortality by day 8-10.

Overall, shRNA-expressing vectors offer several advantages over traditional synthetic siRNAs namely enhanced stability, prolonged expression and lower immune response [39]. By presenting shRNA constructs on DNA plasmids, these systems effectively evade dsRNA-mediated activation of Toll-like receptor (TLR) 3. Furthermore, the intrinsic processing of shRNA by endogenous cellular machinery implies a decreased propensity for eliciting inflammatory reactions via cytoplasmic dsRNA receptors [39]. Moreover, shRNA-expressing vectors allow selective targeting of particular cell types, reducing potential off-target effects on non-target cells by incorporating cell-type specific promoters [71].

I.2.3.1. Minicircles as shRNA expressing systems

Despite being far less immunogenic than viruses, unmethylated CpG dinucleotide and other bacterial motifs of plasmids can induce host inflammatory responses and transcriptional silencing of episomal transgenes [72–74]. Moreover, the larger size of conventional plasmids often reduces transfection efficiencies [74–77]. These limitations can be overcome using minicircles (MCs) that are small vectors free of bacterial backbone sequences (e.g., antibiotic resistance gene, origin of replication, and inflammatory sequences intrinsic to bacterial DNA) and capable of high levels of transgene expression, that potentially meet the clinical requirements for safe and long-lasting gene expression [78,79]. MCs are generally synthesised in recombinant bacteria and result from an *in vivo* recombination process: the parental plasmid (PP) carries the eukaryotic expression cassette flanked by two recognition sites of a site-specific recombinase,

that upon induction originate a replicative miniplasmid (MP) carrying the undesired backbone sequences, and a MC carrying the therapeutic expression unit (**Figure I.5**) [78,79].

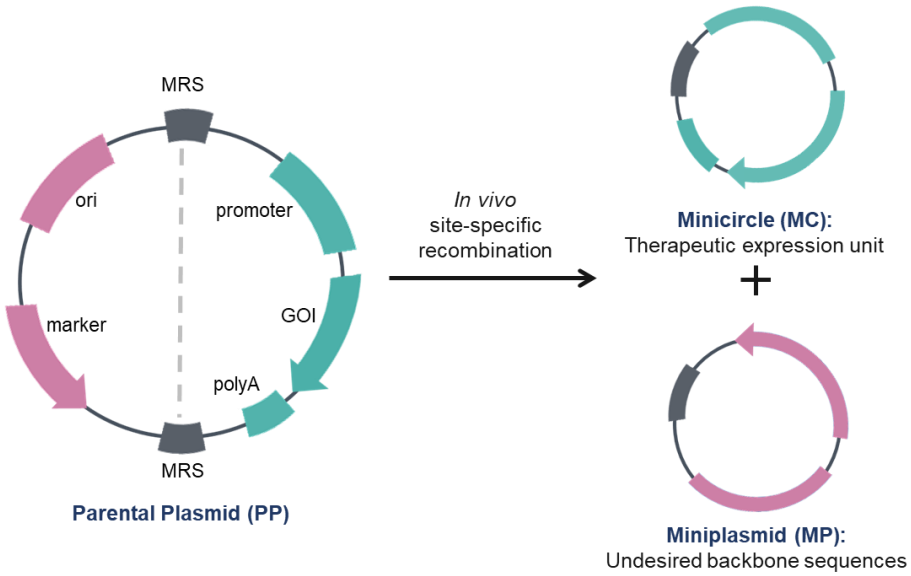

Figure I.5 - Schematic representation of the recombination of a parental plasmid (PP) into a minicircle (MC), carrying the therapeutic expression unit, and a miniplasmid (MP), containing the undesired backbone sequences, which are flanked by two multimer resolution sites (MRS). Abbreviations: ORI, origin of replication; GOI, gene of interest.

The potential of minicircles has been demonstrated in several gene therapy preclinical studies for the treatment of various diseases, including skin wounds [80], primary ciliary dyskinesia [81], pancreatic cancer [82] and ovarian cancer [83]. In this context, shRNA-expressing MCs appear as a promising gene-targeting therapy by combining the prolonged biostability of plasmid DNA, gene silencing capabilities of siRNA, and improved transfection efficiency of MCs [84–88]. As an example of the great potential of shRNA-encoding MCs, Zhao and colleagues reported that MC targeting anaplastic lymphoma kinase showed increased transfection efficiency compared to a conventional plasmid while gene silencing was equivalent to siRNAs, effectively reducing the growth of anaplastic large cell lymphoma cells *in vitro* [86] Moreover, MC demonstrated increased stability in human serum (>48 h), compared to plasmid and siRNA which were only stable for 0.5 and 2 h, respectively [86]. Another example is the inhibition of HIF-1-alpha degradation through MC-expressing shRNA that targets prolyl hydroxylase-2 which showed to significantly improve neovascularization and blood flow recovery compared with a conventional plasmid or PBS, in a murine hindlimb ischemia model [88].

I.2.4. RNAi-based anti-angiogenic strategies

RNAi-based anti-angiogenic strategies have demonstrated positive effects as modulators of angiogenesis *in vitro* and *in vivo*, by silencing pro-angiogenic factors [89]. The VEGF regulatory pathway is undoubtedly a promising target when developing anti-angiogenic gene-targeting therapies. Different formulations of siRNA that target VEGF and its receptors achieved a high anti-tumour effect in tumour-bearing mice [90–92], and effectively reduced pathologic angiogenesis in mouse models of corneal neovascularisation [93,94]. For example, intravenous administration of polyethyleneimine (PEI) nanoparticles bearing siRNAs targeting VEGFR2 into mice tumours led to decreased levels of VEGFR2 within the tumours, as well as a reduction in both tumour angiogenesis and growth [92]. Clinical studies have already been exploring siRNA-based therapeutics in the context of angiogenesis namely for treating of AMD by targeting VEGF (bevasiranib, phase III, NCT00499590) or VEGFR1 (AGN211745/sirna-027, phase II, NCT00395057) [48].

Beside siRNAs, plasmid and viral expression vectors have been used as anti-angiogenesis agents. For instance, lentiviral vectors expressing shRNA targeting VEGF inhibited tumour angiogenesis and growth, and increased apoptosis of pancreatic cancer cells *in vitro* and *in vivo* [95]. In another context, specific knockdown of VEGFR2 in retinal endothelial cells using a lentivirus encoding the shRNA under control of the vascular endothelial-cadherin promoter, demonstrated to be promising novel therapeutic approach for retinopathy of prematurity [96]. Moreover, plasmids expressing shRNA against VEGF-A were shown to have great anti-angiogenesis efficacy, regressing corneal neovascularisation in a mouse model of corneal injury [67] and inhibiting of tumour growth in subcutaneous tumour mice models [97].

In addition, silencing of other molecules of VEGF regulatory pathway has been shown to prevent angiogenesis, including transcriptional activator of VEGF under hypoxic conditions HIF-1-alpha [98] and PlGF, which signals EC to undergo angiogenesis directly through VEGFR1 and potentiates VEGF-A action by activating the crosstalk between VEGFR1 and VEGFR2 [99,100]. For instance, siRNA-based PlGF silencing ameliorated liver injury, inflammation and fibrosis in fibrotic mice, while reducing microvessel density and angiogenic factors HIF-1-alpha, VEGF and VEGFR1 [100].

Besides VEGF, other proteins are notable mediators of angiogenesis, among which EGF receptor [70], Ang-2 [101], heparanase [102], TGF-β co-receptor endoglin [103] and protein tyrosine kinase c-Src [68] and their RNAi-mediated silencing have demonstrated positive effects in preventing tumour angiogenesis and metastasis. For example, siRNA targeting endoglin locally electrotransfected into mammary-adenocarcinoma-bearing mice three times on each consecutive day successfully decreased target-mRNA levels causing a significantly decrease in the number of blood vessels and overall growth of tumours [103]. Another study showed that the delivery of a plasmid vector system encoding a shRNA targeting human c-Src to xenografted pancreatic carcinoma tumours in mice, downregulated angiogenic factors VEGF and CD34 (i.e. indicator of microvessel density in tissues) and caused a reduction of tumour size [68].

I.3. Extracellular vesicles (EVs)

I.3.1. Fundamentals of EVs: biogenesis, composition and uptake

EVs are nano-sized lipid bilayer structures secreted by cells that enclose a variety of cellular components and mediators and facilitate the targeted delivery of their functional cargo to nearby or distant cells [104,105].

Vesicle formation and secretion were first acknowledged in the 1980s by Johnstone and Stahl groups when investigating membrane biochemistry and trafficking during reticulocyte maturation [106,107], being identified as a cellular process for waste disposal [108]. Currently, EVs are strongly established as essential mediators of intercellular communication by transporting numerous proteins, lipids and nucleic acids, and thus able to modulate many normal physiological and pathological conditions (**Figure I.6-A**) [104,105,109].

Due to their robust potential as natural biomedicines, drug delivery systems (DDS) and diagnostic biomarkers, EVs have gained increasing attention in the past decade [110]. EVs have the intrinsic capacity to cross biological barriers, including plasma/endosomal membranes and blood-brain barrier (BBB) [111] and demonstrate reduced immunogenicity and low toxicity in the spleen and liver [105,112]. These unique attributes are rendering EVs attractive DDS allowing them to overcome limitations often associated with synthetic nanocarriers. In fact, EVs seem to be internalized more efficiently and deliver their therapeutic agent several orders of magnitude more efficiently than synthetic nanoparticles [113,114].

Generally, EVs are a heterogeneous population that is generally categorized into three subsets based on their biogenesis: exosomes, microvesicles and apoptotic bodies (**Figure I.6-B**) [104,105]:

Exosomes (Exo) are small membrane vesicles with a diameter of 40 to 150 nm released from cells by the fusion of an intermediate organelle of the endocytic pathway - the multivesicular body (MVB) - with the cell surface. The biogenesis of Exo initiates with the formation of the MVB through the maturation of early endosomes. During this process, the membrane of MVBs suffers inward budding, forming intraluminal vesicles (ILVs) sequestering proteins and nucleic acids [104,105,115] that are specifically sorted by the endosomal sorting complex required for transport (ESCRT) [116], lipids (e.g., ceramides) [117], and tetraspanins [104,118]. MVB can either direct proteins to lysosomes for degradation or be transported and fused to the plasma membrane for the release of ILVs that are then referred to as Exo [104,105,115]. Due to their biogenesis, ESCRT proteins and their accessory proteins, such as ALG-2-interacting protein X (ALIX) and tumour susceptibility gene 101 (TSG101) are expected to be found in Exo regardless of the type of cell from which they originate. Other proteins reported to be abundant in Exo include membrane proteins of the tetraspanin family (e.g., CD63, CD9 and CD81), lysosomal-associated membrane proteins (Lamps), heat shock proteins (HSP) and other cytosolic proteins, such as RAB GTPases and annexin that participate in intracellular trafficking [104,105,115].

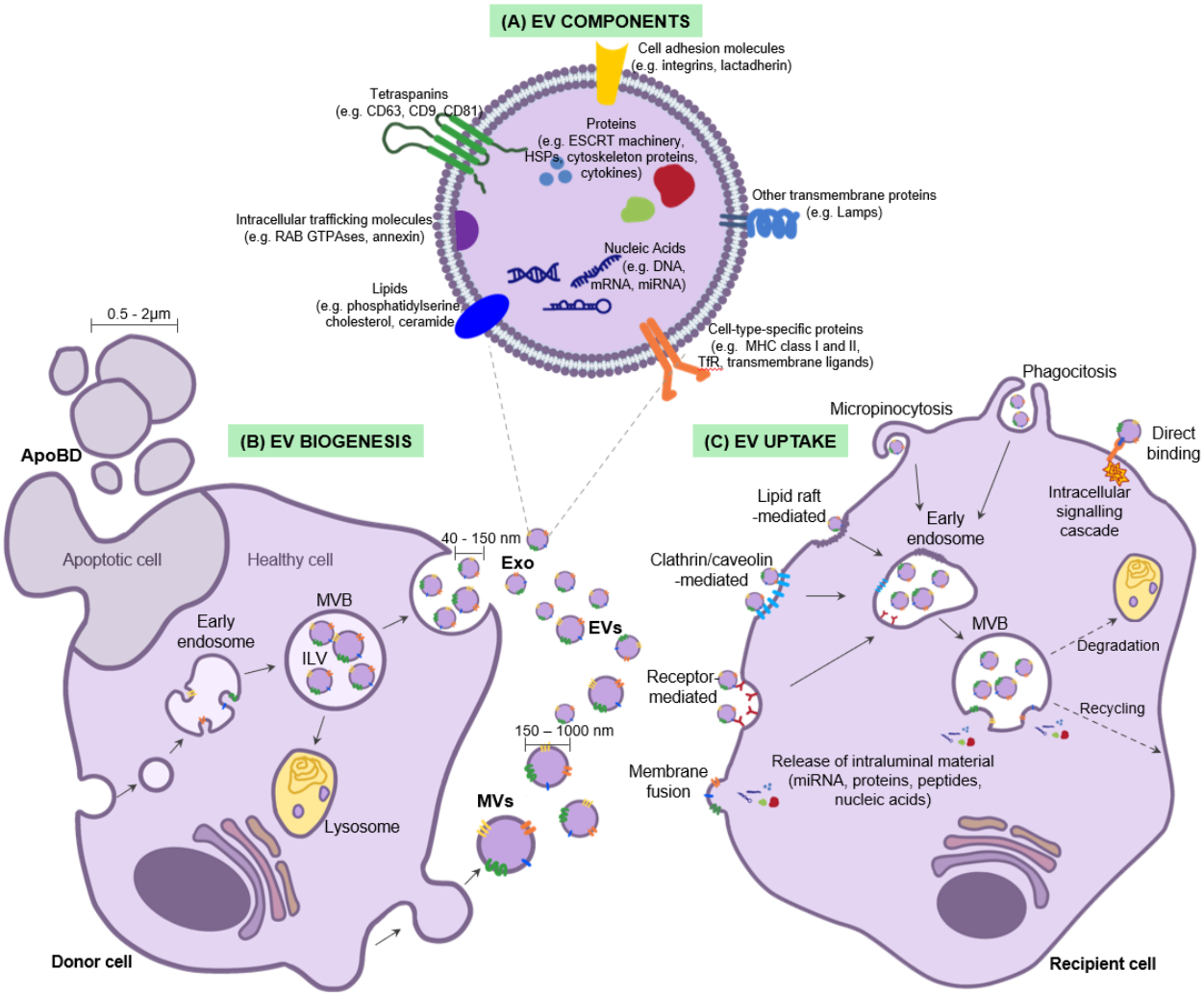

Figure I.6 - Basics of extracellular vesicle (EV) biology. **(A)** General composition of EVs: EVs are nano-sized lipid bilayer structures that enclose a variety of cellular components including cytosolic and transmembrane proteins, bioactive lipids and nucleic acids. **(B)** Biogenesis of the different subsets of EVs: EVs are formed either by the disassembly of an apoptotic cell into subcellular fragments as apoptotic bodies (ApoBD), the budding of the plasma membrane, in which case they are referred to as microvesicles (MVs) or as intraluminal vesicles (ILVs) within the lumen of multivesicular bodies (MVBs). MVBs fuse with the plasma membrane to release ILVs that are then called exosomes (Exo). **(C)** Mechanisms of uptake of EVs by the recipient cells: EVs can induce a downstream signalling cascade in the recipient cell via direct binding or transfer of their intraluminal content by membrane fusion or endocytosis-mediated internalisation. The internalised EVs follow the endosomal pathway and can either be recycled back to the plasma membrane, degraded in the lysosome or undergo endosomal escape releasing their intraluminal cargo. ESCRT—endosomal sorting complex required for transport; HSP—heat shock protein; Lamp—lysosomal-associated membrane proteins; MHC—major histocompatibility complex; PS—phosphatidylserine; TfR—transferrin receptor. Reproduced from [109].

Microvesicles (MV) or ectosomes are larger membrane vesicles, ranging from 50 nm to 1µm in diameter, that result from direct outward budding and fission of the plasma membrane [104,105]. This process is mediated by the local redistribution of the protein and lipid components of the plasma membrane, which modulates changes in membrane curvature and rigidity [119]. Ca^{2+} accumulation induces the activation of proteolytic enzymes (e.g., calpain) and lipid

translocases (e.g., flippases, floppases and scramblases) that disrupts the equilibrium of the phospholipids between the two leaflets that cause the physical bending of the membrane and loss of membrane-cytoskeleton connection, facilitating vesicular release [104,120]. Additionally, membrane budding is associated with lipid rafts which are specialized regions of the plasma membrane that are enriched in cholesterol, glycosphingolipids, and glycosyl-phosphatidylinositol (GPI)-anchored proteins. Caveolin-1, a structural protein of caveolae lipid rafts, has been shown to regulate the formation and cargo sorting of MV [121]. Although membrane budding occurs through a different process than Exo formation, it also depends on endosomal machinery including the ESCRT components, tetraspanins and RAS GTPases [104,119]. Other proteins that are found abundant in MVs include cytoskeletal proteins, such as actin, and plasma membrane-associated proteins [104,120,121].

Finally, apoptotic bodies (ApoBD) that range from 500 nm to 2 µm in diameter are also generated from the cell surface, however, these are only released during the disassembly of an apoptotic cell into subcellular fragments. As a result, ApoBD contain a wide range of cellular components possibly including chromatin/DNA fragments, cytosol portions, degraded proteins, or even intact organelles [122].

Besides the sorted proteins, Exo and MV also contain a variety of nucleic acids, including DNA, mRNA and different classes of non-coding RNAs, namely miRNAs, long non-coding RNAs (lncR), and circular RNAs [104,105,115]. Although the exact mechanism that regulates the sorting of RNA species into EVs is still unknown, some RNA-binding proteins (RBP) have been found to participate in RNA sorting through the recognition of specific sequence motifs. For example, sumoylated heterogeneous nuclear ribonucleoprotein A2/B1 is an RBP and has been reported to regulate miRNA trafficking into EVs by binding to specific motifs (GGAG/CCCU) [123].

Once secreted, EVs can interact with the target cells either located within the microenvironment or in distant sites travelling through blood and other body fluids. This interaction is facilitated by numerous mediators, including tetraspanins, integrins, lipids, lectins, heparan sulfate proteoglycans and other ECM components [104]. The direct binding of EVs can induce a downstream signalling cascade in the recipient cell via ligand-receptor interactions (e.g., antigen presentation, immune modulation and morphogen signalling) [104,115]. For instance, EVs have been reported to act as carriers in the long-range transfer of the canonical lipid-anchored morphogens Hedgehog (Hh) and Wnts to recipient cells which induce several physiological processes, such as stem cell maintenance, tissue repair and metabolism [124].

Alternatively, EVs can transfer their intraluminal cargo to the recipient cells either by direct membrane fusion or endocytosis. Endocytosis is the main uptake mechanism and occurs through different pathways: receptor-mediated endocytosis, clathrin-mediated endocytosis, caveolin-mediated endocytosis, lipid raft-mediated endocytosis, phagocytosis and micropinocytosis [104,115]. The internalised EVs follow the early endosomal pathway in which they can either be recycled back to the plasma membrane, degraded in the lysosome and used as a metabolites source, or undergo endosomal escape, through back fusion with the limiting membrane MVB, releasing their contents to the cytosol (**Figure I.6-C**) [104,115].

Although the mechanism by which cells discriminate the fate of the internalised EVs is poorly understood, the delivery capacity of EVs has been largely demonstrated. The release of their intraluminal content triggers alterations in the recipient cells by the action of nucleic acids, including miRNA and mRNA, that regulate gene expression, and other important genetic elements, including genomic DNAs, mitochondrial DNAs and long noncoding RNAs [104,115]. EVs also release protein and peptide cargos that induce a functional response in the recipient cells. For example, in dendritic cells, protein cargos of EVs can be processed and used in antigen presentation regulating immune response [104,125].

Due to the overlapping sizes and absence of proteins that are restricted to each population, all the different vesicles can be collectively referred to as EVs, as proposed by the International Society for Extracellular Vesicles (ISEV) [126].

I.3.2. Manufacture of EVs

In clinical settings, large doses of EVs are required, ranging from 10^{10} to 10^{11} total administrated vesicles [127,128]. In stark contrast, most preclinical studies still use conventional planar culture systems (e.g., T-flask) and fetal bovine serum (FBS)-supplemented culture media formulations for cell expansion and resort to non-scalable low-purity grade methods for EV isolation (e.g., polymer-based precipitation methods and ultracentrifugation) [128,129], all of which hampers their translation into the clinic by failing to meet the necessary dose and safety requirements. Thus, a large-scale EV manufacturing workflow, that includes scalable platforms from the upstream to the downstream, needs to be implemented to generate high EV yields with great purity levels [130].

I.3.2.1. Production of EVs

Depending on the cell source, EVs present specific properties and signalling molecules conferring them unique clinical potential. Among others, mesenchymal stromal cells (MSC), immune cells, including macrophages, dendritic cells (DC), T cells and natural killer (NK) cells, neural cells and red blood cells (RBC) are being investigated as EV-producers for their therapeutic effects [131]. Currently, EVs derived from MSC isolated from different tissues (mainly bone marrow, umbilical cord, and adipose tissue) are the primary focus of clinical research [132]. Besides their intrinsic therapeutic properties and safety profile, *ex vivo* expansion capacity of the EV-producing cell source is a crucial factor when aiming at clinical treatments. Moreover, expansion and EV secretion rates are notably different depending on the cell source, which impact the cost of final product. For instance, some studies have reported that umbilical cord-derived MSC have an increased expansion capacity and produce the highest EV yields when compared to MSC isolated from adipose tissue (MSC(AT)) and bone marrow (MSC(M)) [133–135].

The selection of the culture platform is a critical step when producing EV-enriched conditioning media. Generally, plasticware containers, such as Petri dishes, T-flasks, multiwell plates, are the simplest and most commonly used culture vessels. Their used is mainly directed

towards research purposes and becomes a challenge in applications that demand a large number of cells owing to the lack of scalability. To avoid laborious and unsustainable scale-out when high cell densities are required, other plasticware-based culture systems were developed. In particular, multi-layered flasks were designed to scale-up single layered T-flasks by increasing the surface area while maintaining the footprint. For example, Andriolo and colleagues developed of a good manufacturing practice (GMP)-grade manufacturing method for cardiac-progenitor-cells-derived EVs using sixteen 1,720 cm^2 multi-layered flasks (HYPERFlasks® from Corning®) [136]. Sophisticated advances to these systems include closed systems densely packed thin individual surfaces with perfusion mechanisms for the continuous medium supply in laminar flow [137], but have not yet been used for EV production. An alternative platform with flask configuration is the Integra CELLine system which consists of a two-compartment culture flask with a semi-permeable membrane separating a cell-containing compartment from a larger medium compartment, allowing high cell concentrations. This system allowed a 12-, 8- and ~15-fold increase in EV concentration (measured as protein content) compared to traditional T-flasks, when cultivating mesothelioma, NK and bladder carcinoma cells, respectively [138,139]. Despite reducing the cost and labour of the production, the scalability of this system is limited.

When upscaling EV production, bioreactors are the most promising strategy by allowing monitoring and control, as well as sustaining high cell densities and the subsequent production of large volumes of EV-enriched conditioned medium (CM). Generally, bioreactors yield increased cell numbers in a more cost-effective manner compared to static cultures, by increasing the surface-to-volume ratio and minimizing culture time, manipulations and consumables [140]. Hollow-fiber bioreactors are one of the most used configurations when upscaling EV production, accommodating high cell densities and multiple-day retrieval of EV-enriched CM. The setup is composed of cylindrical permeable hollow fibers, in which cells are typically cultivated in the extracapillary space, while medium recirculates through the intracapillary space constantly providing nutrients by tangential flow [130]. For example, hollow-fiber systems operating in a perfusion mode with medium recirculation was used to collect EVs from MSC(M) and NK throughout a 25- and 20-day period, respectively, yielding large EV numbers [141,142]. Some limitations of hollow fiber bioreactors include the impossibility of *in situ* cell growth monitoring, lack of homogeneity in the extracapillary space and difficulties in cell harvesting [130].

Microcarriers provide a surface for adherent cells to growth in suspension while offering a high surface-area-to-volume ratio [143]. Multiple microcarrier-based stirred platforms have been implemented to maximise cell expansion and EV production, including spinner flasks [144–146] and vertical-wheel systems [133,147,148]. When cultivating WJ-derived MSC (MSC(WJ)) increased EV productivity 3- and 20-fold compared to static cultures, when using vertical-wheel systems [133,147] and spinner flasks [144], respectively. Stirred-tank reactor (STR) platforms further improve EV yields and process standardisation by continuously monitoring the cell culture microenvironment, controlling not only temperature, but also fine-tuning dissolved oxygen and pH [149–151]. Similarly, fully controlled STR systems also induced an increase in EV secretion when compared to two-dimensional static systems [150,151]. Besides causing significant intracellular

pathways and expression alterations that regulate EV secretion, laminar or turbulent flow-induced shear stress causes cell membrane tension and elongation, leading to fragmentation and spontaneous self-assembly of vesicles [152]. Despite being advantageous for EV secretion, excessive shear stress produced by the impeller could be a problem, particularly for delicate cell types [130]. The wave bioreactor system employs a wave motion generated by a rocking platform, which provides a good cell/microcarriers suspension and with negligible shear stress [130]. Dooley and colleagues have used the wave bioreactor for large-scale production of EVs derived from suspension-adapted HEK293 cells in 10- or 25-L working volumes [153]. Moreover, the growth of MSC as 3D aggregates under wave motion has showed to promote EV secretion, yielding 2-fold higher numbers of EVs per cell than the 2D monolayer cultures [154].

Besides agitation [147], other physiological stimuli have been shown to enhance EV secretion, including low oxygen tension (e.g., ranging from 0.5% to 5% O_2, compared to controls) [155–157], low pH (e.g., pH 4 or 6) [158,159] and high temperature (e.g. 40 or 42ºC) [159,160]. For instance, culture of MSC(AT) in hypoxia (5% O_2) boosted the yield secreted EVs by 2.6-fold [157]. As another example, thermal stress at 40°C for 1 hour increased the production of EVs in human leukemia/lymphoma T and B Cells by 3- and 22-fold, respectively [159,160].

Additionally, EV yields can be enhanced with chemical compound supplementation. For example, studies have reported that adiponectin [161], combined N-methyldopamine and norepinephrine [162] or combined interferon-gamma (IFN-γ) and TNF-α [163] can robustly increase EV secretion by MSC. Similarly, incubation with cytokines TNF-α, IL-8 or Leukotriene B4 for 20 min, stimulated EV production in activated neutrophils by a factor of 2-3 compared to non-simulated cells [164]. As another example, ethanol treatment significantly enhanced EV secretion by primary hepatocytes in a time and dose dependent manner [165]. It is important to note that these manipulations also have an impact on EV cargo, and consequently function and therapeutic potency, which needs to be thoroughly investigated.

Equally important is the selection of a suitable culture medium formulation, with the use of serum-/xeno(geneic)-free (S/XF) options being indispensable when moving towards GMP compliant conditions. However, most preclinical studies still employ FBS-containing media formulations [166]. Besides ethical concerns related to animal welfare, the ill-defined composition, wide batch-to-batch variability, risk of animal pathogen contamination, and xenogeneic-antigen transmission associated with FBS supplementation discourage its application in clinical settings [167]. Moreover, during conditioning periods for EV collection, it is essential to employ culture media depleted of EVs to avoid cross-contamination of the final preparation, while simultaneously not compromising cell health and EV productivity, in order to conserve process efficiency [166,168]. For example, MSC incubated in medium supplemented with EV-depleted human platelet lysate (hPL) maintained cell survival and cumulative EV production for three successive periods of 72h, which was not observed when standard starving conditions were used [169]. Furthermore, EV-depleted hPL supplement sustained the survival and EV production of other cell types, including human primary endothelial colony forming cells and two non-adherent human cell lines, Jurkat and THP-1 [169]. Alternatively, other chemically defined, serum-free media have

been explored for conditioning periods for EV production. Zhu and colleagues tested ten commercially available media for cell growth and EV production by human amniotic epithelial cells, as well as evaluating their impact on surface markers and composition of EVs [170].

Using a luciferase-engineered EVs to quantify EV secretion, Bost and colleagues demonstrated that the culture media used during the EV production stage impacts EV productivity in which non-supplemented Opti-MEM® led to an increase in the production of HEK293T-derived EVs, in comparison to Opti-MEM or DMEM (i.e. Dulbecco's Modified Eagle's Medium) supplemented with 10% FBS or EV-depleted FBS [171].

Typically, EV collection periods are focused on a single 24h to 72h CM batch at the end of culture [133,146–150]. Still, collection frequency also influences the final EV yield, and it should be further investigated. In fact, Patel and colleagues reported that mid-period collection of the CM led to an increase of approximately 2-fold in the total number of MSC-EVs produced when compared to a single collection at 6h, 12h and 24h [172]. In addition, macrophage-produced CM harvested at 24h, 48h or 72h presented a similar concentration of EVs, showing no particle accumulation [173]. These findings suggest that EV production may function as a balanced intercellular communication system and the removal of particles promotes additional secretion, and continuous collection of the CM might be a promising strategy to improve EV yields. Importantly, other factors such as cell passage or cell seeding during the conditioning period also have an impact of EV secretion productivity and should be optimized to potentiate the production output [172].

Other strategies applied to increase EV yields include the genetic modification of the parental cells and the generation of cell-derived nanovesicles (CDNs) that are EV mimics formed by the serial extrusion of cells through filters. For instance, human MSC(M) were engineered to overexpress metalloreductase STEAP3, syndecan-4 and L-aspartate oxidase proteins, which are involved in the biogenesis of Exo, significantly increasing EV production [174]. However, genetic engineering can be challenging in primary cells, while being time-consuming and costly. In contrast, CDNs generation strongly reduces production time and cost, while potentially increasing production yield by up to 250-fold [175]. Wang and collaborators demonstrated that the yield of extruded MSC-derived CDNs was 20-fold higher than secreted EVs, and the myocardial protective effects in a myocardial infarction (MI) mouse model were preserved [176].

I.3.2.2. Isolation of EVs

Generally, following upstream processing, the CM need to be clarified from remaining cells and larger debris, typically using centrifugation or filtration. Afterwards, EVs need to be concentrated and separated from the impurities present in the CM, which can be accomplished by different purification methods [177].

The most widely implemented method for EV isolation is differential ultracentrifugation (UC). In fact, a worldwide survey conducted by the International Society of Extracellular Vesicles (ISEV) in 2020 revealed that more than 75% of participants employed UC as primary method of EV isolation [178]. The method consists of a series of centrifugation steps with progressive speed

that separates the components in the liquid based on their sedimentation rates which differ in size and density. For EV preparations, the applied centrifugal forces typically vary between 100,000 to 120,000×*g,* depending on the rotor type [177]. Administration of EVs isolated by differential UC from cell derived CM have already been shown beneficial for several pathological diseases. For instances, UC yielded MSC-derived EVs capable of stimulated bone growth and regrowth of neurons in osteogenesis imperfecta and spinal cord injury (SCI) mouse models, respectively [179,180]. However, UC results in particle aggregation and can have negative impacts in the integrity and functionality of prepared EVs due to incomplete contaminant separation. Moreover, UC have long dead-end times and lack of scalability [130,177,181,182].

Another common approach is polymer-based precipitation that relies on the addition of water-excluding precipitants, like polyethylene glycol (PEG) and derivatives, which causes the originally solved components to become insoluble and precipitate and allows their subsequent sedimentation by low-speed centrifugation [177]. PEG precipitation has been able to concentrate EVs from cell culture supernatants in both small and large scales, providing higher particle yields and purity and being more reproducible than differential UC [183]. Although polymer-based precipitation is a simple, cost-effective method to isolate EVs [177], it yields low-purity samples due to co-precipitation of proteins and residual polymer matrix, possibly affecting their biological activity [181,184], thus not delivering the high quality required for clinical applications. Nevertheless, this approach has been widely used for EV enrichment, namely using easy-to-use commercially available kits (e.g., ExoQuick® or Total Exosome Isolation®), and the yielded EVs have demonstrated beneficial effect in numerous pre-clinical diseases models, namely graft-versus-host disease (GvHD) [185] and ischemic stroke [186].

Other methods for EV isolation have proved to be more scalable alternatives, including filtration and chromatography-based techniques [177,187].

Ultrafiltration (UF) has been widely used to isolate EVs from relatively dilute samples using membranes with a molecular weight cut-off (MWCO) typically ranging from 10-500 kDa. The method is often performed using centrifugal UF which offers simplicity; however, large sample volumes lead to long processing times and often filter plugging, which results in loss of sample, and sample contamination by proteins [187]. Alternatively, tangential flow filtration (TFF) is a size-base separation method in which the feed flows tangentially over the membrane surface at low pressure, thus preventing membrane fouling over time (e.g., filter cakes and clogging) and minimizing shear stress forces, contrary to dead-end filtration like UF. The feed recirculates through a closed system composed of a reservoir and filter modules, such as hollow fiber units or membrane-containing cassettes. Over time, the feed volume decreases, concentrating particles that are larger than the filter pores size and depleting the retentate of pore-passing molecules. TFF is also used for diafiltration, where the original feed solvent can be gradually replaced with a different buffer [177,187]. This can be applied to change buffers during multiple purification steps and it is widely applied in the formulation step. TFF is a suitable method for large-scale EV isolation, allowing the processing of larger volume samples in a time-efficient and reproducible manner, thus generating high EV yields. A comparative study showed that when processing large

volumes of CM, TFF concentrates EVs with improved yields, removal of single macromolecules and aggregates, batch-to-batch consistency in half the processing time, when compared to UC, while maintaining comparable physicochemical characteristics [188].

For increased purity levels, TFF can be combined with distinct chromatography techniques, relying on size, charge or affinity to separate EVs from residual proteins and other biomolecular contaminants [177,187]. Among these, size-exclusion chromatography (SEC) is the most frequently combined technique [187]. SEC consists of a porous stationary phase that, like TFF, separates EVs based on their molecular size or hydrodynamic volumes. Essentially, larger particles flow through the stationary phase being eluted first, whereas smaller particles enter the pores being retarded in their flow [177]. This separation technique renders EV preparations with high yields and improved purity without compromising their morphological integrity and functionality [189,190]. For example, when added to stimulated T cells, SEC-isolated EVs derived from MSC(WJ) CM inhibited their proliferation by 34%, contrarily to non-purified CM and EVs isolated by UC in which no effect was observed [191].

Alternatively, anion-exchange chromatography (AEC) exploits the interactions between negatively charged EVs and a porous stationary phase material modified with positively charged functional groups or cations (e.g., quaternary amines as strong anion exchanger or diethylaminomethyls as weak anion exchanger) [177,187]. Basically, negatively charged compounds in the mobile phase, like EVs in cleared CM, bind to cationic groups in the stationary phase, and are separated from non-binding molecules. Elution of the bound compounds is typically accomplished by increasing salt concentration or lowering the pH [177]. Different AEX chromatography columns have been used to isolate EVs from the CM of MSC [192–194] and other cell lines [195,196]. Interestingly, Seo and colleagues were able to isolate cytotoxic T-lymphocyte-derived EVs with high purity and separate two EV subpopulations, namely bioactive exosomes and microvesicle-like EVs, using an AEX chromatography method [196]. Heath and colleagues demonstrated the effectiveness of AEX chromatography as a single step approach for isolating of cell-derived EVs using a monolithic column with quaternary amine functionality, resulting in EVs with higher purity and integrity compared to TFF [197]. Of notice, the presence of nucleic acids in the feed, as in CM, might force their removal enzymatically (e.g., Benzonase treatment) as pre-chromatography step [177].

Lastly, affinity chromatography is based on specific ligands immobilized in the stationary phase that bind to target compounds leading to their selective retention through washing steps and subsequent elution by appropriate buffers. Concerning EV isolation, the ligands can be antibodies, peptides, and transmembrane proteins or other affinity agents such as heparin [177,187]. For example, Barnes and colleagues have demonstrated that heparin-based affinity chromatography can be used to efficiently purify EV derived from neural stem cell with higher particle recovery and similar purity when compared to SEC. Interestingly, it allowed the separation of EVs into three populations based on their affinity to the heparin column, revealing variations in TSG101 expression and tetraspanin immunophenotype [198]. Moreover, single domain antibodies-copolymer matrix was used as stationary phase of immunoaffinity chromatography for

the isolation of EVs from CM [199]. The single domain antibodies were selected by direct panning on vesicle-enriched fractions [200], allowing the developed affinity chromatography-based isolation method to successfully recover EVs from CM and human plasma [199]. In addition to being a highly selective purification method, affinity chromatography allows the isolation of EVs originating from particular cell types using specific ligands (e.g., anti-CD105 (endothelial cell-specific EVs) or anti-CD171 (neuron-derived EVs) [187]. For instances, immunoaffinity chromatography with monolithic columns immobilized with monoclonal antibodies against CD61, allowed the isolation of a highly specific population of platelet-derived EVs from blood plasma [201]. Some limitations include difficulties in eluting the bounded EVs and high cost of the specific ligands [187].

Although chromatography techniques can yield highly purified EVs, the samples are often too diluted or in inappropriate buffers and therefore an additional concentration/diafiltration step is required, thus affecting the overall EV yield [177]. Other emerging technologies to isolated EVs include asymmetric flow field-flow fractionation and diverse microfluidic platforms [187].

To date, there is no gold-standard technique for EV isolation. Generally, there is a relative relationship between EV yield and purity and the selection of the EV enrichment method depends on the desired application. Nonetheless, a scalable, reproducible and cost-effective isolation platform capable of isolating EVs with satisfactory quality and yield is crucial when envisioning the clinical use of EVs [177,187]. Each method present different levels of key parameters for EV manufacturing, as summarized by Pincela Lins and colleagues [130] (**Table I.3**).

Table I.3- Levels of key performance parameters in EV manufacturing for the current EV purification methods: Yield refers to the quantity of EVs recovered; Purity reflects the ratio of EV content with contaminants; Scalability includes the feasibility to scale-up without increasing time and costs; Costs include consumables and personnel spent for processing sample; Time consists of the overall processing time of samples. The arbitrary units are listed as + (low), ++ (intermediate), +++ (high). Adapted with permission from [130].

Method	Yield	Purity	Scalability	Cost	Time
Ultracentrifugation	+++	++	+	++	+++
Polymer precipitation	+++	+	++	+	+
Tangential flow filtration	+++	++	+++	+++	++
Size-exclusion chromatography	+	+++	++	++	++
Anion-exchange chromatography	++	++	++	++	++
Affinity chromatography	+	+++	+	+++	+++

I.3.3. Strategies to bioengineer EVs

Despite the potential of EVs to be used as natural delivery vehicles, several bioengineering strategies have been applied to maximize their therapeutic efficacy. This can be achieved using two major strategies: cargo engineering and surface engineering. Essentially, by customizing the therapeutic payload of EVs or enhancing their selectivity to target cells, bioengineered EVs have the potential to become more personalized and targeted DDS (**Figure I.7**) [109].

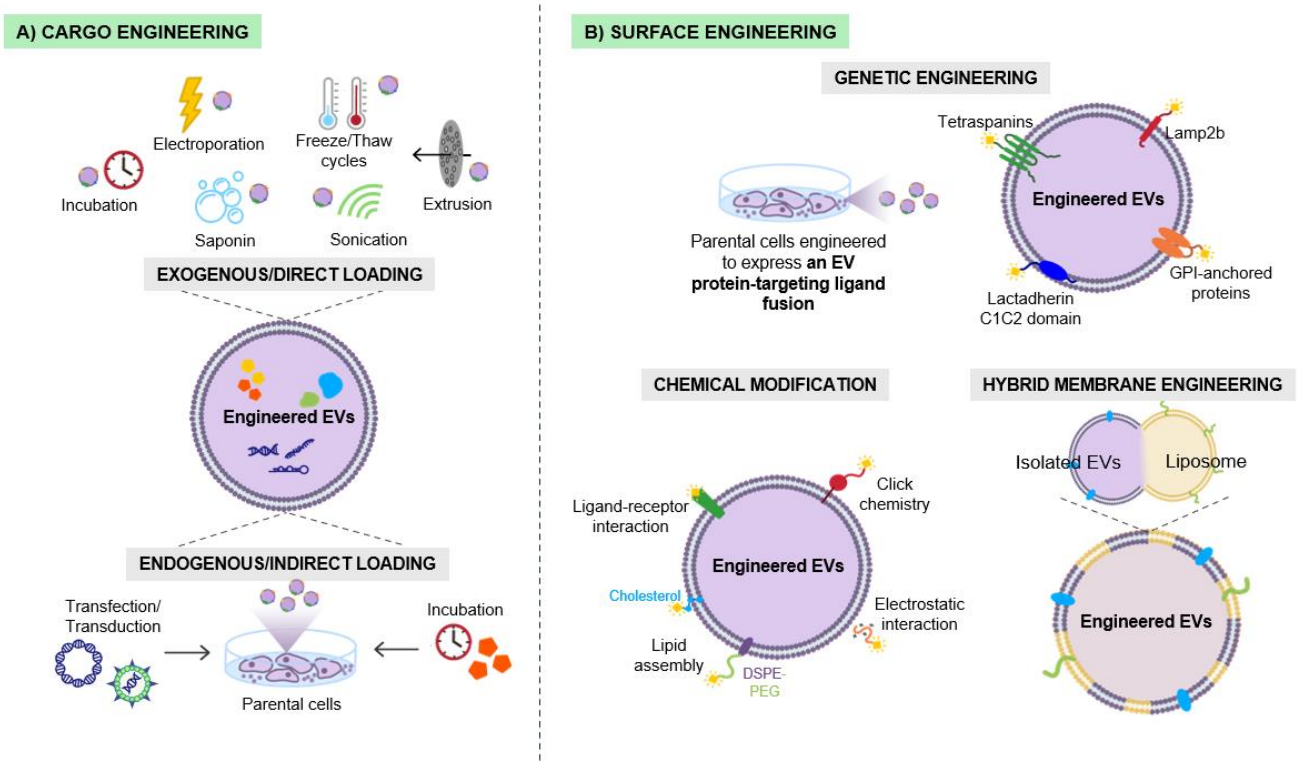

Figure I.7 - Strategies to maximize the therapeutic efficacy of extracellular vesicles (EVs). **(a)** Cargo engineering of EVs by exogenous/direct loading, through external incorporation of cargo into isolated EVs, or endogenous/indirect loading, by providing the parental cells with the means to naturally incorporate the desired cargo during EV biogenesis. **(b)** Surface engineering of EVs: The parental cells can be genetically engineered to produce EVs displaying transmembrane protein-targeting ligand fusions. The isolated EVs can be chemically modified, by anchoring targeting moieties to the surface of isolated EVs through covalent bonds, lipid self-assembly or other non-covalent reactions. Hybrid membrane engineering allows the fusion of isolated natural EVs and synthetic liposome nanoparticles. DSPE—1,2-distearoyl-sn-glycero-3-phosphoethanolamine; GPI—glycosyl-phosphatidylinositol; Lamp—lysosomal-associated membrane proteins; PEG—polyethylene glycol. Adapted from [109].

I.3.3.1. Cargo customization

EVs can be artificially loaded with different therapeutic agents, including small molecules, drugs, proteins, and different RNA species, such as siRNA and miRNA. The incorporation of extrinsic cargo into EVs requires the manipulation of the EVs or the parental cells. This can be accomplished by two methods: exogenous/direct loading, with the external incorporation of cargo

into isolated EVs; and endogenous/ indirect loading, by providing the parental cells with the means to naturally incorporate the desired cargo during EV biogenesis (**Figure I.7-A**)

I.3.3.1.1. Exogenous cargo loading

Exogenous loading occurs after EV isolation by direct encapsulation of the desired therapeutic cargo through various processes, including co-incubation [202–205], electroporation [205–209], sonication [204,205,210,211], freeze-thawing [204], extrusion [211,212] and permeation by a detergent-based compound [204,211] (**Figure I.7-A**).

Incubation is a passive loading method that has been used to encapsulate hydrophobic drugs into EVs. For example, EVs co-incubation with Curcumin (Cur) improved its bioavailability and anti-inflammatory effect in a mouse model of inflammation [202]. Similarly, hydrophobically modified siRNA were successfully encapsulated in EVs derived from glioblastoma cells through co-incubation [203].

Alternatively, different active loading strategies have been employed to physically or chemically permeabilize the hydrophobic membrane of EVs, allowing the transient diffusion of hydrophilic molecules into their intraluminal space.

For instance, electroporation relies on the exposure of the EV-membrane to high-intensity electrical pulses and has been widely used to facilitate the loading of different cargos, including siRNA [111,206], miRNA [207,213,214], DNA [215,216] and other small molecules [208]. Moreover, Usman and collaborators explored electroporation to engineer EVs derived from human red blood cells (RBC) for the delivery of antisense oligonucleotides, Cas9 mRNA, and guide RNAs, to CRISPR–Cas9 edit the recipient cells [209].

The sonication method has also been described to promote the active loading of a variety of small nucleic acids into EVs, using a low-intensity ultrasound frequency [210]. Interestingly, Kim and colleagues reported that sonication provided the greatest loading capacity of paclitaxel (PTX) into macrophage-derived EVs, when compared to incubation and electroporation [205].

Freeze-thawing involves the combination of EVs with the cargo at room temperature, followed by repeated cycles of freezing (at −80^{o}C or in liquid nitrogen) and thawing, allowing for cargo incorporation through membrane deformation. Although some studies reported that freeze-thawing led to EV aggregation [204,217], Hettich and co-workers showed that this method demonstrated a great loading efficiency of hydrophilic compounds while maintaining the structural and biological characteristics of the EVs [218]. This method also has been applied to produce hybrid vesicles by actively fusing the membrane of EVs and liposomes (further reviewed below) [217].

Alternatively, permeation by the detergent-based compound saponin is a method used to chemically load EVs, which induces the formation of membrane pores without its destruction by removing cholesterol. For instance, this technique was applied to load the large protein catalase into EVs derived from macrophages, which resulted in a loading efficiency comparable to sonication and extrusion methods [211]. This method showed the most efficient loading (~50%)

when encapsulating doxorubicin (DOX), compared to 37ºC and room temperature co-incubations and freeze-thaw cycles [204].

Finally, extrusion is a technique used to artificially produce vesicles by breaking up the cells and then reforming the contents into EVs mimetics while retaining some of the physical and biological characteristics of secreted EVs. For example, Jang and colleagues produced EV mimetics from monocytes or macrophages harbouring different chemotherapeutics drugs using serial extrusion through filters with diminishing pore sizes (10-, 5-, and 1 μm). Remarkably, EVs mimetics presented a similar in vivo anti-tumour activity, compared to naturally secreted EVs [212].

Overall, the incubation method is a straightforward strategy that preserves the integrity of the EV membrane, but it has low loading efficiency and is only compatible with hydrophobic cargos. In opposition, active loading methods present higher loading efficiencies. However, these are still limited in their technical complexity and often disrupt membrane/cargo integrity and stability and promote aggregation [204,205,211,219–221].

I.3.3.1.2. Endogenous cargo loading

Endogenous loading depends on the availability of desired cargo in the producer cell and the subsequent use of the cellular machinery for its incorporation into EVs. The introduction of the exogenous cargo into the producer cell can be achieved by passive loading through simple incubation or active loading through the genetic manipulation of the parental cells (**Figure I.7-A**). Simple incubation has been mostly used to endogenous incorporate small drugs into EVs [222,223].

In contrast, genetic manipulation has been used to bioengineer EVs to harbour small non-coding RNAs and mRNA/proteins of interest. For instance, THP-1 monocytes genetically engineered to transiently overexpress miRNA-939 secreted EVs loaded with the produced miRNA. One possible cellular mechanism for its incorporation into the EVs was the recognition of its RBP binding motif GGAG [213]. Endogenous miRNA-loading was also studied by Lee and colleagues through the engineering of a stable producer cell line. Human embryonic kidney (HEK) 293T cells, were engineered to express the miRNA-124, typically repressed in Huntington's disease (HD) using a retroviral expression system. The produced EVs were enriched in miRNA-124 and induced the silencing of the target gene REST after injections into a mouse HD model [224].

Active and specific RNA loading into EVs can be improved using the Targeted and Modular EV Loading (TAMEL) technology that resorts to an EV-enriched protein to anchor an RNA-binding domain (RBD) on the intraluminal side of EVs. Essentially, the RBD binds to RNA presenting the specific sequence motifs and actively incorporates them into EVs. Hung and colleagues constructed a plasmid encoding for EV-enriched protein Lamp2b fused with the RBD MS2. This approach substantially enhanced the loading of RNA-cargo with the sequence recognized by the MS2-RBD (up to 6-fold) [225]. Similarly, EVs were engineered to load a specific

RNA by fusing the tetraspanin CD9 with human antigen R (HuR), an RBP that interacts with miRNA-155 with high affinity [226].

Apart from small RNAs, proteins and mRNAs can also be endogenously loaded into EVs by transfection/transduction of the parental cells with the gene encoding the desired cargo. Mizrak and co-workers first reported that overexpression of the desired gene prompts the loading of the corresponding mRNA and protein into EVs. The authors transfected HEK 293T cells to express high levels of the enzyme cytosine deaminase fused to uracil phosphoribosyltransferase (CD-UPRT) that converts the prodrug 5-fluorocytosine (5-FC) into a cytotoxic cancer agent 5-fluorouracil. The isolated EVs were loaded with CD-UPRT mRNA/protein inducing *in vivo* tumour regression in a mouse model, upon injection and systemic treatment with 5-FC [227]. Similarly, in another study, A549 lung cancer cells were transduced with an adenoviral vector encoding the cystic fibrosis transmembrane conductance regulator gene, which is mutated in patients with cystic fibrosis (CF). EV-mediated delivery of produced mRNA/protein to CF cells corrected the deficiency in chloride channel activity [228].

Synthetic therapeutics can also be encapsulated into EVs by transfection of the parental cells. For example, after transfection of HEK 293T cells with synthetic siRNA that targets the expression of hepatocyte growth factor (HGF), there was an increased secretion of HGF-harbouring EVs with an inhibitory effect on tumour growth and angiogenesis *in vitro* and *in vivo* [229].

Generally, endogenous loading strategies allow relatively simple and stable production of EVs with engineered cargo, while preserving EV-membrane integrity and the function of the loaded cargo. However, these approaches are often time-consuming and expensive compared to exogenous methods, have limited loading efficiency and can cause a negative impact on parental cells [220,221].

I.3.3.2. Surface functionalization

In vivo administered EVs suffer from rapid clearance mostly by uptake into cells in the liver, spleen, gastrointestinal tract and lungs [230]. The surface of EVs is critical for their biodistribution, tropism and therapeutic effect and its modification can endow EVs with additional targeting to specific cell types, abilities to cross different biological barriers and extended lifespan *in vivo* until reaching the target location [231–233]. Numerous strategies have been investigated to functionalize the surface of EVs: genetic manipulation, by engineering the parental cells to produce EVs displaying transmembrane targeting moieties; chemical modification, by anchoring targeting moieties to the surface of isolated EVs; and hybrid membrane engineering, by conjugating isolated natural EVs and synthetic liposome nanoparticles (**Figure I.7-B**).

I.3.3.2.1. Genetic manipulation of parental cells

Typically, the parental cells can be genetically engineered to produce EVs with the desired surface features by modifying native EV-transmembrane proteins with exogenous ligands

that are recognized by the recipient target cells, including proteins/peptides, antibodies and lipid-raft associated components (**Figure I.7-B**).

In a pioneer study by Alvarez-Erviti and colleagues, the surface of dendritic cells-derived EVs was engineered to improve their brain targeting after systemic administration. Targeting was achieved by transfection with a plasmid encoding Lamp2b fused to the central nervous system (CNS)-specific rabies viral glycoprotein (RVG), resulting in increased brain accumulation after intravenous injections in a mouse model [111]. Since then, Lamp2b has been the most widely used protein anchor in surface engineering approaches. For instance, Lamp2b fused to αγ integrin-specific peptide iRGD and human epidermal growth factor receptor 2 (HER2)-binding affibody, showed improved EV-tropism towards integrin-positive breast cancer cells and HER2-expressing tumour cells, respectively [208,234].

Other transmembrane proteins are used to anchor specific ligands. Liang and collaborators engineered HEK 293T cells to express a fusion between tetraspanin CD63 and Apo-A, a known target of the scavenger receptor class B type 1 receptor that is highly expressed by liver cancer cells. The produced EVs were effectively internalized by human liver cancer HepG2 cells via receptor-mediated endocytosis [214]. Similarly, due to its localization on the membrane of EVs, the C1C2 domain of lactadherin has been explored as an anchor for different recombinant proteins, such as carcinoembryonic antigen and HER2 [235]. Moreover, GPI-anchored proteins (associated with lipid rafts) were used to display a nanobody that targets epidermal growth factor receptor (EGFR), a well-studied oncogene, on the surface of EVs to target tumour cells expressing this receptor [236].

Apart from improving the affinity and selectivity of EVs to target cells/tissues, genetic modification can be used to produce EVs displaying tags that increase their lifespan. Kamerkar and colleagues engineered fibroblasts to overexpress CD14, which is an integrin-associated transmembrane protein described to protect cells from phagocytosis. CD47-enrich EVs showed higher circulation retention times by evading phagocytosis by monocytes and macrophages, in a mouse model [233].

I.3.3.2.2. Chemical modification

Alternatively, the targeting ligands can be incorporated into the surface of EVs by chemical modification after their isolation, relying on covalent bonds, hydrophobic insertions, lipid self-assembly or other non-covalent reactions (**Figure I.7-B**).

The simplest method is by the direct incorporation of hydrophobic/amphiphilic molecules into the naturally hydrophobic membrane of EVs. Phospholipid 1,2-dimyristoyl-sn-glycero-3-phosphoethanolamine (DMPE)- and 1,2-distearoyl-sn-glycero-3-phosphoethanolamine (DSPE)-polyethylene glycol (PEG) derivatives can accumulate in the membrane of EVs and have been successfully used to immobilize targeting ligands. For instance, macrophage-derived EVs containing PTX were modified with anisamide-DSPE-PEG moiety to target the sigma receptor, which is overexpressed by lung cancer cells [237]. Additionally, phospholipid-PEG derivatives increase EV stability *in vivo,* prolonging circulation times that potentially increases the

accumulation of EVs in target tissues and specific cargo delivery [238]. Similarly to phospholipid derivatives, cholesterol can self-assemble into EVs due to its hydrophobicity. In this context, Huang and colleagues explored the potential of cholesterol-conjugated AS1411 DNA aptamer to mediate the targeted delivery of EVs to nucleolin which is overexpressed on the surface of leukemia cells [239]. Likewise, a bacteriophage Φ29 RNA has been engineered to incorporate cholesterol-conjugated EGFR RNA aptamer and used to decorate EVs carrying siRNA as a targeted anti-tumour treatment [240].

Click-chemistry (copper-catalyzed azide-alkyne cycloaddition) is a highly efficient covalent reaction between an alkyne and azide that forms a triazole linkage, which has been successfully applied to functionalize the surface of EVs [241]. In a study by Lee and collaborators, alkyne-functionalised EVs were decorated with various functional agents using copper-free click chemistry, to allow their specific delivery to cancer cells [242]. Moreover, Jia and colleagues conjugated the membrane of macrophages-derived EVs with RGERPPR peptide, a specific ligand of neuropilin-1 (NPR-1) which is overexpressed in glioma cells, using a cycloaddition reaction with sulfonyl azide. The peptide-displaying EVs were able to cross the BBB and facilitate glioma recognition [232].

Non-covalent approaches include receptor-ligand binding and electrostatic interactions and have also been implemented to functionalize the surface of EVs. For instances, superparamagnetic nanoparticles (NPs) were conjugated to the transferrin receptors of blood-derived EVs. This strategy allowed an efficient separation of EVs from the blood and endowed EVs with a robust targeting ability under an external magnetic field [243]. By relying on electrostatic interactions, Nakase and Futaki engineered HeLa-derived EVs with a combination of cationic lipids and a pH-sensitive fusogenic peptide GALA, enhancing cell membrane binding and EV uptake, and subsequent cytosolic release of their cargo [244].

I.3.3.2.3. Hybrid membrane engineering

The surface of EVs can also be functionalized using hybrid membrane engineering that result from the capacity of the lipid bilayer of EVs to spontaneously fuse with other membrane structures. Isolated natural EVs and decorated synthetic liposomes can be fused into hybrid nanoparticles without affecting their intrinsic properties (**Figure I.7-B**).

The surface properties of EVs can be easily modified using liposomes embedded with peptides/antibodies as targeting moieties. In this context, Li and colleagues fused tumour cell-derived EVs with liposomes modified with tumour-targeting peptides. The hybrid EVs allowed highly efficient drug loading and were strongly enriched in the tumour areas [245]. Sato and collaborators formulated engineered hybrid EVs by fusing their membrane to different synthetic phospholipid liposomes using the freeze-thaw method and confirmed that the delivery function of the EVs can be modified by changing their properties and lipid composition [231]. Moreover, EVs fusion with functionalized liposomes via PEG-mediated reaction has shown to facilitate the enrichment of EVs with exogenous lipophilic or hydrophilic compounds, while preserving their intrinsic content and biological properties [246]. Also, through simple incubation, EV–liposome

nanovesicles were generated and demonstrated to be able to efficiently encapsulate large plasmids, including the CRISPR-Cas9 expression vectors, similar to the liposomes. However, these could be endocytosed by MSC and express the encapsulated genes, unlike liposomes [247]. Using the co-extruding method, Jhan and co-workers fused EVs with a suspension of different synthetic lipids by serial extrusion through membranes (400, 200 and 100 nm). This method allowed the formation of vesicles with controlled size and a 43-fold increase in production compared to native EV secretion [248]. In an alternative approach by Zhang and colleagues, hybrid membrane engineering was used to develop multifunctional artificial EVs. Essentially, membrane proteins from RBC and breast cancer cells were incorporated into synthetic liposomes. The engineered hybrid EVs exhibited anti-phagocytosis capacity during circulation (high level of CD47 from RBC) and the tumour-homing ability (EpCAM, galectin 3 and N-cadherin from cancer cells) for targeted drug delivery [249].

The formation of EV-liposome hybrids has also been reported as a method to functionally deliver nucleic acids (e.g., siRNA and pDNA) to target cells [247,250].

I.4. Mesenchymal stromal cells and derived extracellular vesicles

Mesenchymal stromal cells (MSC) are a diverse subset of adult, fibroblast-like, multipotent precursors capable of differentiate into multiple cell lineages, such as osteoblasts, chondrocytes and adipocytes [251]. MSC are present in perivascular locations, on both arterial and venous vessels, from nearly all tissues in the adult body, providing stromal support to the maintenance of a dynamic and homeostatic tissue microenvironment [252,253].

MSC were described for the first time in 1970 by Friedenstein and co-workers, as a rare population of colony forming unit - fibroblasts (CFU-F), residing in the bone marrow (BM) of guinea-pigs and mice [254,255]. Since then, cells with similar characteristics have been found from cultures of virtually all adult and foetal organs tested [256]. Some of the reported tissue sources include adipose tissue (AT), Wharton's jelly (WJ), and dental pulp (DP) [257,258].

With the increased interest in the therapeutic potential of MSC, the differences in their isolation, expansion and characterization, along with difficulties in their identification in mixed populations of cells, challenged the comparison of the outcomes of different studies. To address these issues, the International Society for Cellular Therapy (ISCT) proposed a minimum criteria to define MSC: adherence to plastic when maintained under standard culture conditions; expression of the cell surface molecules CD105, CD73 and CD90, and lack of expression of the hematopoietic markers CD34, CD45, CD14 (or CD11b), CD79α (or CD19) and major histocompatibility complex (MHC) II class cellular receptor HLA-DR; and *in vitro* differentiation into osteoblasts, adipocytes and chondrocytes [259]. In 2019, ISCT updated their criteria for defining MSC to include their tissue-source origin and functional assays to demonstrate their therapeutic mode of action [260].

MSC are one of the most extensively explored cell types for cell-based therapeutics to treat a wide range of diseases. The main therapeutic attribute of MSC is their ability to locally modulate the tissue microenvironment by secretion of a wide spectrum of trophic factors including growth factors, cytokines and adhesion molecules [261,262]. These biologically active molecules can have a positive paracrine effect on tissue repair and regeneration namely immunomodulation [263], inhibition of inflammation and anti-fibrosis [262], [264], angiogenesis [265], support of proliferation and differentiation of progenitor cells and recruitment of endogenous cells [266,267]. For instance, MSC significantly support wound healing by polarizing macrophages anti-inflammatory M2 activation, promoting angiogenesis and enhancing the survival and migration of fibroblasts [268]. In the context of central nervous system (CNS) regeneration, MSC can facilitate neurogenesis by preventing apoptosis of endogenous neural cells and promoting axon re-extension by inhibiting the effect of extrinsic factors derived from the external environment of damaged areas [269].

Since the first clinical trial of an MSC-based therapy in 1995 [270], MSC continue to spark the interest of the scientific community namely in clinical settings, achieving a total of 1476 clinical studies in March 2023, which are focused primarily on the treatment of the musculoskeletal, nervous, cardiovascular, and immune-related disorders [271]. MSC have proven to be exceptionally safe being presently approved for clinical use. For instance, in 2018, an allogeneic AT-derived MSC (MSC(AT)) product – Alofisel – was approved by the European Medicines Agency (EMA) for the treatment of complex refractory perianal fistulas in the context of Crohn's disease (CD) [272,273].

One of the major signalling effectors of the secretome of MSC are EVs [274,275]. Since EVs are anticipated to preserve significant features of parental cells, MSC have been extensively investigated as EV producers. Mesenchymal stromal cells derived-extracellular vesicles (MSC-EVs) share therapeutic properties with MSC [276] and can influence recipient cells, both at genetic and biochemical levels, modulating several physiological processes [274,275]. Compared to MSC, EVs can be even safer since these do not self-replicate and do not cause microvasculature entrapment [277,278]. Also, EVs present good stability during storage, making them promising candidates for off-the-shelf therapeutics [279]. Extensive research has shown that MSC-EVs hold various therapeutic roles including immune regulation, anti-inflammatory effects, and tissue regeneration [280]. For example, MSC(M)-derived EVs, induced the expression of chondrocyte markers while inhibiting catabolic and inflammatory markers in osteoarthritis (OA)-like chondrocytes *in vitro*, and reduced cartilage and bone degeneration *in vivo* in the collagenase-induced OA murine model [281]. Moreover, EVs derived from MSC(WJ) enhanced the proliferation and migration of human immortal keratinocyte line HaCaT and human skin fibroblasts *in vitro* and accelerated cutaneous wound healing in mice *in vivo*, by transferring miRNA-27b and repressing Itchy E3 ubiquitin protein ligase [282]. In addition, Han and colleagues demonstrated that MSC(M)-derived EVs carrying TGF-β upregulated the expression of Smad6, inhibited the excessive differentiation of neural stem cells into astrocytes, and promoted

regeneration of neurons in spinal cord injured rats, resulting in a better neurological outcome [283].

MSC can efficiently mass-produce EVs by withstanding large-scale expansion and immortalization, enabling a sustainable and reproducible EV production process [284], which together with the above-described features suggests MSC as a suitable candidate to produce EV-based therapeutics. Despite the undoubted therapeutic potential of unmodified MSC-EVs, improvements are still needed in what concerns target selectivity and payload potency, and bioengineering strategies have been widely employed to potentiate the benefits of MSC-EVs as DDS.

I.4.1. Bioengineered MSC-EVs as Improved Drug Delivery Systems

I.4.1.1. Loading MSC-EVs with therapeutic cargo

Different types of therapeutic cargo have been loaded into MSC-EVs, including nucleic acids, proteins and small molecules. Either endogenously, by manipulation of parental MSC, or exogenously, through manipulation of isolated EVs, cargo engineering of MSC-EVs has been shown to improve their therapeutic efficacy towards a particular clinical application (**Table I.4**).

miRNAs are promising new therapeutics for treating many diseases. MSC-EVs have emerged as a promising vehicle for delivering miRNA, thus many researchers have been engineering MSC to express or harbour these molecules.

For instance, human BM-derived MSC (MSC(M)) were transduced with lentivirus vectors containing miRNA-124a which silences Forkhead box A2 expression, inducing aberrant intracellular lipid accumulation. Quantitative PCR demonstrated that the produced EVs contained approximately 60-fold higher levels of miRNA-124a, compared to non-modified MSC-derived EVs. miRNA-124a-carrying EVs resulted in a significant *in vitro* reduction in viability and clonogenicity of glioma stem cells (GSC), and treated mice harbouring intracranial GSC xenografts after systemic administration [285]. In addition, other miRNAs have been endogenously loaded into MSC-EVs and demonstrated anti-cancer potential, including miRNA-379 [286] and miR-16-5p [287] and miRNA-424 [288] through post-transcriptional regulation of tumour-related genes expression of ciclo-oxigenase-2, integrin α2 and transcriptional factors MYB, respectively.

Table I.4- Overview of the potential strategies and applications of cargo-engineered mesenchymal stromal cells derived-extracellular vesicles (MSC-EVs). Reproduced from [109].

Type of strategy	Cargo	Application	Therapeutic Effect	MSC source	Ref.
Nucleic Acids					
Endogenous loading (transduction)	miRNA-122	Liver fibrosis	Inhibited fibrosis	Human/mouse AT	[289]
	miRNA-124a	Glioblastoma	Increased survival of GSC-injected mice	Human BM	[285]

	miRNA-126	Skin wounds	Increased re-epithelialization, angiogenesis, and collagen maturity	Human SM	[290]
	miRNA-17-92	Ischemic stroke	Enhanced axon-myelin remodelling and functional recovery after stroke	Rat BM	[291]
	miRNA-379	Breast cancer	Inhibited tumour growth	Human BM	[286]
	miRNA-let7c	Renal fibrosis	Decreased fibrosis	Human BM	[292]
	mRNA-CD-UPRT	Cancer	Inhibited tumour growth	Human AT, BM, DP and WJ	[293]
Endogenous loading (transfection)	miRNA-126	Ischemic stroke	Increased neurogenesis and improved functional recovery after stroke	Rat AT	[294]
	miR-133b	Spinal cord injury	Inhibited inflammatory response and induced nerve function repair	Rat BM	[295]
	miRNA-150-5p	Rheumatoid arthritis	Inhibited synoviocyte hyperplasia and angiogenesis	Mouse BM	[296]
	miRNA-155-5p	Osteoarthritis	Increased proliferation and migration, suppressed apoptosis and enhanced ECM secretion of osteoarthritic chondrocytes	Human SM	[297]
	miR-16-5p	Colorectal cancer	Inhibited tumour growth	Human BM	[287]
	miRNA-181c	Burn-induced inflammation	Decreased inflammation	Human WJ	[298]
	miRNA-22	Spinal cord injury	Inhibited inflammatory response and induced nerve function repair	Rat BM	[299]
	miRNA-26a	Spinal cord injury	Promoted axonal regeneration and neurogenesis	Rat BM	[300]
	miRNA-29b	Alzheimer's Disease	Reduced the pathological effects of amyloid-β peptides	Rat BM	[301]
	miRNA-424	Ovarian cancer	Inhibited tumorigenesis and angiogenesis	Human BM	[288]
	miRNA-92a-3p	Osteoarthritis	Enhanced cartilage development and homeostasis	Human BM	[302]
Exogenous loading (electroporation)	miRNA-124	Ischemic stroke	Increased neurogenesis	Mouse BM	[303]
	miRNA-132	Myocardial infarction	Enhanced neovascularization and preserved heart functions	Mouse BM	[304]
	miRNA-499a-5p	Endometrial cancer	Inhibited tumour growth and metastasis	Mouse BM	[305]
	miRNA-590-3p	Myocardial infarction	Promoted cardiomyocyte proliferation and cardiac regeneration	Rat BM	[306]
	siRNA-CTGF	Spinal cord injury	Increased axon regeneration and motor function after SCI	Rat BM	[307]

	siRNA-galectin-9	Pancreatic ductal adenocarcinoma	Inhibited tumour growth	Human BM	[308]
	siRNA-Kras	Pancreatic ductal adenocarcinoma	Inhibited tumour growth	Human BM	[309]
	siRNA-PLK-1	Bladder cancer	Increased cytotoxicity and apoptosis	Human BM	[310]
	si-SHN3	Osteoporosis	Enhanced osteogenic differentiation and vessel formation and inhibited osteoclast formation	iPSC	[311]
Exogenous loading (incubation)	cholesterol-modified miRNA-210	Ischemic stroke	Increased angiogenesis and survival of ischemic brain mice	Mouse BM	[312]
	siRNA-PTEN	Spinal cord injury	Increased functional recovery of spinal cord lesion in rats	Human BM	[313]
Exogenous loading (transfection reagent)	miR-326	Inflammatory bowel disease	Inhibited the synthesis and production of inflammatory factors	Human WJ	[314]
Proteins					
Endogenous loading (protein transduction)	Akt	Myocardial infarction	Increased angiogenesis and cardiac regeneration	Human WJ	[315]
	Ang-2	Skin wounds	Increased angiogenesis and accelerated wound healing	Human WJ	[316]
	Osteoactivin	Osteoporosis	Increased proliferation and osteogenesis of MSC and attenuated bone loss in ovariectomized rat	Rat BM	[317]
	PEDF	Ischemic stroke	Ameliorated cerebral ischemia-reperfusion injury in rats	Rat AT	[318]
Small molecules					
Endogenous loading (incubation)	Iron oxide NPs	Skin wounds	Improved targeting under an external magnetic field and enhanced wound healing	Human WJ	[319]
	PTX	Pancreatic adenocarcinoma	Decreased tumour growth	Mouse BM	[223]
	TXL	Metastatic breast cancer; Ovarian cancer; Lung carcinoma	Inhibited tumour growth	Human WJ	[320]
	Venofer	Cancer	Increased tumour cell death under an external magnetic field	Human AT, BM, DP and WJ	[321]
Exogenous loading (dialysis)	DOX	Osteosarcoma	Inhibited tumour growth	Mouse BM	[322]
Exogenous loading (electroporation)	DOX	Colon adenocarcinoma	Inhibited tumour growth	Mouse BM	[323]
	NCTD	Hepatocellular Carcinoma	Inhibited tumour growth	Human BM	[324]

Exogenous loading (electroporation/sonication)	GEMP/PTX	Pancreatic ductal adenocarcinoma	Increased homing and penetration and anti-tumour potency	Human BM	[325]
Exogenous loading (extrusion)	PTX	Breast cancer	Decreased tumour growth	Human BM	[326]
Exogenous loading (freeze-thaw)	polypyrrole NPs	Diabetic peripheral neuropathy	Reduced the neural and muscular damage under electric stimulation	Rat BM	[327]
Exogenous loading (incubation)	Cur	Ischemic stroke	Decreased inflammation	Mouse BM	[328]
Exogenous loading (incubation; sonication)	TKI	Anaplastic thyroid cancer	Increased radioiodine-sensitivity	Human AT	[329]

AT- adipose tissue; BM- bone marrow; CD-UPRT- cytosine deaminase fused to uracil phosphoribosyltransferase; CTGF- connective tissue growth factor; Cur- Curcumin; DOX- doxorubicin; DP- dental pulp; ECM- extracellular matrix; GEMP- gemcitabine monophosphate; GSC- glioma stem cells; iPSC- induced pluripotent stem cells; NCTD- norcantharidin; NPs- nanoparticles; PEDF- pigment epithelium-derived factor; PLK-1- serine/threonine-protein kinase; PTX- paclitaxel; SCI- spinal cord injury; SHN3- schnurri-3 protein; SM- synovial membrane; TKI- tyrosine kinase inhibitor; TXL- taxol; WJ- Wharton's jelly.

In the context of skin regeneration, Li and colleagues explored the potential of EVs derived from MSC transfected with miRNA-181c mimics, which has a critical role in regulating inflammation, specifically in attenuating skin burn-induced inflammation. The results demonstrated that the engineered EVs suppressed the TLR4 signalling pathway, reducing NF-κB/p65 activation, and alleviated inflammation in burned rats more effectively than EVs produced by non-transfected MSC [298]. In another study, EVs secreted by MSC derived from the synovial membrane (SM) engineered to overexpress miRNA-126 demonstrated to be able to heal full-thickness skin defects in a diabetic rat model [290]. On the other hand, MSC(AT)-derived EVs endogenously loaded with miRNA-126 also showed prospective effects in the treatment of ischemic stroke [294].

MSC have also been engineered to produce miRNA-containing EVs that attenuate fibrosis. For instance, miRNA-122-engineered EVs inhibited fibrosis by reducing proliferation and collagen maturation of hepatic stellate cells through miRNA-122-induced downregulation of target genes such as insulin-like growth factor receptor-1, cyclin G-1, and prolyl-4-hydroxylase α-1 [289]. Moreover, MSC(M) engineered to overexpress miRNA-let7c generated EVs that inhibited the upregulated expression of fibrotic genes in neighbouring rat kidney tubular epithelial cells and attenuated renal fibrosis *in vivo* in a mouse model of unilateral ureteral obstruction [292].

Envisioning a therapeutic strategy for rheumatoid arthritis (RA), MSC-EVs were engineered to harbour the miRNA-150-5p, by transfection of the parental cells. miRNA-150-5p-loaded EVs decreased migration and invasion of RA synoviocytes and downregulated tube formation *in vitro,* by targeting matrix metalloproteinase 14 and vascular endothelial growth factor. These MSC-EVs also reduced clinical arthritic scores and joint destruction in an *in vivo* RA mouse model [296]. In addition, a study on EVs derived from miRNA-92a-3p-expressing MSC showed enhanced cartilage development and prevented its degradation by targeting *wnt5a* in a collagenase-induced OA mouse model [302]. Furthermore, EVs secreted by miRNA-155-5p-

overexpressing SM-derived MSC promoted ECM secretion *in vitro* by targeting Runx2, and effectively prevented OA in a mouse model [297].

Studies have found that MSC-EVs mediated delivery of miRNA showed a positive effect in neurodegenerative diseases and mitigate the damage caused by CNS injuries. Jahangard and colleagues engineered MSC to produce EVs encapsulating miRNA-29, which is downregulated in Alzheimer's Disease (AD) and silences the expression β-site amyloid precursor protein cleaving enzyme 1 and Bcl-2 interacting mediator of cell death. miRNA-29-EVs caused a reduction of the pathological effects of amyloid-β peptides after injection into the hippocampus of a rat model of AD, namely by improving spatial learning and memory deficits [301]. Furthermore, the lentivirus-based modification of MSC to overexpress the miRNA-17-92 allowed the production of EVs that enhanced axon-myelin remodelling and motor electrophysiological recovery after stroke in an *in vivo* mouse model [291]. Spinal cord injury (SCI) recovery has been investigated using MSC-EVs endogenously loaded with miRNA-133b which is a key player in the differentiation of neurons and the outgrowth of neurites. miRNA-133b-EVs showed to activate signalling pathway proteins involved in the survival of neurons and the regeneration of axons, reduce the volume of the lesion and promote the regeneration of axons after systemic injection into a rat model of SCI [295]. In addition, recent studies reported that MSC-EV-mediated delivery of miRNA-22 and miRNA-26a could represent novel therapeutic approaches for the treatment of SCI [299,300].

To date, only a few studies have been reported to develop mRNA-loaded EVs. Among these, a study by Altanerova and colleagues describes a strategy where MSC from different tissue sources were modified by retrovirus transduction to overexpress the suicide gene CD-UPRT. The mRNA-CD-UPRT was incorporated into the secreted EVs and induced cell death in the presence of prodrug 5-FC upon internalization by tumour cells [293].

Therapeutic siRNAs have also been delivered using MSC-EVs. For example, MSC(M)-derived EVs were electroporated with siRNA targeting oncogenic Kras. The modified MSC-EVs induced the suppression of oncogenic Kras and increased the survival of several mouse models with pancreatic cancer [309]. Similarly, serine/threonine-protein kinase (PLK-1)-targeting siRNA were electroporated into MSC(M)-derived EVs. siRNA-PLK-1-carrying EVs delivery to bladder cancer cells resulted in the suppression of PLK-1 and contributed to cell cycle arrest and apoptosis [310]. In a different context, MSC-EVs were loaded with a siRNA that silences the expression of phosphatase and tensin homolog (PTEN), which is one of the major intrinsic impediments to axonal growth, aiming at improving the regenerative ability of neurons after SCI [313]. Moreover, Huang and colleagues demonstrated that siRNA-targeting the connective tissue growth factor (CTGF) encapsulated in MSC-EVs also has a positive effect on functional recovery after SCI [307].

Synthetic miRNA mimics have also been exogenously encapsulated into MSC-EVs. For instance, MSC-EVs were electroporated with the miRNA-132 that targets RASA1, an essential negative regulator of vascular sprouting and vessel branching. The bioengineered EVs promoted angiogenesis in *vitro* and enhanced neovascularization and preserved heart functions in an *in vivo* MI mouse model [304]. In another study, MSC-EVs harbouring miRNA-499a-5p inhibited

endometrial tumour growth and angiogenesis *in vitro* and *in vivo,* by directly targeting to upregulated gene VAV3, [305]. Using a different strategy, Wang and collaborators exogenously loaded EVs secreted by human MSC(WJ) with a miRNA mimic using a commercial transfection reagent. miRNA-326-carrying MSC-EVs suppressed the activation of NF-κB signalling pathway and the reduced expression levels of neddylation-related enzyme molecules, inhibiting the synthesis and production of related inflammatory factors and relieving dextran sulfate sodium (DSS)-induced inflammatory bowel disease (IBD) in a mouse model, compared to unmodified MSC-EVs [314].

Protein loading into EVs was also investigated by genetic manipulation of parental MSC. For example, serine/threonine kinase Akt, which plays an important role in promoting cell proliferation and inhibiting cell apoptosis, was transduced into human MSC(WJ) using an adenovirus system. Western blot semi-quantification revealed that the produced EVs harboured significantly higher levels of Akt than the control EVs. The produced EVs harboured higher levels of Akt and demonstrated increased angiogenic effects *in vitro* and *in vivo* and promoted superior cardiac regeneration in an acute MI mouse model, compared to control EVs [315]. Similarly, Ang-2 loaded into MSC(WJ)-derived EVs through its lentiviral-based overexpression by parental cells. Ang-2-carrying EVs enhanced angiogenesis and accelerated cutaneous wound healing *in vivo* [316]. Moreover, EVs secreted by pigment epithelium-derived factor (PEDF)-overexpressing MSC(AT), showed to ameliorate cerebral ischemia-reperfusion injury in an *in vivo* rat model by activating autophagy and suppressing neuronal apoptosis [318]. Furthermore, MSC(M) were transduced to overexpress osteoactivin. The produced MSC-EVs stimulated the proliferation and osteogenic differentiation of MSC(M) via the activation of Wnt/β-catenin signalling and promoted bone regeneration in an ovariectomized rat model of postmenopausal osteoporosis (OP) [317]. Using exogenous loading, Rajendran and colleagues encapsulated TKI into EVs produced by human MSC(AT) by direct incubation or sonication. Sonicated TKI-EVs enhanced iodine avidity in radioactive iodine-refractory thyroid cancer compared with free-TKI treatment [329].

MSC-EVs have proven to be efficient delivery vehicles for small anti-cancer drugs. For example, MSC incubated with PTX have been shown to secrete EVs presenting a high drug concentration as quantified by high-performance performance liquid chromatography (HPLC) analysis. PTX-loaded EVs and induced a dose-dependent inhibition of human pancreatic adenocarcinoma cell proliferation, reducing tumour growth by up to 50% [223]. Using an alternative approach, Kalimuthu and collaborators have directly incorporated PTX into MSC-EVs by serial extrusion through 10-, 5-, and 1-μm polycarbonate membrane filters. These vesicles demonstrated their significant therapeutical effects against breast cancer both *in vitro* and *in vivo* [326]. As a prospective approach to surpassing chemoresistance of the pancreatic ductal adenocarcinoma (PDAC), a combination therapy of gemcitabine monophosphate (GEMP) and PTX delivered by MSC-EVs was developed, using electroporation and sonication as loading methods, respectively [325]. Despite the low encapsulation efficiencies determined by HPLC (5.92% and 2.62% for GEMP and PTX, respectively), GEMP/PTX-loaded EVs showed a great anti-tumour efficacy *in vitro* and *in vivo* in a PDAC orthotopic mouse model [325]. Furthermore,

the anti-cancer drug DOX was also successfully packed into MSC-EVs using different endogenous loading methods, including electroporation or dialysis [322,323]. UV–Vis spectroscopy-mediated quantification showed that electroporation yielded a higher DOX encapsulation efficiency with a maximum level of 35% [323]. Other small anti-cancer drugs have been packed into MSC-EVs and exhibited improved therapeutic effects, including taxol (TXL) [320] and norcantharidin (NCTD) [324]. Another promising approach consists in loading other small molecule drugs into MSC-EVs to treat inflammation or tissue regeneration besides malignant tumours. For example, isolated MSC(M)-derived EVs were incubated with Cur to engineer EVs with anti-inflammatory properties. After administration into a mouse model of ischemic stroke, Cur-carrying EVs suppressed the inflammatory response and cellular apoptosis in the lesion region of an ischemic stroke mouse model, more effectively than non-modified EVs or Cur alone [328].

Finally, MSC-EVs can be packed with synthetic NPs. For instances, magnetic NPs were incorporated into MSC-EVs, using an MSC-mediated assembly process. Essentially, MSC were incubated with iron oxide NPs and the secreted EVs were loaded with the NPs. After injection and magnet guidance, the NP-harbouring EVs showed significantly enhanced accumulation at the site of injured skin, demonstrating to induce a faster wound reduction with increased collagen deposition and high blood vessel density [319]. Similarly, in another study, MSC-EVs were loaded with Venofer, a carbohydrate-coated ultrasmall superparamagnetic iron oxide nanoparticles (SPION), by incubating MSC with a Venofer-heparin-protamine sulfate complex overnight. The secreted Venofer-carrying EVs were successfully internalized by the tumour cells and facilitated their ablation via cytotoxic hyperthermia by applying an alternating magnetic field [321]. Some studies have also reported the modification of cargo of MSC-EVs by hybrid membrane engineering strategies. Singh and colleagues assembled MSC(M)-derived EVs and liposomes containing polypyrrole (Ppy) NPs, using the freeze–thaw method. Ppy-NPs naturally possess electrical conductivity, which can promote nerve regeneration and ameliorate diabetic peripheral neuropathy (DPN). After intramuscular injection into a DPN mouse model, Ppy-NPs-encapsulating hybrids in combination with electrical stimulation reduced the neural and muscular damage [327].

I.4.1.2. Improving the therapeutic potential of MSC-EVs via surface engineering

Apart from cargo modification, different bioengineering strategies have been used on MSC-EVs to functionalize their surface. Essentially, by genetic engineering of parental MSC or direct chemical modification of isolated EVs, the surface of MSC-EVs has been manipulated to enhance their therapeutic properties and improve target selectivity, aiming at developing potent targeted therapies with reduced adverse effects (**Table I.5**).

Table I.5 - Overview of the potential strategies and applications of surface-engineered mesenchymal stromal cells derived-extracellular vesicles (MSC-EVs). Reproduced from [109].

Type of strategy	Surface modification	Application	Therapeutic effect	MSC source	Ref.
Genetic engineering of EV surface	cTnI-targeting peptide	Myocardial infarction	Improved targeting to ischemic heart	Rat BM	[306]
	HER2-specific DARPins	Breast cancer	Improved uptake by HER2+ cells	N/A	[330]
	IL-2	Cancer	Activated human $CD8^+$ T-killers	Human AT	[331]
	IL-6ST decoy receptors	Duchenne muscular dystrophy	Counteracted the effects of pathological signalling pathways	Human BM	[332]
	CSTSMLKAC peptide	Myocardial infarction	Improved targeting to ischemic heart	Mouse BM	[333]
	PD-L1	Autoimmune Diseases	Improved recognition and inactivation of immune cells	Mouse BM	[334]
	RVG	Ischemic stroke	Increased targeting to ischemic brain	Mouse BM	[303]
	TNF-α	Cancer	Inhibited tumour growth	Human N/A	[335]
	TRAIL	Cancer	Increased selective apoptosis	Human N/A	[336]
Chemical-based surface engineering	5TR1 DNA aptamer	Colon adenocarcinoma	Improved targeting to tumours	Mouse BM	[323]
	BM-specific RNA aptamer	Osteoporosis	Improved targeting to bone marrow	Mouse BM	[337]
	c(RDGyK) peptide	Ischemic stroke	Improved targeting to ischemic brain	Mouse BM	[312,328]
	IL-4- receptor targeting peptide	Anaplastic thyroid cancer	Improved targeting to tumours	Human BM	[338]
	LJM-3064 aptamer	Multiple sclerosis	Increased affinity to myelin-producing cells; Induced immunomodulatory and remyelination effects	Mouse BM	[339]
	OXA	Pancreatic ductal adenocarcinoma	Induced immunogenic tumour cell death	Human BM	[308]
	RVG	Alzheimer's disease	Improved targeting to brain tissues	Mouse BM	[340]
	SDSSD peptide	Osteoporosis	Improved targeting to osteoblasts and bone-forming surfaces	iPSC	[311]
	SPION	Melanoma subcutaneous cancer	Improved targeting under an external magnetic field	Human N/A	[335]
	εPL-PEG-DSPE	Osteoarthritis	Increased uptake and retention in cartilage	iPSC	[341]
	Macrophage membranes fractions	Spinal cord injury	Increased levels of ischemic region-targeting molecules and improved targeting to injury	Human WJ	[342]
Hybrid membrane engineering	Monocyte membranes fractions	Myocardial infarction	Improved targeting to ischemic myocardium	Rat BM	[343]

PEGylated liposomes	Cancer	Decreased internalization by macrophages	Mouse BM	[246]
Platelet membrane fractions	Myocardial infarction	Improved targeting to injured myocardium and enhanced cellular uptake by endothelial cells and cardiomyocytes	Human BM	[344]

AT-adipose tissue; BM- bone marrow; cTnI- cardiac troponin I; DARPin- designed ankyrin repeat protein; DSPE- 1,2-distearoyl-sn-glycero-3-phosphoethanolamine; HER2- human epidermal growth factor receptor 2; IL- interleukin; IL-6ST- cytokine interleukin 6 signal transducer; iPSC- induced pluripotent stem cells; OXA- oxaliplatin; PD-L1- programmed cell death-ligand 1; PEG- polyethylene glycol; RVG- rabies viral glycoprotein; SPION- superparamagnetic iron oxide nanoparticles; TNF-α- Tumour necrosis factor; TRAIL- tumour necrosis factor-related apoptosis-inducing ligand; WJ- Wharton's jelly; εPL- ε-polylysine.

The conjugation of peptides on the surface of MSC-EVs has been shown to improve their targeting towards organs or tissues, demonstrating prospective effects in the treatment of different types of cancer, heart and brain diseases. Many researchers have been using genetic engineering to generate recombinant peptides that are displayed on the surface of MSC-EVs, usually by fusing a targeting ligand to an EV membrane-enriched peptide/protein. Envisioning the targeting delivery of drugs to the brain, Yang and colleagues developed neuron-specific targeting EVs by engineering MSC to overexpress Lamp2b fused with RVG. After systemic administration into a mouse model of cortical ischemia, RVG-displaying MSC-EVs efficiently deliver the exogenously loaded miRNA-124 to the ischemic region and ameliorate brain injury by promoting neurogenesis [303]. Similarly, MSC(M) were transduced to overexpress Lamp2b fused with ischemic myocardium-targeting peptide (IMTP) CSTSMLKAC and produce cardiac cell-targeting EVs. Intravenously injected IMTP-displaying EVs showed enhanced accumulation in the MI region and significantly increased capillary density, inhibited inflammatory response, reduced infarct size and preserved cardiac function, compared to naked EVs [333]. Alternatively, a peptide targeting cardiac troponin I (cTnI), which is highly expressed in the MI, was used as an EV membrane-displaying ligand for the targeted delivery of miRNA-590-3p to the ischemic area. The MSC-EVs decorated with the cTnI-targeting peptide effectively accumulated in the infarct area along the cTnI concentration gradient [306]. Gomari and collaborators improved the efficiency of MSC-EVs for targeted anti-cancer drug delivery by transducing the parental cells with a lentivirus encoding Lamp2b fused with HER2-specific designed ankyrin repeat protein (DARPin), which are synthetic peptides with high binding affinity and specificity to their target protein. The engineered EVs were preferentially uptaken by HER2-overexpressing breast cancer cells compared to normal cells, effectively delivering DOX and siRNA molecules [330].

Surface modification of MSC-EVs can be used not only to improve targeting but to introduce an additional therapeutic moiety. For instance, tumour necrosis factor (TNF-α)-related apoptosis-inducing ligand (TRAIL) is a widely studies anti-cancer agent that selectively triggers an extrinsic apoptotic pathway in malignant cells [345]. In this context, Yuan and colleagues found that EVs secreted by genetically engineered TRAIL-expressing MSC selectively induced apoptosis in eleven cancer cell lines and were able to partially overcome TRAIL resistance in cancer cells [336]. As another example, MSC were transfected to overexpress a plasmid encoding fusion protein of cell-penetrating peptides (CPP) and TNF-α which resulted in the secretion of

EVs with TNF-α anchored in the membrane. Compared to unmodified EVs, TNF-α-EVs significantly enhanced tumour cell growth inhibition *through* induction of the TNFR I-mediated apoptotic pathway *in vitro* and *in vivo* [335]. Xu and colleagues proposed a platform for the treatment of autoimmune disease by developing activated immune cells-specific targeting EVs. For that, MSC were modified to overexpress programmed cell death-ligand 1 (PD-L1), whose receptor is highly express in autoimmune pathological tissues and involved in the signalling pathway of inhibition of immune responses and preservation of immune homeostasis. The PD-L1-expressing MSC-EVs were recognized by various activated immune cells including T cells, macrophages and dendritic cells with high expression of PD-L1 receptor, in a DSS-induced colitis mouse model. Additionally, the engineered EVs restored tissue lesions by reconfiguring the local immune microenvironment [334]. Moreover, MSC(AT) were engineered with lentivirus encoding IL-2, a cytokine that stimulates anti-cancer immunity, for its EV-mediated delivery, aiming at reducing systemic toxicity. IL-2-EVs were able to activate human CD8+ cytotoxic T cells, which effectively killed human triple-negative breast cancer cells; however, these failed to suppress the proliferation of human peripheral blood mononuclear cells (PBMCs) [331]. In another study, MSC were engineered to produce EVs displaying pro-inflammatory cytokine IL-6 signal transducer decoy receptors at their surface to selectively inhibit the IL-6 trans-signalling pathway, a specific mediator in chronic inflammatory response, while not interfering with the classical signalling properties of this cytokine. IL-6-decoy receptor-decorated EVs demonstrated their decoy activity by inducing a reduction in STAT3 phosphorylation in the quadriceps and gastrocnemius muscles of Duchenne muscular dystrophy mouse model [332].

Chemical engineering has been largely investigated in incorporating targeting moieties into the surface of MSC-EVs, including peptides, RNA/DNA aptamers and drugs. For example, Zhang and colleagues conjugated the surface of MSC-EVs with the c(RGDyK) peptide, known to target the ischemic brain by binding to integrin $\alpha_v\beta_3$ in reactive cerebral vascular endothelial cells, using bio-orthogonal copper-free click chemistry. Essentially, the reactive dibenzylcyclootyne-conjugated EVs formed a covalent bond with an azide group on the lysine of the c(RGDyK) peptide. After intravenous administration into a mouse model of ischemic stroke, the engineered EVs successfully targeted lesions within ischemic brain tissue [328]. This strategy allowed the accumulation of EV-loaded cholesterol-modified miRNA-210 in the lesion region and promote microvascular angiogenesis [312]. In another study, MSC-EVs were chemically functionalized via a reaction between an aptamer-conjugated aldehyde and the amino group of EV-membrane proteins. Basically, the surface of EVs was conjugated with an MSC(M)-specific RNA aptamer to improve BM targeting. After intravenous injection, the engineered EVs successfully targeted the BM and promoted bone regeneration in OP and femur fracture mouse models, contrarily to non-functionalized EVs, which accumulated in the liver and lungs [337]. Similarly, Bagheri and colleagues engineered the surface of MSC(M)-derived EVs with the 5TR1 DNA aptamer that has a high affinity with MUC1, a transmembrane mucin glycoprotein overexpressed in different types of cancer cells. Click chemistry led to the formation of a covalent bond between carboxylate-modified 5TR1 aptamer and amine group on the surface of EVs. After intravenous injection into

a mouse model of colon adenocarcinoma, the 5TR1 aptamer-EVs exhibited higher tumour accumulation and faster liver clearance in comparison with unmodified EVs [323]. Using the same reaction, Shamili and co-workers conjugated MSC-EVs with the LJM-3064 DNA aptamer which has a strong affinity toward myelin, and demonstrated remyelination induction, aiming at establishing a novel approach for managing multiple sclerosis (MS). LJM-3064 aptamer-EVs showed a higher affinity for the myelin basic protein-producing cells *in vitro*, and synergistically induced immunomodulatory and remyelination effects in the experimental mouse model of MS [339]. To overcome the immunosuppressive tumour microenvironment of PDAC, an EV-based dual DDS of siRNA-galectin-9 was developed to block the galectin-9/dectin-1 axis and reverse immunosuppression caused by tumour-associated macrophages, and prodrug oxaliplatin (OXA), to act as immunogenic cell death-trigger and kill the tumour cells by inhibiting DNA synthesis and repair. After exogenous loading of siRNA-galectin-9, OXA was added to the MSC-EVs obtaining a stable maleimide-thiol conjugate, through vortexing [308]. MSC-EVs cancer-targeted delivery can also be achieved with magnetism. For example, SPION were conjugated with transferrin (Tf) using click chemistry. Afterwards, Tf-SPION were assembled to the surface of MSC-EVs by transferrin–transferrin receptor-mediated interaction. The engineered EVs were used for cancer-targeted delivery of TNF-α (described above), under an external magnetic field in a mouse model of melanoma subcutaneous cancer [335].

Another chemical strategy used to engineer the surface of MSC-EVs has been lipid-assembly. For instance, Gangadaran and colleagues functionalized the surface of MSC-EVs with a peptide that targets IL-4 receptor, which is upregulated in various types of tumours, using a membrane phospholipid-based linker composed of dioleylphosphatidylethanolamine (DOPE), methoxy PEG, and succinyl-N-hydroxy-succinimidyl (NHS) ester. The IL-4-receptor-targeting peptide EVs induced a faster internalization into human anaplastic thyroid cancer cells *in vitro* compared to EV-displaying a control peptide. Additionally, engineered EVs showed to efficiently target tumours in a xenograft mouse model, in contrast to control EVs that predominantly localized in the liver and spleen [338]. Using a similar strategy, MSC(M)-derived EVs were conjugated with the RVG peptide using a DOPE-NHS linker. The RVG-displaying EVs enhanced their binding to the cortex and hippocampus upon intravenous administration in a mouse model of AD, ameliorating spatial learning and memory impairments [340]. Alternatively, bone-targeting EVs were developed through conjugation with the peptide SDSSD modified with a diacyl lipid tail via hydrophobic insertion. The peptide-displaying EVs specifically delivered the exogenously loaded siRNA targeting schnurri-3 (SHN3) to osteoblasts and bone-forming surfaces via SDSSD/periostin interactions [311].

Feng and colleagues engineered MSC-EVs with a positively charged surface by simple incubation with a novel cationic amphiphilic macromolecule ε-polylysine (εPL)-PEG-DSPE, in order to enhance EVs intra-articular bioavailability in OA therapy. In contrast with unmodified EVs, electropositive MSC-EVs demonstrated increased chondrocyte uptake and retention ability in cartilage, leading to an enhanced OA treatment [341].

Some studies have also modified the surface of MSC-EVs by engineering hybrid nanocarriers. For instance, PEG-mediated fusion of MSC-EVs with functionalized liposomes with various liposome-to-EV ratios has allowed the manipulation of the EV-membrane properties, namely cellular uptake. In fact, PEGylated liposomes-EV hybrids, enabled a lower internalization by macrophages *in situ* [246]. In another study, membrane MSC-EVs were fused with platelet membrane fractions in the presence of PEG, in order to enhance their accumulation in injured tissues. Compared to unmodified MSC-EVs, the cellular uptake of hybrid EVs was significantly enhanced in endothelial cells and cardiomyocytes, but not macrophages. Additionally, the hybrid EVs showed improved targeting to injured myocardium and enhanced therapeutic potency in a mouse model of MI [344]. Similarly, Zhang and colleagues generated monocyte mimics-EVs hybrids to improve the delivery efficiency of MSC-EVs to ischemic myocardium, by mimicking the recruitment feature of monocytes [343]. Moreover, Lee and collaborators fabricated EVs hybrids by fusing the membrane of MSC(WJ) and macrophages through serial extrusion of cells via microporous and nanoporous filters. The engineered hybrid EVs largely accumulated in the SCI area after the *in vivo* systemic injection, due to the increased levels of ischemic region-targeting molecules compared to MSC-EVs [342].

I.4.1.3. Clinical translation of bioengineered MSC-EVs

In the past few years, more than forty clinical trials have been registered to address the innate potential of MSC-EVs for the treatment of different diseases, including bronchopulmonary dysplasia (NCT03857841), burn wounds (NCT05078385), OA (NCT05060107), AD (NCT04388982), dystrophic epidermolysis bullosa (NCT04173650), CD (NCT05130983), periodontitis (NCT04270006) and COVID-19 associated pneumonia (NCT04276987; NCT04491240) (listed in “clinicaltrials.gov” on 01st February 2024 using the terms “MSC exosomes OR MSC extracellular vesicles”). However, there are still several hurdles hampering the clinical application of non-modified MSC-EVs, namely their short half-life, poor targeting ability, rapid clearance from the target area and inefficient payload [230].

Significant advances have been made in developing strategies to bioengineer MSC-EVs to overcome these limitations. Functionalization of MSC-EVs with targeting ligands using genetic manipulation or chemical modification makes them more directed and efficient therapeutics (**Table I.4**). Moreover, the modification of the intraluminal composition of MSC-EVs through their complementation with specific exogenous payloads potentially enables the establishment of personalized treatments (**Table I.3**). In this context, the combination of these two bioengineering strategies is expected to contribute towards the development of personalized MSC-EV-based therapies with improved targeting and therapeutic potency in the treatment of a multitude of diseases, including cancer, brain and heart disorders, as well as bone injuries (**Figure I.8**).

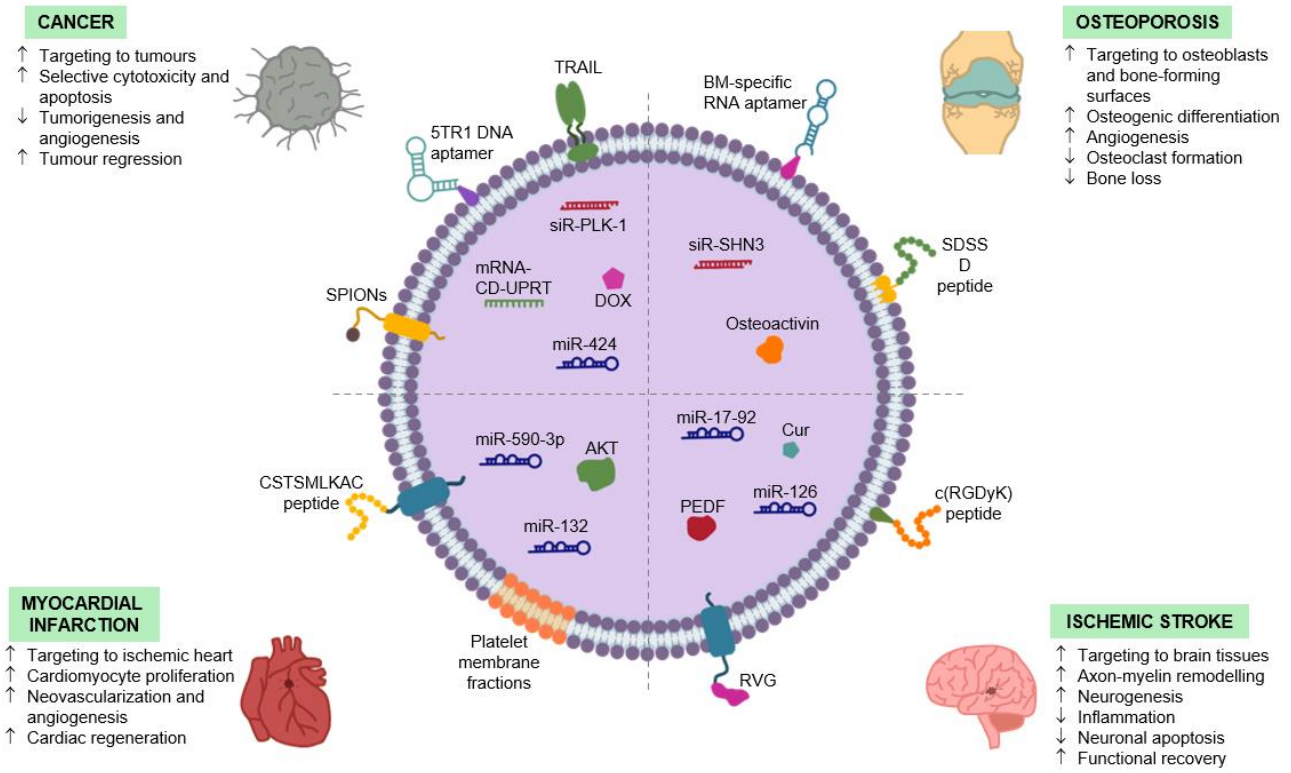

Figure I.8 - Representative applications of bioengineered MSC-EVs with improved therapeutic payload and target specificity in the treatment of cancer [288,293,308,310,322,335,336], osteoporosis [317,337,482], myocardial infarction [304,306,315,333,344] and ischemic stroke [291,294,303,312,318,483]. CD-UPRT- cytosine deaminase fused to uracil phosphoribosyltransferase; Cur- Curcumin; DOX- doxorubicin; PEDF- pigment epithelium-derived factor; PLK-1- serine/threonine-protein kinase; RVG- rabies viral glycoprotein; SHN3- schnurri-3 protein; SPION- superparamagnetic iron oxide nanoparticles; TRAIL- tumour necrosis factor-related apoptosis-inducing ligand. Reproduced from [109].

Clinical studies have already been exploring MSC-EVs as DDS of nucleic acids for the treatment of different diseases. miRNA-124-loaded MSC-EVs have been found to ameliorate brain injury by promoting neurogenesis after ischemia [303]. In this context, a phase I/II clinical trial (NCT03384433) is evaluating the effect of allogenic MSC-EVs enriched with miRNA-124 as a treatment for acute ischemic stroke patients. The patients are expected to receive the miRNA-124-MSC-EVs by intraparenchymal injection, one month after stroke onset. In this study, measurements of treatment-derived adverse events, including stroke recurrences, brain oedema and seizures and measurements of the degree of disability of stroke patients will be conducted within a period of 12 months after therapy administration. Additionally, MSC-EVs containing siRNA targeting oncogenic $Kras^{G12D}$ mutations are being tested against PDAC in a phase I clinical trial (NCT03608631). PDAC patients are expected to receive the siRNA-$KRAS^{G12D}$-EVs through intravenous administration on days 1, 4, and 10, with repeated treatments every 14 days. The primary objectives of this study are the assessment of a maximum tolerated dose and the identification of dose-limiting toxicities. Secondary objectives include the pharmacokinetics of

circulating EVs, the assessment of overall response and disease control rates and the evaluation of the median progression-free survival and median overall survival with therapy. Another phase I clinical trial (NCT05043181) will be testing the therapeutic potential low-density lipoprotein (LDL) receptor (LDLR)-mRNA in the treatment of homozygous familial hypercholesterolemia (HoFH). HoFH patients carry a functional loss mutation of the LDLR gene causing severely elevated plasma LDL-cholesterol and premature coronary heart disease [346]. In this clinical study, MSC(M) will be engineered with a LDLR-expressing virus vector and the produced LDLR-mRNA-enriched EVs will be used as HoFH therapy. A total of three treatments with an interval of 7±1 days will be injected into the patients through abdominal puncture, testing six EV doses. The primary outcome will be measuring the changes in total cholesterol, LDL-cholesterol, high-density lipoprotein-cholesterol and triglyceride and the secondary outcome will be the assessment of the degree of coronary stenosis and the volume and stability of carotid artery plaques.

Other registered studies have been using EVs from other sources as DDS, namely EVs from erythrocytes loaded with methotrexate to treat malignant ascites (NCT03230708) and EVs from HEK-293 cells loaded with an antisense oligonucleotide (ASO) targeting STAT6 in advanced hepatocellular carcinoma and metastasis from gastric and colorectal cancer patients (NCT05375604). In what concerns surface engineering, three trials using EVs overexpressing the CD24 receptor are being conducted to treat COVID-19-related conditions (NCT04747574, NCT04902183, NCT04969172) [132].

Despite the substantial amount of research on bioengineered MSC-EVs as improved drug delivery therapeutics, only a few of them have been investigated in clinical settings. One major contributing factor is that most methods used in pre-clinical models for the production and isolation of EVs have low yields, insufficient purity profiles and are hardly scalable (e.g., conventional planar cell culture systems as T-flasks for MSC-EV production and ultracentrifugation or precipitation-based EV isolation methods) [347].

Furthermore, the reproducible manufacture of an EV-based product at a clinical scale is challenging when using MSC as parental cells due their limited lifespan and inherent batch-to-batch or donor-to-donor variations [348]. MSC immortalization is a possible approach to tackle these limitations and facilitate large-scale EV production. Some studies have reported that immortalization (e.g., by *MYC* transgene integration) did not confer tumorigenic activity to MSC and their secreted EVs [349]. Still, MSC-EVs produced by immortalized cells will always raise safety concerns in what concerns their tumour-promoting effects. An alternative approach to increase the yield and homogeneity of MSC-EVs is using induced pluripotent stem cells (iPSC) as a source of MSC [311,341]. iPSC-derived MSC potentially allow unlimited cell supply, which lowers the manufacturing costs and increases the scalability potential for the production of a GMP-grade EV product [348].

In addition, most of the methods reported to bioengineer the content and surface of MSC-EVs are still at the pre-clinical level and with limited scalability. Due to the lower loading efficiencies often associated with exogenous loading, cargo engineering of MSC-EVs has mostly been explored by endogenous loading through the genetic modification of the parental cells,

which is still troublesome in primary cells and has unpredictable loading efficiencies [220,221]. To overcome these limitations, Yang and collaborators established a novel cellular nanoporation-based strategy for large-scale loading of mRNA into MSC-EVs. Essentially, MSC were cultured on a specifically designed biochip, transfected with plasmid DNAs and induced to release EV harbouring the transcribed RNAs by an electrical stimulus. Compared with bulk electroporation, cellular nanoporation generated up to 50-fold more EVs with one thousand-fold higher levels of transcripts [350]. Furthermore, surface modification of previously isolated MSC-EVs has shown great signs of progress regarding efficiency and scalability, avoiding the complexity of genetic engineering strategies [220].

I.5. Motivation, aims and outline of the thesis

Several diseases include excessive angiogenesis as part of the pathology, including malignancies, ocular diseases like DR and AMD, and inflammatory diseases like psoriasis and RA [19–24]. VEGF, plays a central role in angiogenesis by stimulating endothelial cell functions (e.g., mitogenesis, migration, sprouting and tube formation) and potentiates vascular permeability, which precedes and accompanies angiogenesis [4,11,12]. Besides participating in physiological angiogenesis, VEGF actively contributes to the progression of excessive angiogenesis-related disorders [19–24].

RNA interference-based anti-angiogenic strategies have demonstrated positive effects as modulators of angiogenesis *in vitro* and *in vivo*, by silencing pro-angiogenic factors [89]. VEGF regulatory pathway is undoubtedly a promising siRNA target when developing anti-angiogenic gene-targeting therapies, having achieved high anti-tumour effects in tumour-bearing mice [90,91] and reduced pathologic angiogenesis in corneal neovascularisation models [93,94]. Expression vectors encoding shRNAs can be used as an alternative to synthetic siRNAs [55], and MCs emerge as a promising option by being minimalistic vectors free of bacterial backbone sequences capable of high levels of transgene expression [78]. Combining the prolonged biostability of plasmid DNA, gene silencing capabilities of siRNA, and improved transfection efficiency of MCs, shRNA-expressing MCs appear as a promising gene-targeting therapy [84–87].

EVs are cell-derived nano-sized lipid membranous structures that modulate cell-cell communication by transporting a variety of biologically active cellular components. The potential of EVs in delivering functional cargos to targeted cells, their capacity to cross biological barriers, as well as their high modification flexibility, make them promising drug delivery vehicles for cell-free therapies [104,105,109]. MSC are considered a promising source for producing EVs for biomedical applications, given their intrinsic therapeutic benefits, exceptional safety profile, and efficient *ex vivo* expansion capacity [130,276]. In addition, MSC-EVs can be bioengineered to enhance their therapeutic cargo and increase their selectivity toward target cells, which has been shown to improve their therapeutic potential in numerous pre-clinical animal models [109]. Despite the promising prospects of EVs in therapeutic applications, a lack of robust and scalable manufacturing processes for their production and functionalisation hinders their clinical translation.

This thesis aimed to develop a cell-free anti-angiogenic gene-based therapy, relying on shRNA-expressing MCs that target the expression of key players of VEGF regulatory pathway and the use of MSC-EVs as delivery system. The project comprised three main research objectives: i) the development of shRNA-expressing MCs; ii) the establishment of a platform for the large-scale manufacturing of MSC-EVs; iii) the engineering of MSC-EVs by direct loading of the MCs.

Chapter I includes a general introduction to angiogenesis, anti-angiogenic strategies, and the role of VEGF in health and excessive angiogenesis-related diseases. Then, it delves into RNAi technology and shRNA-expressing systems, particularly MC vectors. Moreover, it discusses EVs touching on their biogenesis, composition, uptake, manufacturing, and bioengineering. Lastly, it introduces MSC as EV producers, highlighting the therapeutic potential of MSC-EVs and their progress as DDS and clinical translation.

Chapter II focus on the development of shRNA-expressing MCs targeting VEGF-A and VEGFR2. Scalable processes were implemented to produce and purify the supercoiled MCs. Transfection experiments and *in vitro* functional angiogenesis assays were performed to evaluate the silencing and anti-angiogenic potential of the MCs.

Chapter III features the establishment of a platform for the manufacturing MSC-EVs integrating fully scalable upstream and downstream processes. MSC(WJ) were expanded in STR under S/XF-free conditions and endured a 3-day continuous EV production stage in EV-depleted medium. After the isolation process, the EV yield was assessed and MSC-EVs were characterized concerning their biochemical and biophysical properties.

Chapter IV explores the use of MSC-EVs as a delivery system of RNAi molecules. MSC-EVs were engineered by direct loading shRNA-expressing MCs using multiple methods. The loading efficiency was assessed, and functional delivery of the EV-MC complexes was evaluated using a GFP-reporter system.

Chapter V summarises the main achievements of each experimental chapter while proposing future studies and discusses the challenges that need to be overcome to broadly establish EVs as nucleic acid delivery vehicles.

Chapter II.

DEVELOPMENT OF SHRNA-EXPRESSING MINICIRCLES THAT SILENCE VEGF AND ITS RECEPTOR

II.1. Abstract

Vascular Endothelial Growth Factor (VEGF) holds significant importance in modulating angiogenesis not only in normal physiology but also in pathological conditions characterized by excessive angiogenesis. Current treatments using inhibitors of VEGF and its receptors have shown efficacy in various angiogenesis-related disorders. Nevertheless, alternative anti-angiogenic agents are being investigated envisioning increased therapeutic efficacy, and RNA interference (RNAi)-based strategies have shown great promise at targeting key regulators of angiogenesis.

This study explores the anti-angiogenic potential of RNAi-based gene therapy targeting VEGF-A and VEGFR-2 using short hairpin RNA (shRNA)-expressing minicircles (MC), devoid of bacterial sequences, aiming for a safer and more sustained gene expression. The development of shRNA-expressing MCs involved the construction of the parental plasmids (PP) and large-scale manufacturing of the correspondent MC. After production and *in vivo* recombination into MC and miniplasmid (MP) in *E. coli* BW2P, the supercoiled MCs were purified through a combination of targeted enzymatic relaxation of the MP and multimodal chromatography. Transfection experiments using human breast cancer cells and human umbilical vein endothelial cells revealed significant knockdown effects at both mRNA and protein levels through quantitative assays, after microporation with the MC-shVEGF and MC-shVEGFR2, respectively. While *in vitro* functional angiogenesis assays provided valuable insights concerning the MCs effect on pro-angiogenic capacity of the transfected cells, further optimization is needed to accurately evaluate the biological impact of MC-mediated VEGF-A and VEGFR-2 silencing.

Overall, this work sheds light on the effectiveness and applicability of MC-derived RNAi systems in targeting pro-angiogenic molecules, emphasizing their promise as a novel non-viral, therapeutic approach for excessive angiogenesis.

II.2. Background

Angiogenesis is a basic physiological process defined by the formation of new blood vessels from pre-existing ones [4,6]. In normal physiology, angiogenesis is essential for organ development, the female reproductive system and tissue repair in healthy adults [6,7]. This process is closely regulated by the balance between angiogenic activators and inhibitors in the extracellular environment of endothelial cells (EC) [6]. Pro-angiogenic factors are secreted by various cell types including EC, fibroblasts, smooth muscle cells, platelets, inflammatory cells, and cancer cells [4]. The local concentration of factors can be influenced by physiological or pathologic responses to injury, chronic inflammation, or cancer [4]. Some well-known angiogenic growth factors and cytokines are vascular endothelial growth factor (VEGF), fibroblast growth factor (FGF), tumour necrosis factor-alpha (TNF-α), transforming growth factor-beta (TGF-β), and angiopoietins [4].

VEGF plays a central role in angiogenesis, stimulating EC mitogenesis, migration, sprouting and tube formation. VEGF also potentiates vascular permeability, which precedes and accompanies angiogenesis [4,11,12]. VEGF family currently comprises five members: VEGF-A, VEGF-B, VEGF-C, VEGF-D and placental growth factor (PlGF). VEGF-A is the key regulator of blood vessel growth and exerts its biological effect through interaction with two VEGF-specific receptor tyrosine kinases, VEGF receptor 1 (Flt-1) and VEGF receptor 2 (VEGFR2) (KDR/Flk-1) that are strongly expressed on EC [11,12,16]. VEGFR2 is considered the primary signal transducer for angiogenesis through PLCγ-PKC-MAPK, PLCγ-PKC-eNOS-NO, TSAd-Src-PI3K-Akt, SHB-FAK-paxillin, SHB-PI3K-Akt, and NCK-p38-MAPKAPK2/3 pathways, mediating EC survival, proliferation, migration and induction of vascular permeability [17].

Besides actively participating in physiological angiogenesis, VEGF has a pathological role in many disorders including malignant, ocular such as age-related macular degeneration (AMD) and diabetic retinopathy (DR), and inflammatory conditions, such as rheumatoid arthritis and psoriasis [19–24]. The Food and Drug Administration (FDA) has approved a spectrum of drugs designed to prevent angiogenesis by inhibiting VEGF or its receptors. Among these are anti-VEGF monoclonal antibody Bevacizumab, anti-VEGFR-2 monoclonal antibody Ramucirumab, human recombinant fusion protein Aflibercept that acts as a decoy receptor by binding to VEGF-A, VEGF-B, and PlGF, small-molecule Tyrosine Kinase Inhibitors Sunitinib and Sorafenib, and aptamers Pegaptanib, an oligonucleotide with high-affinity binding to VEGF-165 [6,25]. Moreover, other treatment categories are being explored as alternative anti-angiogenesis agents, namely gene therapy, RNA interference (RNAi) therapy, and Chimeric antigen receptors (CAR)-T cell therapy [6].

RNAi-based anti-angiogenic strategies have demonstrated positive effects as modulators of angiogenesis *in vitro* and *in vivo*, by silencing pro-angiogenic factors [89]. Among many, VEGF regulatory pathway is undoubtedly a promising target when developing anti-angiogenic gene-targeting therapies. Different formulations of small interference RNA (siRNA) that target VEGF and its receptors achieved a high anti-tumour effect in tumour-bearing mice [90,91] and effectively reduced pathologic angiogenesis in mouse models of corneal neovascularisation [93,94]. siRNAs have the advantage of executing their function by complete Watson–Crick base pairing with mRNA, whereas monoclonal antibody and small molecule drugs rely on the recognition of often complex spatial configurations of target proteins [49]. Moreover, siRNA-mediated post-transcriptional silencing prevents target protein translation and a single siRNA molecule can mediate the degradation of multiple mRNA molecules, making it a very efficient and specific therapeutic modality [49,50]. An alternative approach to delivering siRNA sequences is expressing systems that encode short hairpin RNA (shRNA), which are double-stranded folded stem-looped RNAs that after transcription are exported to the cytosol, recognised, and processed by endogenous enzyme Dicer into approximately 19-22-nucleotide long RNA molecules that induce RISC-mediated target-specific mRNA degradation [55,351]. Plasmid and viral expression vectors have been shown to successfully induce transient or stable shRNA-mediated gene silencing. For instance, lentiviral vectors expressing shRNA targeting VEGF inhibited tumour

angiogenesis and growth, and increased apoptosis of pancreatic cancer cells *in vitro* and *in vivo* [95]. Despite high delivery efficiencies and potentially stable gene expression, concerns about the safety, immunogenicity and latent pathogenic effects of viral vectors hamper their clinical application [352]. Plasmids are a safer and easy-to-handle alternative to deliver shRNAs for efficient therapeutic gene silencing [67–69]. For example, a shRNA-expressing plasmid vector targeting c-Src, a non-receptor protein tyrosine kinase overexpressed in many solid tumours, inhibited tumour angiogenesis *in vivo* [68]. In another case, shRNA-VEGF-A plasmids were shown to regress corneal neovascularisation in a mouse model of corneal injury [67].

Despite being far less immunogenic than viruses, plasmids contain unmethylated CpG dinucleotide and other bacterial motifs that can induce host inflammatory responses and transcriptional silencing of episomal transgenes [72–74]. Moreover, the larger size of conventical plasmids often reduces transfection efficiencies [74–77]. These limitations can be overcome using MCs that are small vectors free of bacterial backbone sequences (e.g., antibiotic resistance gene, origin of replication, and inflammatory sequences intrinsic to bacterial DNA) and capable of high levels of transgene expression, that potentially meet the clinical requirements for safe and long-lasting gene expression [78,79]. MC are generally synthesised in recombinant bacteria and result from an *in vivo* recombination process: the parental plasmid (PP) carries the eukaryotic expression cassette flanked by two recognition sites of a site-specific recombinase, that upon induction originate a replicative miniplasmid (MP) carrying the undesired backbone sequences, and a MC carrying the therapeutic expression unit [78,79]. The potential of MCs has been demonstrated in several gene therapy preclinical studies envisioning the treatment of various diseases, including skin wounds [80], primary ciliary dyskinesia [81], pancreatic cancer [82] and ovarian cancer [83]. As an example of the great potential of shRNA-encoding MCs, Zhao and colleagues reported that MC targeting anaplastic lymphoma kinase showed increased transfection efficiency compared to a conventional plasmid while gene silencing was equivalent to siRNAs, effectively reducing the growth of anaplastic large cell lymphoma cells *in vitro* [86].

In this work, shRNA-expressing MCs that silence VEGF-A (MC-shVEGF) and its receptor (MC-shVEGFR2) were developed, envisioning the establishment of a novel gene-based therapy for excessive angiogenesis disorders. After construction of the corresponding shRNA-expressing PP, their large-scale production and *in vivo* recombination was accomplished using *E. coli* BW2P. Purification of supercoiled MCs involved a combination of targeted enzymatic relaxation of the MP followed by multimodal chromatography. To confirm the silencing potential of the shRNA-expressing MCs, transfection experiments were performed using a human breast cancer cell line and endothelial cells, and the percentage of knockdown at the mRNA and protein levels was assessed by quantitative real-time PCR and ELISA, respectively. The effect of MC silencing on the pro-angiogenic capacity of the transfected cells was evaluated through *in vitro* functional angiogenesis assays. Overall, this study provides important insights in what concerns the implementation of an MC-derived RNAi-based system that targets pro-angiogenic molecules.

II.3. Materials and methods

II.3.1. Cell lines and cell culture

Human breast cancer cells MDA-MB-231 were cultured using high glucose Dulbecco's modified Eagles' medium (DMEM) (Gibco, Life Technologies), supplemented with 10% (v/v) of heat-inactivated fetal bovine serum (FBS) (Lonza), and 1% (v/v) Antibiotic-Antimycotic (A/A) (Gibco, Life Technologies) and passaged between 2 and 3 times per week, by enzymatic harvesting with trypsin 0.05%. Human umbilical vein endothelial cells (HUVEC) were cultured using Endothelial Cell Growth Medium-2 BulletKit™ (EGM™-2, Lonza) and passaged at 80–90% confluency after enzymatic detachment with Accutase (Invitrogen, Life Technologies). Cells were incubated at 37°C and 5% CO_2 in a humidified atmosphere.

II.3.2. Design and construction of shRNA-expressing parental plasmids

For the construction of the shRNA-expressing vector targeting different molecules, the parental plasmid pMINILi-CVGN2 previously developed by our group [353,354], was used as a backbone template. Briefly, this plasmid contains an expression cassette with a green fluorescent protein (GFP)-vascular endothelial growth factor (VEGF) gene fusion under transcriptional control of the human cytomegalovirus (CMV) immediate-early promoter and a bovine growth hormone (BGH) polyadenylation signal. The eukaryotic expression cassette is flanked by two multimer resolution sites (MRS) and the miniplasmid portion includes a pMB1 origin of replication (ori), kanamycin resistance selection marker (KanR), and a recognition site for the nicking endonuclease Nb.BbvCI (**Supplementary Figure II.1**). In this work, the eukaryotic cassette was replaced by the sequence of the polymerase III promoter (U6-promoter) which is capable of originating a well-defined shRNA transcript [355] followed by the insertion of the shRNA sequences that will target VEGF, VEGFR2 and GFP (negative control) (**Figure II.1**).

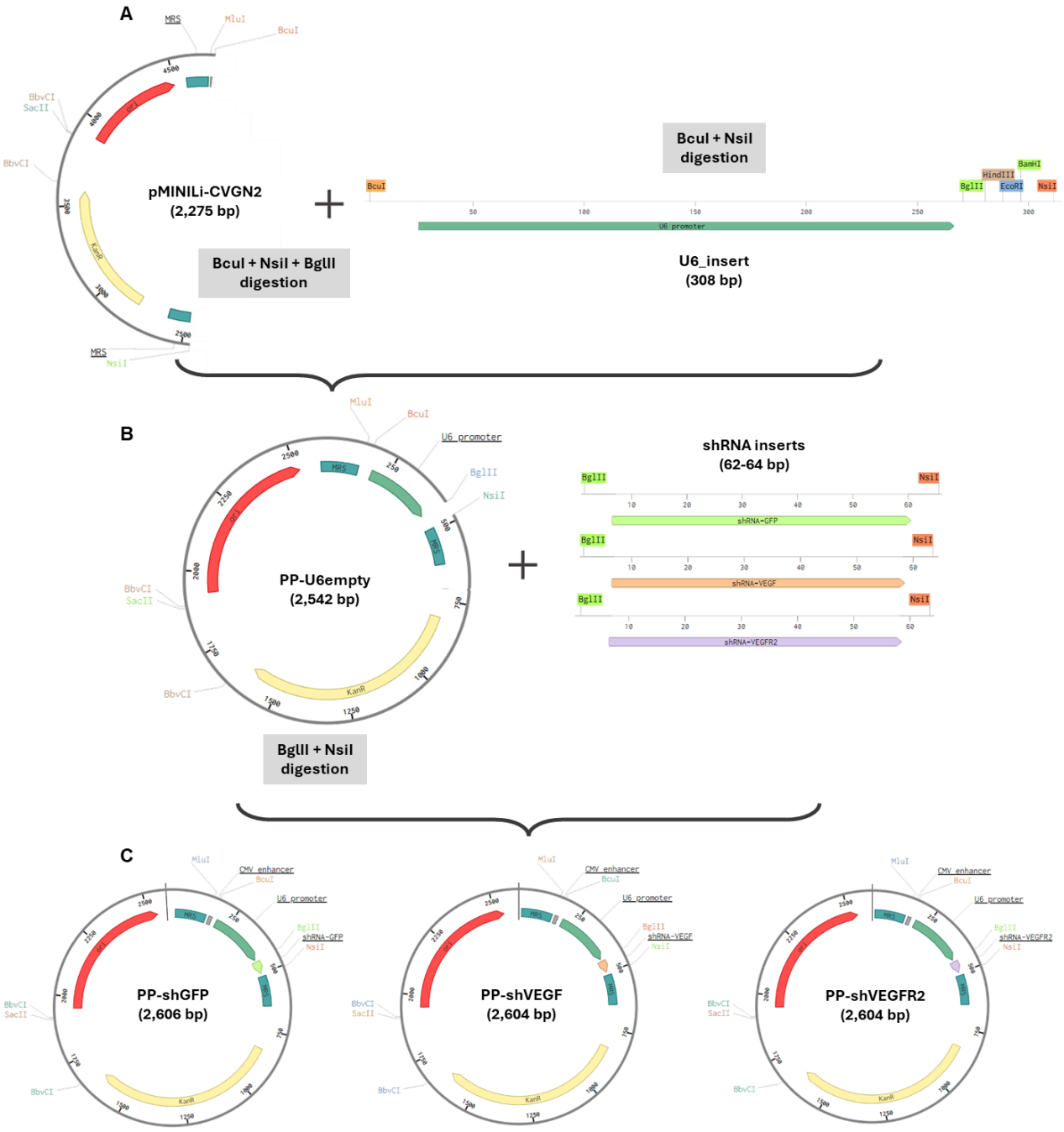

Figure II.1- Schematic representation of the construction of shRNA-expressing parental plasmids. **(A)** Ligation of the digested parental plasmid pMINILiCVGN2 backbone and U6-promoter-containing insert for constructing the PP-U6empty. **(B)** Ligation of the digested parental plasmid PP-U6empty with the different annealed sequences of shRNA inserts. **(C)** Plasmid maps of PP-shGFP, PP-shVEGF and PP-shVEGFR2.

II.3.2.1. *In silico* design of the U6 promoter sequence and shRNA-inserts

The new eukaryotic cassette was designed to contain the U6 promoter sequence and multiple cloning sites (MCS) flanked by restriction enzyme sites of BcuI and NsiI to allow its insertion on the PP backbone.

For the construction of the PP targeting the different molecules, target sequences of siRNA which have been shown to efficiently silence gene expression of VEGF, VEGFR2 and GFP in different human cell lines were selected for the respective shRNA inserts (**Table II.1**) A pair of DNA oligonucleotides (outsourced, STABVIDA) were designed for each target gene containing the sequence of the passenger strand followed by a loop sequence and finally, the sequence of the guide strand, allowing the transcript to fold back on itself forming a shRNA, analogously to natural miRNA [356]. The selected 9-nt loop sequence 5'-TTCAAGAGA-3' is based on a naturally occurring miRNA sequence [357]. The oligonucleotides exhibit overhangs of the restriction enzymes BglII and NsiI digested recognition sequence to facilitate its insertion into the parental plasmid (**Table II.1**).

Synthetic siRNAs, targeting the same location as the shRNA, were also designed including deoxythymidine dinucleotide overhangs in the passenger strand to improve strand selection [358], and were chemically synthesised (outsourced, STABVIDA).

Table II.1- Sequences of shRNA inserts composed by the passenger and guide strands separated by the loop sequence in italic (BcuI and NsiI digested sequences overhangs in bolt) for cloning into pMINILi-CVGN2 PP backbone. The RNA target sequence is also depicted.

Gene	shRNA insert sequence (5' to 3')	Target sequence (5' to 3')	Ref.
VEGF	Forward: **GATCT**ATGTGAATGCAGACCAAAG*TTCAAGAG* *A*CTTTGGTCTGCATTCACATTTTTTT**ATGCA**	AUGUGAAUGCAGACCAAAG	[359–361]
	Reverse: **T**AAAAAAATGTGAATGCAGACCAAAG*TCTCTTG* *AA*CTTTGGTCTGCATTCACAT**A**		
VEGFR2	Forward: **GATCT**GGGCTTTACTATTCCCAGC*TTCAAGAGA* GCTGGGAATAGTAAAGCCCTTTTT**ATGCA**	GGGCUUUACUAUUCCCAGC	[362,363]
	Reverse: **T**AAAAAGGGCTTTACTATTCCCAGC*TCTCTTGA* *A*GCTGGGAATAGTAAAGCCC**A**		
GFP	Forward: **GATCT**GCAAGCTGACCCTGAAGTTC*TTCAAGA* *GA*GAACTTCAGGGTCAGCTTGCTTTTT**ATGCA**	GCAAGCUGACCCUGAAGUUC	[364,365]
	Reverse: **T**AAAAAGCAAGCTGACCCTGAAGTTC*TCTCTTG* *AA*GAACTTCAGGGTCAGCTTGC**A**		

II.3.2.2. Construction of the shRNA-expressing parental plasmids

The vectors were transformed into chemically competent *Escherichia coli* DH5α by heat shock throughout construction. The new eukaryotic cassette containing the U6-promoter sequence was cloned and outsourced into a pUC57 vector (2,710 bp) (Nzytech). For the construction of the PP-U6empty, the vectors pMINILi-CVG and pUC57 were digested with BcuI (Thermo Fisher Scientific), NsiI (Promega) and BglII (Promega) restriction enzymes for 3 hours at 37°C. The digested pDNA was separated by a 1% agarose gel electrophoresis and the correct fragment was extracted from the gel with NZYGelpure kits (Nzytech) according to the manufacturer's instructions. The fragments ligation was performed overnight at 4°C with a vector: insert ratio of 1:5 using T4 DNA ligase (3U/ µL; Promega) (**Figure II.1- A**). Afterwards, the pDNA of *E. coli* DH5α clones was extracted using NZYMiniprep kit (Nzytech), according to the manufacturer's instructions, and the restriction pattern after MluI and BamHI (Promega) digestion was evaluated through 1% agarose gel separation. To further validate the insertion, DNA sequencing was performed on the construct (STABVIDA) using the following primer sequence (MP-R3): ATTCCGGTTCGCTTGCTGTC.

To construct the final PP vectors, the shRNA insert oligonucleotides (**Table II.1**) were resuspended in 10 mM Tris, pH 8.0; 50 mM NaCl; 1 mM EDTA and annealed by incubation at 95°C for 2 min, followed by a gradual decrease to 25 °C for 45 min, and finally decrease to 4°C. The new PP-U6-empty was digested with BglII (Promega) and NsiI (Promega) for 3 hours at 37°C and the desired fragment was obtained as described above. Afterwards, the annealed dsDNA oligonucleotide (insert) was ligated to the digested PP-U6empty with a vector: insert ratio of 1:7 using T4 DNA ligase (3U/ µL; Promega) for 3 hours at room temperature (**Figure II.1- B**). *E. coli* DH5α clones were confirmed by restriction pattern after BamHI (Promega) and SacII (Thermo Fisher Scientific) and DNA sequencing with the primer ATTCCGGTTCGCTTGCTGTC The confirmed parental plasmids were identified as PP-shVEGF, PP-shVEGFR2, and PP-shGFP, including the name of the respective shRNA-targeting gene (**Figure II.1- C**).

II.3.3. Production and *in vivo* recombination of the parental plasmids

The producer strain *E. coli* BW2P developed by our group [366] was used for the production and *in vivo* recombination of the different PP into MP and MC. This strain expresses the ParA resolvase gene under the transcription control of the arabinose inducible expression system pBAD/AraC which catalyses the intramolecular recombination between the two MRS. The process was adapted from established protocols [353,367]. Briefly, cells from an overnight pre-inoculum were used to inoculate 100 mL Erlenmeyer flasks containing 30 mL of LB medium (Nzytech) supplemented with 30 µg/mL kanamycin (Amresco) and 0.5% (w/v) glucose (Merck) with a starting optical density at 600 nm (OD_{600nm}) of approximately 0.1. Cultures were incubated at 37 °C and 250 rpm until $OD_{600nm} \approx 2.5$ has been reached. Afterwards, the appropriate volume was used to inoculate 2 L Erlenmeyer flasks containing 500 mL of LB medium (Nzytech) supplemented with 30 µg/mL kanamycin (Amresco) at an $OD_{600nm} \approx 0.1$ which were incubated at

37 °C and 250 rpm. Recombination was induced at an $OD_{600nm} \approx 2.5$, by adding 0.01% (w/v) L-(+)-arabinose (Merck). Recombination was allowed to proceed for 1 hour at 37 °C and 250 rpm. Cells were harvested from the culture by centrifugation at 6,000xg for 15 min at 4ºC and stored at -20ºC for further processing.

II.3.4. Purification of the supercoiled minicircles

For the purification of the different MCs, the pDNA species were recovered and purified from the producer cells using the QIAGEN Plasmid Plus Maxi Kit (Qiagen) according to the manufacturer's instructions. Afterwards, to reduce the sample volume the purified pDNA was precipitated with 0.3M sodium acetate and 70% (v/v) of ethanol for 1h at -20ºC. The pDNA was pellet by centrifugation at 12,500xg, 4ºC for 30min. The pellet was washed with ice-cold 70% (v/v) of ethanol and centrifuged for another 20min. Finally, the airdried pellet was resuspended in 150 μL UltraPure™ DNase/RNase-Free Distilled Water (Life Technologies). The subsequent isolation of the MC from the other species in the mixture was based on the method established by Silva-Santos and colleagues [367]. Firstly, an *in vitro* digestion with Nb.BbvCI (New England Biolabs) to nick one of the strands of the MP and of the non-recombined PP, converting them into their open-circular (oc) counterparts, was completed. The reaction was performed for 2 h at 37ºC in a total volume of 250μL using the CutSmart buffer 1x (New England Biolabs) and a ratio of using of 1-10 U of enzyme per 100 μg of total nucleic acids. Finally, supercoiled (sc) MC was isolated from the other species in this mixture by multimodal chromatography, performed using a Triton 10/50 column (Cytiva) packed with 5 mL of multimodal chromatography Capto™ adhere resin (Cytiva) connected to an ÄKTA Purifier 10 system (Cytiva). The mobile phase consisted of mixtures of buffer A (10 mM Tris-HCl, 1 mM EDTA, pH 8) and buffer B (2 M NaCl in 10 mM Tris-HCl, 1 mM EDTA, pH 8). The absorbance of the eluate was continuously measured at 254 nm by a UV detector positioned after the column outlet and the system was operated at 1 mL/min. The column was equilibrated with 3 column volumes (CV) of 41.5% buffer B (≈74 mS/cm). The samples were conditioned with a buffer containing 830 mM NaCl in 10 mM TE, to a final volume of 1mL. Unbound material was washed out of the column with 2 CV of 41.5% buffer B. Elution steps were then performed with 3 CV of 46% B (≈81 mS/cm) and 3 CV of 100% B (≈152 mS/cm). The fractions collected were analysed by agarose gel electrophoresis. Finally, the MC-containing fractions were concentrated/diafiltrated to a volume of approximately 100 μL mL of UltraPure™ DNase/RNase-Free Distilled Water (Life Technologies) using an ultrafilter with a molecular weight cut-off of 30 kDa (Amicon® Ultra-4, Merck Millipore) previously passivated overnight with a solution 5% (v/v) Tween-20 in distilled water. The final DNA concentration was determined by spectrophotometry at 260nm, using a Nanodrop (GE Healthcare), and MC integrity and purity was evaluated by agarose gel electrophoresis.

II.3.5. Transfection of the shRNA-expressing minicircles into target cell lines

To evaluate the potential of the MCs that silence VEGF (MC-shVEGF) and VEGFR2 (MC-shVEGFR2), transfection experiments were performed using MDA-MB-231 and HUVEC, respectively. Transfection was performed through microporation using the Neon™ Transfection System 10 µL Kit (Life Technologies) and the procedure was adapted from previous work from our group [368–370]. Essentially, $2x10^5$ cells were resuspended in buffer R (Life Technologies) and 0.5 µg of the appropriate MC to a final volume of 10 µL. Cell suspensions were microporated using 1 pulse at 1,000 V for 40 ms using the 10 µL Neon™ Tips (Life Technologies), and incubated with 90 µL of Opti-MEM™- Reduced Serum Medium (Gibco) for 20 min. Finally, cells were plated onto 12-well plates previously coated with 0.1% (v/v) gelatin (Sigma) in phosphate-buffered saline (PBS) 1x and cultured in corresponding culture media. Control conditions include non-microporated cells (Non-microp), cells microporated with buffer R (Microp), cells microporated with MC that silences GFP (MC-shGFP) as a negative control, and microporation with 50nM of synthetic siRNAs that silence the same target-mRNA region (si-VEGF and si-VEGFR2) as a positive control.

Cells and culture supernatants were collected at different timepoints post-transfection and centrifuged for 7 min at 350xg and 10 min at 360xg, respectively, before -80ºC storage. At each collection timepoint, cell number and viability were estimated using the Trypan Blue Solution, 0.4% (Gibco, Life Technologies) exclusion method. Cell recoveries were determined at day 2 for all conditions, by calculating the ratio between the number of viable cells in the microporation condition and the non-microporated control condition (Non-microp).

II.3.6. Evaluation of the silencing potential of shRNA-expressing minicircles

II.3.6.1. Evaluation of minicircle-derived silencing at the mRNA level

Total RNA was extracted from transfected cells pellets with RNeasy Mini Kit (Qiagen), according to the manufacturer's instructions. Afterwards, 250-500 ng of RNA were converted to cDNA with the High-Capacity cDNA Reverse Transcription Kit (Life Technologies), with a single cycle of 10 min at 25ºC, 120 min at 37°C and 5 min at 85ºC in a thermal cycler (T100™ Thermal Cycler, Bio-Rad). Quantitative real-time polymerase chain reaction (RT-qPCR) was performed using StepOnePlus™ Real-Time PCR System (Applied Biosystems), using NZY qPCR Green ROX plus kit (Nzytech) with a reaction mixture composed by 0.4 µM of specific primers (**Table II.2**), 25 ng of cDNA template and 1x NZY qPCR Green Master Mix to a final volume of 12 µL. After 10min at 95ºC, 40 cycles of 15 sec at 95°C and 1 min at 60ºC were performed. The $2^{-\Delta\Delta CT}$ method of relative gene expression quantification was applied to determine the fold change in target-mRNA expression [371]. Glyceraldehyde 3-phosphate dehydrogenase (GAPDH) was used as the housekeeping gene and cells microporated with buffer R (Microp), as the reference

condition. The percentage of knockdown of the target gene in the microporated cells, was calculated by subtracting the normalized $2^{-\Delta\Delta CT}$ from 1 (defined by the level of expression for the control sample) and multiplying by 100 [372].

Table II.2 - List of primers for the target-mRNA quantification through RT-qPCR.

Gene	Primer sequence (5' to 3')
GAPDH	Forward: TTGATTTTGGAGGGATCTCG Reverse: GAGTCAACGGATTTGGTCGT
VEGFR2	Forward: GAAATGACACTGGAGCCTAC Reverse: GAGACATGGAATCACCACAG
VEGF-A	Forward: CAACTTCTGGGCTGTTCTC Reverse: CTCTCCTCTTCCTTCTCTTCT

II.3.6.2. Evaluation of minicircle-derived silencing at the protein level

VEGF levels of culture supernatants of transfected MDA-MB-231 collected 2-days after microporation were diluted 5x and quantified using Human VEGF Quantikine® Enzyme-Linked Immunosorbent Assay (ELISA) kit (R&D Systems), according to the manufacturer's instructions.

VEGFR2 levels of HUVEC lysates prepared 2-days after microporation were quantified using Human VEGFR2/KDR Quantikine® ELISA kit (R&D Systems), according to the manufacturer's instructions. Cell lysates were prepared with Cell Lysis Buffer 2 (R&D Systems) to a concentration of 1.5×10^6 cells/mL.

Samples absorbance at 450nm (and 540nm to correct for optical imperfections in the plate) was measured using the plate reader Infinite® 200 PRO, NanoQuant, Tecan Trading AG (Männedorf, Switzerland). The concentration of each sample was determined based on a calibration curve, after blank correction.

II.3.6.3. Evaluation of minicircle-derived silencing through angiogenesis functional studies

In vitro functional angiogenesis assays - tube formation assay and scratch assay [373] - were used to assess the impact of MC silencing on the pro-angiogenic potential of the transfected cells. Functional assays were performed using conditioned medium (CM) of transfected MDA-MB-231 and transfected HUVEC to evaluate the anti-angiogenic effect of the MC-shVEGF and MC-shVEGFR2, respectively.

To prepare CM for the functional assays, transfected MDA-MD-231 were cultured for 2 days after microporation. Afterwards, the medium was replaced by Endothelial Growth Basal Medium -2 (EBM-2, Lonza) and incubated for 24 h. CM was collected, centrifuged for 10 min at 360xg and stored at -80ºC.

For the *in vitro* tube formation assay, 50 µL of CM derived from MDA-MB-231 microporated with buffer R (Microp) and microporated with MC that silences GFP (MC-shGFP) and VEGF (MC-shVEGF) were used to cultivate HUVEC (incubated overnight in EBM-2) on µ-Slide 15 Well 3D plates (Ibidi) (5×10^3 cells/well) previously coated with 10 µL of Matrigel® Basement Membrane Matrix (Corning) for 6 h at 37ºC and 5% CO_2 in a humidified atmosphere. Each condition was performed in triplicate using EGM-2 and EBM-2 as positive and negative controls, respectively. Images were acquired using a bright field microscope DMI 3000B (Leica) and tube formation was evaluated (total segments length, number of junctions and number of meshes), using the Angiogenesis Analyzer plugin of ImageJ software [374]. Data represents the average quantification using CM from two independent transfection experiments.

For the scratch assay, HUVEC were seeded at $1.5x10^5$ cell/cm^2 in 2-well culture inserts (Ibidi) placed on 24-well plate, and cultured in EGM-2 for 24h. After, overnight incubation in EBM-2, inserts were removed, and cells were treated with 250µl transfected MDA-MB-231 CM. Cells were monitored over time for a total of 24h and bright field images were analysed using the ImageJ software to determine the percentage of scratch closure relative to the initial scratch area. Each condition was tested in one well, using EGM-2 and EBM-2 as positive and negative controls, respectively. Data represents the average quantification using CM from two independent transfection experiments.

Alternatively, HUVEC microporated with buffer R (Microp) and microporated with MC that silences GFP (MC-shGFP) and VEGFR2 (MC-shVEGFR2) were seeded at $1.5x10^5$ cell/cm^2 in the 2-well culture inserts (Ibidi) and the remaining cells were plated in 24-well plates previously coated with 0.1% gelatin for the tube formation assay. Cells were detached and used in the functional assays as aforementioned using EBM-2 supplemented 2% FBS and 30 ng/ml of VEGF (R&D systems) as culture media [375], and non-microporated cells (Non-microp) as control. Data represents the quantification of one single transfection experiment.

II.3.7. Statistical analysis

All data is presented as mean ± standard error of the mean (SEM). Statistical analysis was performed using GraphPad Prism 9 software. Significance was determined using a one-way ANOVA followed by a post-hoc Tukey's multiple comparison test; *p<005, **p<0.01, ***<0.001, ****<0.0001.

II.4. Results

II.4.1. A shRNA-encoding expression system was constructed using parental plasmid vectors

To develop the shRNA-expressing MCs that silence pro-angiogenic targets VEGF, VEGFR2 and negative control GFP, a PP harbouring the sequence of the polymerase III U6-promoter in the eukaryotic was constructed. Unlike CMV, this promoter can generate a well-

defined shRNA transcript [355]. pMINILi-CVGN2 [353,354] was used as a PP backbone template and the U6-promoter insert was synthesised and cloned into a pUC57 vector. To remove the eukaryotic cassette and preserve the MRS and MP sequences, the pMINILi-CVGN2 was digested with BcuI, NsiI and BglII restriction enzymes, and the desired fragment of 2,275 bp was extracted from the gel (dashed box; **Figure II.2-A**). Likewise, the pUC57 vector was digested with BcuI and NsiI restriction enzymes to isolate the U6-promoter insert of 308 bp (dashed box**; Figure II.2-B**). After the transformation of the ligated fragments into *E.coli* DH5α, a clone candidate was selected and its restriction pattern matches the one expected for the digestion of the newly constructed PP (PP-U6empty) with MluI and BamHI (2,269 bp + 314 bp) (**Figure II.2-C**), confirming the appropriate insertion of U6-fragment into the PP backbone.

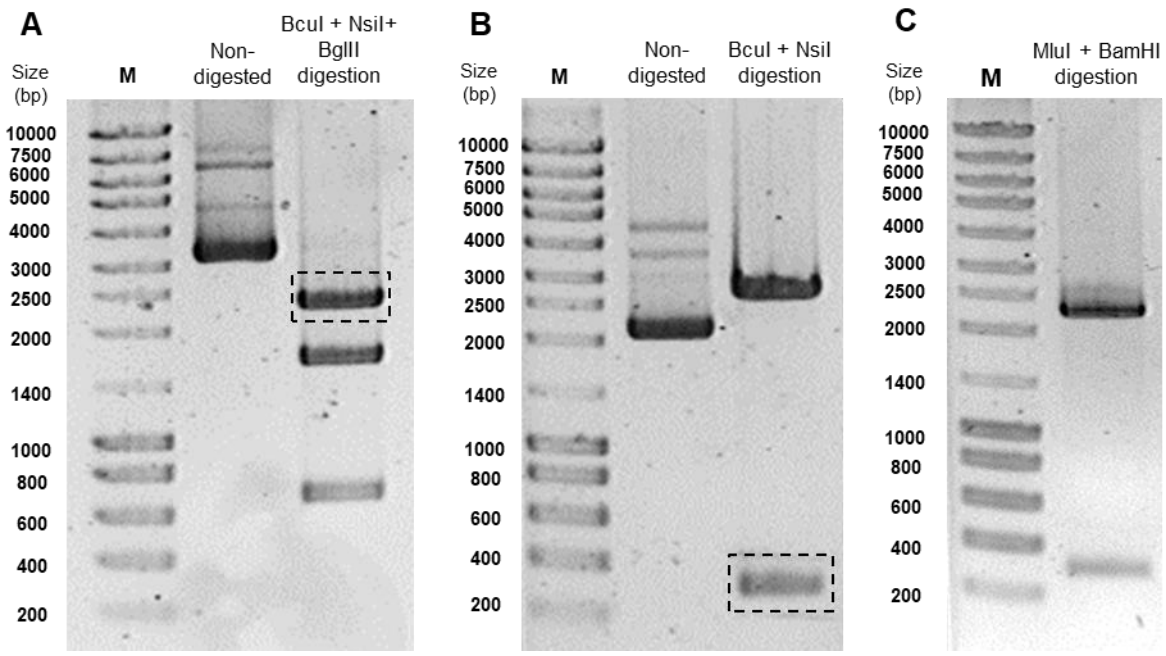

Figure II.2- Agarose gel electrophoresis analysis of the digested plasmids. **(A)** Parental plasmid pMINILi-CVGN2 pDNA before (lane 2) and after restriction digestion with BcuI, NsiI and BglII (lane 3). **(B)** pUC57 plasmid harbouring the U6-promoter sequence pDNA before (lane 2) and after restriction digestion with BcuI and NsiI (lane 3). The dashed box highlights the fragments used in the subsequent construction of the PP-U6empty vector. **(C)** Restriction pattern analysis of pDNA of a clone candidate harbouring PP-U6empty after digestion with MluI and BamHI. Lane M - molecular weight marker NZYDNA Ladder III (Nzytech).

Lastly, to construct the final vectors encoding the shRNA sequences that target VEGF, VEGFR2 and GFP, the different inserts were cloned into the PP-U6empty. Therefore, the desired fragment of 2,542 bp was extracted from the gel after PP-U6empty digestion with BglII and NsiI (dashed box; **Figure II.3-A)**. The annealed oligonucleotide inserts exhibit overhangs of the restriction enzymes BglII and NsiI digested sequence (highlighted in bold; **Table II.1**) and were readily ligated into the digested PP backbone by complementary extremities. The restriction pattern analysis of pDNA of clone candidates harbouring PP-shGFP, PP-shVEGF and PP-

shVEGFR2 after digestion with BamHI and SacII showed a linearized pDNA resulting from the loss of the BamHI restriction site (**Figure II.3-B**), which confirms that the shRNA sequences were readily inserted into the PP-U6empty (**Figure II.1- C**).

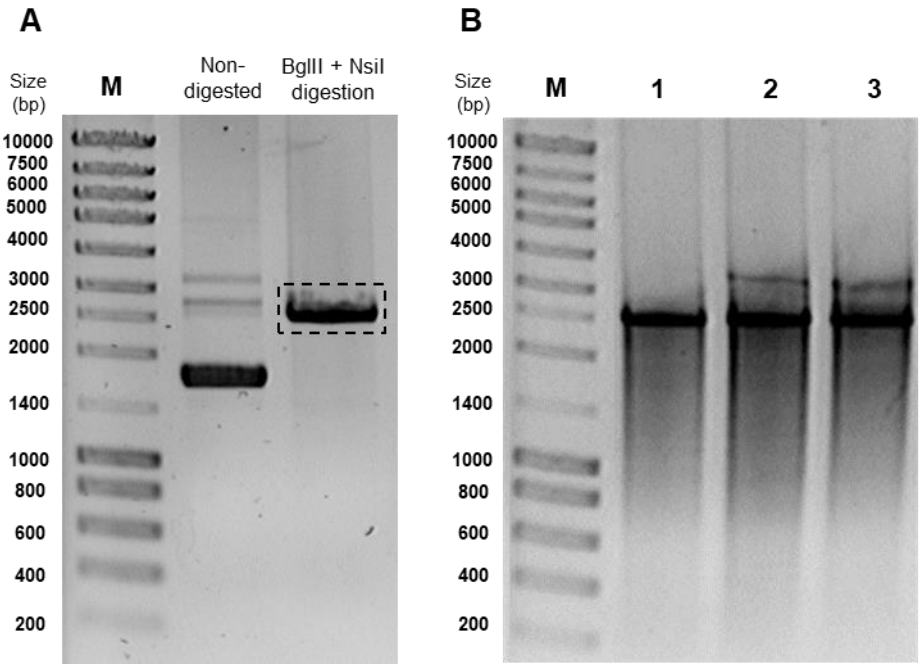

Figure II.3 - Agarose gel electrophoresis analysis of the digested plasmids. **(A)** Parental plasmid PP-U6empty pDNA before (lane 2) and after restriction digestion with and NsiI (lane 3). The dashed box highlights the fragments used in the subsequent construction of the shRNA-encoding PP vectors. **(B)** Restriction pattern analysis of pDNA of clone candidates harbouring PP-shGFP (1), PP-shVEGF (2) and PP-shVEGFR2 (3) candidates after digestion with BamHI and SacII. Lane M - molecular weight marker NZYDNA Ladder III (Nzytech).

II.4.2. shRNA-expressing parental plasmids were produced and recombined using *E. coli* BW2P

E. coli BW2P was used for the production and *in vivo* recombination of the shRNA-expressing PPs. This plasmid producer strain contains the ParA resolvase gene under transcriptional control of pBAD/AraC promoter/operator system, induced by arabinose and repressed by glucose. ParA resolvase catalyses the recombination of PP into MP and MC [353,366].

E. coli BW2P cells harbouring the different shRNA-encoding PPs were grown and OD_{600nm} was monitored over time (**Figure II.4)**. The recombination into MC and MP was induced by the addition of L-(+)-arabinose at an $OD_{600nm} \approx 2.5$ (highlighted in grey; **Figure II.4**), corresponding to the late exponential phase to allow cell number and PP production maximization before induction [376]. Growth curves of *E. coli* BW2P harbouring the different PP replicated similarly, reaching approximate OD_{600nm} values after 1 hour of recombination (3.8 ± 0.10), which was expected since the plasmids are very similar (**Figure II.4**).

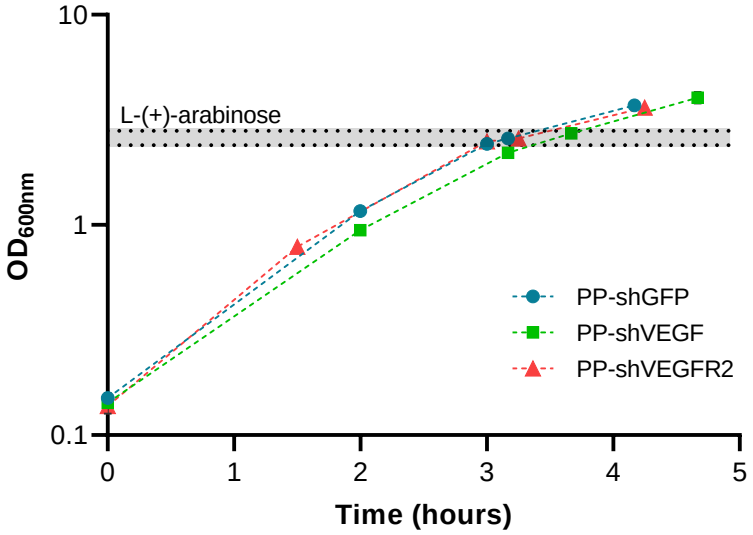

Figure II.4 - Growth curves of *E. coli* BW2P harbouring the parental plasmids PP-shGFP, PP-shVEGF and PP-shVEGFR2 in logarithmic scale. Bacterial growth was performed in 500mL LB medium supplemented with 30 µg/mL kanamycin, at 37ºC and 250 rpm. Values are a mean ± SEM (n=4). The range of OD_{600nm} values in which recombination into MP and MC was induced by L-(+)-arabinose is shown in grey.

To confirm the *in vivo* recombination of the newly constructed shRNA-encoding PPs, samples were collected before and after recombination induction. A representation of this analysis is shown in **Figure II.5** using *E. coli* BW2P harbouring the PP-shGFP. Essentially, before induction, supercoiled (sc) PP form predominates (lane 1, **Figure II.5**). The fact that MC and MP species are absent is a clear indication that no recombination occurs before L-(+)-arabinose addition. In contrast, after 1h of recombination, the generation of MP and MC is detected by the presence of the corresponding bands of sc MP at ~1,400bp and sc MC at ~500bp and the absence of the PP bands (lane 2, **Figure II.5**), confirming the high recombination efficiency of the system used to express the ParA resolvase.

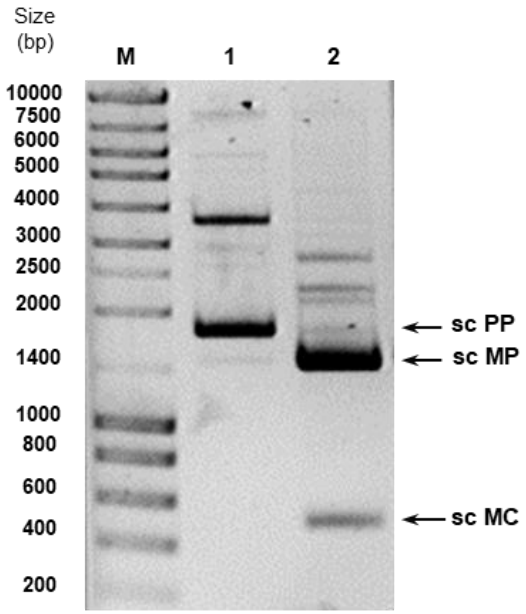

Figure II.5 - Agarose gel electrophoresis analysis of the *in vivo* recombination of PP-shGFP. pDNA purified from *E. coli* BW2P cells collected before (lane 1) and 1 hour after induction of recombination with L-(+)-arabinose (lane 2). Lane M - molecular weight marker NZYDNA Ladder III (Nzytech). Abbreviations: sc PP- supercoiled parental plasmid; sc MP- supercoiled miniplasmid; sc MC- supercoiled minicircle.

II.4.3. Combination of targeted enzymatic relaxation and multimodal chromatography allowed supercoiled shRNA-expressing minicircles purification

After the production and *in vivo* recombination of the shRNA-expressing PP into its MP and MC counterparts, the primary purification of the total pDNA *E. coli* BW2P cells was accomplished using a commercially available kit. This system relies on alkaline lysis and anion-exchange resin columns for RNA, proteins, metabolites, and other low-molecular-weight impurities elimination. Gel electrophoresis analysis demonstrated that after primary purification of the cell lysate, the sc isoform of both MPs and MCs are the two major components of the solution (lane 1, **Figure II.6**). Afterwards, enzymatic digestion with Nb.BbvCI, which recognises specific target sequences located on the prokaryotic backbone of the PP and therefore on MP (**Figure II.1**-C), was used to convert sc molecules into the corresponding oc forms by nicking one of the MP strands, and eventual residual non-recombined PP strands, at the target site [353]. The results showed that 2 h after Nb.BbvCI digestion, the sc MP (lane 1, Figure II.6) was readily converted into its oc counterpart (lanes 2**, Figure II.6**) whereas sc MC remained unmodified (lanes 1 and 2**,** Figure II.6). After digestion, the sample comprised essentially a mixture of sc MC and oc MP and other residual isoforms and multimers (lanes 2, **Figure II.6**).

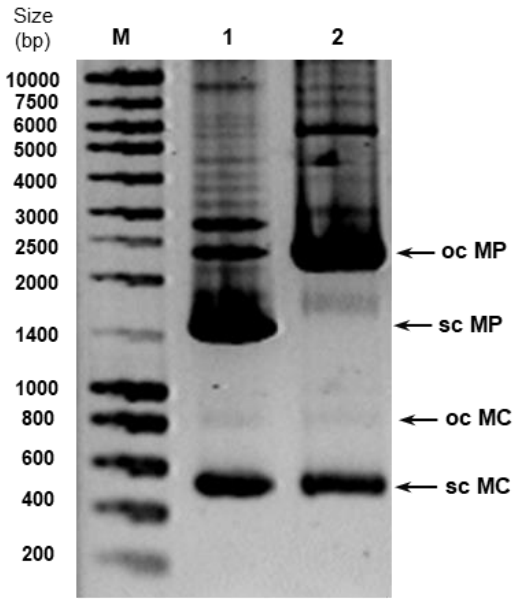

Figure II.6 - Agarose gel electrophoresis analysis of recombined pU6-shGFP before and after digestion with endonuclease Nb.BbvCI. Samples were collected after plasmid purification with the HiSpeed® Plasmid Maxi Kit (Qiagen) (lane 1) and after digestion with endonuclease Nb.BbvCI, for 2 hours at 37ºC (lane 2). Lane M - molecular weight marker NZYDNA Ladder III (Nzytech). Abbreviations: sc MC- supercoiled minicircle; oc MP- open circular miniplasmid; sc MP- supercoiled miniplasmid.

To isolate the sc MC from the other species, multimodal chromatography with a Capto adhere ligand was performed. MC-containing samples were pre-conditioned with NaCl up to a final concentration of 830 mM and loaded onto a pre-equilibrated Capto™ adhere column. Unbound material was washed with 41.5% B (830 mM, ≈ 74 mS/cm) and elution was accomplished using two steps with increasing salt concentration, the first at 46% B (920 mM, ≈81 mS/cm) and the second at 100% B (2 M, ≈152 mS/cm). The chromatogram obtained (**Figure II.7-A**) is characterized by an early peak at 41.5% B, another peak at 46% B and a final peak at 100% B. Agarose gel electrophoresis analysis of the collected fractions (**Figure II.7-B**) demonstrated that the first peak represents the elution of oc isoform of the MP, the second peak corresponds to the sc MC elution and the last peak results from the high salt concentration and the elution of strongly bound impurities. The MC-containing fractions (14-18) were diafiltrated/concentrated and agarose gel electrophoresis analysis was completed to evaluate the MC integrity and purity of the sample. The isolation of the shRNA-expressing MCs (~500 bp) was successful as its sc isoform is the predominant constituent of the sample (**Supplementary Figure II.2**). Overall, the isolation process yielded 15.1 ± 2.55 µg of MC (mean ± SEM; n=14), which corresponds to a production of 21.9 ± 3.79 µg of MC/ L of bacterial growth and 10.6 ± 1.74 µg of MC/ gram of dry cell weight (DCW), considering the coefficient 0.5 gDCW/L/OD_{600} unit [377].

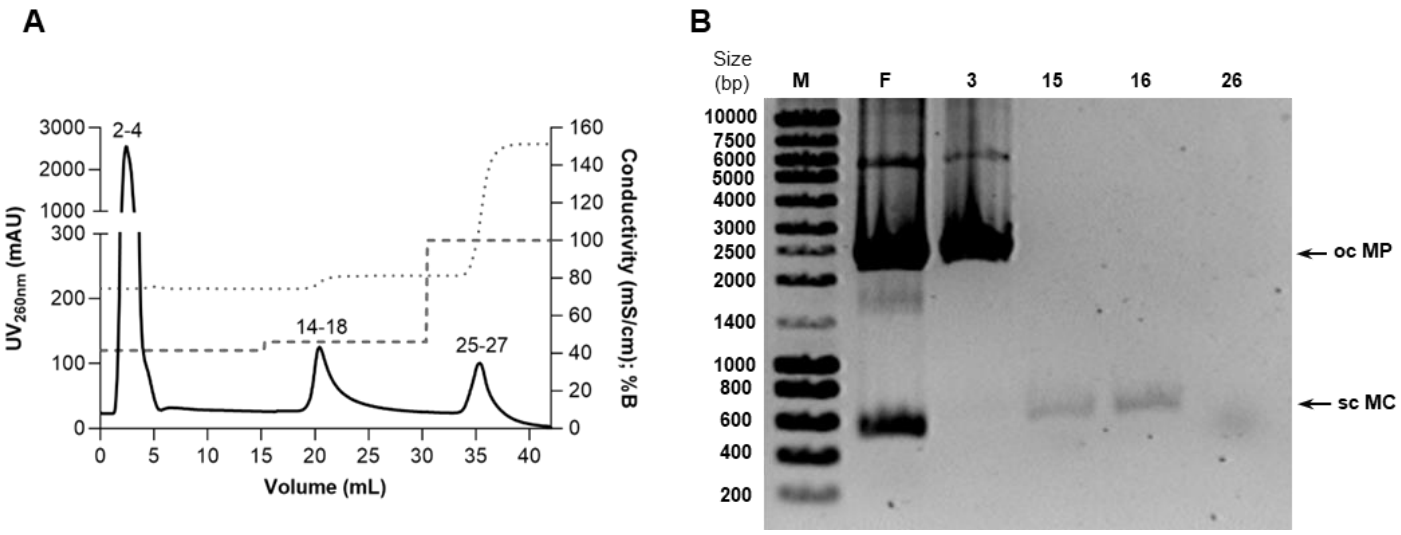

Figure II.7- Isolation of sc minicircle of pU6-shGFP from the oc species in the mixture by multimodal chromatography. **(A)** Chromatogram obtained using a Capto™ adhere column and a series of elution steps with increasing NaCl concentration. Numbers over peaks correspond to the collected fractions. Black continuous line: absorbance at 254 nm; grey dashed line: conductivity (mS/cm); grey dotted line: percentage of buffer B (%B). **(B)** Agarose gel electrophoresis analysis of fractions collected during the chromatographic run. The numbers above each lane correspond to fractions collected (10 µL of feed sample (F); 20µL of sample for fraction 3; 30 µL of sample for fractions 15, 16 and 26). Lane M - molecular weight marker NZYDNA Ladder III (Nzytech). Abbreviations: oc MP- open circular miniplasmid; sc MC- supercoiled minicircle.

II.4.4. shRNA-expressing minicircles silence the target genes at mRNA and protein levels

To evaluate the silencing potential of the MC-shVEGF and MC-shVEGFR2, transfection experiments were performed using MDA-MB-231, a human breast cancer cell line known to secrete pro-angiogenic molecules [378], and HUVEC that have high density of VEGF surface receptors [379], respectively. Microporation was used as the transfection method, using non-microporated cells (Non-microp) and cells microporated with buffer R (Microp) as controls. MC-shGFP and si-VEGF or si-VEGFR2 were used as negative and positive silencing controls, respectively. The impact of the delivery system on cell recovery by day 2 and the proliferative capacity of the transfected cells was evaluated (**Figure II.8**). Cells microporated with buffer R (Microp) showed high cell recoveries (~95%) whereas cells microporated with nucleic acids showed lower cell recovery. For each cell line, cells microporated with MCs and siRNA demonstrated comparable cell recoveries. These were slightly lower for HUVEC compared to MDA-MB-231 when transfected with the MCs (~77% vs ~60%) (**Figure II.8 – A**). Despite the lower cell recoveries, high viabilities (≥ 90%) were observed after MC/siRNA transfection for both cell lines. Although control conditions (Non-microp and Microp) displayed the highest cell numbers throughout 7 days, cells transfected with nucleic acids were able to proliferate **(Figure II.8 – B)**, reaching comparable final fold increase values in total cell number (from day 2) compared to non-microp**.**

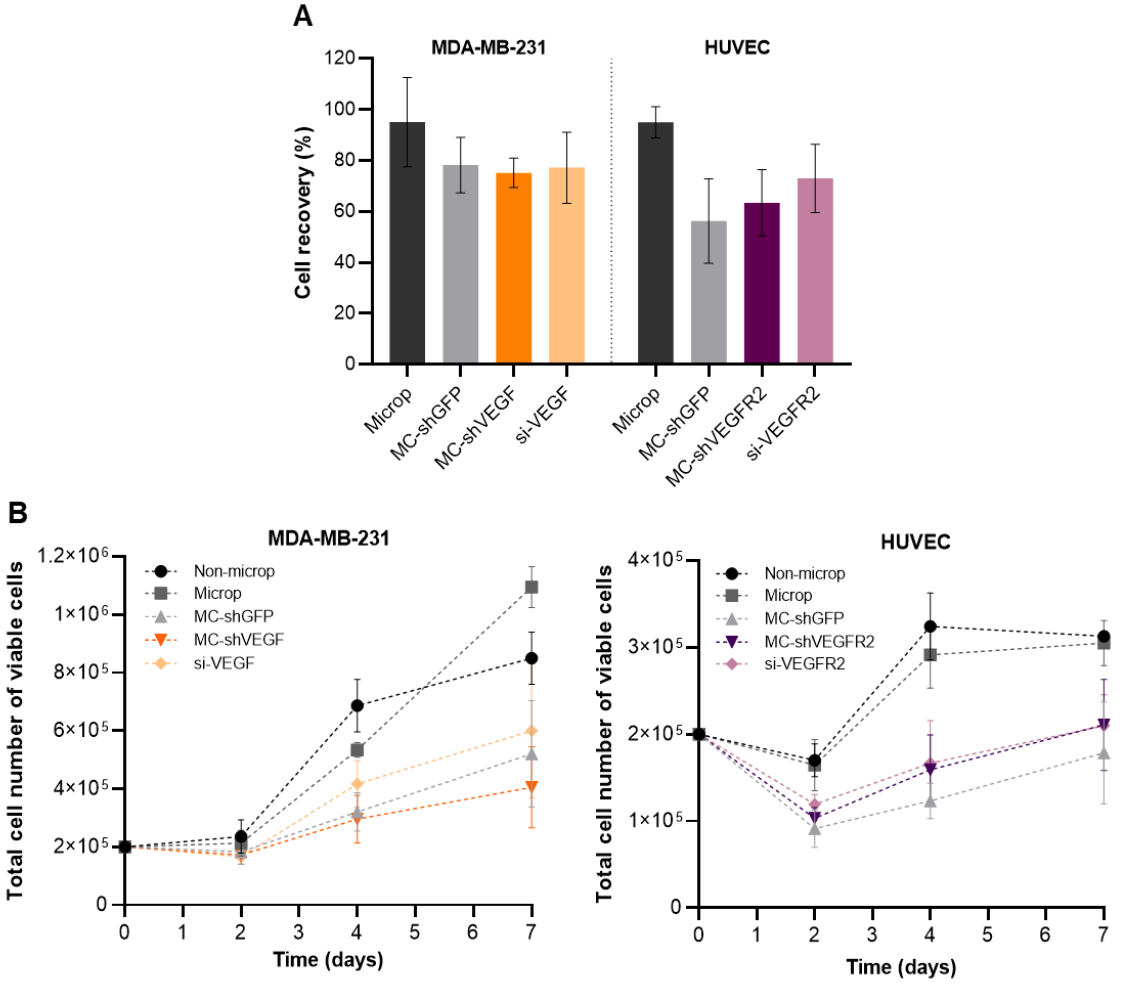

Figure II.8- Analysis of the behaviour of MDA-MB-231 and HUVEC after microporation with the MC-shVEGF and MC-VEGFR2, respectively. **(A)** Cell recovery 2 days after microporation. Non-microporated cells (Non-microp) and microporated with buffer R (Microp) were used as controls. MC-shGFP and si-VEGFR2 were used as negative and positive silencing controls, respectively. **(B)** MDA-MB-231 (right panel) and HUVEC (left panel) proliferation after microporation. Total number of viable cells before (0) and 2-, 4- or 7-days post-microporation is shown. Values represent the mean ± SEM of three independent experiments. No statistically significant differences were found between conditions, using a one-way ANOVA followed by a post-hoc Tukey's multiple comparison test.

The effect of the shRNA-expressing MCs on the expression levels of the specific target gene was assessed at various timepoints following microporation using RT-qPCR and ELISA (**Figure II.9 and Figure II.10**).

MC-shVEGF transfection resulted in a significant decrease of VEGF-mRNA expression in MDA-MB-231, 2 and 4-day post-microporation when compared to the control (Microp) (**Figure II.9-A**). Although not statistically significant when compared to the control, MC-shVEGF showed a significant decrease in VEGF-mRNA expression 7-days post-microporation compared to the negative control vector MC-shGFP. Transfection with MC-shGFP resulted in a slight increase in the number of VEGF-mRNA copies compared to the control at certain timepoints (**Figure II.9-A**).

MC-shVEGF induced a VEGF-mRNA knockdown of 71 ± 3.0%, 78 ± 1.4% and 45 ± 9.1% in MDA-MB-231, 2- 4- and 7-day after transfection, respectively. Overall, negative control MC-shGFP did not cause significant alterations on VEGF expression when compared to the control. MC-shVEGF-mediated VEGF silencing was comparable to VEGF knockdown induced by synthetic siRNA positive control (si-VEGF) for all timepoints tested (**Figure II.9 - A**).

The VEGF protein profiles of CM from microporated MDA-MB-231 were consistent with those obtained at the mRNA level (**Figure II.9-B)**. Cells transfected with the MC-shVEGF secreted less VEGF (19 ± 2.7 pg/10,000 cells) compared to the control (106 ± 12.5 pg/10,000 cells) (**Supplementary Figure II.3-A**), corresponding to an 82 ± 2.6% decrease in VEGF production (**Figure II.9-B**).

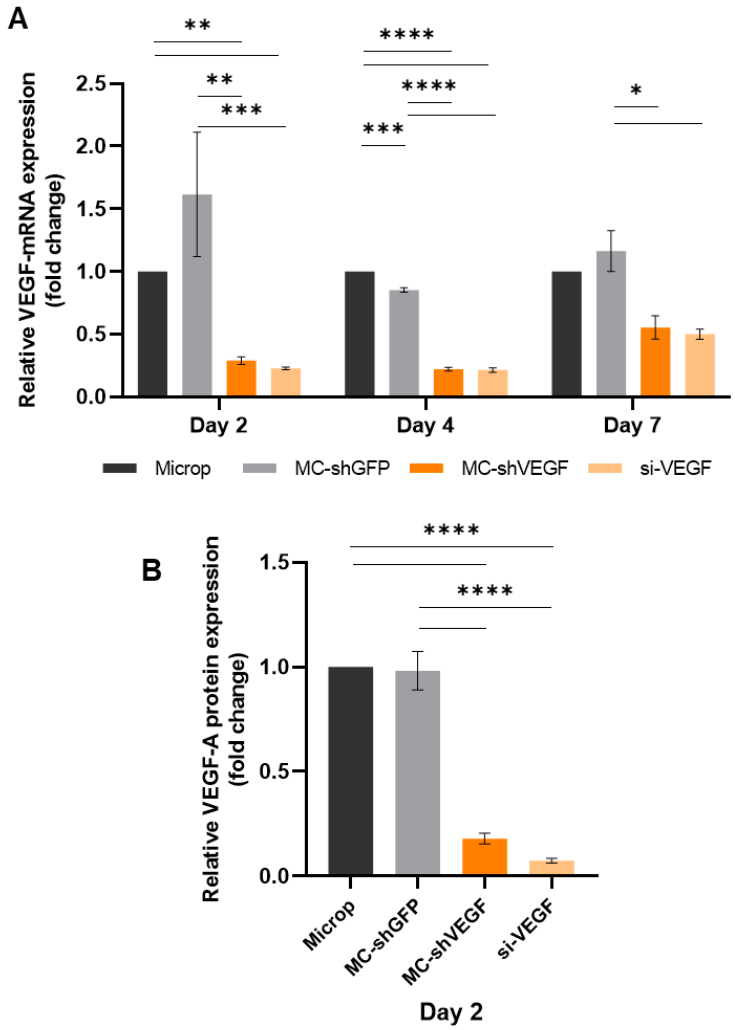

Figure II.9 – Evaluation of VEGF expression in MDA-MB-231 at different timepoints after microporation with MC-shVEGF. **(A)** Relative mRNA expression of VEGF in transfected MDA-MB-231 cells, assessed through RT-qPCR using the $2^{-\Delta\Delta Ct}$ method with GAPDH as the endogenous control gene and microporated with buffer R (Microp) as control condition. **(B)** Relative human VEGF protein levels measured in CM of transfected MDA-MB-231, using an ELISA assay. MC-shGFP and si-VEGF were used as negative and positive silencing controls, respectively. Values represent the mean ± SEM of three independent experiments. Statistical analysis was performed using a one-way ANOVA followed by a post-hoc Tukey's multiple comparisons test; *p<005, **p<0.01, ***p<0.001, ****p<0.0001.

Transfection of HUVEC with MC-shVEGFR2 resulted in a significant decrease in VEGFR2-mRNA expression when compared to the control (**Figure II.10-A**), corresponding to maximum knockdown of 55.7 ± 13.1%, 4 days after microporation. Although not statistically significant, a MC-shVEGFR2-mediated silencing effect can be observed at day 2 and even at day 7 (**Figure II.10-A**). At day 2, MC-shVEGFR2 induced a significant decrease in VEGFR2-mRNA expression compared cells microporated with the negative control MC-shGFP, which induced a slight overexpression of VEGFR2-mRNA relatively to the control (**Figure II.10-A**). Once again, MC-shVEGFR2-mediated silencing was comparable to the silencing induced by the synthetic siRNA positive control (si-VEGFR2) for all tested timepoints, except for day 2, in which the latter generated a superior knockdown (70 ± 4.5% vs 32.9 ± 10.3%, respectively) (**Figure II.10-A**).

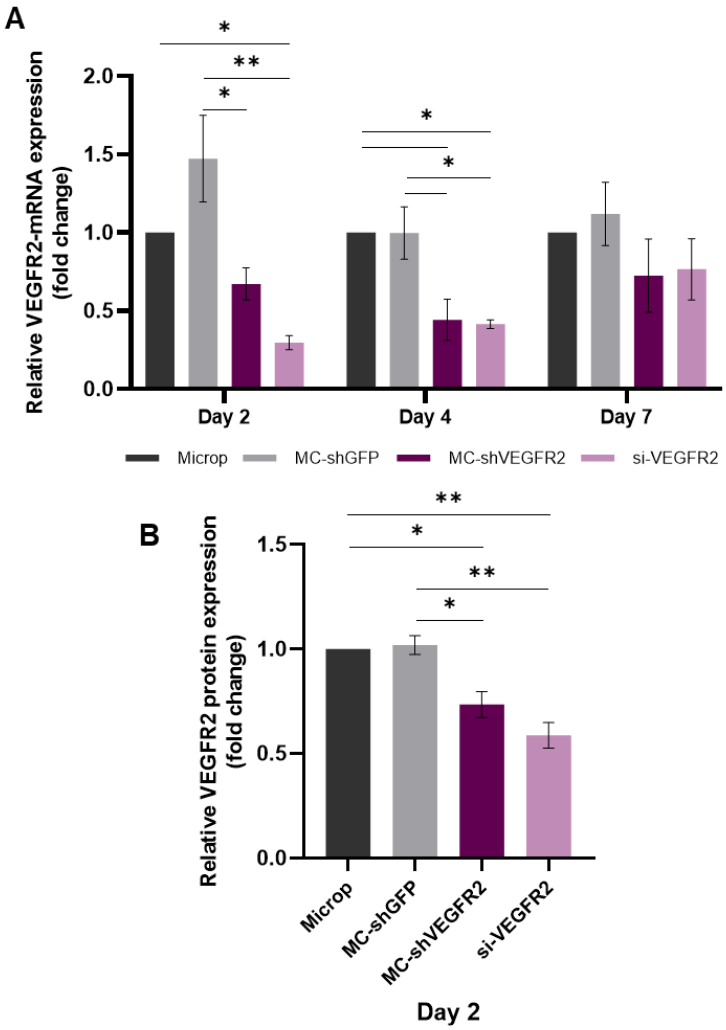

Figure II.10- Evaluation of VEGFR2 expression in HUVEC at different timepoints after microporation with MC-shVEGFR2. **(A)** Relative mRNA expression of VEGFR2 in transfected HUVEC cells, assessed through RT-qPCR using the $2^{-\Delta\Delta Ct}$ method with GAPDH as the endogenous control gene and microporated with buffer R (Microp) as control condition. **(B)** Relative human VEGFR2 levels measured in lysates of transfected HUVEC, using an ELISA assay. MC-shGFP and si-VEGFR2 were used as negative and positive silencing controls, respectively. Values represent the mean ± SEM of three independent experiments. Statistical analysis was performed using a one-way ANOVA followed by a post-hoc Tukey's multiple comparisons test; *p<005, **p<0.01.

VEGFR2-protein expression on HUVEC microporated with MC-shVEGFR2 and si-VEGFR2 was significantly decreased when compared to control conditions (Microp and MC-shGFP) (**Figure II.10-B)**. The lysates of cells transfected with the MC-shVEGFR2 contained less VEGFR2 protein (9.7 ± 2.3 pg/100,000 cells) compared to the control (13 ± 2.3 pg/100,000 cells) (**Supplementary Figure II.3-B**), representing a 27 ± 6.2% decrease in VEGFR2 expression when compared to the corresponding control. This observation is consistent with the results obtained from RT-qPCR (**Figure II.9-A,B**).

II.4.5. *In vitro* angiogenesis assays were used to evaluate the functional effect of shRNA-expressing minicircles silencing

The impact of MC silencing on the pro-angiogenic capacity of the transfected cells was evaluated through *in vitro* functional angiogenesis assays: tube formation and scratch assay [373].

To evaluate the anti-angiogenic potential of MC-shVEGF, the CM of transfected MDA-MB-231, was used to cultivate HUVEC on Matrigel coated surfaces and their re-organization capacity and formation of tube-like structures was evaluated (**Figure II.11**). Tube formation was quantitively assessed by measuring total segments length, number of junctions and number of meshes that comprise of the complete joining of multiple segments and junctions. No statistically significant differences were found between conditions in which HUVEC were cultured in CM of transfected MDA-MB-231 and negative control EBM-2. Contrarily to what was anticipated, CM from cells microporated with buffer R (Microp) that is expected to be composed of different pro-angiogenic molecules, including VEGF, showed a similar capacity to induce tube formation as the baseline EBM-2 (**Figure II.11**). For assay validation, a positive control using EGM-2 confirmed tube formation capacity by HUVEC (**Supplementary Figure II.4**). Additionally, the effect of MC-shVEGF on the capacity of MDA-MB-231 to induce cell migration/proliferation of HUVEC, and consequent closing of a scratch were also evaluated (**Figure II.12**). At 12h post-treatment with CM of transfected MDA-MB-231, no statistical differences were found between conditions and the percentage of scratch closure was comparable to EBM-2 baseline (**Figure II.12**). Moreover, after 24h of incubation, the scratch area of negative control EBM-2 and CM conditions was larger than at starting point (data not shown). Once again, this result suggests that the CM might not be sufficiently enriched in pro-angiogenic molecules or could contain factors that are repressing HUVEC functions. Overall, these preliminary results of tube formation and scratch assay indicate that further optimisation in the CM production protocol is required to allow a more sensitive analysis of the effect of MC-shVEGF-mediated silencing on the pro-angiogenic capacity of MDA-MB-231.

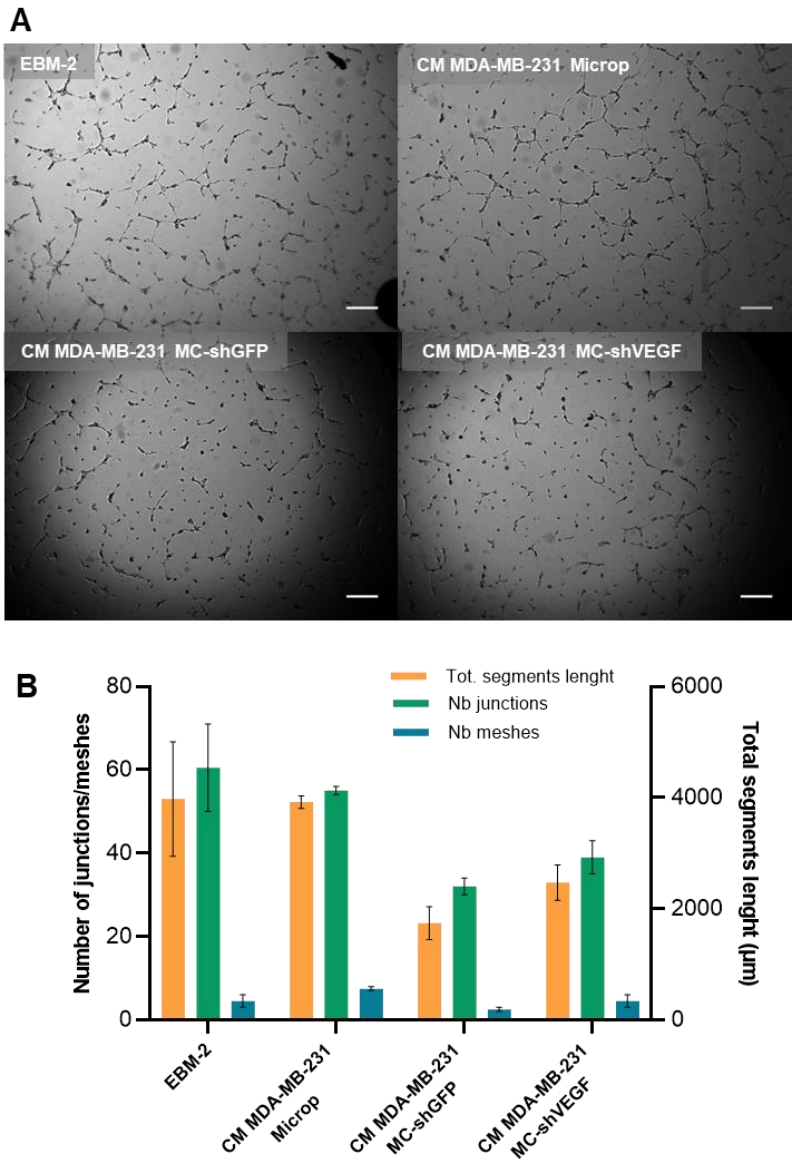

Figure II.11 - *In vitro* tube formation assay using conditioned medium (CM) of MDA-MB-231 after transfection with the MC-shVEGF. **(A)** Representative images of tube formation assay following 6h incubation of HUVEC with CM of cells transfected with MC-shVEGF. Microporated with buffer R (Microp) and MC-shGFP were used as transfection controls. EBM-2 was used as negative control of the assay. Scale bar: 250 µm. **(B)** Tube formation was quantitively assessed by measuring the number of junctions and meshes and total length of the segments formed by HUVEC 6h after incubation with the CM of transfected cells. Values represent the mean ± SEM of two independent experiments. No statistically significant differences were found between conditions, using a one-way ANOVA followed by a post-hoc Tukey's multiple comparison test.

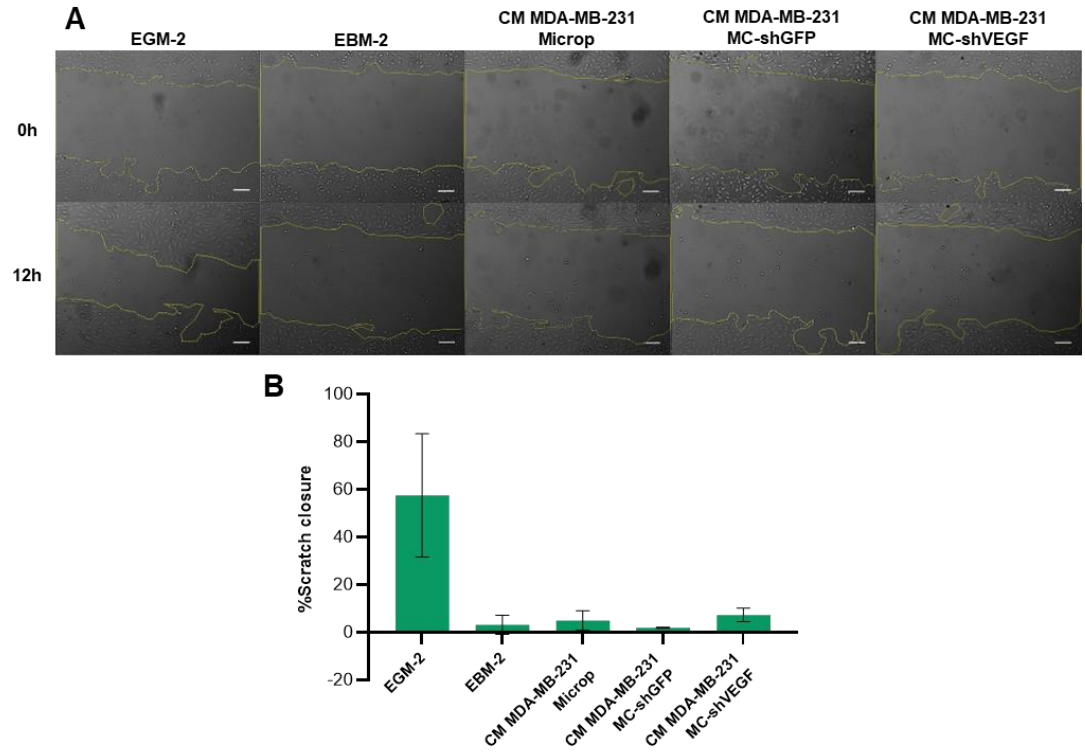

Figure II.12- Scratch assay using conditioned medium (CM) of MDA-MB-231 after transfection with the MC-shVEGF. **(A)** Representative images of scratch assay following 12h incubation of HUVEC with CM of cells transfected with MC-shVEGF. Microporated with buffer R (Microp) and MC-shGFP were used as transfection controls. EGM-2 and EBM-2 were used as positive and negative controls of the assay, respectively. Scale bar: 100 µm. **(B)** Quantification of scratch closure percentage, 12h after treatment with the CM of transfected cells. Values represent the mean ± SEM of two independent experiments. No statistically significant differences were found between conditions, using a one-way ANOVA followed by a post-hoc Tukey's multiple comparison test.

To assess the anti-angiogenic potential of MC-shVEGFR2, transfected HUVEC were cultured on Matrigel coated surfaces and scratch inserts to evaluate their capacity to form tube-like structures (**Figure II.13**) and to migrate/proliferate (**Figure II.14**), respectively, when cultured in EBM-2 supplemented 2% FBS and 30 ng/ml of VEGF. This preliminary experiment showed that HUVEC transfected with the MCs presented a reduced angiogenic capacity in the tube formation assay, by forming a lower number of junctions and meshes and shorted segments when compared to the controls non-microp and microp. Moreover, MC-shVEGFR2 appears to induce a slightly stronger effect in preventing the formation of tube-like structures in comparison to MC-shGFP (**Figure II.13**). Considering the scratch assay, HUVEC transfected with the MC-shVEGFR2 showed a reduced migration/proliferation, and consequent ability to close the scratch when cultured in medium with reduced serum content supplemented with VEGF, in comparison to control non-microp and microp and cells microporated with MC-shGFP (**Figure II.14**). After 24h of incubation, the percentage of scratch closure was ≥80% for all conditions, with the exception of HUVEC transfected with the MC-shVEGFR2 in which a ~56% closure was observed (**Figure**

II.14-B). Nevertheless, to evaluate the statistical significance of these differences and consolidate the anti-angiogenic effect of MC-shVEGFR2, replicates of these experiments need to be performed.

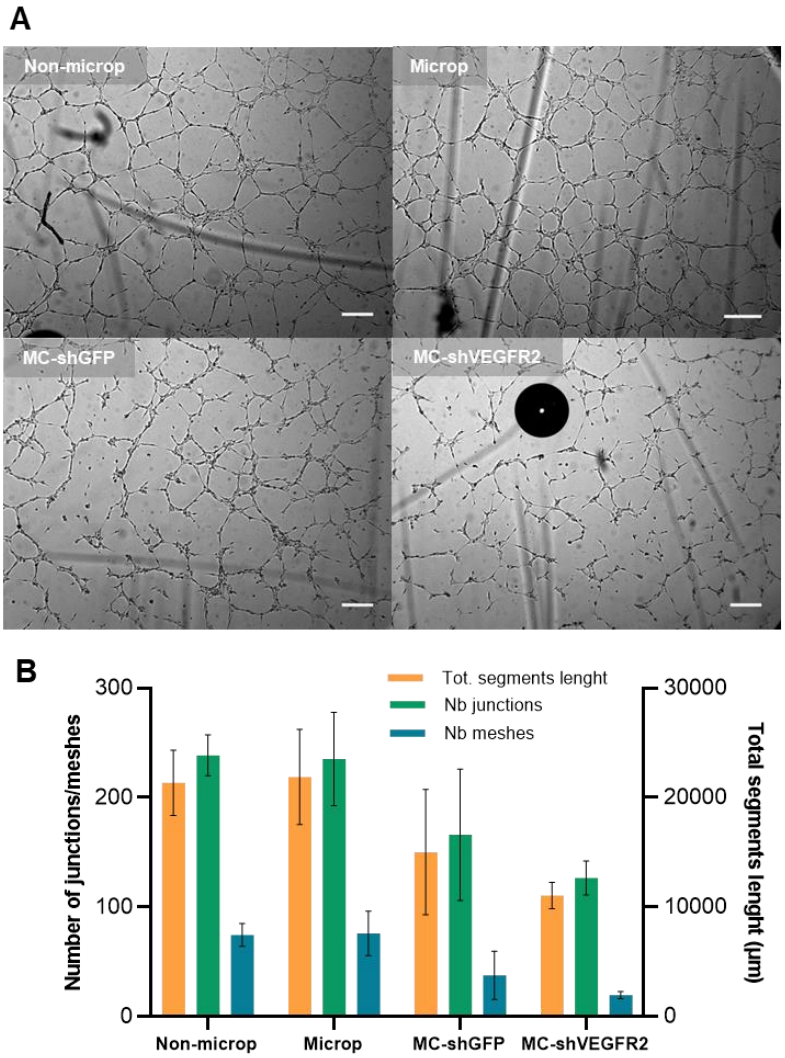

Figure II.13 - *In vitro* tube formation assay with HUVEC transfected with the MC-shVEGFR2. **(A)** Representative images of tube formation assay following 6h incubation of HUVEC transfected with MC-shVEGFR2. Non-microporated cells (Non-microp) and cells microporated with buffer R (Microp) and MC-shGFP were used as controls. Scale bar: 250 µm. **(B)** Tube formation was quantitively assessed by measuring the number of junctions and meshes and the total length of the segments formed by HUVEC after 6h of incubation. Values represent the mean ± SD of one experiment (n=3, technical replicates).

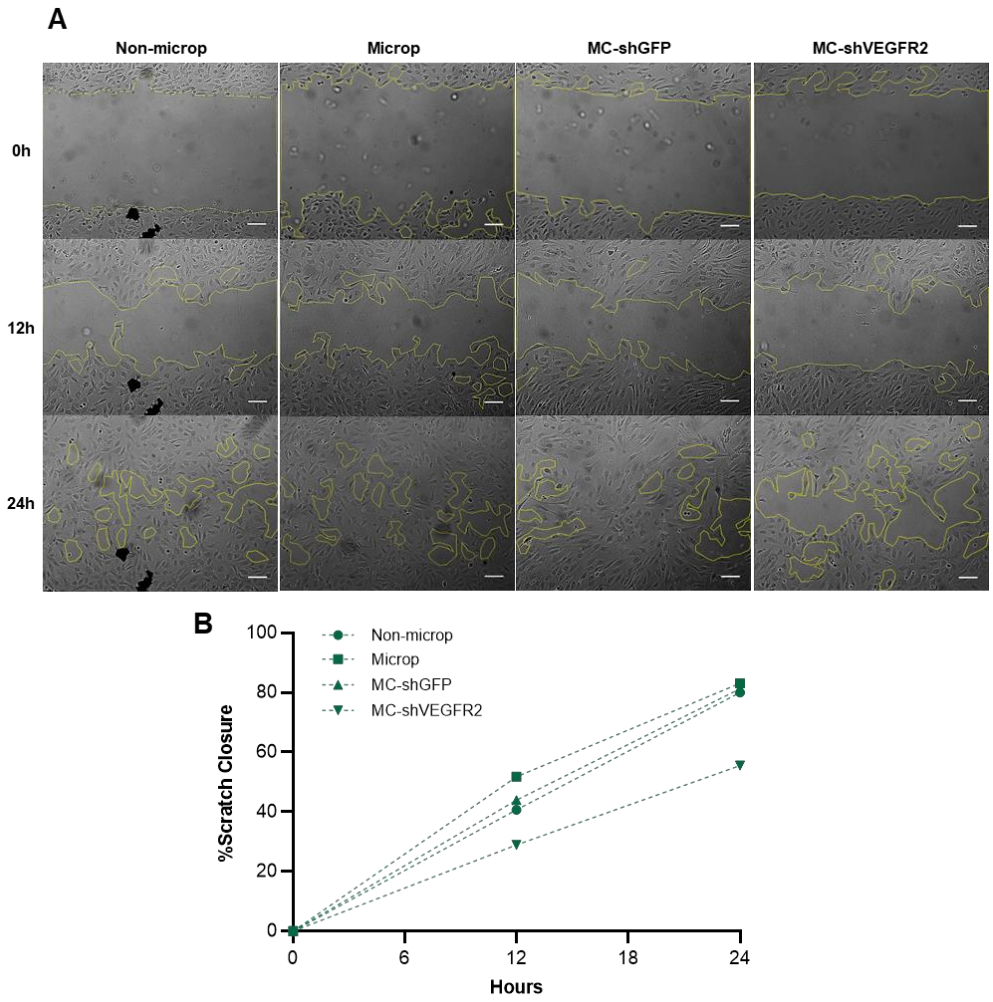

Figure II.14 - Scratch assay with HUVEC transfected with the MC-shVEGFR2. **(A)** Images of scratch assay following 24h incubation of transfected HUVEC in EBM-2 supplemented with 2% FBS and VEGF. Non-microporated cells (Non-microp) and cells microporated with buffer R (Microp) and MC-shGFP were used as controls. Scale bar: 100 µm. **(B)** Quantification of scratch closure percentage at 12h and 24h of incubation.

II.5. Discussion

Angiogenesis plays a fundamental role in physiological development and pathological conditions and is tightly regulated by a balance of angiogenic activators and inhibitors [6]. Among the pro-angiogenic factors, VEGF and its receptors hold significant importance in modulating EC functions and have become key targets for therapeutic interventions [11,12,16,17]. Current treatments utilizing inhibitors against VEGF or its receptors have shown efficacy in various angiogenesis-related disorders, including monoclonal antibodies, recombinant fusion proteins, small-molecule and aptamers [6,25]. Nevertheless, alternative anti-angiogenic agents are still under investigation envisioning increased therapeutic efficacies.

RNAi-based strategies targeting key regulators of angiogenesis have shown great promise at addressing a spectrum of angiogenesis-associated disorders [89]. Taking advantage

of the considerable expertise on plasmid and viral vector delivery field, RNAi-mediated silencing can be accomplished using expressing systems encoding shRNA that are recognised by cellular machinery and processed into functional siRNA molecules [55,351]. Plasmids are a safer, easy-to-handle alternative for therapeutic shRNA-mediated gene silencing [67–69]; however, their bacterial motifs can still induce host inflammatory responses and transcriptional episomal silencing and their bigger size reduces transfection efficiencies. [72,73,75–77]. MCs, given their small size and absence of bacterial backbone sequences, can overcome these limitations allowing for high levels of transgene expression [78,79]. Combining the prolonged biostability of plasmid DNA, gene silencing capabilities of siRNA, and improved transfection efficiency of MCs, shRNA-expressing MCs appear as a promising gene-targeting therapy [84–87]. A study comparing siRNAs, shRNA-expressing plasmid and MC, reported higher transfection efficiencies in hard-to-transfect cells for MC compared to a conventional plasmid while presenting a silencing effect equivalent to siRNAs [86]. Moreover, MC demonstrated increased stability in human serum (>48 h), compared to plasmid and siRNA which were only stable for 0.5 and 2 h, respectively [86].

In this work, shRNA-expressing MCs that silence VEGF-A (MC-shVEGF) and its receptor (MC-shVEGFR2) were developed, envisioning the establishment of a novel gene-based therapy for excessive angiogenesis disorders. This work builds upon previous studies from our group that aimed the development of scalable manufacturing processes for MC vectors [353,367] and the engineering of hard-to-transfect mesenchymal stromal cells (MSC) with MC-encoding VEGF envisioning an *ex vivo* gene therapy to enhance angiogenesis [369,380].

The widespread use of MC is limited by challenges in achieving optimal cell yields, efficient recombination, and complete purification from MPs and residual PPs. *E. coli* strains have been used for the *in vivo* recombination of the PP, through the expression of different inducible recombinases, including λ-integrase [381], Cre-recombinase [382], FLP-recombinase [383], ϕC31-integrase [384] and ParA-resolvase [385]. In this work, the production and *in vivo* recombination of the PP was accomplished using *E.coli* BW2P strain developed by our group [366] that expresses the ParA resolvase gene under the transcription control of the arabinose inducible expression system pBAD/AraC, which catalyses the intramolecular recombination between the two MRS in PP. This strain also has improved L-arabinose uptake, contributing to increased expression of resolvase [353]. Here, this producer system allowed the efficient recombination of the shRNA-expressing PP, 1h after L-arabinose induction, corroborating the previous results in which another PP was almost undetectable after 1 h and 2 h of recombination showing a 96.6% ± 2.6% recombination efficiency after 2h [353]. At the end of culture, lower quantities of MC are obtained in comparison to the MP counterparts since the latter continues undergoing replication after recombination. To facilitate the subsequent purification process of the MC, a reduced recombination time could be investigated in the future to prevent the unwanted replication of MP impurities. Overall, the recombination of the shRNA-expressing PP originated a MP of 2,108 bp and MC of 496 bp, confirming the possible application of this system to produce MC of smaller size (previously of 2,475 bp [353,367] and 1,715 bp [369]).

Unlike standard plasmid DNA, the purification of supercoiled MC is complex and faces processing challenges since MC production yields MP and residual non-recombined PPs with their corresponding topoisomers that present similar size and physicochemical properties. As a result, traditional chromatographic methods alone have been proven ineffective for MC purification and innovative strategies have been focusing on the degradation or topological modification of MP and PP impurities prior to chromatographic purification [386]. The MC purification methodology implemented herein combines the targeted relaxation of MP impurities by the action of nicking endonuclease Nb.BbvCI and multimodal chromatography [367]. In contrast to the method developed by Kay and colleagues, which rely upon *in vivo* I-SceI–mediated degradation of MP species that is encoded in the bacterial genome [387], the targeted Nb.BbvCI enzymatic relaxation occurs *in vitro*, being more easily controlled. Nb.BbvCI digestion readily converted the sc MP into the corresponding oc form, while the shRNA-expressing MC remained in its sc conformation. Afterwards, the separation of sc MC from the other isoforms in the mixture was accomplished using multimodal chromatography, and this represents the most valuable topological form for gene therapy applications [388,389]. Multimodal chromatography was performed using a series of elution steps with increasing NaCl concentrations and the N-benzyl-N-methyl ethanolamine ligand (Capto™ adhere) which features a charged nitrogen atom for electrostatic interaction, a phenyl group for hydrophobic and aromatic interactions and hydroxyl and ether groups for hydrogen bonding. The order of elution observed reflects the increasing degree of base exposure in oc DNA, sc DNA and RNA, caused by the initial bending induced by electrostatic binding of the charged nitrogen of the matrix to the phosphate backbone of the nucleic acids. The exposed bases are available for other interactions to occur, including cation-π, π-π stacking and hidrogenbonding that reinforce the electrostatic binding and generate a network of non-covalent bonds between the molecules and the matrix [367]. In fact, our results showed that the oc species elute first followed by sc MC with the increase in salt concentration, which disrupts of ionic interactions, decreasing base exposure and strength of the bond network [367]. Alternatively, hydrophobic interaction chromatography (HIC) could have been used in the final step of the purification due to its well-known ability to fractionate plasmid topoisomers and proven ability to isolated sc MCs after Nb.BbvCI action [353,369]. However, NaCl is less harmful to the environment than ammonium sulfate, which is generally used in HIC.

Altogether, this combined method was effective for the purification of MCs in their sc isoforms virtually free from MPs, PPs and RNA, which are much smaller than the ones purified previously (above 3x larger), confirming the robustness and flexibility of the process. The purified MC yields obtained herein (21.9 ± 3.79 µg/L of bacterial growth culture) are acceptable considering that the yields reported by others ranged between 0.13 mg/L and 1.5 mg/L and are tipically obtained when purifying much larger MCs with resultant final preparations often enriched in other species and isoform impurities [381,390–393]. Moreover, it is important to consider that when transfecting smaller vectors, a reduced amount is required to deliver the equivalent number of DNA molecules. Overall, this method was effective for the purification of supercoiled shRNA-expressing MCs, supporting the subsequent transfection experiments.

Transfection studies were conducted using the cancer cell line MDA-MB-231, known to secrete pro-angiogenic factors among which VEGF-A [378], and HUVEC, which have high densities of VEGF surface receptors [379], to assess the silencing effect of the MC-shVEGF and MC-shVEGFR2, respectively. Microporation was selected based on previous studies from our group aiming at achieving high cell transfection efficiencies without compromising cell viability and recovery [369,370]. This method demonstrated to be a reliable and efficient method to genetically modify MSC *in vitro* through the transfer of both MCs [369] and larger conventional vectors [368,370]. Moreover, electroporation after plasmid injection has also been an efficient *in vivo* gene delivery system [394,395]. In this work, MDA-MB-231 and HUVEC microporated without nucleic acids showed excellent cell recoveries (~95%), while those transfected with MCs demonstrated lower recoveries. Still, the latter maintained high viabilities and exhibited comparable proliferative capacity to non-microporated cells, as previously reported for microporated MSC [369,370]. Cell recoveries after transfection with MCs, were ~77% and ~60% for MDA-MB-231 and HUVEC, respectively, which are comparable to those for bone marrow MSC after transfection with a MC vector (~72%) [369].

The effect of shRNA-expressing MC on the corresponding target expression was evaluated at the mRNA and protein levels. RT-qPCR results showed that MDA-MB-231 transfection with MC-shVEGF, induced a significant decrease in VEGF expression up to 7 days, with a maximum knockdown of 78 ± 1.4% 4-days post-microporation. Moreover, 2-days after microporation, MC-shVEGF transfection induced a decrease of 82 ± 2.6% in the secreted VEGF-protein. Of notice, the negative control MC-shGFP did not lead to any significant changes in VEGF expression when compared to the control group, and the VEGF silencing induced by MC-shVEGF was similar to the silencing achieved by the positive control siRNA (si-VEGF) at all the timepoints tested. The VEGF-targeting system developed herein exerted a potent gene silencing effect in breast cancer cells which was superior to others reported using various silencing systems, cell models and transfection methods. For example, Chen and colleagues reported that the delivery of a VEGF-A-shRNA expression plasmid polyplexes into mouse colon adenocarcinoma cells, showed a knockdown of ~75%, 48 h after treatment [97]. In another study, breast cancer cells MCF7 and pancreatic cancer cells PANC-1 transfected with pDNA-encoding a shRNA targeting VEGF using RGD-conjugated polymer complexes demonstrated a maximum decreased VEGF gene expression of ~67% and ~71%, respectively [396]. Interestingly, a shRNA-expressing lentivirus vector with high gene transduction efficiency induced ~71% and ~51% at mRNA and protein level in a human pancreatic carcinoma cell line 3-days after transduction [95], which is once again comparable to our non-viral system. Concerning the MC-shVEGFR2 induced a reduction in VEGFR2-mRNA for up to 7 days, with a maximal knockdown of 56 ± 13 %, 4 days after microporation. This effect was similar to the one cause by synthetic si-VEGFR2 transfection with the exception of day 2 in which a knockdown of 77 ± 1.3 % was observed. Moreover, the silencing effect was confirmed at the protein level, in which MC-shVEGFR2 induced a 27 ± 6.2% decrease in the VEGFR2 expression by HUVEC. Considering that non-immortalised endothelial cells have been largely recognized as hard-to-transfect cells [397], our system induced a high

inhibition efficiency. Other studies have shown the potential of silencing VEGFR2 in the context of preventing tumour angiogenesis and growth or retinopathy, using synthetic siRNA molecules and lentiviral vectors [96,362]. The silencing of VEGFR-2 expression by synthetic siRNA-targeting VEGFR2 decreased ~81% of target expression in human ovarian carcinoma cell line DOV13 [362]. In another study, the expression of VEGFR2 mRNA was reduced in ~56% after rat retinal microvascular endothelial cells transduction with lentiviral vector that delivered shRNA-VEGFR2 under control of the vascular endothelial-cadherin promoter, in comparison to the empty vector [96].

Functional angiogenesis assays work as a crucial platform to evaluate the biological impact of MC-mediated VEGF-A and VEGFR-2 silencing. In this work, CM derived from MDA-MB-231 transfected with MC-VEGF was used as a treatment for tube formation and scratch assay which reflects the migration/proliferation capacity of EC. However, the established methodology failed to give conclusions regarding the effect of VEGF-silencing on EC functions, since MDA-MB-231-derived CM presented similar capacity to induce tube formation and scratch closure as the baseline EBM-2 (negative control). The first was expected to be enriched in different pro-angiogenic molecules including VEGF, as reported by others [378,398], and have an increased capacity to induce EC functions when compared to basal medium. For instance, previous studies have shown that treatment with MDA-MB-231-derived CM enhanced endothelial colony-forming cells migration through scratch closure and tube formation potential in comparison to control medium [398]. Moreover, testing a similar system, Yoo and colleagues demonstrated that the presence of CM produced by the human malignant glioma cell line U343 transduced with shVEGF-oncolytic-adenovirus disrupted the capillary-like network formed by HUVEC, significantly reducing the relative tube length by ~49%, contrasting with the organized structures formed under control conditions [399]. These preliminary results suggest that our CM production protocol needs further optimization to accurately analyse the effect of MC-shVEGF on the pro-angiogenic capacity of MDA-MB-231. For instances, alternative media for conditioning should be evaluated (e.g., DMEM supplemented with 10% FBS and L-glutamine or EBM-2 supplemented with 2% FBS and L-glutamine) and the conditioning period could also be extended (e.g., 48h) [398,399].

On the other hand, preliminary angiogenesis functional assays using HUVEC transfected with the MC-shVEGFR2 showed that transfected cells presented a reduced angiogenic capacity to form tube-like structures and to close scratches when cultured in reduced serum media supplemented with VEGF, in comparison to control cells. However, additional experiments are needed to confirm the statistical significance of these alterations and the anti-angiogenic effect of MC-shVEGFR2. On the same line of work, a previous study reported that human retinal endothelial cell transfected with aldose-reductase-targeting siRNA expressed decreased levels of VEGFR2 and showed a decreased migration capacity with incomplete wound closure (~65%) in the presence of VEGF, when compared to non-transfected and scrambled siRNA controls [400]. In another study, siRNA-mediated silencing of paxillin significantly reduced HUVEC tube formation, characterized by a decrease in tube length, in the absence or presence of VEGF-A.

Moreover, the knockdown of paxillin inhibited the VEGF-A-induced adhesion, proliferation and migration of the HUVEC [401].

Overall, although functional studies to determine the biological effect of MC-mediated VEGF-A and VEGFR2 silencing *in vitro* are still required, this work sheds light on the effectiveness and applicability of MC-derived RNAi systems in targeting pro-angiogenic molecules, emphasizing their promise as a novel non-viral, gene-based therapeutic approach for excessive angiogenesis. Importantly, by using the system established herein other pathological genes could potentially be targeted, aiming at different diseases or biological contexts other than anti-angiogenesis therapy.

II.6. Supplementary material

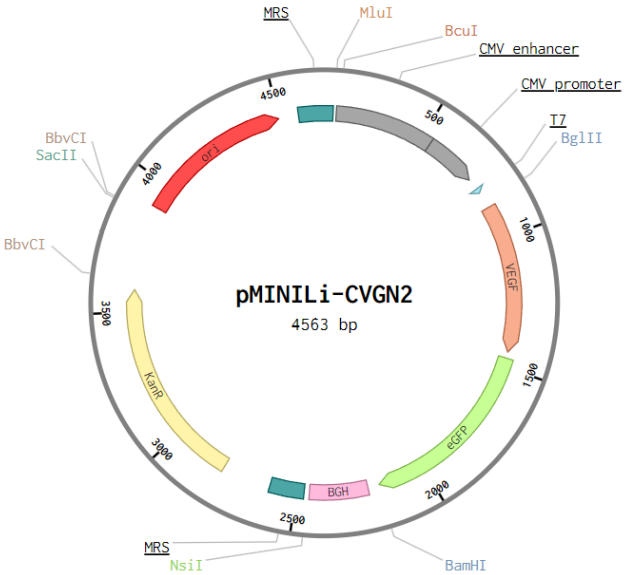

Supplementary Figure II.1 - Schematic representation of parental plasmid pMINILi-CVGN2. plasmid contains an expression cassette with a green fluorescent protein (GFP)-vascular endothelial growth factor (VEGF) gene fusion under transcriptional control of the human cytomegalovirus (CMV) immediate-early promoter and a bovine growth hormone (BGH) polyadenylation signal. The eukaryotic expression cassette is flanked by two multimer resolution sites (MRS) and the miniplasmid portion includes a pMB1 origin of replication (ori), kanamycin resistance selection marker (KanR), and a recognition site for the nicking endonuclease Nb.BbvCI.

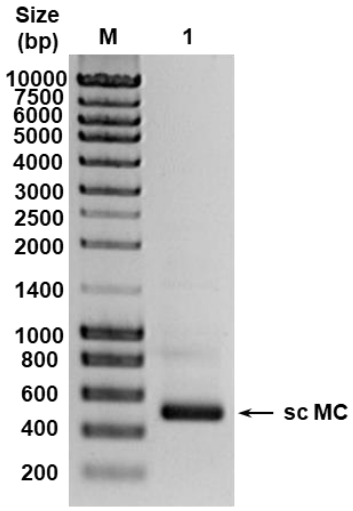

Supplementary Figure II.2 - Agarose gel electrophoresis analysis of the supercoiled minicircle originated from pU6-shGFP after diafiltration/ concentration of the multimodal chromatography fractions (1µL, lane 1). Lane M - molecular weight marker NZYDNA Ladder III (Nzytech). Abbreviations: sc MC- supercoiled minicircle.

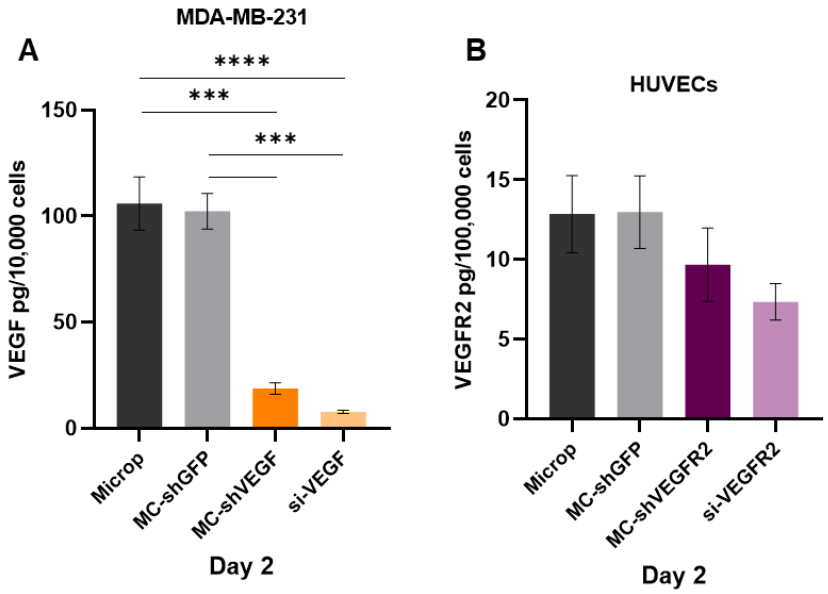

Supplementary Figure II.3 – Human VEGF-A and VEGFR2 protein levels measured after transfection of target cells with MC-shVEGF and MC-shVEGFR2, respectively, using ELISA assays. **(A)** Secreted human VEGF-A levels measured in CM of transfected MDA-MB-231; **(B)** Secreted human VEGFR2 levels measured in lysates of transfected HUVEC. MC-shGFP and si-VEGF/si-VEGFR2 were used as negative and positive silencing controls, respectively. Values represent the mean ± SEM of three independent experiments. Statistical analysis was performed using a one-way ANOVA followed by a post-hoc Tukey's multiple comparisons test; ***p<0.001, ****p<0.0001.

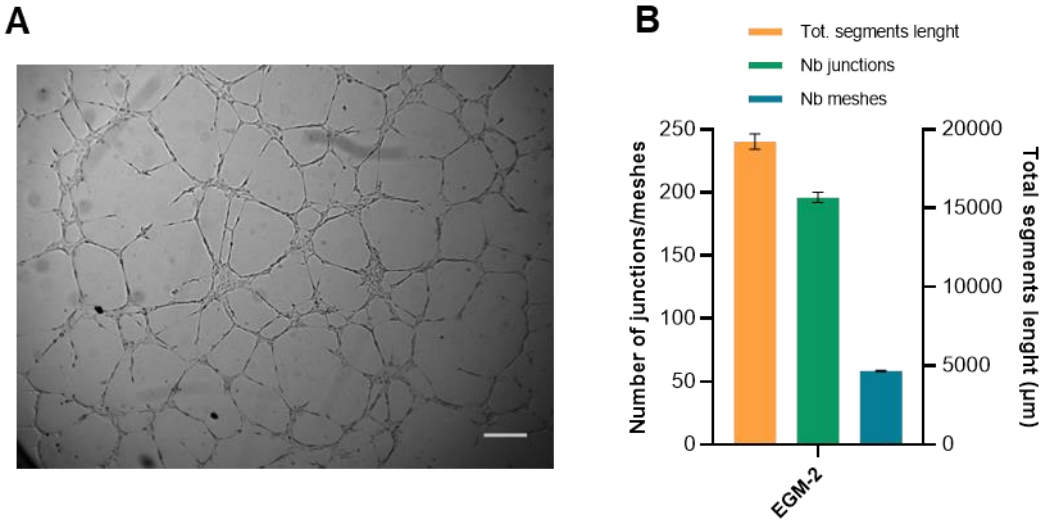

Supplementary Figure II.4 - *In vitro* tube formation assay using Endothelial Cell Growth Medium-2 (EGM-2). **(A)** Representative image of tube formation assay following 6h incubation of HUVEC with EGM-2. Scale bar: 250 µm. **(B)** Tube formation was quantitively assessed by measuring the number of junctions and meshes and total length of the segments formed by HUVEC 6h after incubation with EGM-2. Values represent the mean ± SEM of two independent experiments.

Chapter III.

MANUFACTURING OF MESENCHYMAL STROMAL CELL-DERIVED EXTRACELLULAR VESICLES IN A STIRRED TANK REACTOR SYSTEM

The contents of this chapter will be partially published as:

Ulpiano, C., Salvador, W., Franchi-Mendes, T., Lin, C., Milligan, W., Rodrigues, C.A.V., Cabral, J.M.S., Fernandes-Platzgummer, A., Monteiro, G. A., da Silva, C.L. Continuous collection of human mesenchymal stromal cell-derived extracellular vesicles manufactured in stirred-tank reactors under xenogeneic-free conditions (to be submitted).

III.1. Abstract

Mesenchymal stromal cell (MSC)-derived extracellular vesicles (MSC-EVs) are an important component of the paracrine action of MSC and have demonstrated beneficial effects in various pre-clinical disease models. However, most studies still use planar culture systems and fetal bovine serum (FBS)-supplemented culture media formulations for MSC manufacturing, along with non-scalable low-purity grade methods for EV isolation, failing to meet the necessary doses and safety requirements and thus hindering the clinical translation of MSC-EVs.

In this work, we established a platform for the manufacturing of MSC-EVs by integrating fully scalable upstream and downstream processes able to comply with Good Manufacturing Practices (GMP) standards. Wharton's jelly-derived MSC (MSC(WJ)) were expanded using Dissolvable microcarriers in a controlled stirred tank bioreactor operated under combined fed-batch and perfusion mode using human platelet lysate (hPL)-supplemented medium. Then, a 3-day EV production stage, featuring continuous harvesting of the conditioned medium (CM), was established using a novel serum-/xeno(geneic)-free exosome depleted-hPL supplement. For the isolation of MSC-EVs from the CM, a scalable process was implemented by pairing tangential flow filtration (TFF) and anion-exchange chromatography (AEC). Isolated MSC-EVs were characterised using nanoparticle tracking analysis, protein and zeta potential quantification, western blot analysis of EV protein markers, transmission electron microscopy and uptake studies of fluorescently labelled-EV by target cells.

The developed system sustained the efficient expansion of MSC(WJ), reaching a total of $(6.0 \pm 0.18) \times 10^7$ cells after 7 days, which represents a ~30-fold expansion. Upon a 3-day continuous harvesting of CM, EVs were isolated by TFF/AEC and particle quantification confirmed the total collection of $(1.9 \pm 0.38) \times 10^{12}$ EVs without compromising the integrity and particle secretion rate of MSC(WJ), corresponding to the manufacturing of $(1.2 \pm 0.31) \times 10^4$ EVs/cell/day. MSC-EVs presented high purity levels ($(5.7 \pm 2.7) \times 10^9$ particles/μg), a homogeneous small size distribution with a mean diameter of ~120 nm, a surface charge of ~-23mV, positive detection of tetraspanins CD9 and CD63 and syntenin-1 and displayed a typical cup-shaped morphology. MSC-EVs were readily incorporated by endothelial cells and two human breast cancer cell lines.

Overall, the platform established herein allowed reproducible, high-yield manufacturing of clinically relevant numbers of MSC-EVs with high purity and generally accepted characteristics concerning size, surface charge, morphology and cellular internalisation that validate their potential application as natural therapeutics or drug delivery vehicles.

III.2. Background

Extracellular vesicles (EVs) are small membrane-enclosed structures of 50 – 1,000 nm in diameter that are actively secreted by cells and harbour a variety of biologically active molecules, including proteins and nucleic acids [104]. Although originally identified as cellular waste, EVs are currently established as essential mediators of cell-cell communication that can induce alterations in nearby or distant recipient cells [104,108]. EVs have the innate capacity to efficiently cross biological barriers and demonstrate reduced immunogenicity/toxicity, therefore being extensively investigated as potential therapeutics and natural drug delivery vehicles [105,110,112].

Mesenchymal stromal cells (MSC) are one of the most explored EV-producing cell types for biomedical applications [280]. MSC-derived EVs (MSC-EVs) are an important component of the paracrine action of MSC on tissue repair and regeneration [402]. Like their parental cells, MSC-EVs demonstrate immunomodulatory and anti-apoptosis properties and the ability to regulate endogenous cell functions [276,403]. In addition, MSC-EVs can be bioengineered to enhance their therapeutic cargo and increase their selectivity toward target cells, which has been shown to improve their therapeutic potential in numerous pre-clinical animal models [109]. MSC have been extensively tested in clinical trials for numerous conditions, demonstrating their safety [272,273,404]. Besides sharing this attribute, MSC-EVs do not self-replicate and have a lower risk of microvasculature entrapment, making them potentially safer than MSC [277,278]. Furthermore, MSC-EVs can be easily handled and endure different types of preservation [279]. Overall, these features suggest that MSC-EVs are a suitable candidate for off-the-shelf cell-free therapeutics.

MSC-EVs have demonstrated great beneficial effects in a variety of pre-clinical disease models, either as natural therapies or drug delivery vehicles [109,274]. For instance, MSC-EVs have been shown to reduce peribronchial and perivascular inflammation in a mouse model of chronic obstructive pulmonary disease [405] and promote neuroregeneration and modulate peripheral immune responses in a mouse model of ischemic stroke [406]. In another study, MSC-EVs exogenously loaded with a small drug norcantharidin exerted significant anti-tumour effects and induced hepatocyte repair in a mouse model of hepatocellular carcinoma [324]. As yet another example, in a collagenase-induced osteoarthritis mouse model, EVs generated from miR-92a-3p-expressing MSC demonstrated improved cartilage formation and delayed its degradation [302].

In clinical settings, large doses of MSC-EVs are required, ranging from 10^{10} to 10^{11} total administrated vesicles [127]. For example, an ongoing trial for the treatment of acute respiratory distress syndrome (ARDS) (NCT04602104) is administering a daily aerosol inhalation of $1.6x10^{9}$ MSC-EVs for a week, while an ongoing trial for the treatment of osteoarthritis (NCT05060107) is applying a single intra-articular injection of $5x10^{11}$ MSC-EVs. In stark contrast, standard EV manufacturing processes present low EV yields, poor purity levels and lack scalability (e.g., conventional planar culture systems such as T-flasks, polymer-based precipitation methods and ultracentrifugation), therefore hindering MSC-EV translation to the clinic [130]. Thus, a large-scale

MSC-EV manufacturing workflow, including scalable upstream and downstream processes, needs to be implemented to generate high EV yields with great purity levels [130].

Concerning large-scale MSC culture, the use of bioreactor platforms combined with microcarriers is a promising strategy for increasing cell density, as well as sustaining the subsequent production of large volumes of EV-enriched conditioned medium (CM) [130]. Microcarriers provide surface area for MSC adhesion and growth under suspension conditions, while offering a high surface-area-to-volume ratio [143]. Multiple microcarrier-based stirred platforms have been implemented to maximise MSC expansion and MSC-EV production, including spinner flasks [144–146] and vertical-wheel systems [133,147,148]. Stirred-tank reactors (STR) further improve EV yields and process standardisation by continuously monitoring and control of the cell culture microenvironment, namely temperature, dissolved oxygen and pH [149–151]. Moreover, shear stress associated with dynamic stirred culture conditions promotes higher EV secretion from MSC when compared to static conditions [133,144,147,150,151]. Hollow-fiber bioreactors are an alternative when upscaling MSC-EV production, accommodating high cell densities and multiple-day continuous retrieval of EV-enriched CM [141,407], but the impossibility of *in situ* cell growth monitoring, lack of homogeneity in the extracapillary space and difficulties in cell harvesting remain significant limitations.

Aside from the culture platform, another important factor to keep in mind when upscaling MSC-EV production is the MSC source used, since cell doubling rates and EV secretion differ notably across sources, impacting final product costs [130,133]. Some studies have reported that umbilical cord-derived MSC produce the highest EV yields when compared to MSC isolated from adipose tissue (MSC(AT)) and bone marrow (MSC(M)) [133,134], making this a particularly advantageous source. Equally important is the selection of a suitable culture medium formulation, with the use of serum-/xeno(geneic)-free (S/XF) options being indispensable when moving towards Good Manufacturing Practices (GMP) compliant conditions. However, most preclinical studies still employ fetal bovine serum (FBS)-containing media formulations [166]. In addition, during the conditioning periods for EV-enriched CM collection, it is also essential to employ a culture medium depleted of EVs to avoid cross-contaminating the final preparation, while not compromising cell fitness and EV productivity, in order to conserve process efficiency [166,168].

Our group has previously established platforms for MSC expansion and subsequent EV isolation combining different sources of MSC and serum-free/xeno-free culture media in stirred systems [133,146,149]. Recently, our group reported an efficient system for MSC(WJ) expansion under S/XF conditions using Dissolvable microcarriers (DMC) and scalable spinner flasks. With the implemented intermittent agitation regimen, MSC(WJ) adhesion rates were over 90% at day 1, yielding a ~16-fold expansion after 6 days of culture, corresponding to full and homogeneous occupancy of the microcarriers. Moreover, this culture platform allowed a subsequent 24h EV production stage, by switching to a basal medium formulation, without compromising MSC(WJ) integrity [146]. Using an alternative S/XF strategy, a single-use vertical-wheel culture system was implemented for MSC expansion and EV production employing human platelet lysate (hPL) supplementation for the cell expansion stage and basal DMEM for the subsequent 48h

conditioning period [133]. A comparison between MSC isolated from three sources (bone marrow, adipose tissue and umbilical cord derived-WJ) and static and dynamic conditions demonstrated that MSC(WJ) cultured under stirred conditions yield the highest EV concentrations [133], which is aligned with previous findings [144].

Following upstream processing, a scalable downstream process that includes the concentration and separation of EVs from the contaminants present in the CM is required to manufacture MSC-EVs at a clinical scale. The most widely used isolation process is still ultracentrifugation, despite the recognized limitations among which are potential incomplete contaminant separation, long dead-end times and lack of scalability [130,181,182]. Other methods for EV isolation have proved to feature easier scalability, including filtration and chromatography-based techniques. Tangential flow filtration (TFF) is a suitable method for large-scale EV isolation, allowing the processing of larger volume samples in a time-efficient and reproducible manner, thus generating high EV yields [187]. For additional purity, TFF can be combined with distinct chromatography techniques, relying on size, charge or affinity to separate EVs from residual proteins and other biomolecular contaminants [166,187]. Among these, size-exclusion chromatography (SEC) is the most frequently combined technique. Similar to TFF, SEC separates EVs based on their molecular size or hydrodynamic volumes, rendering EV preparations with high yields and improved purity without compromising their morphological integrity [187,189,190]. Alternatively, anion-exchange chromatography (AEC) exploits the interactions between negatively charged EVs and an anion exchanger with positively charged functional groups or cations [187]. This technique has already been used to isolate EVs from cell cultures, showing increased EV recoveries compared to other isolation methods, such as ultracentrifugation and ultrafiltration coupled with SEC [189,408].

In this work, we implemented a platform for continuous harvesting of EVs using a microcarrier-based STR culture system in order to maximize MSC-EV production yields. After preliminary experiments under static conditions and using spinner flasks, we established a platform for manufacturing MSC-EVs by integrating fully scalable upstream and downstream processes. Umbilical cord-derived Wharton's jelly MSC (MSC(WJ)) were used for the robust production of EVs, combining Dissolvable microcarriers (DMC), S/XF exosome-depleted hPL supplemented medium and a fully controlled STR. This system sustained the efficient expansion of MSC followed by a 3-day perfusion EV production stage in stirred conditions, without compromising the integrity of the producing cells. For the isolation of MSC-EVs, a scalable process was implemented by pairing TFF and AEC. Overall, our platform allowed reproducible, high-yield manufacturing of MSC-EVs with consistent and generally accepted characteristics concerning size, surface charge, purity, morphology and cellular internalization, while being able to comply with GMP standards.

III.3. Materials and methods

III.3.1. MSC(WJ) isolation and expansion under static conditions

MSC were isolated from the Wharton's Jelly of human umbilical cord samples in hPL-supplemented medium according to the protocol described by Soure *et al.* [409]. Samples were obtained from healthy donors after written informed consent according to Directive 2004/23/EC of the European Parliament and of the Council of 31 March 2004 on setting standards of quality and safety for the donation, procurement, testing, processing, preservation, storage and distribution of human tissues and cells (Portuguese Law 22/2007, June 29), with the approval of the Ethics Committee of the respective clinical institution (Protocol iBB/SGO-CHLO nº. 1277, May 2012). Cryopreserved MSC(WJ) were thawed and plated on T-flasks at a cell density of 3,000 cells/cm^2 and cultured in low glucose Dulbecco's Modified Eagle's Medium (DMEM) (Gibco, Life Technologies), supplemented with 5% (v/v) of hPL UltraGRO™-PURE gamma-irradiated (GI) (AventaCell Biomedical) and 1% (v/v) antibiotic-antimycotic (A/A) (Gibco, Life Technologies) (DMEM-hPL). Cells were maintained at 37ºC and 5% CO_2 in a humidified atmosphere. At 80% confluency, MSC(WJ) were detached with TrypLE™ Select Enzyme, 1x (Gibco, Life Technologies) for 7 min at 37ºC. Cell number and viability were estimated using the Trypan Blue Solution, 0.4% (Gibco, Life Technologies) exclusion method.

III.3.2. MSC-EV containing conditioned medium (CM) production under static conditions

MSC(WJ) were seeded onto 6-well plates at 3,000 cells/cm^2 and cultured for 4-5 days (>90% confluency) in DMEM-hPL. Afterwards, culture medium was removed and cells were washed twice with 1x phosphate-buffered saline (PBS), before subsequently being cultured in DMEM supplemented with 5% (v/v) of Exosome depleted hPL UltraGRO™-PURE GI (AventaCell Biomedical) and 1% (v/v) A/A (DMEM-hPL-EVd) for CM production. CM was collected at 24h, 48h and 72h timepoints in two different modes; (i) without any medium renewal throughout 3 days; and (ii) with medium renewal every 24h. MSC-EV containing CM was centrifuged at 2,000xg for 15 min, filtered using Millex-HV Syringe Filter Unit with Durapore® PVDF membrane, 0.45 µm (Millipore), and stored at -80ºC until total particle number quantification using nanoparticle particle analysis (NTA), as described in section III.3.8.1.

III.3.3. MSC(WJ) expansion and MSC-EV production in spinner flasks

MSC(WJ) from three independent donors (passages 4-5) were used to inoculate the spinner flasks. Corning® Dissolvable microcarriers (DMC), composed of polygalacturonic acid and pre-coated with Synthemax II, were weighed to achieve an area of 540 cm^2 and were hydrated according to manufacturer's instructions. After microcarriers addition to the spinner flasks, 1x10^6 MSC were added to the vessels (Bellco Glass, 100 mL), equipped with 90º paddles,

radial flow, and a magnetic stir bar with an initial working volume of 40 mL, corresponding to a seeding density of approximately 1,850 cells/cm^2. The spinner vessel was previously treated with with Sigmacote® (Sigma-Aldrich). A summary of the agitation regimen, culture volume and medium exchange are depicted in **Table III.1**. Briefly, during the 6/7-day expansion stage, MSC(WJ) were cultured in DMEM-hPL with an intermittent agitation regime of 5 min at 40 rpm and 30 min at 0 rpm. Fresh culture medium was added and changed throughout expansion as detailed in **Table III.1**. After expansion, cell-containing microcarriers were washed twice with 40 mL of PBS and resuspended in DMEM-hPL-EVd to complete a working volume of 40 mL. During the 3-day MSC-EV production stage, the agitation was set to 50 rpm and CM was collected and replaced every 24h. Each day, MSC-EV containing CM was precleared from cell debris by centrifugation at 2,000xg for 15 min, followed by filtration using a Stericup® Quick Release Durapore® PVDF membrane 0.45 µm (Millipore) bottle-top filter and stored at -80 ºC until total particle number quantification using NTA and EV isolation.

Table III.1 - Culture parameters used in the microcarrier-based expansion of MSC(WJ) and subsequent EV production in the spinner flask culture system, including the culture time, agitation regimen, culture media and working volume implemented at each stage.

Culture parameter	**MSC expansion (6/7 days)**			**EV production (3 days; 24h-batches)**
Agitation regimen	Intermittent cycles: 5' at 40 rpm; 30' at 0 rpm			50 rpm
Culture medium	DMEM + 5% hPL UltraGRO™-PURE GI			DMEM + 5% Exosome depleted hPL UltraGRO™-PURE GI
Working volume (mL)	40 (day 0-1)	50 (day 2)	80 (day 3 – onwards) 50% medium change on day 5	40

III.3.4. MSC(WJ) expansion and CM production in stirred-tank reactors

MSC(WJ) from three independent donors (passages 4-5) were cultured for 10 days in a 250 mL glass DASbox® Mini Bioreactor System (Eppendorf) equipped with an 8-blade 60°-pitch impeller and sensors for monitoring temperature, pH and dissolved oxygen (DO). The glass vessel was treated with Sigmacote® before use. DASware® control software (Eppendorf™) was employed to control the process parameters within the chosen set points (T= 37 ºC and pH= 7.2). Oxygen was supplied to the stirred tank reactor (STR) by the introduction of 100% air, corresponding to 21% pure O_2, through the headspace. A schematic workflow of the culture parameters used in the MSC(WJ) expansion and MSC-EV production stages in a fully controlled STR system is depicted in **Figure III.1**. Briefly, two million cells were seeded onto 1,080 cm^2 of Synthemax II–coated DMC (Corning®), corresponding to a seeding density of approximately 1,850 cells/cm^2, and inoculated into the STR with an initial working volume of 80 mL. During the 7-day cell expansion stage, MSC(WJ) were cultured in DMEM-hPL with an intermittent agitation regime of 5 min at 50 rpm and 30 min at 0 rpm [146]. From day 1 to day 4, continuous fed-batch

was performed at a constant rate of 1.92 mL/h until reaching a volume of 160 mL. From day 5 to day 7, medium perfusion at a constant rate of 3.33 mL/h was carried out until completely replacing the medium. A micro sparger with a pore size of 10 µm was employed as a filter to ensure the retention of microcarriers during perfusion. Before the subsequent MSC-EV production stage, cell-containing microcarriers were washed with 200 mL of PBS and resuspended in 100 mL DMEM-hPL-EVd. During the 3-day MSC-EV production stage, the agitation was set to 60 rpm and CM was collected through perfusion at a rate of 8.33 mL/h which corresponds to a production of 200 mL of CM per day. Each day, MSC-EV-containing CM was precleared from cell debris and stored as described above.

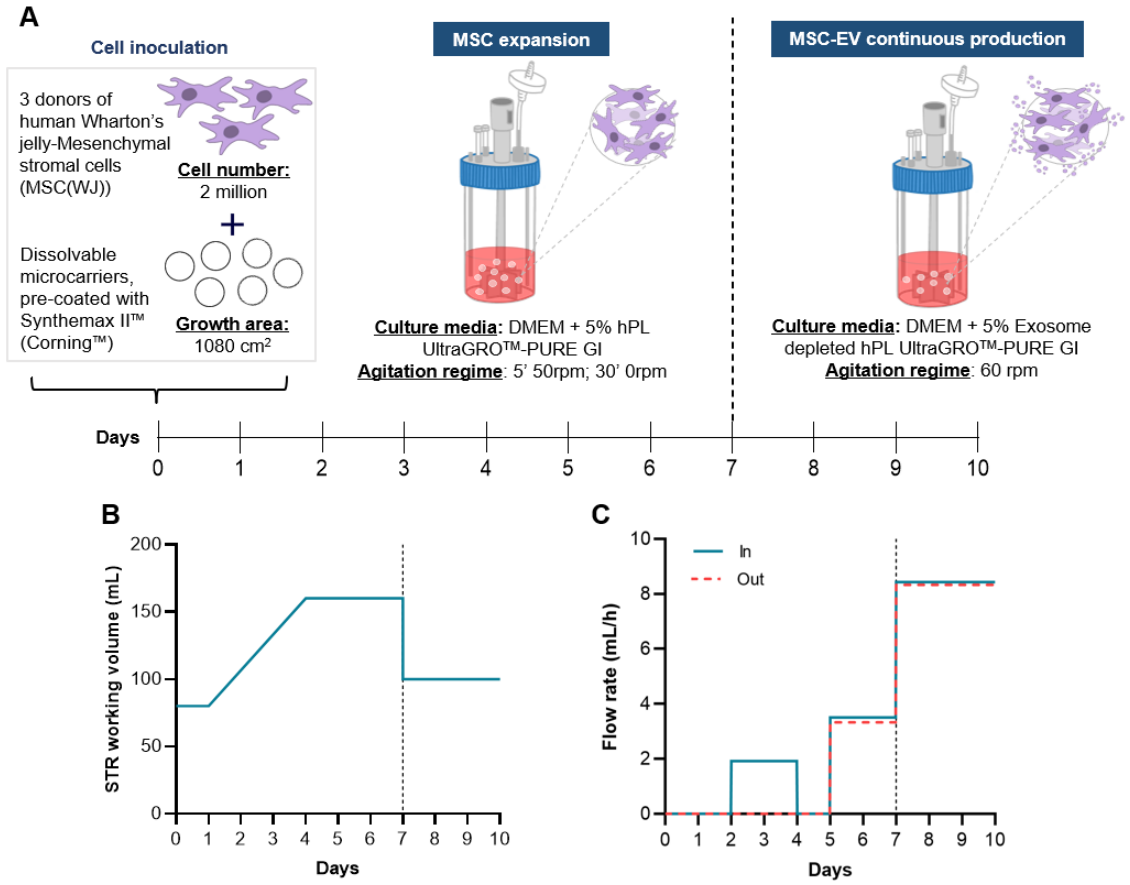

Figure III.1 - Schematic workflow of the culture parameters used in the microcarrier-based expansion of MSC(WJ) and subsequent EV production in a fully controlled stirred-tank reactor (STR) system. **(A)** Schematic representation of cell inoculation conditions, culture medium and agitation regimens implemented throughout the MSC(WJ) expansion and MSC-EV production stages. **(B)** STR working volume during MSC(WJ) expansion and MSC-EV production (stages are separated by the dashed line). **(C)** Culture medium flow rate in and out of the STR during MSC(WJ) expansion and MSC-EV production (stages are separated by the dashed line).

III.3.5. Monitoring of culture parameters and cell imaging on microcarriers

III.3.5.1. Cell number quantification

Throughout the stirred cultures, cell number assessment was performed as described in Bandarra-Tavares *et al*. [146] by collecting two independent 1 mL samples of MSC(WJ) culture from the STR at 60 rpm. For cell detachment, microcarriers were washed twice with PBS and enzymatically digested, for 7 min at 37 ºC and 600 rpm in Thermomixer® comfort (Eppendorf AG), with 0.5 mL of a solution composed of 2.6% Pectinase (Sigma-Aldrich), 2% EDTA (Sigma-Aldrich) and 95.4% TrypLE™ 1x (Gibco). The reaction was stopped by adding 1 mL of DMEM-hPL and the total number of viable cells was estimated using the Trypan Blue exclusion method. The specific growth rate (μmax) and doubling time (td) of MSC(WJ) during the exponential growth phase were calculated as described in Fernandes-Platzgummer *et al.* [149].

III.3.5.2. Glucose and lactate concentrations analysis

For glucose and lactate monitoring, the supernatant of the samples of MSC(WJ) culture was collected daily and centrifuged at 360 x g for 10 min. Glucose and lactate concentrations were determined through membrane-bound immobilized enzyme quantification using the YSI 2500 Biochemistry Analyser (Yellow Springs Instrument).

III.3.5.3. Cell viability and distribution on the microcarriers

Additional 0.5 mL samples of MSC(WJ) culture were collected for cell imaging on microcarriers. Cell distribution on the microcarriers was evaluated by nuclei staining with 4′,6-diamidino-2-phenylindole (DAPI) (Sigma-Aldrich) at 1 μg/mL. Cell viability on microcarriers was assessed by staining viable cells with Calcein-AM (Sigma-Aldrich) at 1 μM. Additionally, on day 10 of STR culture, dead cells were stained using ethidium homodimer III (EthD-III) at 1 μM. Images were acquired using a fluorescence microscope DMI 3000B (Leica).

III.3.6. MSC(WJ) harvesting and characterization after STR culture

At the end of the STR culture (day 10), MSC(WJ) were harvested from the microcarriers inside the STR vessel. After CM harvesting through the perfusion filter, cell-containing microcarriers were washed with 200 mL of PBS and subsequently digested with 55 mL of microcarrier dissolution solution at 37ºC and 100 rpm for 15-20 min, resulting in cell detachment. The reaction was stopped by adding 55 mL of DMEM-hPL and MSC(WJ) were centrifuged and collected for further characterization according to the criteria defined by the International Society for Cell and Gene Therapy (ISCT) Committee [259]. Immunophenotypic analysis of MSC(WJ) was performed by flow cytometry with a panel of anti-human monoclonal antibodies: CD90-PE, CD44-PerCP-Cy5.5, CD73-FITC, CD105-PE, CD34-FITC, HLA-DR-FITC, CD80-PE, CD45-PerCP-Cy5.5, CD19-FITC (Becton Dickinson, BD). LIVE/DEAD™ Fixable Far Red Dead Cell

Stain Kit (Invitrogen, Life Technologies) was used to assess cell viability. Samples were acquired with a minimum of 10,000 events using a BD FACSCalibur™ Flow Cytometer (BD) and data was analysed using FlowJo™ Software (BD).

MSC(WJ) multilineage differentiation capacity was also evaluated. For osteogenic and adipogenic differentiation, MSC(WJ) were seeded onto 24-well plates at 3,000 cells/cm^2 and cultured for 4-5 days in DMEM-hPL. Afterwards, the culture medium was replaced by respective differentiation medium, StemPro™ Adipogenesis Differentiation Kit or StemPro™ Osteogenesis Differentiation Kit (Gibco). For chondrogenic differentiation, spheroids composed of 100,000 cells were generated by applying the hanging-drop technique. After 24h, the spheroids were placed on ultra-low attachment 24-well plates (Corning) with Mesencult™-ACF Chondrogenic Differentiation Kit (STEMCELL Technologies) medium. Differentiation medium was replaced twice a week for 21 days. Following this, adipocyte-produced lipid droplets were stained with Oil Red O, osteocyte progenitors were stained with alkaline phosphatase (ALP) and chondrocyte-secreted extracellular matrix proteins were stained with Alcian Blue as described in Santos *et al.* [410].

III.3.7. Isolation of MSC-EVs from conditioned media

The CM collected from the stirred cultures (i.e., 3 day - conditioning phase) was thawed on ice and pooled for MSC-EV isolation. A schematic representation of the EV isolation process is represented in **Figure III.2.** The employed EV purification method was adapted from Silva *et al* [408]. Firstly, using a Minimate™ EVO TFF system, the of CM was concentrated/diafiltrated using a Minimate™ 100 kDa MWCO Omega™ Membrane (Cytiva) to a volume of 50 mL of nuclease buffer composed of 50 mM Tris-HCl (Fisher Scientific), 20 mM NaCl (Fisher Scientific), pH 8. The diafiltrated sample was then supplemented with 5 mM of $CaCl_2$ and digested with 5U/(mL of initial CM) of Micrococcal nuclease (MNase) for 75 min at 37^{o}C with 600 rpm agitation in Thermomixer® comfort (Eppendorf AG). Afterwards, the digested sample was concentrated/diafiltrated to a volume of 20 mL of chromatography buffer A (50 mM HEPES, 20 mM NaCl, pH 7). Subsequently, AEC was performed using a Triton 5/50 column (Cytiva) packed with 1 mL of Capto™ Q ImpRes resin (Cytiva) connected to an ÄKTA Purifier 10 system (Cytiva). The column was pre-equilibrated with a buffer composed of 50 mM HEPES, 180.7 mM NaCl, pH 7, (10.5% buffer B (50 mM HEPES, 2M NaCl, pH 7), ≈23 mS/cm). The EV-containing sample was pre-conditioned with 10.5% buffer B and two and three chromatographic runs using a 10 mL volume sample were performed for EV-samples from spinners and STR, respectively. Unbound material was washed with 15 column volumes (CV) of 10.5% B, and stepwise elution was completed with 10 CV of 60% B (≈95/100 mS/cm) and 7 CV of 100% B (≈142/150 mS/cm). Finally, the EV-containing fractions were concentrated/diafiltrated to a volume of approximately 0.5 mL in PBS using an ultrafilter with a molecular weight cut-off of 30 kDa (Amicon® Ultra-4, Merck Millipore) previously passivated overnight with a solution 5% (v/v) Tween-20 in distilled water.

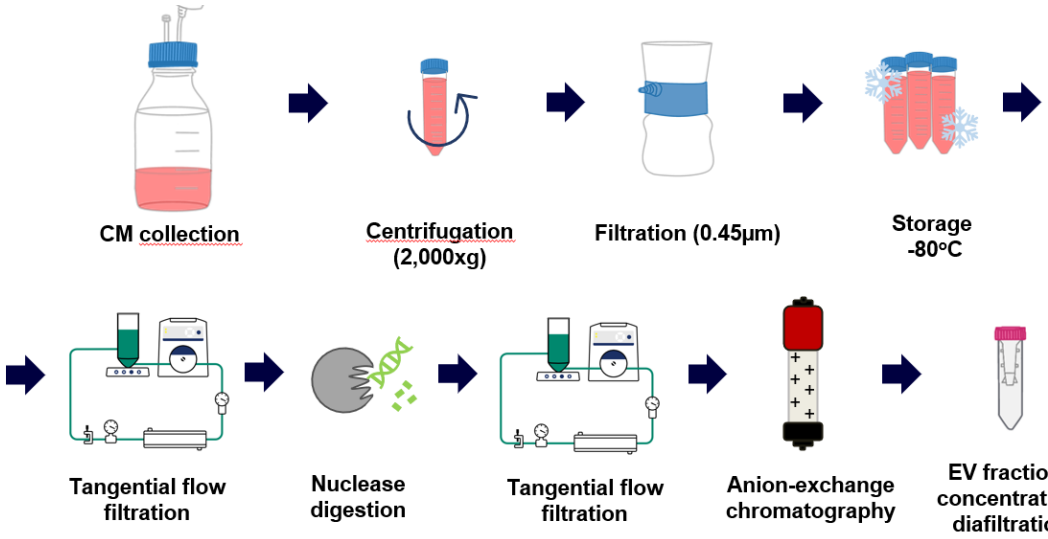

Figure III.2 - Schematic workflow of EV isolation from MSC(WJ) stirred cultures.

III.3.8. Characterization of isolated MSC-EVs

III.3.8.1. Nanoparticle particle analysis (NTA)

Particle quantification and size distribution profiles of EV-containing CM and isolated MSC-EV samples were obtained by NTA using a Nanosight LM14C instrument (Malvern). Samples were diluted in PBS to achieve a final particle concentration ranging between 10^8 and 10^9 particles/mL and measured using the standard operation procedure (SOP) as follows: camera level 13; screen gain 1; time of acquisition 30 sec; number of captures 5 (each capture with fresh sample). Video recording was acquired and analysed using NanoSight NTA version 3.4 (Malvern).

III.3.8.2. Protein quantification

Total protein of isolated MSC-EVs samples was determined using Micro BCA™ Protein Assay Kit (Thermo Scientific™) according to manufacturer instructions for the microplate procedure. Samples were lysed in RIPA buffer (Merck Millipore) 1x at room temperature (RT) for 10 min and diluted 10 times in PBS. Sample concentration was determined by applying a second-order polynomial curve fit to the bovine serum albumin (BSA) standards prepared in 0.1x RIPA in PBS solution. Absorbance was measured at 562 nm using the plate reader (Infinite® 200 PRO, NanoQuant, Tecan Trading AG, Männedorf, Switzerland). Two replicates were quantified for each sample. To assess the purity of the MSC-EV samples, the particle-to-protein ratio (PPR), which consists of the ratio between the total particle number and total protein of the sample [181], was determined.

III.3.8.3. Zeta potential

MSC-EV samples were diluted 10,000 times in distilled water. Samples were loaded into disposable capillary cells DTS1070 (Malvern Instruments) and analysed using the SOP set up for a sample refractive index of 1.45 (protein), dispersant refractive index of 1.33 (water), system temperature of 25°C, and sample equilibration time of 2 min. Each sample was measured in 3 runs, each resulting from subruns ranging from 10 to 100 in automatic mode. Measurements were performed with a Zetasizer Nano ZS (Malvern), and Malvern Zetasizer software version 7.10 was used to collect and analyse the data.

III.3.8.4. Western blot analysis of EV protein markers

The positive EV-protein markers CD9, CD63, Syntenin-1 and the negative marker Calnexin were evaluated in isolated MSC-EV samples using Western blot, with whole cell lysate (WCL) of MSC(WJ) harvested from the STR cultures as control. For the WCL samples, cells were lysed in RIPA buffer 1x supplemented with cOmplete™ Protease Inhibitor Cocktail (Roche) and centrifuged at 12,000xg for 15 min at 4 ºC, after which supernatants were recovered. EV and WCL samples (2 μg of total protein, corresponding to ~$1x10^{10}$ EVs) were diluted in PBS, NuPAGE™ LDS Sample buffer and NuPAGE™ Sample Reducing Agent (Invitrogen, Life Technologies) (except for tetraspanins detection, where non-reducing conditions were used), denatured at 95 ºC for 10 min and loaded in 4–12% Bis–Tris polyacrylamide precast gels (Invitrogen, Life Technologies). Electrophoresis was run at 130 V in MES SDS Running Buffer for 1 h and the proteins were subsequently transferred into nitrocellulose membranes using a Power Blotter System (Invitrogen, Life Technologies). Membranes were blocked with 5% BSA solution in 1x tris buffered saline with tween (TBST) for 1 h at RT and incubated overnight at 4 ºC with primary antibodies anti-CD9 (CBL162, Merck), anti-CD63 (556019, BD), anti-Calnexin (610523, BD) and anti-Syntenin-1 (ab133267, Abcam) at 1:1000 concentration. After extensive washing with TBST, membranes were incubated with HRP-conjugated secondary antibodies anti-Mouse (G-21040, Invitrogen) and anti-Rabbit (HAF008, R&D Systems) at 1:20,000 concentration for 1 h at RT. Finally, after secondary antibody washing with TBST, SuperSignal™ West Pico PLUS Chemiluminescent Substrate (Thermo Fisher Scientific) was applied for membrane revelation according to manufacturer instructions. Images were acquired using an iBrightTM CL1500 Imaging System (Invitrogen, Life Technologies).

III.3.8.5. Transmission electron microscopy

Transmission Electron Microscopy (TEM) imaging of MSC-EV samples was conducted using a negative staining protocol. Firstly, the 100 mesh formvar/carbon-coated copper grids were glow-discharged. Samples were mixed (1:1) with formaldehyde 4% in 0.1 M PBS and then added to the prepared grids and incubated for 5 min at RT. Afterwards, the grids were washed in 10 drops of distilled water and stained in 1 drop of uranyl acetate 2% by incubation for 5 min at RT

in the dark. Imaging was performed using a Tecnai G2 Spirit BioTWIN Transmission Electron Microscope (FEI Company™) operating at 120 kV and data was acquired with an Olympus-SIS Veleta CCD Camera.

III.3.8.6. EV uptake by target cells

Human umbilical vein endothelial cells (HUVEC), and human breast cancer cell lines MDA-MB-231 and MCF-7 were used as target cells for the EV uptake assays. HUVEC were cultured in EGM-2 Endothelial Cell Growth Medium-2 (Lonza) and breast cancer cells were cultured in high-glucose DMEM (Gibco) supplemented with 10% (v/v) fetal bovine serum (FBS) (Gibco) and 1% (v/v) A/A.

Isolated MSC-EVs were labelled with the fluorescent dye AlexaFluor 647 NHS ester (Invitrogen, Thermo Fisher) or PKH67 Green Fluorescent Cell Linker Kit for General Cell Membrane Labelling (Sigma Aldrich). EVs (3-4x10^{10} EVs) were mixed with sodium bicarbonate (pH 8.3, 100 mM final concentration) and 0.625% v/v AlexaFluor 647 NHS ester (10 mg/mL in DMSO) and incubated for 1 hour at 37°C and 450 rpm. EVs were then diluted in PBS and quenched in 100 mM Tris-HCl in a final volume of 100 µL, for 20 min at RT. Alternatively, EVs were added to 0.2 µL of PKH67 diluted in 50 µL of Diluent C. The mixture was then completed to a final volume of 100 µL by adding Diluent C and incubated for 5 min at RT. Mock dye treatments were prepared for both probes by replacing the EVs with PBS. Labelled-EVs were immediately purified from unbound dye using Exosome Spin Columns MW3000 (Invitrogen) according to manufacturer instructions.

The day before the EV uptake experiment, HUVEC, MDA-MB-231 and MCF-7 (50,000 cells) were plated onto flat-bottom 96-well plates. Labelled-EVs were then added to the target cells at a concentration of approximately 2x10^{10} particles/mL in culture medium supplemented with Exosome-depleted FBS (Gibco) and incubated for 6 h at 37 °C. Afterwards, cells were harvested and subjected to flow cytometry using a FACSCalibur™ Flow Cytometer (BD). The percentage of EV-containing cells and the relative EV uptake based on median fluorescence intensity (MFI) values (ratio of labelled-EV MFI to mock dye MFI) were analysed using FlowJo™ Software (BD).

III.3.9. Statistical Analysis

Statistical analysis was carried out using GraphPad Prism 9 software. Data were collected from three independent experiments and depicted as mean ± standard error of the mean (SEM) unless noted otherwise. Statistical tests are detailed in each figure legend, and all significant differences are indicated in the graphs.

III.4. Results

III.4.1. EV-depleted human platelet lysate was unable to support MSC(WJ) expansion

The need to employ a culture medium depleted of EVs throughout the conditioning stage to produce the EV-enriched CM prompt us to evaluate the capacity of a newly developed exosome-depleted human platelet lysate (hPL-EVd) supplement (AventaCell Biomedical) in promoting/maintaining the expansion potential of MSC(WJ). To this end, cells were cultivated on 12-well plates with culture medium with different concentrations of the supplement, using cells grown in culture medium supplemented with complete hPL as control (**Figure III.3**). At the end of culture, MSC(WJ) showed high viability (≥98%) for every conditions; however, the cells were not able to grow when using hPL-EVd, reaching a maximum fold-expansion of 1.7 ± 0.083 and 2.7 ± 0.32 by day 9, when cultured with 5% and 10% supplementation, respectively (**Figure III.3 – A,B)**, while presenting a very elongated morphology (**Figure III.3 – C**). In contrast, MSC(WJ) grown in

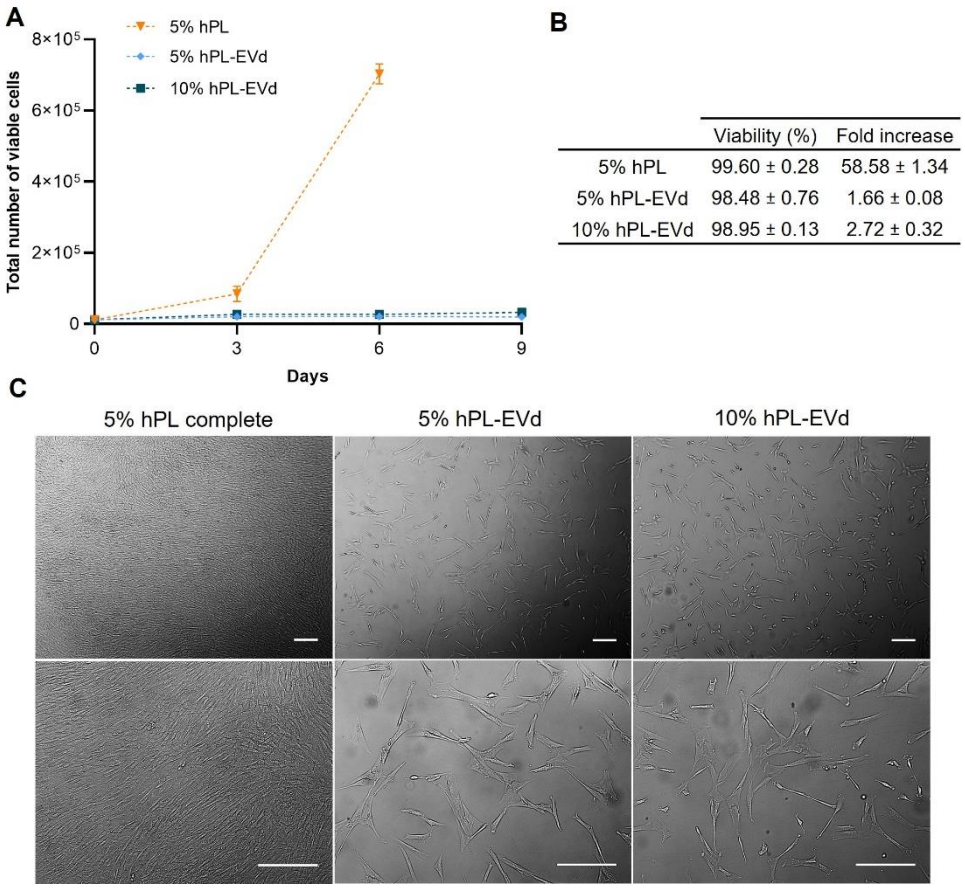

	Viability (%)	Fold increase
5% hPL	99.60 ± 0.28	58.58 ± 1.34
5% hPL-EVd	98.48 ± 0.76	1.66 ± 0.08
10% hPL-EVd	98.95 ± 0.13	2.72 ± 0.32

Figure III.3 – MSC(WJ) expansion in culture medium supplemented with exosome-depleted human platelet lysate (hPL-EVd). **(A)** Total number of viable cells cultured with concentrations of hPL-EVd throughout 9 days. **(B)** Viability (%) and fold-increase in expansion at the end of culture. **(C)** Representative images of MSC(WJ) morphology at the end culture. Scale bar: 250 μm. Cells grown in culture medium supplemented with complete hPL were used as control. Graph values are presented as mean ± SEM of 3 independent donors (n=3).

culture medium supplemented with complete hPL reaching a maximum fold-expansion of 59 ± 1.3 by day 6 (**Figure III.3 – A, B)** and presented the typical cellular morphology (**Figure III.3 – C**). Therefore, in the following studies, hPL-EVd was employed for the medium conditioning stage only, while standard hPL-based medium was used for cell expansion.

III.4.2. Medium renewal enhanced MSC(WJ) particle production under static conditions

For EV production, MSC are typically cultured in EV-free medium during conditioning periods ranging from 24 to 72 hours [133,150,411]. To evaluate cell fitness and particle accumulation in the CM throughout 72 h, MSC(WJ) were cultured for 24 h, 48 h and 72 h periods with/without medium renewal every 24 h, using hPL-EVd as culture medium supplement (**Figure III.4**).

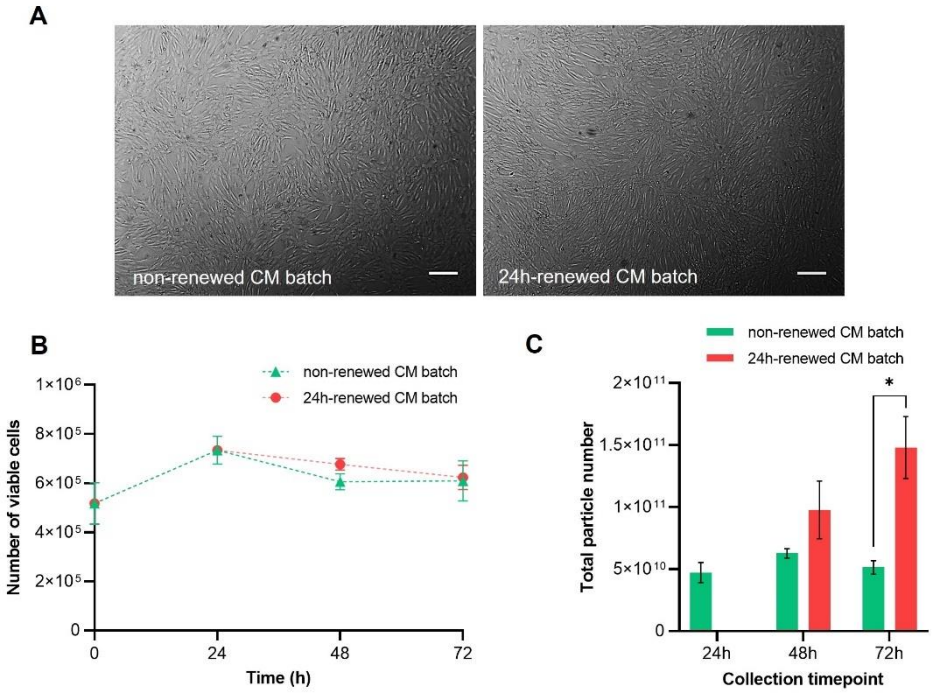

Figure III.4 - Evaluation of particle accumulation in MSC(WJ) conditioned medium (CM) during 72h. **(A)** Representative images of MSC(WJ) morphology at the end of the 72h-conditioning period. Scale bar: 250 μm. **(B)** Total number of viable cells cultured without any medium renewal (green) and with medium renewal every 24h (red). **(C)** Total number of particles produced up to the respective timepoint, without any medium renewal (green) and with medium renewal every 24h (red), determined from nanoparticle tracking analysis (NTA) measurements. Graph values are presented as mean ± SEM of 3 independent donors (n=3). Statistical analysis was performed using a one-way ANOVA followed by a post-hoc Tukey's multiple comparisons test; *p<0.05.

After 72h, MSC(WJ) cultured in DMEM-hPL-EVd showed high cell survival with viability of 99 ± 0.54% and 99 ± 0.16%, with and without 24h-medium renewal, respectively, and presented typical cellular morphology (**Figure III.4-A**). Additionally, no significant alterations in cell number were observed throughout the 72 h and the number of MSC(WJ) cultured with/without

medium renewal every 24h was comparable (**Figure III.4-B**). The total number of particles in the CM was similar for the different conditioning periods when no medium was replaced, showing that there was no accumulation of particles throughout time (**Figure III.4-C**). Moreover, the total number of particles secreted by MSC(WJ) was superior when cells were cultured with 24h-medium renewal cycles compared to cells cultured without medium renewal (**Figure III.4-C**). After 72h, 24h-medium renewal allowed a significant fold increase of 2.8 ± 0.17 in the total number of particles produced by MSC(WJ), compared to the condition where no medium was exchanged (**Figure III.4-C**). This shows that several EV collection cycles using the same parental cells can be performed, potentially maximising EV production.

III.4.3. MSC(WJ) expansion and multiple EV collection batches were accomplished in a microcarrier-based spinner flasks

Based on the work performed by our group [133,146], a S/XF microcarrier-based stirred culture system was implemented envisioning large-scale production of MSC-EVs. This system combines the use of DMC and hPL-supplemented medium for the expansion of MSC(WJ) followed by EV production aided by a novel EV-free hPL supplement particularly developed for EV manufacturing. Initial adhesion efficiency of MSC(WJ) to microcarriers was 87 ± 5.4% on day 1 and the cells were successfully expanded, with a maximum fold-expansion of 37 ± 3.4 having been achieved after 6 or 7 days depending on the donor. MSC(WJ) exhibited exponential growth with a μmax and td were 0.55 ± 0.043 day^{-1} and 1.3 ± 0.10 days, respectively, reaching an average of (3.7 ± 0.34) x 10^6 cells (**Figure III.5-A**). Upon the conditioning medium stage for EV production, a 0.58 ± 0.13-fold decrease in cell number was observed between the beginning and end of the stage (72 h) (**Figure III.5-A**). Glucose consumption and lactate secretion profiles showed a decrease in glucose levels concomitant with an increase in lactate concentration throughout culture. During the EV production stage, glucose was completely consumed every 24h (**Figure III.5-B**). Nuclei staining showed cell distribution and a progressive increase in the number of cells per microcarrier (**Figure III.5-C**). Cell viability throughout culture was assessed by calcein-AM staining, showing highly viable cells on the microcarrier surface with typical MSC elongated morphology. In the last day of EV production, although viable, cells demonstrated a more spherical morphology on the microcarriers surface, which could possibly lead to cell detachment if the culture was prolonged (**Figure III.5-C**). NTA measurements of the CM corresponding to each collection period during the 3-day EV production stage showed no significant differences in the number of total accumulated particles and the particle secretion rate of MSC(WJ), demonstrating an average particle yield factor before EV isolation of (3.2 ± 0.57) x 10^4 particles/cell/day (**Figure III.5-D**).

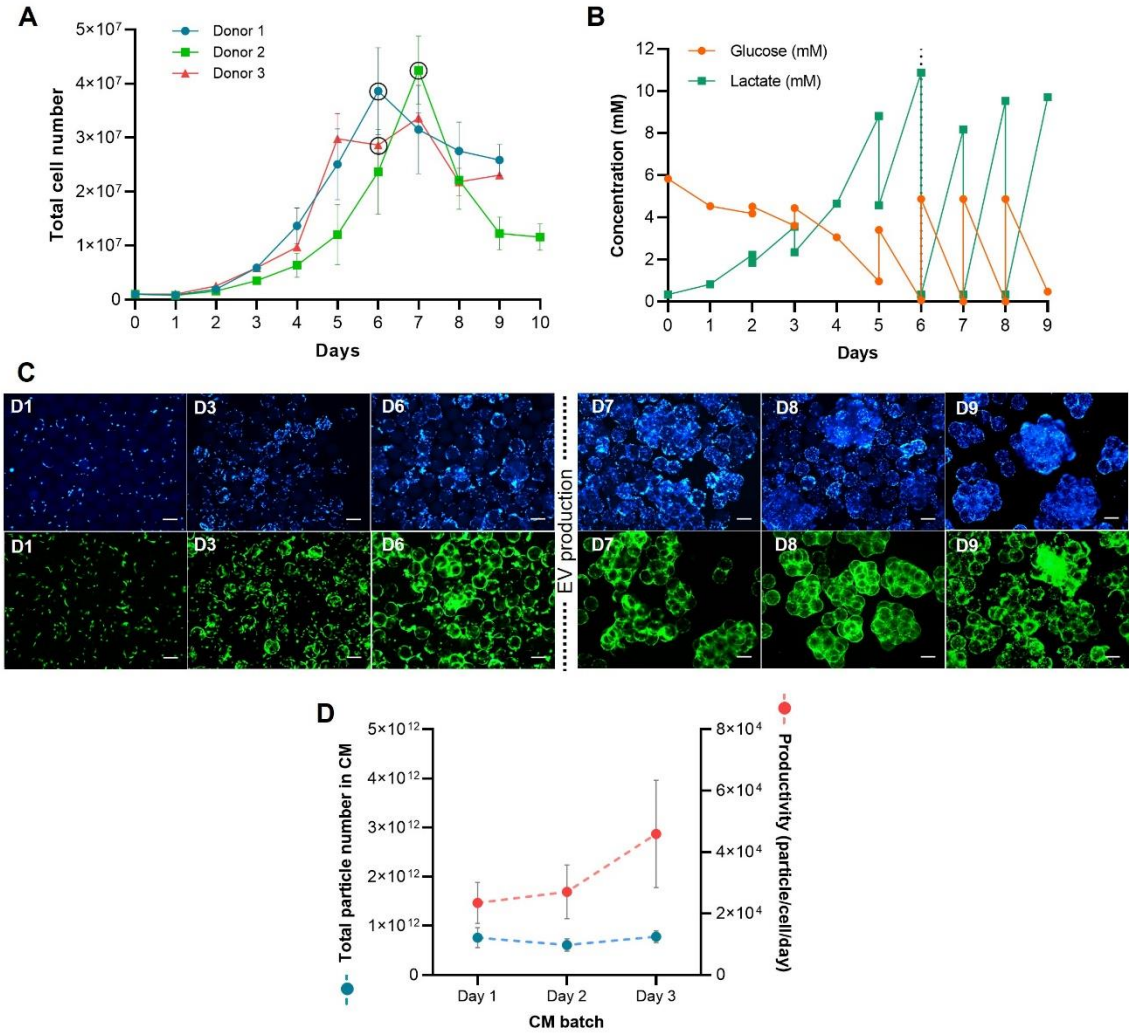

Figure III.5 - Microcarrier-based expansion of MSC(WJ) and subsequent EV production in spinner flasks. **(A)** Growth curve of MSC(WJ) throughout the 9/10-day culture in spinner flask depicted as total cell number. The EV production stage started on day 6-7 and is highlighted with a black circle. **(B)** Representation of glucose and lactate concentration measurements throughout spinner culture (donor 1). **(C)** Representative images of cell distribution on microcarriers obtained through DAPI staining (blue) (top panel), and cell viability assessment obtained through Calcein-AM staining (green) (bottom panel), throughout spinner flask culture (donor 1). MSC(WJ) expansion and EV production stages are separated by the dashed line. **(D)** Total particle number (blue) and particle secretion rate of MSC(WJ) (red) throughout the 3-day EV production stage, determined from the nanoparticle tracking analysis (NTA) measurements of the conditioned medium (CM) of each day. Scale bar: 250 µm. All table and graph values are presented as mean ± SEM of 3 independent donors (n=3). No statistically significant differences were found using a one-way ANOVA followed by a post-hoc Tukey's multiple comparisons test.

III.4.4. EVs were successfully isolated from microcarrier-based stirred MSC(WJ) cultures using a scalable isolation process

After the 3-day conditioning medium stage, EVs were successfully isolated from the CM of MSC(WJ) cultures using a scalable process (**Figure III.2**). After CM filtration and concentration using TFF and nucleic acid digestion, AEC allowed further separation of soluble proteins from EVs. The protein contaminants were eluted in the flowthrough, while the resin-adsorbed-EVs were subsequently eluted by increasing the ionic strength (**Figure III.6**).

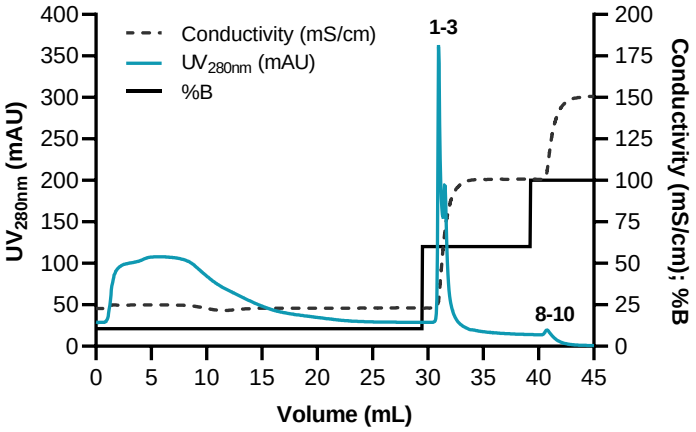

Figure III.6 – Chromatogram obtained after injection of EV-containing sample derived from MSC(WJ) cultured in spinner flasks into a Capto™ Q ImpRes column pre-equilibrated with a buffer composed of 50 mM HEPES, 180.7 mM NaCl, pH 7, (10.5% buffer B, ≈23 mS/cm). Unbound material was washed with 15 CV of 10.5% B, and stepwise elution was performed with 10 CV of 60% B (≈100 mS/cm) and 7 CV of 100% B (≈150 mS/cm). Numbers over peaks correspond to the collected fractions. Blue continuous line: absorbance at 280 nm; grey dashed line: conductivity (mS/cm); black continuous line: percentage of buffer B (%B).

EV-containing fractions were concentrated and characterised in accordance with the criteria proposed by the International Society for Extracellular Vesicles (ISEV) [412]. A summary of isolated MSC-EV characteristics and yields is displayed in **Table III.2**. NTA was used to determine the size distribution of isolated MSC-EVs, demonstrating an enrichment in particles below 200 nm (**Figure III.7-A**) with a mean and mode diameter of approximately 117 nm and 86 nm, respectively (**Table III.2).** Particle quantification confirmed the total isolation of (3.6 ± 0.46) x 10^{11} EVs (**Table III.2**), which corresponds to a specific EV productivity of (1.4 ± 0.32) x 10^4 isolated EVs per producing cell (**Table III.2**). A particle yield factor of (4.7 ± 0.11) x 10^3 particles/cell/day (**Table III.2**) was calculated as a measure of EV yield, as suggested by Grangier and colleagues [140]. TEM images showed that isolated samples displayed the typical spherical and cup-shaped structure of EVs (**Figure III.7-B**), which results from membrane dehydration during sample preparation [413]. To assess the purity of EV samples, protein quantification was performed to determine the particle-to-protein ratio (PPR). The average PPR value obtained for the isolated EV samples was (4.1 ± 1.3) x 10^9 particles/μg (**Table III.2**). The isolated MSC-EVs expressed

three EV-positive protein markers, namely tetraspanins CD9 and CD63 and syntenin-1, as detected through western-blot (**Figure III.7-C**). Detection was stronger in EV samples compared to WCL controls, confirming the EV-enrichment of isolated samples. Moreover, the negative marker calnexin was not detected in EV samples, in contrast to WCL controls (**Figure III.7-C**).

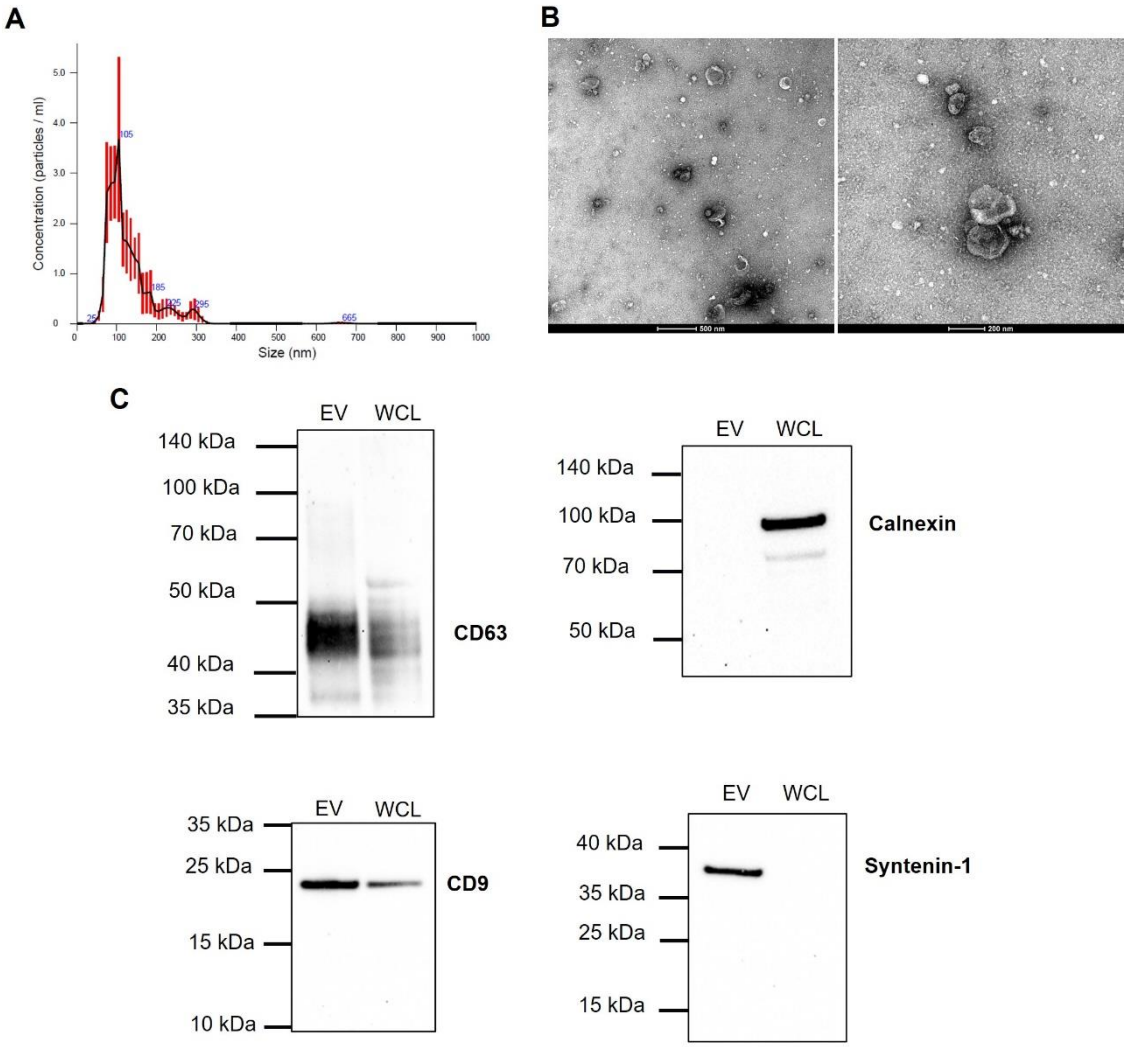

Figure III.7 - Characterisation of isolated EVs produced by MSC(WJ) cultured in spinner flasks. **(A)** Representative size distribution profile of isolated MSC(WJ)-derived EVs obtained by NTA. **(B)** Representative transmission electron microscopy images of isolated EVs after negative staining, at different magnifications. Scale bar: 500 nm (left); 200 nm (right). **(C)** Representative Western-blot images of positive EV markers CD63, CD9 and syntenin-1 and negative EV marker calnexin detection using isolated EV samples and the respective whole cell lysate (WCL) of MSC(WJ).

Table III.2 – Characteristics and yields of EVs isolated from the 3-day conditioned media produced by MSC(WJ) cultured in spinner flasks. Values are presented as mean ± SEM of 3 independent donors (n=3).

EV parameter	Average value for 3 MSC(WJ) donors
Total isolated EV number	(3.6 ± 0.46) x10^{11}
Average size (nm)	117 ± 5.16
Mode of size (nm)	85.8 ± 4.36
Particle-to-protein ratio (total particles/ µg protein)	(4.1 ± 1.2) x10^{9}
Specific EV productivity (EV/cell)	(1.4 ± 0.32) x 10^{4}
Particle yield factor (EV/cell/day)	(4.7 ± 0.11) x 10^{3}

III.4.5. MSC(WJ) expansion and continuous EV collection was accomplished in a microcarrier-based STR culture system

The novel EV-free hPL supplement was also explored for the continuous production of EVs in a controlled and scalable STR system (**Figure III.1-A**). MSC(WJ) adhesion efficiency to microcarriers was 86 ± 4.1% on day 1 of STR culture and the cells were successfully expanded, with a maximum fold-expansion of 30 ± 0.74 having been achieved after 7 days. As seen in the growth curves represented in **Figure III.8-A,** the cells exhibited exponential growth until reaching (6.0 ± 0.18) x 10^{7} cells on day 7, corresponding to a cell density of (3.8 ± 0.11) x 10^{5} cells/mL and (5.6 ± 0.17) x 10^{4} cells/cm^{2}. The calculated µmax and td were 0.55 ± 0.027 day^{-1} and 1.3 ± 0.067 days, respectively. During the EV production stage between days 7 and 10, no significant alteration in cell number was observed and cell concentration remained relatively constant at (5.6 ± 0.28) x 10^{5} cells/mL.

The qualitative occupancy of the DMC throughout MSC(WJ) expansion was evaluated by nuclei staining, through which a progressive increase in the number of cell-loaded microcarriers, along with a gradual increase in microcarrier occupancy from days 1 to 7, was observed (**Figure III.8-B**). This increase was accompanied by microcarrier aggregation as MSC(WJ) expansion reached higher cell densities, being most evident from day 6 onwards (**Figure III.8-B,C**). Calcein-AM staining showed viable cells presenting the characteristic elongated morphology of MSC on microcarrier surfaces throughout STR culture, including during the EV production stage (**Figure III.8-C**). Moreover, Live/Dead images of MSC(WJ) on microcarriers on day 10 of STR culture showed a negligible number of dead cells after cell expansion and EV production (**Supplementary Figure III.1**). Glucose and lactate concentration analysis demonstrated that the adopted feeding scheme (**Figure III.8-C**) successfully prevented glucose depletion and lactate accumulation above critical concentration [414] throughout the 10-day culture (**Figure III.8-D**).

During the EV production stage, glucose and lactate concentrations were maintained constant around 4mM and 2mM, respectively (**Figure III.8-D**).

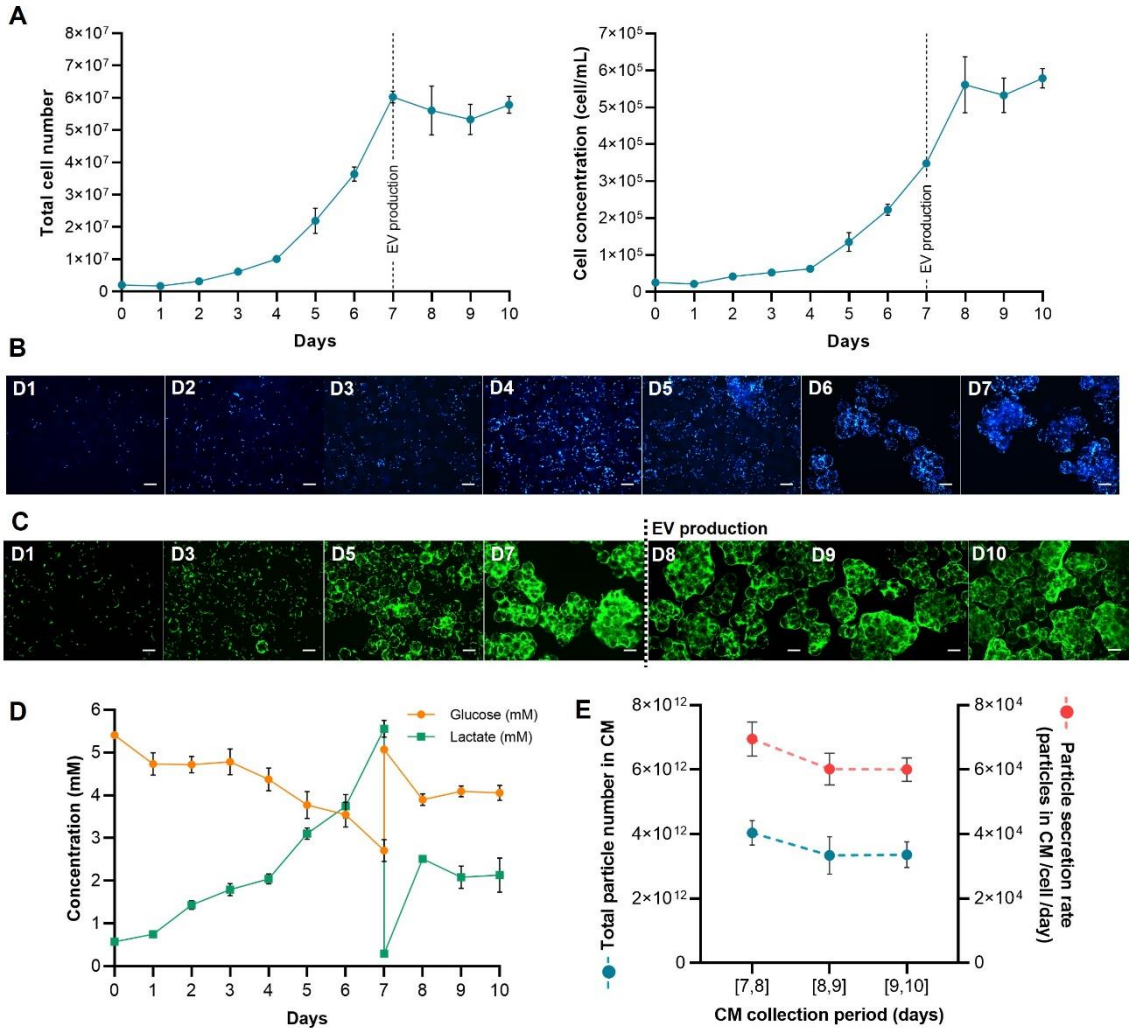

Figure III.8 - Microcarrier-based expansion of MSC(WJ) and subsequent EV production in a fully controlled stirred-tank reactor (STR) system. **(A)** Growth curve of MSC(WJ) throughout the 10-day culture in STR depicted as total cell number (left) and cell concentration (right). The EV production stage started on day 7 and is highlighted by the dashed line. **(B)** Representative images of cell distribution on microcarriers throughout MSC(WJ) expansion in a STR, obtained through DAPI staining (blue). **(C)** Representative images of cell viability assessment throughout STR culture, obtained through Calcein-AM staining (green). MSC(WJ) expansion and EV production stages are separated by the dashed line. **(D)** Glucose and lactate concentration measurements throughout STR culture. **(E)** Total particle number (blue) and particle secretion rate of MSC(WJ) (red) throughout the 3-day EV production stage, determined from the nanoparticle tracking analysis (NTA) measurements of the conditioned media (CM) of each day. Scale bar: 250 µm. All table and graph values are presented as mean ± SEM of 3 independent donors (n=3). No statistically significant differences were found using a one-way ANOVA followed by a post-hoc Tukey's multiple comparisons test.

NTA measurements of the CM corresponding to each collection period during the 3-day EV production stage showed no significant differences in the number of total accumulated particles and the particle secretion rate of MSC(WJ), demonstrating an average particle yield

factor before EV isolation of (6.5 ± 0.26) x 10^4 particles/cell/day (**Figure III.8-E**). The collected CM had an average particle concentration of (1.8 ± 0.13) x 10^{10} particles/mL. Overall, medium supplementation with hPL-EVd allowed the continuous production of EV-enriched CM under stirred conditions without causing significant alterations in the cell number, cell viability and particle secretion rate of MSC(WJ).

III.4.6. MSC(WJ) preserve their cellular identity after continuous EV collection in a STR

On day 10 of STR culture, after the 3-day continuous EV production, MSC(WJ) were harvested from the microcarriers by applying an enzymatic solution and characterised in what concerns their viability, immunophenotype and trilineage differentiation potential according to criteria established by the ISCT [259] (**Figure III.9**). Harvested MSC(WJ) presented a high cell viability of 96.8 ± 2.22% (**Figure III.9-A**), similar to what was visually observed before DMC dissolution (**Supplementary Figure III.1**), showing that cell recovery from the microcarriers did not have a significant negative impact on cell viability. Immunophenotypic analysis demonstrated that after EV production MSC(WJ) expressed high levels (≥95%) of positive cell surface markers CD90, CD44 and CD73 (**Figure III.9-B**). The lower expression detected for positive marker CD105 (74.9 ± 13.1%) is not uncommon after cell expansion under stirred conditions [135,149,150,415]. Moreover, the expression of negative markers CD80, CD19, CD34, CD45, and HLA-DR was negligible (≤3%), further confirming MSC(WJ) immunophenotypic identity (**Figure III.9-B**). After the conditioning stage, MSC(WJ) preserved their multilineage differentiation ability, further validating their identity (**Figure III.9-C**). MSC(WJ) differentiated into the adipogenic lineage, confirmed by the detection of lipid droplets stained in red (left panel, **Figure III.9-C**), the osteogenic lineage, validated by the presence of osteoblast progenitors stained in red (middle panel, **Figure III.9-C**), and the chondrogenic lineage, corroborated by the blue staining of chondrocyte-secreted acidic polysaccharides (right panel, **Figure III.9-C**).

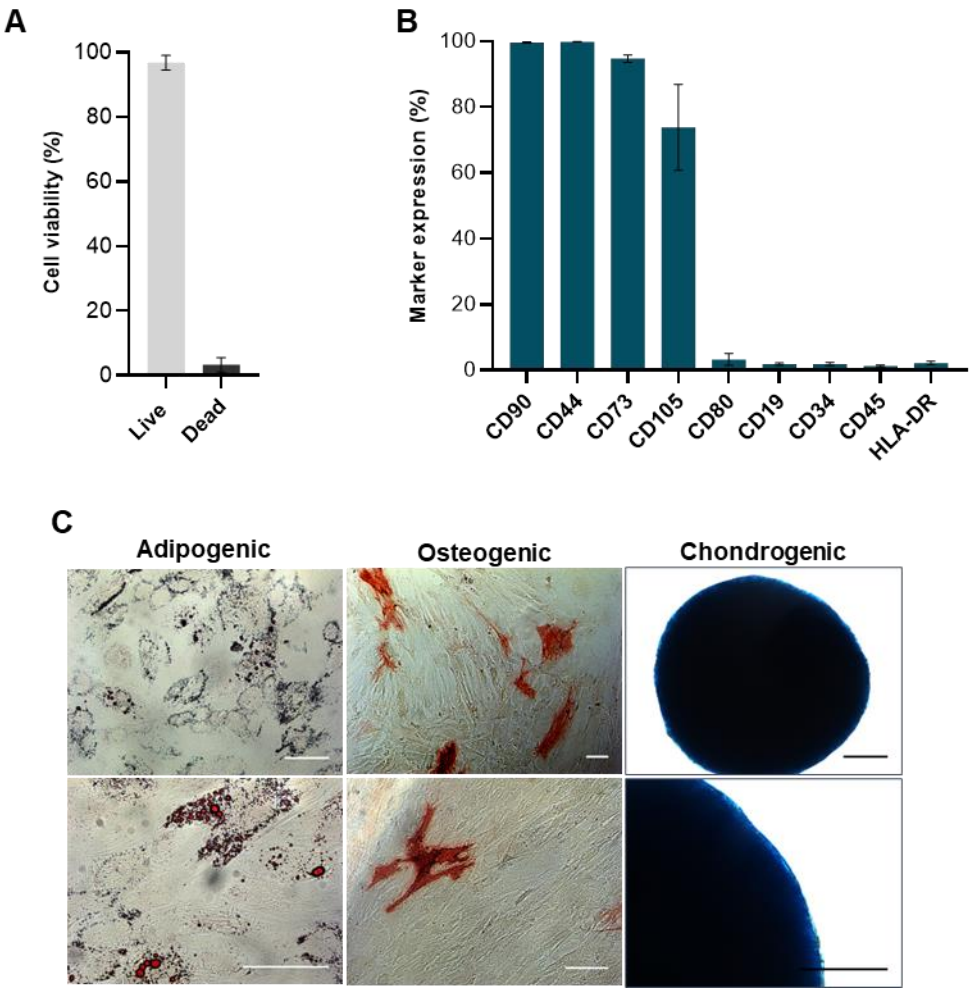

Figure III.9 - Characterisation of MSC(WJ) after microcarrier-based MSC(WJ) expansion and EV production in a fully controlled stirred-tank reactor (STR) system. **(A)** Cell viability after MSC(WJ) expansion and EV production in a STR, assessed by flow cytometry after Live/Dead staining. **(B)** Immunophenotypic analysis after MSC(WJ) expansion and EV production in a STR system through flow cytometry. **(C)** Trilineage differentiation potential of MSC(WJ) after expansion and EV production in a STR: Adipogenic lineage with adipocyte-produced lipid droplets stained using Oil Red O; Osteogenic lineage with osteocyte progenitors stained using Alkaline phosphatase (ALP); Chondrogenic lineage with staining of chondrocyte-secreted extracellular matrix proteins (Alcian Blue). Scale bar: 100 µm. Graph values are presented as mean ± SEM of 3 independent donors (n=3).

III.4.7. Continuously harvested MSC(WJ)-EVs showed robust quality attributes after isolation

After the 3-day continuous production stage, EVs were successfully isolated from the CM of MSC(WJ) cultures using a scalable process (**Figure III.2**). After AEC (**Supplementary Figure III.2**), EV-containing fractions were concentrated and characterised in accordance with the criteria proposed by ISEV [412]. A summary of isolated MSC-EV characteristics and yields is displayed in **Table III.3**. Size distribution profile of isolated MSC-EVs showed an enrichment in particles

below 200 nm (**Figure III.10-A**) with a mean and mode diameter of approximately 120 nm and 106 nm, respectively (**Table III.3).** Particle quantification confirmed the total isolation of (1.9 ± 0.38) x 10^{12} EVs (**Table III.3**) at a concentration of (3.4 ± 0.49) x 10^{12} EVs/mL, which corresponds to a specific EV productivity of (3.6 ± 0.93) x 10^{4} isolated EVs per producing cell and a particle yield factor of (1.2 ± 0.31) x 10^{4} particles/cell/day (**Table III.3**). The total number of isolated EVs and particle yield factor was approximately 5- and 3-fold higher than when using spinner flasks, respectively (**Table III.2**).

TEM images confirmed the presence of individual vesicles of different sizes that display the spherical and cup-shaped structure typical of EVs (**Figure III.10-B**). The zeta potential measurements of isolated MSC-EVs indicated a net negative surface charge of approximately -23 mV (**Table III.3**), as expected. The average PPR value obtained for the isolated EV samples was (5.7 ± 2.7) x 10^{9} particles/μg (**Table III.3**). Western-blot showed that isolated MSC-EVs expressed tetraspanins CD9 and CD63 and syntenin-1, and the detection was stronger in EV samples compared to WCL controls, confirming the EV-enrichment of isolated samples. Contrary to WCL controls, the negative marker calnexin was not detected in EV samples (**Figure III.10-C**). Besides morphological characterisation of MSC-EVs, an uptake assay was performed to validate cell internalization of the isolated MSC-EVs into target cells. MSC-EVs were stained with two different dyes (lipid probe PKH67 and protein probe Alexa647) and incubated with breast cancer cell lines MDA-MB-231 and MCF-7, as well as with HUVEC. After 6h, the percentage of EV-containing cells was high (>85%) for every target cell type (left panel, **Figure III.10-D**). Interestingly, the relative EV internalization was significantly higher for HUVEC in comparison to the breast cancer cell lines (right panel, **Figure III.10-D**), which suggests that HUVECs present an increased affinity to uptake MSC-EVs.

Table III.3 – Characteristics and yields of isolated EVs produced by MSC(WJ) in a controlled stirred-tank reactor for 3 days. Values are presented as mean ± SEM of 2 independent donors (n=2).

EV parameter	Average value for 2 MSC(WJ) donors
Total isolated EV number	(1.9 ± 0.38) x10^{12}
Average size (nm)	120 ± 5.7
Mode of size (nm)	107 ± 8.65
Zeta potential (mV)	-23.4 ± 10.8
Particle-to-protein ratio (total particles/ μg protein)	(5.7 ± 2.7) x 10^{9}
Specific EV productivity (EV/cell)	(3.6 ± 0.93) x 10^{4}
Particle yield factor (EV/cell/day)	(1.2 ± 0.31) x 10^{4}

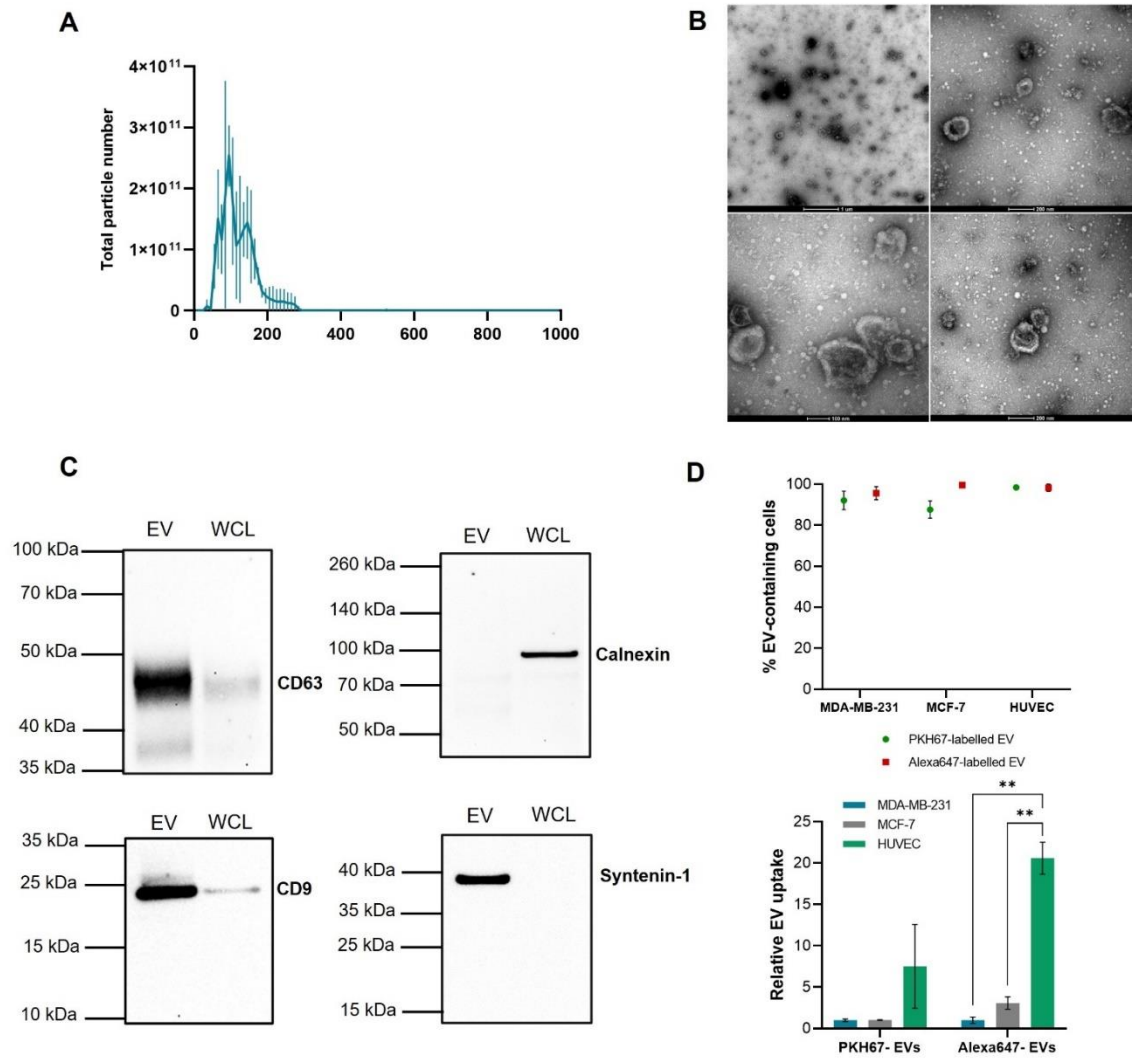

Figure III.10- Characterisation of isolated EVs continuously produced by MSC(WJ) cultured in a fully controlled stirred-tank reactor for 3 days. **(A)** Size distribution profile of isolated MSC(WJ)-derived EVs obtained by NTA. **(B)** Representative transmission electron microscopy images of isolated EVs after negative staining, at different magnifications. Scale bar: 1 µm (top left), 100nm (bottom left), 200 nm (right). **(C)** Representative Western-blot images of positive EV markers CD63, CD9 and syntenin-1 and negative EV marker calnexin detection using isolated EV samples and the respective whole cell lysate (WCL) of MSC(WJ). **(D)** Analysis of EV uptake by target cells MDA-MB-231, MCF-7 and HUVEC after treatment with PKH65-(green) and Alexa647-(red) labelled EVs. The percentage of EV-containing cells (top panel) and the relative EV uptake based on median fluorescence intensities (MFI) values (ratio MFI of labelled-EV to MFI of free dye) (bottom panel) were determined by flow cytometry. Values are presented as mean ± SEM of 2 independent donors (n=2). Statistical analysis was performed using a one-way ANOVA followed by a post-hoc Tukey's multiple comparisons test; **p<0.01.

III.5. Discussion

MSC-EVs have shown great promise as natural therapeutics and drug delivery vehicles in a wide range of pre-clinical disease models [109,274]. Despite their biomedical potential, most preclinical studies still use planar culture systems and FBS-supplemented culture media formulations for MSC expansion and resort to non-scalable low-purity grade methods for MSC-EV isolation, all of which hampers their translation into the clinic by failing to meet the necessary dose and safety requirements. In this context, the implementation of a large-scale manufacturing workflow for MSC-EVs, incorporating scalable upstream and downstream processes, is necessary to provide high-purity EV yields [130,166,182]. Envisioning industrialisation, multiple large-scale systems have been investigated for EV production, among which are two-dimensional multilayer flasks [416] and several three-dimensional culture configurations, such as hollow-fiber bioreactors [141], microcarrier-based cultures [149,150] and 3D aggregates [417]. Several groups have been exploring scalable microcarrier-based stirred platforms for MSC-EV production, including spinner flasks [144–146] and vertical-wheel systems [133,147,148]. Although numerous reports describe the successful large-scale expansion of MSC in microcarrier-based fully controlled STR systems [415,418–423], only a few have applied them to EV manufacturing [149–151].

The present work focused on implementing a scalable platform for continuous harvesting of EVs using a microcarrier-based STR culture system in order to maximize MSC-EV production yields. Aiming at extending cell viability and consequently prolonging the cell conditioning period, we employed a novel S/XF EV-depleted supplement that allowed continuous EV production over a 3-day period. Specifically, MSC(WJ) were expanded on DMC in a STR with intermittent agitation until maximum fold expansion using hPL-supplemented medium followed by EV production in stirred conditions using exosome-depleted hPL-supplemented medium. Both supplements are gamma irradiated as a pathogen reduction technology (PRT) formulation, which is essential to produce a safe MSC-derived product for clinical use [424]. Similar to our previous study using an alternative commercially available S/XF formulation [146] and preliminary studies performed herein using spinner flasks, this new platform allowed MSC(WJ) adhesion to the DMC with an efficiency of 86 ± 4.1%, which is notably higher than the typical ≤50% efficiency reported for MSC(WJ) adhesion when using hPL-stirred cultures employing various microcarriers and agitation regimens [133,135,425,426]. Additionally, taking advantage of the intermittent agitation and by increasing the total available surface area of the microcarriers by 50% in comparison to our previous protocol [146], a total number of (6.0 ± 0.18) x 10^7 cells was reached after 7 days, representing a ~30-fold cell expansion factor, which is superior to most values reported in the literature for MSC expansion under S/XF stirred culture conditions with similar or longer timeframes [133,135,147–150,419,425–427]. The initial cell seeding density (1,850 cell/cm^2) was intentionally lower than what is typically employed for S/XF microcarrier-based MSC expansion, which ranges between 3,000 – 7,000 cells/cm^2 [135,147,150,419,420]. This reduction delayed cell-containing microcarrier aggregation, a phenomenon accelerated by higher initial cell density per microcarrier [428]. Moreover, the homogeneous and full occupancy of the microcarriers was

facilitated by incorporating static periods that promote MSC migration to empty microcarriers throughout culture, without signs of early bead aggregation [146,428,429]. Although a stationary growth phase was not observed, by day 7, the DMC appeared to be aggregated and nearly confluent, yielding a cell density of (5.58 ± 0.17) x 10^4 cells/cm^2. Typically, cell-containing microcarrier aggregation correlates with higher cell densities, which have been shown to promote cell detachment from microcarriers [428]. Therefore, envisioning subsequent EV production, we aimed to initiate this phase with MSC still in a highly viable and proliferative state, to mitigate the impact of the shear stress associated with continuous stirred culture in exosome depleted-hPL medium.

The selection of an appropriate feeding strategy is extremely important to regulate toxic metabolite accumulation, essential nutrient consumption and sustain optimal cell growth [430]. Previous work on MSC expansion has shown that perfusion cultures allow higher cell concentrations and yield superior fold expansions compared to fed-batch feeding strategies [149,419]. In the present work, during MSC(WJ) expansion, the STR operated under continuous fed-batch until day 4, followed by perfusion until day 7. This approach facilitated efficient MSC(WJ) growth by maintaining optimal glucose and lactate levels. For the subsequent EV production stage, the perfusion operation mode was chosen based on the results of particle accumulation in the CM of MSC(WJ) cultured in static conditions with exosome depleted-hPL supplement medium for 72h. The results indicated no accumulation of particles over time, a total particle production 2.84 ± 0.17-fold higher when 24h-medium renewal cycles were performed. Similarly, Patel and colleagues reported that mid-period collection of the CM led to an increase of approximately 2-fold in the total number of MSC-EVs produced when compared to a single collection at 6h, 12h and 24h [172]. Additionally, even when looking at a different cell type, macrophage-produced CM harvested at 24h, 48h or 72h presented a similar concentration of EVs, suggesting no particle accumulation [173]. These findings suggest that EV production may function as a balanced intercellular communication system and the removal of particles promotes additional secretion, a phenomenon that continuous culture systems can take advantage of to improve EV yields. Indeed, during the 3-day EV production stage in the stirred cultures (spinner flasks and STR), there were no significant differences in the total number of accumulated particles and the particle secretion rate of MSC(WJ) throughout time.

In the STR system, EV production was performed under continuous agitation at 60 rpm (visually complying to N_{S1u} criterion [431]) to further stimulate EV production since shear stress associated with stirred culture conditions has been reported to enhance EV secretion from MSC [133,144,147,150,151]. Microcarrier-based stirred cultures of MSC(WJ) increased EV productivity 3- and 20-fold compared to static cultures, when using vertical-wheel systems [133,147] and spinner flasks [144], respectively. Similarly, fully controlled STR systems also induced an increase in EV secretion when compared to two-dimensional static systems [150,151]. Besides causing significant intracellular pathways and expression alterations that regulate EV secretion, laminar or turbulent flow-induced shear stress causes cell membrane tension and elongation, leading to fragmentation and spontaneous self-assembly of vesicles [152]. Importantly, during the 3-day

continuous EV production stage, MSC(WJ) showed high viability and conventional cellular morphology while maintaining the cell number and particle production rate. This demonstrates that the exosome-depleted hPL-supplemented culture medium and stirred culture conditions did not significantly compromise MSC(WJ) integrity. Moreover, at the end of culture, harvested MSC(WJ) presented the standard immunophenotype and trilineage differentiation potential, confirming that this EV production platform preserves MSC(WJ) cellular identity. . These findings align with recent work reported by Lorenzini and colleagues, where MSC incubated for 3 successive periods of 72h in culture medium supplemented with EV-depleted hPL maintained cell survival and cumulative EV production, a phenomenon not observed under standard starving conditions [169]. Interestingly, this study demonstrated that the developed EV-depleted hPL supplement sustained the survival and EV production of other cell types, including human primary endothelial colony forming cells (ECFC) and two non-adherent human cell lines, Jurkat and THP-1 [169].

To the best of our knowledge, the present study is the first to establish an S/XF microcarrier-based STR culture system for the continuous production of primary human MSC-EVs, while others focused on a single 24h to 72h CM batch collection at the end of culture [133,146–150]. Alternative cellular platforms have been explored for production of EVs for longer periods of time. Gobin and colleagues explored a hollow-fiber system operating in perfusion mode with culture medium recirculation, enabling EV collection from MSC(M) throughout a 25-day period, using a chemically defined S/XF with low particle content during the EV production stage [141]. Similarly, natural killer (NK) cells were cultured using a hollow-fiber system with culture medium recirculation for EV production over 20 days (three separate culture batches), yielding large quantities of clinical-grade NK-derived EVs [142].

Following a large-scale upstream process, robust isolation platforms capable of processing large CM volumes are required. Many reported studies on MSC-EV production in scalable stirred systems still rely on polymer-based precipitation kits [133,145,149] and ultracentrifugation [147,148] as EV isolation methods. However, ultracentrifugation lacks scalability and can potentially lead to incomplete contaminant separation, whereas polymer-based precipitation yields low-purity samples due to co-isolation of proteins and residual polymer matrix [130,181,182,184]. TFF, alone or in combination with chromatography, is a scalable EV isolation method that allows the time-efficient processing of large volumes generating high EV yields with improved purity [187]. In fact, Haraszti and colleagues demonstrated that TFF improves the yield of MSC-EVs from CM of 3D stirred cultures by 7-fold compared to ultracentrifugation [144]. In another case, TFF coupled with SEC yielded 5.2-fold increase in EV concentration compared to density gradient ultracentrifugation after isolation of STR MSC(AT) cultures [150]. The EV downstream platform presented herein builds upon previous work by our group, where multiple anion-exchange resins were evaluated for particle recovery and impurity removal from CM derived from STR cultures [408]. The isolation protocol, combining ultrafiltration, nuclease digestion and AEC using the Capto™ Q ImpRes resin successfully recovered 53% of MSC-EVs, while impurity levels complied to regulatory agency requirements [408], outperforming

other isolation methods including UC and ultrafiltration coupled with SEC [189,408]. Other groups have also reported the use of different AEC columns to isolate EVs from the CM of MSC [192–194] and other cell lines [195,196]. Interestingly, Seo and colleagues were able to isolate cytotoxic T-lymphocyte-derived EVs with high purity and separate two EV subpopulations, namely bioactive exosomes and microvesicle-like EVs, using an AEC method [196]. In the present work, by incorporating TFF for the concentration/diafiltration step, a large-scale EV isolation protocol capable of processing large CM volumes (above 600 mL) that yields high EV numbers with great purity in less than 12 hours was successfully established.

A particle yield factor, which depends on both upstream and downstream processes, was proposed by Grangier and colleagues as a useful tool useful tool for comparing large-scale EV manufacturing platforms [140]. For example, using a 0.1L vertical-wheel system and UC as the EV isolation method, a particle yield factor ranging between ~0.5-2.5 x 10^3 particles/cell/day was obtained, depending on the agitation [147]. Moreover, MSC(AT) cultures processed with TFF-SEC yielded a production of ~2.25 x 10^3 particles/cell/day and ~6.65 x 10^3 particles/cell/day, when using static planar flasks and a 0.2L STR, respectively [150]. Haraszti and colleagues reported a particle yield factor of ~1 x 10^4 and ~3.5 x 10^2 particles/cell/day when using TFF and UC to isolate EVs from 2D static cultures of MSC(WJ), respectively [144].

Our platform generated a total number of (1.9 ± 0.38) x 10^{12} EVs, which corresponds to a particle yield factor of (1.2 ± 0.31) x 10^4 particles/cell/day. Interestingly, this factor was 3-fold higher than the one obtained using spinner flask as MSC(WJ) culture system, confirming that continuous collection of EV-containing CM further enhance productivity.

Notably, considering a clinical dose of MSC-EVs ranging from 10^{10} to 10^{11} total administrated nanoparticles [127], the manufacturing platform presented herein can provide at provide at least 10 EV doses and can be easily scaled-up to higher volumes to fit the needs of allogeneic clinical trials. The isolated EVs presented a homogeneous small size distribution with a mean diameter of ~120 nm and displayed a cup-shaped morphology in TEM images, which is in line with MSC-EV characteristics reported in previous studies [146,147,149,150]. The slightly lower negative surface charge of the isolated MSC-EVs (-23.4 ± 10.8 mV) compared to other studies [135,433] could be related to the selected isolation method, which separates EVs from the contaminants relying on their negative charge. The isolation process yielded EV samples with a PPR of (5.7 ± 2.7) x 10^9 particles/μg, which is higher than other EV preparations obtained from CM using other isolation methods [133,144,147,149,434], suggesting superior EV purity. For instance, EVs isolated from the CM of MSC cultured in stirred conditions had a PPR of 0.9 x 10^9 and 1.23 x 10^9 particles/μg when using UC and TFF, respectively [144]. The detection of tetraspanins CD9 and CD63 and syntenin-1 at higher levels in isolated EV samples compared to WCL controls further confirmed EV enrichment and purity of the preparation. EVs may trigger intracellular signalling through receptor-ligand interactions with target cells or by undergoing internalization to deliver their cargo through several mechanisms [435]. The isolated MSC-EVs were readily internalized by HUVEC and breast cancer cell lines, validating their potential application as natural therapeutics or drug delivery vehicles.

Overall, in this work, we integrated fully scalable and potentially GMP-compliant upstream and downstream processes that allowed reproducible, high-yield manufacturing of clinically relevant numbers of MSC-EVs with generally accepted characteristics in less than 2 weeks, representing an important step on the road to make MSC-EV-based therapies economically viable and widely available in a routine clinical setting.

III.6. Supplementary material

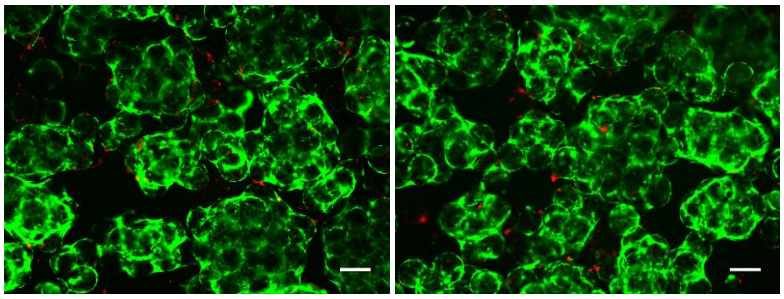

Supplementary Figure III.1 - Representative Live/Dead images of MSC(WJ) on microcarriers on day 10 of STR culture after MSC(WJ) expansion and EV production. Viable cells were stained with Calcein-AM and are shown in green while dead cells were stained with Ethidium Homodimer III (EthD-III) and are depicted in red. Scale bar: 250 µm.

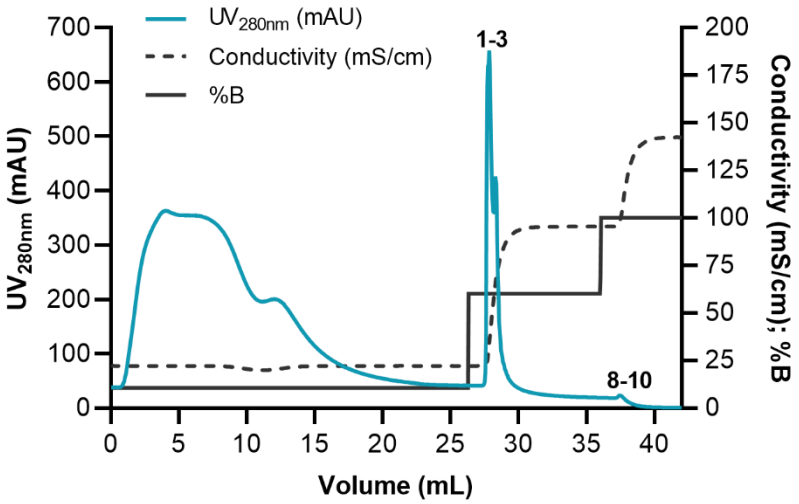

Supplementary Figure III.2- Chromatogram obtained after injection of EV-containing sample into a Capto™ Q ImpRes column pre-equilibrated with a buffer composed of 50 mM HEPES, 180.7 mM NaCl, pH 7, (10.5% buffer B, ≈23 mS/cm). Unbound material was washed with 15 CV of 10.5% B, and stepwise elution was performed with 10 CV of 60% B (≈95 mS/cm) and 7 CV of 100% B (≈142 mS/cm). Numbers over peaks correspond to the collected fractions. Blue continuous line: absorbance at 280 nm; grey dashed line: conductivity (mS/cm); black continuous line: percentage of buffer B (%B).

Chapter IV.

ENGINEERING OF MSC-EVS WITH SHRNA-EXPRESSING MINICIRCLES

IV.1. Abstract

Gene-based therapies hold promise for treating a wide array of diseases, but their efficacy is hindered by challenges namely in transporting large, fragile, negatively charged molecules such as DNA and RNA across cellular membranes. Extracellular vesicles (EVs) emerge as a natural delivery system that overcomes the limitations of synthetic nanocarriers. Ranging in size from 50 to 1,000 nm, these lipid bilayer structures facilitate intercellular communication by transporting various biologically active molecules. EVs are capable of encapsulating, protecting, and delivering therapeutic cargo to target cells, crossing biological barriers while presenting reduced immunogenicity and toxicity profiles.

EVs can be loaded with various therapeutic agents, including small molecules, proteins, and nucleic acids. Incorporating extrinsic cargo into EVs can be accomplished through direct or indirect loading, with the first being an easier, faster, and more flexible approach. Various loading methods, including co-incubation, electroporation, sonication and extrusion enable the incorporation of therapeutic nucleic acids (e.g., microRNA and siRNAs) into EVs. Although few studies have reported efficient DNA-loading into EVs, possibly due to its large size and conformation limitations, electroporation has enabled the effective EV encapsulation of plasmid vectors, in particular minicircles (MC). MCs are minimalist plasmid vectors making their incorporation into EVs presumably simpler than large conventional plasmids.

This work aimed to develop a novel anti-angiogenic gene-based therapy using mesenchymal stromal cell-derived EVs (MSC-EVs) as delivery vehicles of shRNA-expressing MCs that target key players in the vascular endothelial growth factor (VEGF) regulatory pathway. MSC-EVs retain the immunosuppressive activity and immunomodulatory properties of MSC. Moreover, MSC are extremely safe and efficient EV producers. Here, most work was performed using a reporter system composed by an MC that targets GFP (MC-shGFP) as cargo and GFP-expressing HEK293T cells (HEK-GFP+) as recipient cells. MSC-EVs loading was tested by passive incubation, microporation, sonication, liposome hybrids formation and using an EV transfection reagent. The loading efficiency of the MC into MSC-EVs was quantified using two alternative approaches, using real-time quantitative polymerase chain reaction (RT-qPCR) or fluorescently-labelled MCs. The functional EV-mediated delivery of MC-shGFP into HEK-GFP+ cells was evaluated by flow cytometry. Results showed low loading efficiencies (<7%) and no significant decrease in the median fluorescent intensity of HEK-GFP+ after MC-loaded EVs delivery, suggesting that the complexes were unable to induce a functional effect. Synthetic-siRNA-loaded EVs were also ineffective in decreasing the median fluorescent intensity. Globally, this work provided use of MSC-EVs delivery systems for shRNA-expressing MCs, indicating that several challenges need to be overcome to broadly establish EVs as nucleic acid delivery vehicles.

IV.2. Background

Gene-based therapies continue to advance, aiming at developing novel medicines for a broad range of diseases [444]. The main challenge limiting its *in vivo* application is the difficulty of transporting large, fragile, and negatively charged molecules, like DNA and RNA, through cellular membranes while ensuring a safe and efficient therapeutic effect. Tailored delivery systems are one of the strategies to improve the efficacy of gene therapy, aiming at extending their circulation time, avoiding mononuclear phagocyte uptake, and efficiently ensuring their transport into the cell cytoplasm without lysosomal degradation [445]. However, most delivery systems are based on synthetic nanocarriers which present limitations regarding toxicity and rapid clearance [446].

Extracellular vesicles (EVs)-based delivery offers an alternative to synthetic nanocarriers as natural vehicles that can load, protect, and deliver therapeutic cargo to nearby or distant cells. EVs are lipid bilayer structures with sizes ranging from 50 to 1,000 nm that modulate cell-cell communication by transporting a variety of biologically active molecules, including cytosolic and transmembrane proteins, bioactive lipids and nucleic acids [104,105]. EVs have the intrinsic capacity to cross biological barriers, including plasma/endosomal membranes and blood-brain barrier (BBB) [111]. Moreover, EVs present reduced immunogenicity and low toxicity in the spleen and liver [105,112], demonstrating to be an advantageous delivery system. In fact, studies have reported that EVs were internalized more efficiently and delivered their therapeutic agent several orders of magnitude more efficiently than synthetic nanoparticles [113,114]. EVs can be further bioengineered to alter their surface properties to improve their therapeutic efficacy and target-specificity [109]. EVs have been successfully loaded with different therapeutic agents, including, small molecules, drugs, proteins, and different RNA species, such as small interference RNA (siRNA) and microRNA (miRNA). Generally, the incorporation of extrinsic cargo into EVs can be accomplished by two methods: direct loading, with the external incorporation of cargo into isolated EVs; and indirect loading, by providing the parental cells with the means to naturally incorporate the desired cargo during EV biogenesis, typically by genetic engineering [109]. When compared to the laborious process of gene engineering methods, direct EV loading is a much easier, faster, and more flexible approach. Direct loading can be achieved through multiple processes, including co-incubation [202–205], electroporation [205–209], sonication [204,205,210,211], freeze-thawing [204], extrusion [211,212], permeation by a detergent-based compound [204,211], and complexation with liposomes [247,447].

EVs retain important features of the parental cells, presenting distinct internal and superficial cargos depending on the cell source consequently having different properties, namely, biodistribution and therapeutic effects on recipient cells [230]. Moreover, cell source availability, *ex vivo* expansion ability, and EV secretion capacity are also important factors when considering the high EV number required for an EV-based therapy. As a result, mesenchymal stromal cells (MSC) have been extensively investigated as EV producers [280]. MSC-derived-extracellular-vesicles (MSC-EVs) share immunosuppressive activity and immunomodulatory properties with MSC [276] and can influence recipient cells at genetic and biochemical levels and modulate

various physiological processes [274,275]. Moreover, MSC have proven to be exceptionally safe [272,273], and can efficiently mass-produce EVs by withstanding large-scale expansion and immortalization [284]. In fact, our group (Chapter III) and others have reported on the scalable manufacture of MSC-EVs using systems more readily translatable for clinical settings [134,150].

MSC-EV-mediated drug delivery includes the transport of small molecules (e.g., curcumin or chemotherapeutic drugs), proteins, siRNAs and miRNAs, demonstrating beneficial effects in numerous pre-clinical disease models [109]. For instance, MSC-EVs incubated with curcumin, effectively suppressed inflammatory response and cellular apoptosis in a stroke mouse model, surpassing the effect of curcumin alone [328]. As another example, MSC-EVs electroporated with siRNA targeting Kras were found to induce the suppression of oncogenic Kras and increase the survival of several mouse models with pancreatic cancer [309].

To date, only a few studies have been reported to develop DNA-encapsulating EVs using direct loading methods. For instance, Lamichhane and colleagues reported that DNA loading into MSC-EVs by electroporation was shown to be inefficient and dependent on DNA size and conformation [215]. Alternatively, with an optimized electroporation protocol, an average of 4,200 plasmid copies/EV were loaded into megakaryocytic-derived EV, thus enabling effective delivery of GFP–encoding pDNA to target cells [448]. Moreover, Izco and colleagues demonstrated that short hairpin RNA (shRNA)-expressing minicircles (MCs) can be readily delivered to the central nervous system in a mouse model of Parkinson's disease by murine dendritic cells EVs-modified with a brain-targeting peptide and decrease the target gene expression for prolonged periods [216]. MCs are small vectors free of bacterial backbone sequences and capable of high levels of transgene expression, that potentially meet the clinical requirements for safe and long-lasting gene expression [78,79]. Due to their small size, their incorporation into EVs is presumably simpler than conventional plasmids.

In this work, MSC-EVs were engineered through direct loading of shRNA-expressing MCs, aiming at developing a novel cell-free anti-angiogenic gene-based therapy by targeting the expression of key players of vascular endothelial growth factor (VEGF) regulatory pathway. We explored different methods to load MCs into MSC-EVs through a series of experiments using a reporter system consisting of an MC that targets GFP (MC-shGFP) and GFP-expressing HEK293T cells (HEK-GFP+) as recipient cells, including electroporation, sonication, passive incubation, formation of liposome-EV hybrids, and a transfection reagent. MC loading was quantified using two alternative approaches based on real-time quantitative polymerase chain reaction (RT-qPCR) or fluorescently-labelled MCs. Functional delivery of the complexes was evaluated by flow cytometry of HEK-GFP+ at different timepoints after treatment. Loading experiments using synthetic siRNAs as cargo were also performed. In general, this study highlights that various hurdles must be addressed to widely use MSC-EVs for nucleic acid delivery purposes.

IV.3. Materials and methods

IV.3.1. Cell lines and cell culture

Umbilical cord-derived Wharton's jelly MSC (MSC(WJ)) were obtained and isolated from human samples cultured in static and dynamic conditions as previously described (Chapter III).

HEK293T genetically engineered to constitutively express green fluorescent protein (GFP) (HEK-GFP+) (kindly provided by Dr Vasco Barreto, CEDOC/iNOVA4Health) were cultured using Dulbecco's modified Eagle's medium (DMEM) (Gibco, Life Technologies), supplemented with 10% (v/v) of heat-inactivated fetal bovine serum (FBS) (Lonza), and 1% (v/v) Antibiotic-Antimycotic (A/A) (Gibco, Life Technologies) and passaged between 2 and 3 times per week, by enzymatic treatment with trypsin (Gibco, Life Technologies) 0.05%.

Human umbilical vein endothelial cells (HUVEC) were cultured using Endothelial Cell Growth Medium-2 BulletKit™ (EGM™-2, Lonza) and passaged at 80–90% confluency by enzymatic treatment with accutase (Invitrogen, Life Technologies).

Cells were incubated at 37°C and 5% CO_2 in a humidified atmosphere. Cell number and viability were estimated using the Trypan Blue Solution, 0.4% (Gibco, Life Technologies) exclusion method.

IV.3.2. MSC-EVs production and isolation

To obtain the conditioned medium (CM) for isolation of MSC-EVs, MSC(WJ) were cultured in spinner flasks or stirred-tank reactors, as previously described (Chapter III) using hPL EV depleted formulation (Exosome depleted hPL UltraGRO™-PURE GI, AventaCell Biomedical). For some experiments the CM was produced using T-flasks and MSC were expanded in StemPro™ MSC SFM XenoFree culture medium (Life Technologies), and the conditioning was performed using in StemPro™ MSC SFM XenoFree basal formulation for 48 h.

EVs were isolated from CM using tangential flow filtration (TFF) combined with anion exchange chromatography, as previously described (Chapter III).

IV.3.3. MSC-EV uptake by HEK-GFP+ cells

Isolated MSC-EVs were labelled with the fluorescent dye AlexaFluor 647 NHS ester (Alexa647) (Invitrogen, Thermo Fisher) as previously described (Chapter III). Labelled-EVs were added to plated HEK-GFP+ cells at a concentration of approximately $2x10^{10}$ particles/mL in culture medium supplemented with Exosome-depleted FBS (Gibco) and incubated for 4-6 h at 37°C.

Cells were harvested from 96-well plates and subjected to flow cytometry using a FACSCalibur™ Flow Cytometer (BD). The percentage of EV-containing cells and median fluorescence intensity (MFI) values were analysed using FlowJo™ Software (BD).

Fluorescence images of HEK-GFP+ plated onto 8-well μ-Slide confocal microscope plates (Ibidi) and incubated with labelled-EVs were acquired using a Leica TCS SP5 inverted confocal laser scanning microscope (Leica Microsystems CMS Gmbh) and analysed with ImageJ open-source software.

IV.3.4. Direct loading of MSC-EVs with RNAi molecules

MSC-EVs loading with the MC or siRNA was tested by passive incubation, microporation, Exo-Fect™ transfection, sonication, and liposome hybrids. Depending on the experiment, different doses of EVs (from $1x10^9$ to $1.5x10^{10}$), MC (from 0.1 to 1 μg ; 0.33 to 330 pmol; $2x10^{11}$ to $2x10^{12}$), and siRNA (from 20 to 200 pmol) were used.

Conditions composed of only EVs, MC and siRNA were used as controls depending on the experiment. In selected experiments, Lipofectamine 2000® (Invitrogen™) was used as positive transfection control, according to the manufacturer's instructions.

IV.3.4.1. Electroporation method

EVs were engineered using electroporation performed on a Neon Transfection System ® (Thermo Fisher Scientific) following the manufacturer's protocol. Briefly, EVs and MC/siRNA were mixed, and the final volume was adjusted to 10 μL using the electroporation buffer R. Different ratios of EVs and MC-shGFP/ si-GFP were used, and the mixture was electroporated using different pulse widths, voltages and numbers of pulses, according to the previously reported literature [449–452] and also others (electroporation settings detailed throughout Section IV.4.). Then, the mixture was incubated for 30 min at 37ºC.

IV.3.4.2. Exofect™ method

MSC-EVs were transfected with MC-shGFP using the Exo-Fect™ Exosome Transfection Kit (Systems Biosciences) according to the manufacturer's instructions. Briefly, 1 μL of Exo-Fect™ solution was combined with the MC and purified MSC-EVs, resulting in a final volume of 15 μL in PBS 1x. The mixture was incubated at 37°C in a shaker for 10 min, and immediately placed on ice to arrest the reaction. To terminate the reaction, ExoQuick-TC reagent was gently added in a 1:5 (v/v) ratio of ExoQuick to EV and the mixture was incubated on ice for 30 min. Afterwards, the mixture was centrifugated at 13,000xg for 3 min. After removal of the supernatant, the EV pellet was resuspended in 15 μL of PBS 1x.

IV.3.4.3. Sonication method

EVs were engineered by sonication in a water bath sonicator (USC300T, VWR®). EVs and MC/siRNA were mixed and submitted to two cycles of 45kHz for 30 sec and 1 min incubation on ice. Then, the mixture was incubated for 30 min at 37ºC.

IV.3.4.4. EV-liposome hybrid method

EV-liposome hybrids were engineered by adapting a protocol developed elsewhere [247]. Lipofectamine 2000® and MC/siRNA were diluted in DMEM, respectively, then mixed and incubated at room temperature for 5 min. Afterwards, EVs were added to the plasmid–liposome complex and incubated at 37 °C for 18 h.

IV.3.5. EV loading efficiency quantification

IV.3.5.1. Loading quantification using real-time quantitative polymerase chain reaction (RT-qPCR) after DNase treatment

In a selected experiment, the loading efficiency was quantified using RT-qPCR. MSC-EVs ($1.5x10^9$) were mixed with MC-shGFP (100 ng; $2x10^{11}$ molecules) and submitted to passive incubation or microporation under different experimental conditions: 750V, 20ms and 10 pulses; 1,000V, 20ms and 10 pulses; and 1,500V, 20ms and 5 pulses (protocols detailed above).

Afterwards, a DNase treatment was performed to remove the non-incorporated MC using 2 Units of TURBO™ DNase (2U/µL; Life Technologies) and a final volume of 20 µL according to the manufacturer's instructions. The mixture was incubated at 37°C for 30 min and the reaction was stopped by adding EDTA to a final concentration of 15 mM, and heating at 75°C for 10 min.

Loading efficiency was evaluated by MC quantification by RT-qPCR using StepOnePlus™ Real-Time PCR System (Applied Biosystems), using NZY qPCR Green ROX plus kit (Nzytech) with a reaction mixture composed by 1µL of sample, 1x NZY qPCR Green Master Mix, 0.4 µM of the primers for U6 promoter (Fw 5'-GATACAAGGCTGTTAGAGAGATAA-3' and Rv 5'ACTGCAAACTACCCAAGAAA-3') to a final volume of 12 µL. A calibration curve of 25 pg and six 10-fold serial dilutions, was prepared with pure MC-shGFP. Cycle threshold (Ct) values were plotted against the log of mass and the points were fitted to a linear regression to determine the mass of MC and corresponding DNA copy number for each sample.

IV.3.5.2. Loading quantification using fluorescently-labelled MC

In a selected experiment, to avoid a DNase treatment, the loading efficiency of fluorescently-labelled-MCs was quantified, adapting a protocol developed elsewhere [453].

MC-shGFP was fluorescently labelled using the Label IT® Tracker™ Intracellular Nucleic Acid Localization Kit (Mirus Bio ®) according to the manufacturer's instructions. Briefly, a mixture of 0.5:1 (v:w) ratio of Label IT® Tracker™ Reagent to nucleic acid (2 µg), was incubated at 37°C for 1 h. Afterwards, the DNA was precipitated with 0.1 volume of 5M sodium chloride and 2 volumes of ice-cold 100% ethanol for 1h at -20ºC. The pDNA was pelleted by centrifugation at 14,000xg, 4ºC for 30 min. The pellet was washed with 70% (v/v) ethanol at room temperature for another 20 min. Finally, the airdried pellet was resuspended in 20 µL UltraPure™ DNase/RNase-Free Distilled Water (Life Technologies).

MSC-EVs ($1.5x10^9$) were mixed with labelled-MC (100 ng; $2x10^{11}$ molecules) and submitted to passive incubation, Exo-Fect™ transfection and microporation using 5 or 10 pulses with 20 ms of width and 1,000 or 1,500 V of voltage (protocols detailed above).

Regardless of the method used, all samples were precipitated using ExoQuick-TC reagent, as described in section IV.3.3.4. The supernatant and the pellet were separated, and fluorescence was measured on each fraction. To control for MC precipitation upon treatment, the MC in the absence of EVs was incubated in the same conditions as described above.

The emission spectrum of all samples (excited at λex=555 nm) was measured from λem=560 nm until λem=700 nm using the plate reader Infinite® 200 PRO, NanoQuant, Tecan Trading AG (Männedorf, Switzerland) and the sum of intensities from 560-700nm for each sample was considered to calculate the loading efficiency of each method. The precipitation efficiency on each condition, including the control without EVs, was calculated using the formula: fluorescence intensity of the pellet / (fluorescence intensity of the pellet + fluorescence intensity of the supernatant). For each condition, the fluorescence value of the control was subtracted from the measured value and represented as the percentage of loading efficiency.

IV.3.6. Evaluation of the functional effect of loaded EVs

IV.3.6.1. Functional effect of loaded EVs on HEK-GFP+

The day before the EV delivery experiment, HEK-GFP+ cells (25,000 cells) were plated in 48-well plates and cultured in low glucose DMEM supplemented with 5% Exosome-depleted FBS (Gibco). EVs loaded with the MC and siRNA that silence the expression of GFP were added to the cells in doses ranging from $2x10^4$ to $6x10^5$ EVs/cell, at a concentration ranging from $2.5x10^9$ to $5x10^{10}$ EVs/mL (150-300 μL/well) in low glucose DMEM supplemented with 5% Exosome-depleted FBS (Gibco). After 24 h, ~500 μL of low glucose DMEM supplemented with 5% FBS (Gibco) was added to the cells.

Cells were then harvested at different time points and subjected to flow cytometry using a FACSCalibur™ Flow Cytometer (BD) and the median fluorescence intensity (MFI) values were analysed using FlowJo™ Software (BD).

IV.3.6.2. Functional effect of loaded EVs on HUVEC

The day before the EV delivery experiment, HUVEC (100,000 cells) were plated on 24-well plates and cultured EGM™-2. Loaded EVs with the MC and siRNA that silence the expression of VEGFR2 were added to the cells at a dose of $6x10^4$ EVs/cell, at a concentration of $2x10^{10}$ EVs/mL (300 μL/well) in EGM™-2 supplemented with 2% Exosome-depleted FBS (Gibco). After 24 h, ~500 μL of EGM™-2 was added to the cells. Cells were then harvested after 72 h, and VEGR2-mRNA was quantified by RT-qPCR. Total RNA was extracted from cell pellets with RNeasy Mini Kit (Qiagen), converted to cDNA with the High-Capacity cDNA Reverse Transcription Kit (Life Technologies) and quantified using a NZY qPCR Green ROX plus kit

(Nzytech) and primers for VEGFR2 on a StepOnePlus™ Real-Time PCR System (Applied Biosystems), as previously described (Chapter II).

IV.4. Results

IV.4.1. MSC-EVs are internalized by HEK-GFP+ cells

In Chapter III, besides the morphological characterisation of MSC-EVs, an uptake assay was performed to validate cell internalisation of the isolated MSC-EVs into potential target cells (breast cancer cell lines MDA-MB-231 and MCF-7, and HUVEC). Here, since most work of MSC-EVs engineering was performed using the MC that targets GFP (MC-shGFP), GFP-expressing HEK293T cells (HEK-GFP+) were used as target cells and their capacity to internalise MSC-EVs was evaluated. MSC-EVs were stained with Alexa647, and then incubated with HEK-GFP+ for 5 h. Afterwards, cells were harvested, and flow cytometry was performed. (**Figure IV.1-A, B**).

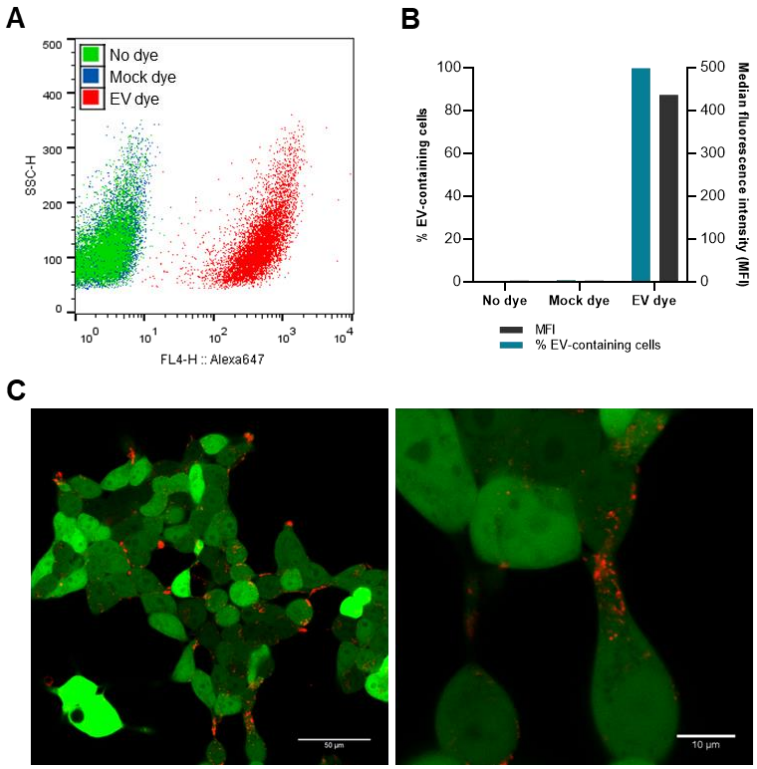

Figure IV.1 - Analysis of EV uptake by HEK-GFP+ cells after treatment with Alexa647-labelled MSC-EVs. **(A)** Flow cytometry analysis of EV uptake by HEK-GFP+ cells after 5h of incubation, represented as an overlay of the dot plots (side scatter height (y) vs. EV fluorescence height (x)) obtained for HEK-GFP+ cells without treatment (No dye) or treated with the dye only (mock dye) or Alexa647-labelled MSC-EVs (EV dye). **(B)** Percentage of EV-containing cells and median fluorescence intensities (MFI) of flow cytometry measurements. **(C)** Representative images of Alexa647-labelled EVs (red) uptake by HEK-GFP+ (green). Scale bars are depicted in each image.

The results demonstrate that virtually all cells were positive for labelled EVs (99.8% of EV-containing cells) (**Figure IV.1-B**). Importantly, HEK-GFP+ treated with mock dye (Alexa647

without EVs) demonstrated no positivity for Alexa 467, showing MFI similar to the one obtained for HEK-GFP+ cells without treatment (No dye) (**Figure IV.1-A, B**). Moreover, after 4 h of incubation with labelled-EVs, HEK-GFP+ were observed by fluorescence microscopy, which further confirmed the MSC-EV uptake (**Figure IV.1-C**).

IV.4.2. Loading quantification was accomplished using two approaches

To quantify the loading efficiency of the MC into MSC-EVs, two alternative approaches were explored. The first strategy included a DNase treatment after loading the MC-shGFP into MSC-EVs to remove the non-encapsulated MC. Afterwards, the EV loading efficiency was evaluated by MC quantification using RT-qPCR. In this case, 100 ng of MC-shGFP were loaded into $1.5x10^9$ MSC-EVs through passive incubation and microporation using different voltages (750, 1,000 and 1,500 V) and numbers of pulses (5 or 10 pulses) of 20 ms (**Table IV.1**), and half of the mixture was quantified. Non-electroporated MC and EV were submitted to the same protocol and used as controls. A calibration curve (**Supplementary Figure IV.1**) allowed the assessment of the MC mass for each loading condition (**Table IV.1**), after subtracting the mass obtained for MC and EV controls. Considering this value and the initial mass of the MC, it was possible to estimate the percentage of loading efficiency for each condition. Moreover, it was possible to determine the number of loaded MC molecules and number of MC molecules loaded per EV for each loading condition (**Table IV.1**). To estimate these values, the number of MC molecules was calculated from the estimated mass of MC, considering the molecular weight of the MC (~$3.08x10^5$ g/mol of dsDNA) and the Avogadro's Number $6.022x10^{23}$ molecules/mol. This value was divided by the number of EVs used (i.e. $7.5x10^8$ particles for all the conditions), based on Nanoparticle tracking analysis (NTA) measurements of EV concentration.

Table IV.1- RT-qPCR quantification of the MC loaded into MSC-EVs using incubation and different microporation conditions as direct loading methods. The estimated MC mass, number of MC molecules and number of MC molecules per EV for each loading condition are shown.

Condition	MC mass (fg)	Loading efficiency (%)	Number of MC molecules	Number of MC molecules/ EV
Incubation	6.1	$1.2x10^{-5}$	$1.2x10^4$	$1.6x10^{-5}$
Microp 750V;20ms;10p	3.9	$0.80x10^{-5}$	$0.80x10^4$	$1.0x10^{-5}$
Microp 1,000V;20ms;10p	9.9	$2.0x10^{-5}$	$2.0x10^4$	$2.6x10^{-5}$
Microp 1,500V;20ms;5p	18	$3.6x10^{-5}$	$3.6x10^4$	$4.8x10^{-5}$

The results showed that the loading efficiencies were extremely low with a number of MC molecules loaded per EV ranging from $1.0x10^{-5}$ to $4.8x10^{-5}$, depending on the loading conditions, which corresponds to less than five molecules of MC loaded into 100,000 EVs (**Table IV.1**). Nevertheless, the results demonstrate that microporation at high voltages (1,000 – 1,500V) improved MC incorporation compared to simple incubation (**Table IV.1**). It is important to consider that the DNase treatment might be influencing the capacity of EVs in delivering the MC since it is

unknown if the MC is completely or partially encapsulated or adsorbed to the EV membrane and the DNase treatment might be disrupting the EV-MC interaction, causing an underestimation of the loading efficiency.

Thus, to avoid a DNase treatment, the MC loading was quantified through an alternative approach using fluorescently-labelled-MCs, adapting a protocol developed elsewhere [453]. MC-shGFP was fluorescently labelled with Rhodamine (100 ng) and loaded into MSC-EVs ($1.5x10^9$ particles) using passive incubation, Exo-Fect™ transfection and microporation using two different settings (**Table IV.2**). Afterwards, samples were precipitated to remove the non-incorporated MC. To control for MC precipitation upon treatment, the MC was incubated in the same conditions as described above. The precipitation efficiency on each condition, including the control without EVs, was calculated (**Table IV.2**). Additionally, for each condition, the fluorescence value of the control was subtracted from the measured value and represented as a percentage of loading efficiency. In the case of Exo-Fect™ transfection, an extra control composed of the reagent and MC without EVs was considered. The precipitation efficiency of the Exo-Fect™-containing conditions revealed that the presence of the reagent facilitates the precipitation of the MC (**Table IV.2**).

Considering the loading efficiency and the initial mass of the MC, it was possible to estimate the mass of loaded MC and the number of MC molecules loaded per EV for each loading condition (**Table IV.2**), calculated as described above. Interestingly, the loading efficiencies, and consequently the number of MC molecules loaded per EV, were much higher than the ones assessed using the previous method, but still below 7% (**Table IV.2**). Once again, conditions in which EVs and MC were submitted to electroporation showed increased loading efficiencies compared to passive incubation, particularly at high voltages (1,500 V) (**Table IV.2**). The Exo-Fect™ reagent alone facilitated the precipitation of the MC and, after subtracting this value, the loading efficiency was lower than for the incubation method, which might not be an accurate estimation (**Table IV.2**)

Table IV.2- Quantification of fluorescently-labelled-MC loaded into MSC-EVs using incubation, the Exo-Fect™ reagent and different microporation conditions as direct loading methods. The precipitation efficiency (%) on each condition, including the controls without EVs was calculated. The estimated loading efficiency (%), mass of loaded MC and number of MC molecules loaded per EV for each loading condition are shown.

Condition	Precipitation efficiency (%)	Loading efficiency (%)	MC mass (ng)	Number of MC molecules	Number of MC molecules/ EV
MC	12	-	-	-	-
MC + Exo-Fect™	86	-	-	-	-
MC + EV + Exo-Fect™	90	3.6	3.6	$7.1x10^9$	4.7
MC + EV + Incubation	16	4.0	4.0	$8.0x10^9$	5.3
MC + EV + Microp 1,000V; 20ms; 10p	16	4.5	4.5	$8.9x10^9$	5.9
MC + EV + Microp 1,500V; 20ms; 5p	18	6.3	6.3	$1.2x10^9$	8.3

IV.4.3. Functional effect of RNAi-loaded MSC-EVs was evaluated by target cell delivery

As aforementioned, most work was performed using a reporter system composed of the MC-shGFP as cargo and HEK-GFP+ as recipient cells. Generally, after MSC-EV loading with the MC-shGFP, the functional delivery of the MC was evaluated by incubating HEK-GFP+ with the EV-MC complexes and cultured in EV-depleted medium for different timepoints. Afterwards, cells were harvested, and flow cytometry was performed to evaluate the effect of the delivered MC-shGFP on the MFI of the recipient cells.

As a first experiment, MSC-EVs were loaded with MC-shGFP using passive incubation, Exo-Fect™ transfection and microporation with two different settings, as performed for the loading quantification experiment (**Table IV.2**), and delivered to HEK-GFP+ at a concentration of $5x10^9$ EVs/mL, representing an approximate dose of $6x10^4$ EVs/cell. After 48h of incubation, the MFI HEK-GFP+ of each condition was quantified through flow cytometry (**Table IV.3**). The results showed that the delivery of EVs loaded by passive incubation and microporation did not cause a decrease in the MFI of HEK-GFP+ compared to the MC control, suggesting that the loaded MC (<7%) was not sufficient to exert a detectable silencing effect on the recipient cells. In contrast, the Exo-Fect™ method induced a decrease in the MFI compared to the MC control, suggesting that the MC was delivered and expressed by the cells. However, MC alone with the Exo-Fect™ reagent also induced a decrease in MFI revealing that this effect seems to be EV-independent.

Table IV.3- Median Fluorescence Intensity (MFI) of HEK-GFP+, 48h after incubation with MC-loaded MSC-EVs, using incubation, the Exo-Fect™ reagent and different microporation conditions as direct loading methods. Fold changes of the MFI for each condition relative to the MC condition were calculated. The corresponding loading efficiencies of each loading method estimated using fluorescently-labelled MC are shown.

Condition	Loading efficiency (%)	MFI of transfected HEK-GFP+	MFI fold change (relative to MC condition)
MC	-	1303	1.0
MC + Exo-Fect™	-	1009	0.76
MC + EV + Exo-Fect™	3.6	1006	0.74
MC + EV + Incubation	4.0	1345	1.0
MC + EV + Microp 1000V; 20ms; 10p	4.5	1374	0.99
MC + EV + Microp 1500V; 20ms; 5p	6.3	1291	1.0

To test a different timepoint after delivery, MSC-EVs loaded by passive incubation and microporation were delivered to HEKF-GFP+ and MFI was evaluated after 72 h. Additionally, the formation of liposome-EV hybrids was explored as an alternative loading method. MC was incubated with lipofectamine 2000® (LF) and then incubated with MSC-EVs for 18 h at 37°C as established by others [247]. In this experiment, LF incubated with the MC for 30 min or 18 h were used as positive transfection controls. The results in **Table IV.4** showed that in the passive incubation condition no changes in the MFI of HEK-GFP+ were observed compared to the MC-only condition, while the microporated condition induced a slight decrease in the MFI of HEK-GFP+ (0.87-fold) (**Figure IV.2-A**). LF-MC complexes induced a higher decrease in the MFI of HEK-GFP+ compared to the MC control confirming that the MC-shGFP can induce a silencing effect on the transfected cells with a decrease of around 40% (**Table IV.4, Figure IV.2**). MC-loaded through the formation of liposome-EV hybrids (LF + EV + MC) induced a decrease in the MFI of HEK-GFP+ compared to the MC control. However, this decrease is similar to LF alone (LF + MC), demonstrating no improved effect with the presence of EVs (**Table IV.4, Figure IV.2-B**).

Table IV.4- Median Fluorescence Intensity (MFI) of HEK-GFP+, 72h after incubation with MC-loaded MSC-EVs, using incubation, microporation and liposome-EV hybrids as direct loading methods. Lipofectamine® (LF) was used as transfection control. Fold changes of the MFI for each condition relative to the MC condition are shown.

Condition		MFI of transfected HEK-GFP+	MFI fold change (relative to MC condition)
30 min	**MC**	1685	1.0
	LF + MC	1000	0.59
	MC + EV + Incubation	1999	1.2
	MC + EV + Microp 750V; 20ms; 10p	1472	0.87
18 h	**LF + MC**	1144	0.67
	LF + EV + MC	1165	0.69

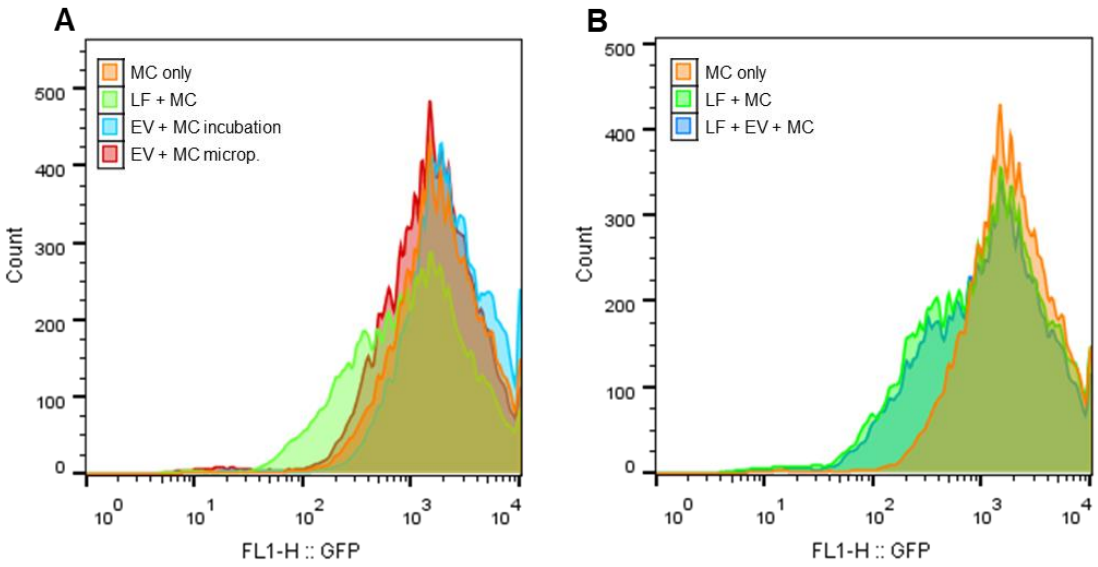

Figure IV.2- Histograms of flow cytometry analysis of HEK-GFP+ 72h after incubation with EVs loaded with MC-shGFP using different loading methods. **(A)** MSC-EVs were loaded with MC-shGFP by passive incubation (EV + MC incubation) and microporation (EV + MC microp.) and incubated with HEKF-GFP+ for 72h. **(B)** MSC-EVs were loaded with MC-shGFP with the formation of liposome-EV hybrids. MC was incubated with Lipofectamine 2000® and then incubated with MSC-EVs (LF + EV + MC). Incubation with the MC only was used as a negative control and Lipofectamine 2000® incubated with the MC was used as a positive transfection control (LF + MC).

Only a few studies have reported the use of direct EV loading methods to encapsulate DNA, being often inefficient and possibly limited by the size and conformation of DNA [215,454]. On the other hand, microRNA and siRNA have been successfully loaded into EVs by a variety of direct loading approaches, the most common being electroporation [308–310,449,450,452]. Therefore, besides testing MC-shGFP loading into MSC-EVs, siRNA that targets GFP (siR-GFP) was also exploited as silencing cargo. In this experiment, $3x10^9$ MSC-EVs were loaded with MC-shGFP (1 μg) or siR-GFP (20 pmol) using passive incubation, microporation using two different settings, sonication, and liposome-EV hybrids, and delivered to HEK-GFP+ at a concentration of $2.5x10^9$ EVs/mL, representing an approximate dose of $1.5x10^4$ EVs/cell. After 48 or 96 h of incubation, the MFI HEK-GFP+ of each condition was quantified through flow cytometry. LF incubated with the MC/siR was used as a positive transfection control (**Supplementary Table IV.1**). The results of the fold change relative to no treatment condition (**Figure IV.3**), showed similar silencing effects in HEK-GFP+ after incubation with MSC-EVs loaded with MC through incubation, microporation and sonication. Moreover, contrarily to what was anticipated, similar silencing effects in HEK-GFP+ after treatment with MSC-EVs loaded MC and siR were observed, rather than a stronger effect for siR, which has been reported to be more easily loaded into EVs. Generally, the silencing effect appears to be more pronounced at the 96h timepoint, being more evident in the LF-containing conditions. Regardless of the timepoint, the silencing effect of the

siR- or MC-loaded EVs using incubation, microporation and sonication was slight (≥0.83-fold change relative to no treatment) when compared to the positive transfection control LF. Concerning the formation of liposome-EV hybrids, MC loading induced a decrease in the MFI of HEK-GFP+ compared to no treatment control, however, it was lower than LF condition alone (0.69-fold vs 0.62-fold at 48 h; 0.39-fold vs 0.29-fold at 96 h). On the other hand, the silencing effect of liposome-EV hybrids was stronger than LF alone when siR was used as cargo (0.49-fold vs 0.77-fold at 48h; 0.27-fold vs 0.55-fold at 96h).

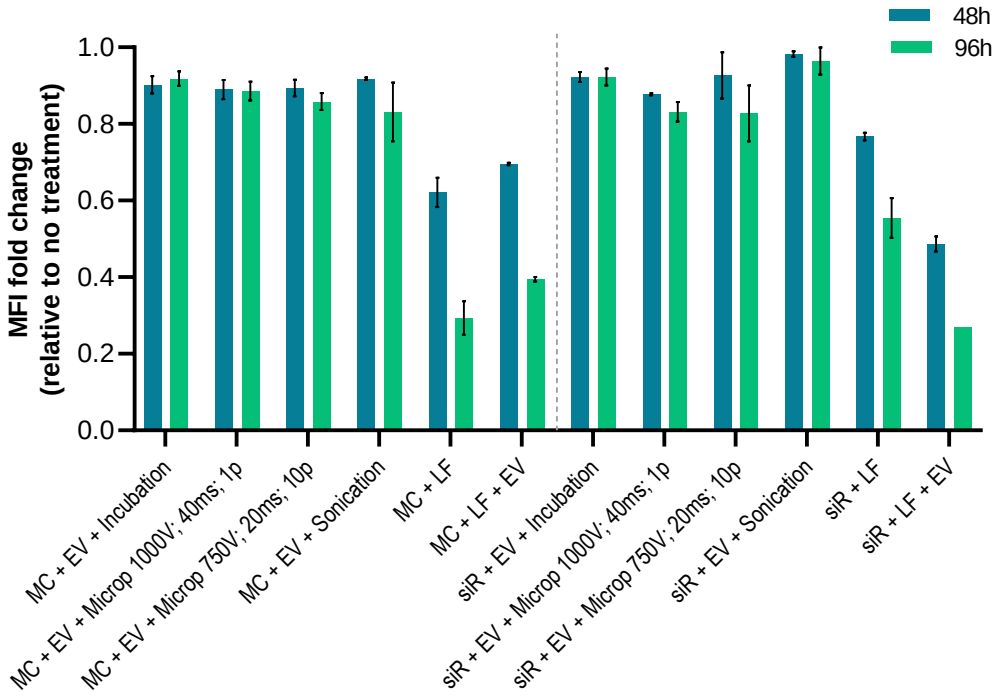

Figure IV.3 - Median Fluorescence Intensity (MFI) of HEK-GFP+, 48h and 96h after incubation with MSC-EVs loaded with MC or siR that target GFP, using incubation, microporation, sonication and liposome-EV hybrids as direct loading methods. Lipofectamine® (LF) was used as transfection control. Values are presented as fold change relative to no treatment condition. Values represent a single experiment with technical duplicates.

Another experiment of siR-GFP loading into MSC-EVs was performed, exploring different microporation settings that have been described in the literature to functionally load different molecules into EVs using the Neon transfection System® [449–452]. An extra condition using the microporation parameters used to efficiently transfect MSC was also included [369,370] (**Table IV.5**). In this case, $1.5x10^{10}$ MSC-EVs were loaded with siR-GFP (200 pmol) and delivered to HEK-GFP+ at a concentration of $5x10^{10}$ EVs/mL, representing an approximate dose of $6x10^{5}$ EVs/cell. The MFI HEK-GFP+ of each condition was quantified through flow cytometry, 72 and 120 h after incubation, using treatment with EVs loaded by passive incubation, EV only and siR only as controls. LF was used as a positive transfection control (**Supplementary Table IV.2**).

Table IV.5- Microporation parameters (voltage, width of the pulse and number of pulses) tested for the loading of siRNAs into MSC-EVs. All conditions, except Microp 4, are reported in the literature to functionally load different molecules into EVs using the Neon transfection System®.

Condition	Voltage; width; number of pulses	Ref
Microp 1	750V; 20ms; 10p	[449]
Microp 2	1,000V; 10ms; 2p	[451]
Microp 3	500V; 1ms; 1p	[452]
Microp 4	1,000V; 40ms; 1p	[369,370]
Microp 5	500V; 10ms; 5p	[450]

The results of the fold change relative to siR only treatment condition (**Figure IV.4**), showed no silencing effects in HEK-GFP+ after incubation with MSC-EVs loaded with siR-GFP regardless of the applied microporation setting, except for Microp 1 which induced a slight decrease in MFI after 120h (0.89-fold change). On the contrary, siR-GFP induced a strong decrease in the MFI of HEK-GFP+ when delivered by LF, which was attenuated by the presence of EV (0.27-fold vs 0.39-fold at 72 h). This effect is contrary to what was observed in the previous experiment and similar to the results of MC-shGFP loading (**Figure IV.5**).

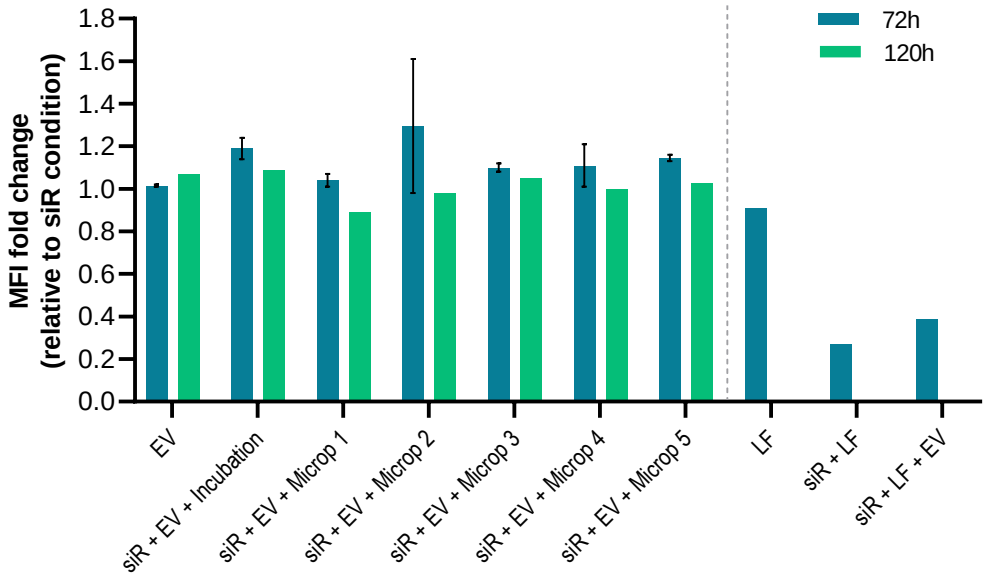

Figure IV.4 - Median Fluorescence Intensity (MFI) of HEK-GFP+, 72h and 120h after incubation with MSC-EVs loaded with siR that target GFP, using incubation and different microporation conditions (**Table IV.5**), and liposome-EV hybrids as direct loading methods. Lipofectamine® (LF) was used as transfection control. Values are presented as fold change relative to siR condition and represent the mean ± SEM of two independent experiments the 120h timepoint except for LF and hybrid conditions which result from a single experiment. Values for 120h represent a single experiment.

A final loading experiment was conducted using the MC that silences vascular endothelial growth factor receptor 2 (VEGFR2) (MC-shVEGFR2) to evaluate the functional effect of loaded EVs delivery on human umbilical vein endothelial cells (HUVEC). In this case, $6x10^9$ MSC-EVs were loaded with MC-shVEGFR2 (1 μg) or siR-VEGFR2 (100 pmol) using microporation (750V, 20ms and 10 pulses [449]) and delivered to HUVEC at a concentration of $2x10^{10}$ EVs/mL, representing an approximate dose of $6x10^4$ EVs/cell. MC-shGFP was used as negative silencing control and LF incubated with MC and si-VEGFR2 was used as a positive transfection control. The mRNA-VEGFR2 expression level of each condition was quantified through RT-qPCR, 72h after treatment with the complexes, using untreated HUVEC as control (**Figure IV.5**). The results showed no silencing effect of VEGFR2 on HUVEC after incubation with the loaded MSC-EVs using siR or MC as cargo, in contrast to LF + siR-VEGFR2 transfection which induced a knockdown of ~57% (**Figure IV.5**). Importantly, while HUVEC incubated with EV-containing conditions presented a cell recovery of >100%, LF transfection of the siR-VEFR2 led to a cell recovery of ~38% and when transfecting MC-shVEGFR2 the cells did not survive.

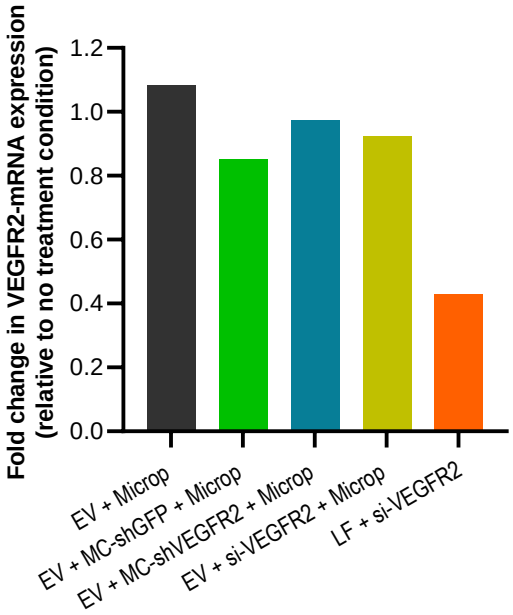

Figure IV.5 - Relative VEGFR2-mRNA expression in HUVEC 72h after incubation with MSC-EVs microporated with MC and siRNA that target VEGF, assessed through RT-qPCR using the $2^{-\Delta\Delta Ct}$ method. GAPDH was used as the endogenous control gene and no treatment HUVEC as the control condition. EVs microporated with MC-shGFP and si-VEGFR2-loaded Lipofectamine® (LF + si-VEGFR2) were used as negative and positive silencing controls, respectively.

IV.5. Discussion

EVs are essential mediators of cell-cell communication, and their ability to transport biologically active molecules and cross biological barriers, along with their favourable safety profile, make them promising delivery systems as an alternative to synthetic nanocarriers. Although the best cell source of EVs is still up for debate and likely dependent on the therapeutic context, MSC have received significant attention due to their intrinsic therapeutic potential [274,275]. Different types of therapeutic payloads have been successfully loaded into MSC-EVs, including nucleic acids, proteins and small molecules, demonstrating positive effects in numerous pre-clinical animal models, namely in the treatment of several types of cancer and degenerative diseases [109]. Some studies have already reached clinical trials, exploring MSC-EVs as delivery vehicles of nucleic acids: EVs enriched with miR-124 as a treatment for acute ischemic stroke patients (NCT03384433); MSC-EVs containing siR targeting oncogenic $Kras^{G12D}$ mutations in pancreatic ductal adenocarcinoma patients (NCT03608631); and low-density lipoprotein receptor (LDLR)-mRNA enriched EVs for the treatment of homozygous familial hypercholesterolemia (NCT05043181).

In this work, we studied the engineering of MSC-EVs with shRNA-expressing MCs aiming at developing a novel cell-free gene-based therapy. This was accomplished using direct loading methods, which are considered easier, faster, and more flexible than the laborious process of genetic engineering methods used for indirect loading. Moreover, direct loading facilitates the use of engineered EVs as versatile off-the-shelf products since previously isolated EVs can be loaded with distinct cargo molecules. Here, besides passive incubation, we tested electroporation, sonication, formation of liposome-EV hybrids and an EV-transfection reagent to actively engineer MSC-EVs with the RNAi molecules. Electroporation, which relies on the exposure of the EV membrane to high-intensity electrical pulses, has been the most widely used method to facilitate the loading of different cargos into EVs, including small molecules [208], siRNAs [111,206], miRNAs [207,213,214], DNA [215,216,448] and CRISPR–Cas9 components [209]. Similarly, the sonication method has promoted the active loading of siRNAs [210] and small molecules [205,325,329] into EVs using a low-intensity ultrasound frequency by transiently opening membrane pores. The formation of EV-liposome hybrids has also been reported as a method to functionally deliver nucleic acids (e.g., siRNA and pDNA) to target cells [247,250]. Finally, the chemical reagent Exo-Fect™ has been used to facilitate the EV-mediated delivery of miRNAs [453], siRNAs [455], pDNA [456] and small molecules [455].

Despite the promise, the effectiveness of EV loading for drug delivery is hindered by the lack of standardized loading metrics, which are commonly used in synthetic vector research but are not consistently applied in EV studies [457,458]. The two main metrics adapted from the drug delivery field that are useful for comparing the performance of EV engineering approaches are encapsulation efficiency, which refers to the percentage of drug encapsulated within the vector, and loading capacity which measures the amount of drug loaded per vector [457,458]. In this work, two distinct approaches have been explored to quantify the loading of MCs into MSC-EVs: RT-qPCR-based quantification of the loaded MC after DNase treatment to remove

non-encapsulated MC and fluorescently-labelled-MC-based quantification after precipitation step to remove the non-interacting MC. These two strategies allowed the estimation of loading efficiency of MC into MSC-EVs and their loading capacity (number of MC molecules per EV) for the different loading methods. In this case, MCs were loaded into MSC-EVs using passive incubation, Exo-Fect™ transfection, and microporation using different voltages and number of pulses.

The first approach offers specificity and quantitative measurements but potentially underestimates the loading efficiency due to the DNase-mediated disruption of EV-MC interactions. The estimated loading capacity using this quantification method ranged from $1.0x10^{-5}$ to $4.8x10^{-5}$ MC molecules per EV, which corresponds to one MC copy per $9.7x10^{4}$ - $2.1x10^{4}$ EVs, being higher when using electroporation at higher voltages. In a recent study, Kang and colleagues used a similar approach to quantify the efficiency of pDNA exogenously loaded into placental-derived EVs [454]. Using electroporation at 200 V, 100 ng of pDNA and an EV dose of $1.0x10^{11}$ particles, ratios of one plasmid per $2.3x10^{3}$ large-EV particles and one plasmid per $3.9x10^{3}$ small-EV particles were obtained. Despite the lower ratios when compared to our results, these correspond to loading efficiencies of less than ~1%. Using passive incubation as direct loading, the obtained ratios were higher and similar to ours [454]. This study demonstrated that only a minor quantity of the initial pDNA was encapsulated, and thus protected by the EVs against the DNase action, being consistent with our results and the findings from Lamichhane and colleagues (<0.2% loading efficiency using pDNA as cargo and PicoGreen assay as quantification method [215]).

In contrast, the second strategy is independent of a DNase treatment, allowing the quantification of the MC that is associated with the MSC-EVs through further interactions other than full encapsulation. As expected, using the same loading methods and an additional one, this strategy estimated improved loading efficiencies and loading capacities when compared with the first approach (10^{5}-fold increase). Nevertheless, the results were consistent with the previous estimations since conditions in which EVs and MC were submitted to electroporation showed increased loading efficiencies when compared to passive incubation, particularly at high voltages (~6.5%). However, it is important to note that this quantification approach is less precise due to the variability associated with the precipitation step and fluorescence-based quantification may not provide as sensitive measurements as RT-qPCR, particularly for low abundance targets. Moreover, the MC labelling process can cause changes in structure/conformation and consequently, influence its association with the EVs. Thus, a combination of both strategies could result in a more reliable quantification.

A large part of EV-engineering studies does not quantify cargo loading, and when reported, the efficiencies are often inconsistent. For instance, using electroporation, loading efficiencies of 30% [449], 2% [215], 60% [448], 15% [459] or 0.09% [460], and 20% [208] were reported when engineering EVs with miRNA, linear dsDNA, pDNA, siRNAs, and doxorubicin, respectively. Aside from the inherent differences in the electroporation systems/protocols and quantification methods used, the discrepancy concerning the loading efficiencies reported can be

affected by other factors, including the physicochemical properties of cargo and EVs that are different depending on the cell source or EV isolation method [457,458]. For instance, in a study by Fuhrmann and colleagues, EVs from different cellular origins (breast cancer cells, endothelial cells, MSC and embryonic stem cells) were loaded with porphyrins with different degrees of hydrophobicity using various methods (electroporation, dialysis, saponin, and extrusion). Loading efficiency was not only dependent on the loading method but also on the hydrophobic nature of the drug and the chemical lipid composition of the vesicles [461]. Additionally, Abreu and collaborators studied miRNA loading into EVs isolated from the CM of human umbilical cord blood-derived mononuclear cells, human urine and commercially available FBS. Depending on the origin, different levels of contaminants were present in the EV preparations, which could be responsible for the reported variations in loading efficiency [453]. Thus, due to the intrinsic differences observed between sources of MSC and derived EVs [166], it would be significant to evaluate if this variability is extended to EV loading ability. Moreover, the impact of EV isolation methods on the MSC-EV loading should be investigated, particularly by exploring the combination of TFF with size-exclusion chromatography [462].

Besides evaluating the efficiency of cargo loading, it is important to provide evidence of EV-cargo functionality after their delivery to recipient cells. In this work, to evaluate the bioactivity of MC-engineered EVs, we used HEK-GFP+ as recipient cells and MC encoding a shRNA that silences GFP expression as cargo. As a first experiment, the methods used in the loading quantification experiment using fluorescently-labelled-MC were replicated (MC copies per EV ratio of ~130) and the MC-loaded EVs were delivered to HEK-GFP+ at an approximate dose of $6x10^4$ EVs/cells. At 48h post-treatment, no decrease in the MFI of HEK-GFP+ was observed, except for Exo-Fect™, suggesting that the amount of MC delivered was not sufficient to induce GFP silencing on the recipient cells. Exo-Fect™ method was excluded since in the absence of EVs the reagent induced the same silencing effect. Subsequent experiments were performed in which EVs were loaded by passive incubation, microporation at different settings, sonication, and incubation with lipofectamine to promote the formation of liposome-EV hybrids. The experiments included higher MC copies per EV ratios (200 and 660), similar EV doses ($2x10^4$ and $1.5x10^4$ EVs/cell) and distinct time points after treatment (72 h and 48 h plus 96 h).

In general, regardless of the timepoint, the silencing effect of MC-loaded EVs was slight or inexistent in comparison to the selected control when using incubation (0.90- to 1.2-fold change), microporation (0.85- to 0.89-fold change) and sonication (0.83- to 0.92-fold change) as loading methods. In contrast, transfection of HEK-GFP+ with the MC induced a strong decrease in MFI compared to the selected control (0.57- to 0.29-fold change), presenting a maximum knockdown of approximately 70% at 96 h after transfection. Concerning the formation of liposome-EV hybrids, a similar decrease in the MFI of HEK-GFP+ was observed when cells were incubated with the MC-loaded hybrids or LF alone, demonstrating that the presence of EVs does not contribute to the observed silencing effect. Nevertheless, it is important to consider that there are some inherent fluctuations in the MFI of HEK-GFP+ between experiments and replicates of

the same experiment, so these slight changes could be artefacts and further investigation is required.

As most of the success of EVs for nucleic acid therapy has been associated with the delivery of RNA molecules as opposed to DNA, we also investigated the EV engineering with siRNA that targets GFP. Interestingly, an experiment performed as a side-by-side comparison with the MC revealed equivalent silencing effects on the MFI of HEK-GFP+ after treatment with MSC-EVs carrying MC and siR. Moreover, subsequent experiments using the siR as cargo were performed using microporation settings described in the literature [449–452]. Overall, no silencing effects in MFI of HEK-GFP+ were observed after treatment with siR-loaded EVs regardless of the applied microporation setting. This was unexpected since small RNAs do not have the limitations of DNA in terms of size and conformation [215,454] and have been successfully loaded into EVs particularly using electroporation [308–310,449,450,452]. Since no loading quantification was performed, it is not possible to determine if the effective amount of loaded siRNA was not sufficient to induce a silencing effect in the recipient cells or if other factors are preventing the functional delivery of the cargo. In addition to using MC-EV complexes targeting GFP, MC-EV aiming at silencing the membrane receptor VEGFR2 in HUVEC were also evaluated. No silencing effect was observed after incubation with the loaded MSC-EVs using siR or MC as cargo, in contrast to siR-VEGFR2 transfection with LF that induced a knockdown of ~57%.

Besides low loading efficiencies, other factors might be preventing the EV-mediated delivery and action of the MC and siRNA in the recipient cells. For instance, the mechanisms of cellular EV uptake and endosomal escape routes need to be efficient so that the nucleic acid cargos can be released and access cytoplasmic targets to eventually elicit biological effects at lower doses. A study has shown that EVs are sorted into endocytic vesicle circuits and colocalize with lysosome throughout time reaching a colocalization of ~50–60% at 48 h [463]. Moreover, Joshi and colleagues, demonstrated that EVs are internalized via endocytosis and only a fraction of them release their cargo from endosomes/lysosomes, ranging from 10% to 24.5% after 2 and 12 h of incubation, respectively, showing that functional delivery of EV cargo is limited and time-dependent [464]. Another important consideration is the EV integrity and composition after direct active loading methods. Such methods (e.g., electroporation and sonication) generate membrane pores that besides disrupting membrane integrity [449,454], could facilitate the leakage of endogenous EV content or cause alterations in the membrane composition, affecting the EV biological activity and target cell uptake. In the future, it would be important to analyse and compare EV characteristics before and after loading to evaluate if it could be a factor contributing to the reduced functional effect observed herein.

In what concerns electroporation as a loading method, further work should include using alternative buffers as all experiments performed herein used the electroporation provided by the electroporation system's manufacturer, whose composition is not described. For instance, in a recent study by Lennaárd and colleagues, eight distinct electroporation buffers were evaluated for the loading of EVs with doxorubicin and presented significant differences regarding EV recovery, loading efficiency and desired biological function [465].

Other loading methods can also be explored, particularly extrusion, which transiently disrupts the lipid bilayer of EVs due to the physical forces applied when the samples are pushed through a membrane of defined pore size. Kalimuthu and colleagues have successfully incorporated paclitaxel into MSC-EVs by serial extrusion through 10-, 5-, and 1-μm polycarbonate membrane filters and engineered EVs demonstrated significant therapeutical effects against breast cancer both *in vitro* and *in vivo* [326]. Moreover, extrusion is one of the preferred methods to generate EV-hybrids with synthetic lipids, namely when developing novel drug delivery systems [466]. Recently, extrusion was used to form stable EV-liposome hybrids loaded with siRNA which were previously incorporated at the hydration step of the lipid film hydration method for the preparation of liposomes [447]. Thus, this approach could be investigated as opposed to the hybridization method explored in this work.

In the future, alternative bioengineering strategies to originate shRNA-containing MSC-EVs can be considered, namely genetically engineering of MSC to express the shRNA and produce EVs harbouring the transcript. Several studies have genetically engineered MSC using transient non-viral systems to produce miR-loaded EVs [109]. For example, Li and colleagues transfected MSC with miR-181c mimics, an anti-inflammation effector. After injection of the produced EVs into rats with severe burns, the levels of miR-181c were significantly increased in the cutaneous wound when compared to EVs produced by non-transfected MSC. Moreover, the engineered EVs suppressed the TLR4 signalling pathway, reducing NF-κB/p65 activation, and alleviated inflammation in burned rats more effectively than innate EVs [298]. As another example, MSC were transfected with a miR-150-5p-encoding plasmid, and the produced EVs showed ~20-fold higher miR-150-5p levels than EVs produced by non-modified MSC. Treatment with these EVs caused the silencing of matrix metalloproteinase 14 and VEGF, which inhibited the migration/invasion of rheumatoid arthritis (RA) synoviocytes and HUVEC tube formation *in vitro,* and reduced clinical arthritic scores and joint destruction in an RA mouse model [296].

To conclude, in this work, we sought to develop a novel anti-angiogenic therapy based on shRNA-expressing MCs using MSC-EVs as natural delivery vehicles. After the shRNA-expressing MCs were successfully designed and manufactured, attempts of MC loading into human MSC(WJ) derived EVs that were manufactured under serum-/xeno(geneic)-free conditions, were performed, envisioning its translation into a clinical setting. Overall, the two quantification strategies implemented herein allowed the assessment of the loading efficiencies and loading capacity of the MC vector into MSC-EVs allowing a comparison between different loading conditions and providing insights into the effectiveness of different methods. The lack of functional effect observed after treatment with RNAi-loaded EVs of target cells underscores the complexity of EV loading, highlighting that the establishment of a universal protocol for EV loading is fundamentally impossible and a lot of optimization needs to take place for each particular system.

IV.6. Supplementary Material

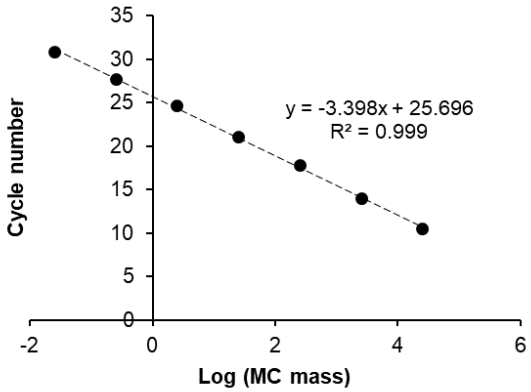

Supplementary Figure IV.1 - Calibration curve constructed using six 10-fold serial dilutions, prepared with pure MC-shGFP. Cycle threshold (Ct) values were plotted against the log of mass and the points were fitted to a linear regression (equation displayed in the graph).

Supplementary Table IV.1 - Median Fluorescence Intensity (MFI) of HEK-GFP+, 48h and 96h after incubation with MSC-EVs loaded with MC or siR that target GFP, using incubation, microporation, sonication and liposome-EV hybrids as direct loading methods. Lipofectamine® (LF) was used as transfection control.

Condition	MFI of transfected HEK-GFP+	
	48h	96h
No treatment	743	468
MC + EV + Incubation	670	429
MC + EV + Microp 1,000V; 40ms; 1p	661	414
MC + EV + Microp 750V; 20ms; 10p	664	401
MC + EV + Sonication	682	389
MC + LF	461	137
MC + LF + EV	516	184
siR + EV + Incubation	685	431
siR + EV + Microp 1,000V; 40ms; 1p	652	389
siR + EV + Microp 750V; 20ms; 10p	688	387
siR + EV + Sonication	730	451
siR + LF	570	259
siR + LF + EV	362	126

Supplementary Table IV.2 - Median Fluorescence Intensity (MFI) of HEK-GFP+, 72h and 120h after incubation with MSC-EVs loaded with siR that target GFP, using incubation, microporation using different parameters and liposome-EV hybrids as direct loading methods. Lipofectamine® (LF) was used as transfection control.

Condition	MFI of transfected HEK-GFP+		
	72h (n=1)	72h (n=2)	120h (n=1)
siR	973	777	1230
EV	982	791	1322
siR + EV + Incubation	1208	882	1346
siR + EV + Microp 1	982	835	1094
siR + EV + Microp 2	956	1252	1208
siR + EV + Microp 3	1055	874	1286
siR + EV + Microp 4	982	939	1230
siR + EV + Microp 5	1104	898	1263
LF	882	-	-
siR + LF	264	-	-
siR + LF + EV	382	-	-

Chapter V.

FINAL REMARKS AND FUTURE DIRECTIONS

The vascular endothelial growth factor (VEGF) and its receptors are crucial for physiological angiogenesis, the process of formation and maintenance of blood vessel structures. However, the excessive or sustained release of VEGF can lead to the development of abnormal vasculature and progression of excessive angiogenesis-related disorders, such as malignancies, ocular pathologies, and inflammatory diseases [19–24]. RNA interference (RNAi)-based strategies have demonstrated great potential as gene-targeting therapies and the VEGF regulatory pathway is undoubtedly a promising target when developing anti-angiogenic therapeutics [90,91,93,94]. In this work, we sought to develop a novel RNAi-based agent to target angiogenesis combining the prolonged biostability of plasmid DNA, gene silencing capabilities of siRNA, and improved safety and transfection efficiency of minicircle (MC) vectors [84–87]. To this end, short-hairpin RNA (shRNA)-expressing MC that silence the expression of VEGF-A and its most potent receptor, VEGF receptor 2 (VEGFR2) were used. As delivery system, we hypothesised the use of extracellular vesicles (EVs), which are cell-derived nanocarriers with an innate capacity to transport functional cargos into targeted cells. EVs have the ability to cross biological barriers and demonstrate reduced immunogenicity and low toxicity [105,111,112], overcoming limitations often associated with synthetic nanocarriers. Mesenchymal stromal cells (MSC) are considered a promising source for producing EVs for biomedical applications, given their intrinsic therapeutic benefits, exceptional safety profile, and robust *ex vivo* expansion capacity [130,276] and were therefore chosen as EV producers in this work. Different types of therapeutic cargo have been loaded into MSC-derived EVs (MSC-EVs), including nucleic acids, proteins and small molecules, using direct and indirect loading methods [109].

Overall, this thesis proposed a novel cell-free anti-angiogenic gene-based therapy, leveraging two key components: shRNA-expressing MCs targeting crucial elements of the VEGF regulatory pathway and MSC-EVs as natural delivery vehicles. The work was divided into three research lines explored in each experimental chapter: the development of shRNA-expressing MCs (Chapter II); the establishment of a platform for the scalable manufacturing of MSC-EVs (Chapter III); and the bioengineering of MSC-EVs by direct loading of the MCs (Chapter IV).

Firstly, the development of shRNA-expressing MCs involved the construction of the parental plasmids (PP) and large-scale manufacturing of the correspondening MC. After production and *in vivo* recombination in *E. coli* BW2P, a 496 bp MC was efficiently originated 1 h after L-arabinose induction. As future studies, a reduced recombination time could be investigated to prevent the unwanted replication of miniplasmid (MP) impurities and facilitate the subsequent MC purification. Afterwards, the combination of targeted MP relaxation by the action of nicking endonuclease *Nb.BbvCI* and multimodal chromatography [367], allowed the effective purification of MCs in their supercoiled isoforms, which is the most valuable topological form for gene therapy applications [388,389], virtually free of MP, PP and RNA unwanted byproducts. The MCs developed herein are much smaller than the ones produced and purified previously (above 3x larger [353,367,369]) confirming the robustness and flexibility of the manufacturing process. Although lower yields were obtained compared to other studies [381,390–393], these were acceptable since our final preparations were exceptionally free from other species and isoform

impurities and we purified much smaller MCs that ultimately require a reduced amount to deliver the same number of DNA molecules. The silencing potential of MCs that target the expression of VEGF-A (MC-shVEGF) and VEGFR2 (MC-shVEGFR2) was evaluated by transfection using human breast cancer cells and human endothelial cells, respectively, as cell models. MC-shVEGF decreased VEGF expression in MDA-MB-231 with a maximum knockdown of ~78% and ~82%, at the mRNA and protein levels, 4- and 2 days after microporation, respectively. Moreover, MC-shVEGFR2 induced a reduction of VEGFR2-mRNA with a maximum knockdown of ~56% at the mRNA level, 4 days after microporation, and ~27% at the protein level, 2 days after microporation. The lower inhibition observed might be explained by the fact that endothelial cells have been largely recognized as hard-to-transfect cells, especially compared to immortalised cells (which are easier to maintain in culture) [397], and thus different cell lines should be transfected to further confirm the silencing effect of the shRNA-expressing system. Nevertheless, in general, the VEGF/VEGFR2-targeting system developed herein exerted an excellent gene silencing effect, which was comparable or superior to others reported using various silencing systems, cell models and transfection methods [95–97,362,396]. Although valuable insights were provided by *in vitro* functional angiogenesis assays, further optimization is needed to accurately evaluate the biological impact of MC-mediated VEGF-A and VEGFR-2 silencing. Once proven to be effective *in vitro*, their anti-angiogenic effects should be evaluated in more complex systems like the chick chorioallantoic membrane (CAM) assay [373] and ultimately using *in vivo* animal models such as immunodeficient mice model for the growth of human tumour xenografts [95,467] or the type 1 diabetic $Ins2^{Akita}$ mouse model of diabetic retinopathy (DR) [468]. Concerning the development of additional shRNA-expressing MC systems, other molecules of the VEGF regulatory pathway have been demonstrated to prevent angiogenesis and could be explored as targets for anti-angiogenic therapy, including transcriptional activator of VEGF under hypoxic conditions, hypoxia-inducible factor (HIF)-1-alpha [98], and placental growth factor (PlGF), which promotes angiogenesis by signalling EC to undergo proliferation and migration directly through VEGFR1 and potentiates VEGF-A action [99]. Moreover, as angiogenesis is a complex process, the synergistic effect of multiple-target interference on angiogenesis through the construction of MCs harbouring multiple shRNA sequences (previously explored by others using different expression systems [469,470]) that target different pro-angiogenic factors is also an interesting approach to investigate in the future.

Simultaneously, a platform the production of the MC delivery system – MSC-EVs – was established. To this end, we have integrated fully scalable upstream and downstream processes potentially compliant with Good Manufacturing Practices (GMP) to develop a platform to produce MSC-EVs at clinical scale. Despite the promising prospects of MSC-EVs in therapeutic applications, most studies still use planar culture systems and fetal bovine serum (FBS)-supplemented culture media formulations for MSC expansion, along with non-scalable low-purity grade methods for EV isolation, hindering their clinical translation [130,140]. Here, umbilical cord-derived Wharton's jelly MSC (MSC(WJ)) were used for the robust production of EVs, combining Dissolvable microcarriers, serum-/xeno(geneic)-free (S/XF) exosome-depleted human platelet

lysate (hPL)-supplemented medium and a fully controlled stirred-tank reactor (STR) (0.25 L). After optimizing parameters such as the cell seeding density per microcarrier surface area and the agitation regimen using spinner flasks, the STR culture system reached a total number of ~6.0 $x10^7$ cells after 7 days, representing a notable ~30-fold cell expansion factor, which is superior to most values reported in the literature for MSC expansion under S/XF stirred culture conditions with similar or longer timeframes [133,135,147–150,419,425–427]. The expansion of MSC(WJ) was followed by a 3-day continuous EV production stage under stirred conditions, which did not compromise the viability and cellular identity of MSC. For the isolation of MSC-EVs, tangential flow filtration (TFF) was coupled with anion exchange (AEX) chromatography to allow the processing of large volumes of conditioned media (CM) (above 600 mL), yielding high EV numbers with great purity levels. Our integrated platform generated a total number of ~1.9 x 10^{12} EVs, which corresponds to a particle yield factor of ~1.2 x 10^4 particles/cell/day. Notably, considering a reported clinical dose of MSC-EVs ranging from 10^{10} to 10^{11} total administered particles [127], the manufacturing platform developed herein can provide at least 10 doses of MSC-EV in less than 2 weeks. Furthermore, MSC-EVs presented the typical cup-shaped morphology, homogeneous small-size distribution and positive detection of syntenin-1 and tetraspanins, CD9 and CD63. Importantly, these MSC-EVs were readily incorporated by target cells, human endothelial cells (i.e., HUVEC) and two human breast cancer cell lines (i.e, MDA-MB-231 and MCF-7). To better characterise and assess the innate therapeutic potential of these MSC-EVs, subsequent experiments should be carried out. These could include transcriptomic and proteomic analysis of the molecular cargo of the EVs produced [436,437] and functional *in vitro* and *in vivo* studies that can demonstrate EV potency [438], namely their hematopoietic support [439,440] and their immunomodulatory [441,442] and proangiogenic activities [150,443]. The evaluation of the capacity of MSC-EV in regulating angiogenesis is particularly important for the application proposed in this thesis. Previous studies have reported the pro-angiogenic potential of MSC-EVs, consistent with the reported features of the parental cells [265,471,472]; however, other studies have reported MSC-EV anti-angiogenic activities in tumours [473–476] and diabetic retina [477,478] microenvironments. The conflicting reports may arise from differences in tissue sources and culture conditions employed, alongside the use of different isolation methods, all of which significantly influence the cargo and surface composition of EVs, thereby impacting their biological functions. Nevertheless, the pro-/anti-angiogenic effect of MSC-EVs will be more transient compared to the shRNA-expressing MCs, which are expected to exert a more prolonged and potent effect once incorporated by recipient cells. For example, MSC-EV loaded with miR-150-5p caused the silencing of matrix metalloproteinase 14 and VEGF, which inhibited the migration/ invasion of RA synoviocytes and HUVEC tube formation *in vitro* and reduced clinical arthritic scores and joint destruction in an RA mouse model [296]. In addition, to further boost MSC-EV production yield, optimization of STR culture parameters could be performed. Besides agitation [147], other physiological stimuli have been shown to enhance EV secretion, including low oxygen tension (e.g., ranging from 0.5% to 5% O_2, compared to controls) [155–157], low pH (e.g., pH 4 or 6) [158,159] and high temperature (e.g., 40 or 42^{o}C) [159,160].

Additionally, MSC-EV yields can be enhanced with chemical compound supplementation, namely using adiponectin [161], N-methyldopamine combined with norepinephrine [162] or interferon-gamma (IFN-γ) combined with tumour necrosis factor-alpha (TNF-α) [163]. Nevertheless, all these manipulations may have an impact on EV characteristics, which needs to be thoroughly investigated and considered depending on the target application.

Lastly, the use of MSC-EVs as a delivery system of RNAi molecules was investigated. We selected direct loading methods because they offer a simpler, faster, and more flexible approach compared to genetic-engineering-based indirect loading, enabling the creation of versatile off-the-shelf engineered EVs by harnessing previously isolated vesicles with distinct cargo molecules. In this thesis, two distinct quantification strategies of MC loading into MSC-EVs were implemented allowing the assessment of encapsulation efficiency and loading capacity, which are key metrics in drug delivery to compare EV loading approaches [457,458], providing valuable insights into the effectiveness of different loading methods. Moreover, through a series of experiments using a reporter system composed of an MC that targets GFP (MC-shGFP) and GFP-expressing HEK293T cells (HEK-GFP+) as recipient cells, we investigated various methods for loading MCs into MSC-EVs, including passive incubation, electroporation, sonication, formation of liposome-EV hybrids and using a transfection reagent. Despite efforts to optimize loading conditions, the results revealed limited or no silencing effects on the target genes, indicating challenges related to MC delivery and action. One hypothesis is that the size of the MC, although extremely small, could still limit its efficient loading, as reported by others when loading DNA into EVs [215,454]; however, EVs loaded with siRNA-targeting GFP were also ineffective in decreasing the median fluorescence intensity of HEK-GFP+, suggesting that the loading failed to complex sufficient molecules to induce a silencing effect after delivery to recipient cells or that other factors are preventing the functional delivery of the RNAi cargos. Generally, this underscores the complexity of EV loading independently of the cargo and highlights the need for further optimization and understanding of the mechanisms involved. In future studies, it would be important to evaluate EV integrity and composition before and after direct active loading methods, such as electroporation and sonication [449,454], which may cause alterations in the EV membrane, thus affecting its biological activity and target cell uptake. Further research should be focused on exploring alternative buffers for electroporation besides the one provided by the manufacturer since buffer composition has been previously found to significantly impact EV recovery, loading efficiency, and biological function [465]. Moreover, alternative direct loading methods can be explored, particularly extrusion, by co-incubating EVs and MCs and subjecting them to physical forces as they pass through a membrane with defined pore size, which transiently disrupts the lipid bilayer of EVs, offering the potential for MC incorporation. In addition, extrusion holds the potential for generating EV-hybrids with synthetic lipids and it could also be investigated as MC delivery system [326,447]. Additionally, alternative strategies to bioengineer MSC-EVs could involve indirect loading by genetically modifying MSC to express shRNA, as demonstrated by previous research using non-viral systems to produce EVs loaded with miRNAs [296,298]. Envisioning its practical translation to a clinical setting, we can conceptualize the

development of an integrated bioprocess for the large-scale generation of endogenously engineered MSC-EVs by coupling transient gene delivery of the MC with the continuous EV production on the STR system. As an example, MSC transient transfection could be accomplished inside the STR using polyethylenimine (PEI), which induces high transfection efficiencies, while being less costly than most commercial reagents [479,480].

Globally, this work sheds light on the effectiveness and applicability of MC-derived RNAi systems in targeting pro-angiogenic molecules, emphasizing their promise as a novel non-viral, gene-based therapeutic approach for excessive angiogenesis. Moreover, we established a platform able to comply with GMP for the robust and high-yield manufacturing of human MSC(WJ)-derived EVs with accepted biochemical and biophysical characteristics, thereby advancing the accessibility of MSC-EV-based therapies for routine therapeutic use. Lastly, attempts to directly load MC into MSC-EVs were performed, envisioning its readily translation to a clinical setting. Although the final goal was not reached, this project provides important insights regarding the potential use of MSC-EVs as drug delivery vehicles, suggesting that several challenges must be addressed to broadly establish EVs as DNA delivery vehicles. Apart from the inherent heterogeneity of MSC and respective secreted EV populations, the differences among the techniques available for EV production, isolation, characterisation and modification contribute to conflicting data between studies. Thus, as we move forward, standardizing loading metrics and full disclosure of EV loading experimental parameters (e.g., amount of molecular cargo, EV numbers, loading solvent in EV/cargo mixtures, detailed loading protocols or EV doses and concentrations used in functional studies) will be imperative to facilitate comparisons between multiple studies and advance the field of EV engineering [481]. In the future, this work has the potential to be extrapolated to the management of a multitude of diseases other than anti-angiogenic therapy, having the flexibility to target the expression of virtually any dysregulated gene.

PUBLICATIONS AND COMMUNICATIONS

PUBLISHED WORK

Papers in Journals

Bandarra-Tavares*, H.; Franchi-Mendes*, T.; Ulpiano, C.; Morini, S.; Kaur, N.; Harris-Becker, A.; Vemuri, M.C.; Cabral, J.M.S.; Fernandes-Platzgummer, A.; da Silva, C.L. (2024). Dual Production of Human Mesenchymal Stromal Cells and Derived Extracellular Vesicles in a Dissolvable Microcarrier-Based Stirred Culture System. *Cytotherapy*, pp.1 – 8 doi:10.1016/j.jcyt.2024.03.001 *equally contributing authors

Ulpiano, C., da Silva, C.L., & Monteiro, G.A. (2023). Bioengineered Mesenchymal-Stromal-Cell-Derived Extracellular Vesicles as an Improved Drug Delivery System: Methods and Applications. *Biomedicines*, *11*(4), 1231. DOI: 10.3390/biomedicines11041231.

Ulpiano, C., da Silva, C.L., & Monteiro, G.A. (2021). Mesenchymal Stromal Cells (MSCs): A Promising Tool for Cell-Based Angiogenic Therapy. *Current Gene Therapy*, 21(5), pp. 382 – 405. doi:10.2174/1566523221666210917114353.

Book chapter:

Silva, M., Ulpiano, C., Bernardes, N., Monteiro, G.A., & da Silva, C.L. (2019). Gene delivery as a tool to improve the therapeutic features of mesenchymal stromal cells: methods and applications. In V. Zimmer (Eds.), *Gene Delivery: Methods and Applications* (pp. 1-75). Nova Science Publishers. ISBN 9781536162684.

SCIENTIFIC COMMUNICATIONS

Poster communications:

Ulpiano,C., Franchi-Mendes, T., Salvador, W., Tavares, H., Rosa, S.S., Fernandes-Platzgummer, A., da Silva, C.L., Monteiro, G.A., Extracellular Vesicles from Mesenchymal Stromal Cells as potential angiogenic modulators through the delivery of RNAi-expressing Minicircles. In ESGCT 30th Annual congress, Brussels, Belgium (2023).

Ulpiano, C., Silva, R.M., Rosa, S.S., Fuzeta, M.A., Fernandes-Platzgummer, A., da Silva, C.L., Monteiro, G.A., Extracellular Vesicles from Mesenchymal Stromal Cells as potential angiogenic modulators through the delivery of RNAi-expressing Minicircles. In 2nd PNEV meeting, Lisbon, Portugal (2023).

Ulpiano, C., Silva, R.M., Rosa, S.S., Fuzeta, M.A., Fernandes-Platzgummer, A., da Silva, C.L., Monteiro, G.A., Extracellular Vesicles from Mesenchymal Stromal Cells as potential angiogenic modulators through the delivery of RNAi-expressing Minicircles. In ISCT 2023, Paris, France (2023).

Ulpiano, C., Fernandes-Platzgummer, A., da Silva, C.L., Monteiro, G.A., Engineering Extracellular Vesicles from Mesenchymal Stromal Cells using Minicircle-derived RNAi Technology. In 27th ESACT meeting, Lisbon, Portugal (2022).

Ulpiano, C., Fernandes-Platzgummer, A., da Silva, C.L., Monteiro, G.A., Engineering Extracellular Vesicles from Mesenchymal Stromal Cells using Minicircle-derived RNAi Technology. In 12th International Meeting of the SPCE-TC, Braga, Portugal (2021)

Ulpiano, C., da Silva, C.L., Monteiro, G.A., Minicircle-derived RNA interference as a novel gene-based anti-angiogenic therapy. In IST PhD Open Days, Lisboa, Portugal (2021).

Ulpiano, C., da Silva, C.L., Monteiro, G.A., RNAi as a tool to inhibit the angiogenic potential of human Mesenchymal Stem/Stromal Cells in malignancy. In MicroBiotec'19 - Congress of Microbiology and Biotechnology, Coimbra, Portugal (2019).

Ulpiano, C., da Silva, C.L., Monteiro, G.A., RNAi as a tool to inhibit the angiogenic potential of human Mesenchymal Stem/Stromal Cells in malignancy. In 10th Annual International (bio)Medical Students Meeting (AIMS), Lisboa, Portugal (2019).

Oral presentations:

Ulpiano, C., and da Silva, C.L, Exosome-depleted hPL Supplements Can Support Robust Cell-derived EV Production. At Aventacell's Global Showcase Presentation in ISCT 2023, Paris, France (2023).

Tavares, H.T.*, Franchi-Mendes, T.*, Ulpiano, C., Morini, S., Becker, A.H., Cabral, J.M.S., Vemuri, M.C., Fernandes-Platzgummer, A., da Silva, C.L., Microcarrier-based xeno(geneic)-free culture system for the scalable production of Extracellular vesicles derived from Wharton's jelly-Mesenchymal stromal cells. In 2nd PNEV meeting, Lisbon, Portugal (2023). *equally contributing authors

Ulpiano, C., Silva, R.M., Rosa, S.S., Fuzeta, M.A., Fernandes-Platzgummer, A., da Silva, C.L., Monteiro, G.A., Extracellular Vesicles from Mesenchymal Stromal Cells as potential angiogenic

modulators through the delivery of RNAi-expressing Minicircles. In Student Network on EVs (SNEV), online virtual format (2023).

Ulpiano, C., Fernandes-Platzgummer, A., da Silva, C.L., Monteiro, G.A., Extracellular Vesicles from Mesenchymal Stromal Cells as potential angiogenic modulators through the delivery of RNAi-expressing Minicircles. In ESACT-UK 33rd Annual Conference, Nottingham, UK (2023).

Ulpiano, C., da Silva, C.L., Monteiro, G.A., Minicircle-derived RNA interference as a novel gene-based anti-angiogenic therapy. In MicroBiotec'21 - Congress of Microbiology and Biotechnology, online virtual format (2021).

REFERENCES

1. Udan, R.S.; Culver, J.C.; Dickinson, M.E. Understanding Vascular Development. *Wiley Interdiscip Rev Dev Biol* **2013**, *2*, 327–346, doi:10.1002/WDEV.91.
2. DeSesso, J.M. Vascular Ontogeny within Selected Thoracoabdominal Organs and the Limbs. *Reproductive Toxicology* **2017**, *70*, 3–20, doi:10.1016/J.REPROTOX.2016.10.007.
3. Banno, K.; Yoder, M.C. Tissue Regeneration Using Endothelial Colony-Forming Cells: Promising Cells for Vascular Repair. *Pediatr Res* **2018**, *83*, 283–290, doi:10.1038/pr.2017.231.
4. Ucuzian, A.A.; Gassman, A.A.; East, A.T.; Greisler, H.P. Molecular Mediators of Angiogenesis. *Journal of burn care & research* **2010**, *31*, 158–175, doi:10.1097/BCR.0b013e3181c7ed82.
5. Potente, M.; Gerhardt, H.; Carmeliet, P. Basic and Therapeutic Aspects of Angiogenesis. *Cell* **2011**, *146*, 873–887, doi:10.1016/j.cell.2011.08.039.
6. Fallah, A.; Sadeghinia, A.; Kahroba, H.; Samadi, A.; Heidari, H.R.; Bradaran, B.; Zeinali, S.; Molavi, O. Therapeutic Targeting of Angiogenesis Molecular Pathways in Angiogenesis-Dependent Diseases. *Biomedicine and Pharmacotherapy* **2019**, *110*, 775–785, doi:10.1016/j.biopha.2018.12.022.
7. Carmeliet, P. Angiogenesis in Life, Disease and Medicine. *Nature* **2005**, *438*, 932–936, doi:10.1038/nature04478.
8. Wang, Z.; Dabrosin, C.; Yin, X.; Fuster, M.M.; Arreola, A.; Rathmell, W.K.; Generali, D.; Nagaraju, G.P.; El-Rayes, B.; Ribatti, D.; et al. Broad Targeting of Angiogenesis for Cancer Prevention and Therapy. *Semin Cancer Biol* **2015**, *35*, S224–S243, doi:10.1016/J.SEMCANCER.2015.01.001.
9. Stitt, A.W.; Curtis, T.M.; Chen, M.; Medina, R.J.; Mckay, G.J.; Jenkins, A.; Gardiner, T.A.; Lyons, T.J.; Hammes, H.-P.; Sim, R.; et al. The Progress in Understanding and Treatment of Diabetic Retinopathy. *Prog Retin Eye Res* **2015**, *51*, 156–186, doi:10.1016/j.preteyeres.2015.08.001.
10. Elshabrawy, H.A.; Chen, • Zhenlong; Volin, M. V; Ravella, S.; Virupannavar, S.; Shahrara, S. The Pathogenic Role of Angiogenesis in Rheumatoid Arthritis. *Angiogenesis* **2015**, *18*, doi:10.1007/s10456-015-9477-2.
11. Ferrara, N.; Gerber, H.-P.; LeCouter, J. The Biology of VEGF and Its Receptors. *Nat Med* **2003**, *9*, 669–676, doi:10.1038/nm0603-669.
12. Hoeben, A. Vascular Endothelial Growth Factor and Angiogenesis. *Pharmacol Rev* **2004**, *56*, 549–580, doi:10.1124/pr.56.4.3.
13. Lal, N.; Puri, K.; Rodrigues, B. Vascular Endothelial Growth Factor B and Its Signaling. *Front Cardiovasc Med* **2018**, *5*, doi:10.3389/FCVM.2018.00039.
14. Dehghanian, F.; Hojati, Z.; Kay, M. New Insights into VEGF-A Alternative Splicing: Key Regulatory Switching in the Pathological Process. *Avicenna J Med Biotechnol* **2014**, *6*, 192.

15. Arcondéguy, T.; Lacazette, E.; Millevoi, S.; Prats, H.; Touriol, C. VEGF-A MRNA Processing, Stability and Translation: A Paradigm for Intricate Regulation of Gene Expression at the Post-Transcriptional Level. *Nucleic Acids Res* **2013**, *41*, 7997, doi:10.1093/NAR/GKT539.
16. Shibuya, M. Vascular Endothelial Growth Factor (VEGF) and Its Receptor (VEGFR) Signaling in Angiogenesis: A Crucial Target for Anti- and Pro-Angiogenic Therapies. *Genes Cancer* **2011**, *2*, 1097–1105, doi:10.1177/1947601911423031.
17. Yang, X.; Yang, Q.; Ma, B.; Wang, X.; Bove, A.M.; Simone, G. Molecular Bases of VEGFR-2-Mediated Physiological Function and Pathological Role. **2020**, doi:10.3389/fcell.2020.599281.
18. LaGory, E.L.; Giaccia, A.J. The Ever-Expanding Role of HIF in Tumour and Stromal Biology. *Nat Cell Biol* **2016**, *18*, 356–365, doi:10.1038/ncb3330.
19. Yoo, S.Y.; Kwon, S.M. Angiogenesis and Its Therapeutic Opportunities. *Mediators Inflamm* **2013**, *2013*, doi:10.1155/2013/127170.
20. Carmeliet, P. VEGF as a Key Mediator of Angiogenesis in Cancer. *Oncology* **2005**, *69 Suppl 3*, 4–10, doi:10.1159/000088478.
21. Ambati, J.; Fowler, B.J. Mechanisms of Age-Related Macular Degeneration. *Neuron* **2012**, *75*, 26–39, doi:10.1016/J.NEURON.2012.06.018.
22. Gupta, N.; Mansoor, S.; Sharma, A.; Sapkal, A.; Sheth, J.; Falatoonzadeh, P.; Kuppermann, B.D.; Kenney, M.C. Diabetic Retinopathy and VEGF. *Open Ophthalmol J* **2013**, *7*, 4–10.
23. Kim, H.R.; Kim, K.W.; Kim, B.M.; Cho, M. La; Lee, S.H. The Effect of Vascular Endothelial Growth Factor on Osteoclastogenesis in Rheumatoid Arthritis. *PLoS One* **2015**, *10*, doi:10.1371/JOURNAL.PONE.0124909.
24. Marina, M.E.; Roman, I.I.; Constantin, A.-M.; Mihu, C.M.; Dumitru Tătaru, A. VEGF Involvement in Psoriasis. *Review Clujul Medical* **2015**, *88*, 247–252, doi:10.15386/cjmed-494.
25. Zhang, A.B.; Mozaffari, K.; Aguirre, B.; Li, V.; Kubba, R.; Desai, N.C.; Wei, D.; Yang, I.; Wadehra, M. Exploring the Past, Present, and Future of Anti-Angiogenic Therapy in Glioblastoma. *Cancers (Basel)* **2023**, *15*, doi:10.3390/CANCERS15030830.
26. Gerriets, V.; Anup, K. Bevacizumab - StatPearls - NCBI Bookshelf Available online: https://www.ncbi.nlm.nih.gov/books/NBK482126/ (accessed on 18 March 2024).
27. Moserle, L.; Jiménez-Valerio, G.; Casanovas, O. Antiangiogenic Therapies: Going beyond Their Limits. *Cancer Discov* **2014**, *4*, 31–41, doi:10.1158/2159-8290.CD-13-0199.
28. Almuhtaseb, H.; Kanavati, S.; Rufai, S.R.; Lotery, A.J. One-Year Real-World Outcomes in Patients Receiving Fixed-Dosing Aflibercept for Neovascular Age-Related Macular Degeneration. *Eye* **2017**, *31*, 878–883, doi:10.1038/eye.2017.6.
29. Diabetic Retinopathy Clinical Research Network et al. Aflibercept, Bevacizumab, or Ranibizumab for Diabetic Macular Edema. *New England Journal of Medicine* **2015**, *372*,

1193–1203, doi:10.1056/NEJMOA1414264/SUPPL_FILE/NEJMOA1414264_DISCLOSURES.PDF.

30. Ng, E.W.M.; Shima, D.T.; Calias, P.; Cunningham, E.T.; Guyer, D.R.; Adamis, A.P. Pegaptanib, a Targeted Anti-VEGF Aptamer for Ocular Vascular Disease. *Nature Reviews Drug Discovery 2006 5:2* **2006**, *5*, 123–132, doi:10.1038/nrd1955.
31. Wilson, R.C.; Doudna, J.A. Molecular Mechanisms of RNA Interference. *Annu Rev Biophys* **2013**, *42*, 217–239, doi:10.1146/annurev-biophys-083012-130404.
32. Lee, R.C.; Feinbaum, R.L.; Ambros, V. The C. Elegans Heterochronic Gene Lin-4 Encodes Small RNAs with Antisense Complementarity to Lin-14. *Cell* **1993**, *75*, 843–854.
33. Alles, J.; Fehlmann, T.; Fischer, U.; Backes, C.; Galata, V.; Minet, M.; Hart, M.; Abu-Halima, M.; Grässer, F.A.; Lenhof, H.P.; et al. An Estimate of the Total Number of True Human MiRNAs. *Nucleic Acids Res* **2019**, *47*, 3353–3364, doi:10.1093/NAR/GKZ097.
34. Bartel, D.P. Metazoan MicroRNAs. *Cell* **2018**, *173*, 20–51, doi:10.1016/J.CELL.2018.03.006.
35. Claycomb, J.M. Ancient Endo-SiRNA Pathways Reveal New Tricks. *Current Biology* **2014**, *24*, R703–R715, doi:10.1016/J.CUB.2014.06.009.
36. Asikainen, S.; Heikkinen, L.; Wong, G.; Storvik, M. Functional Characterization of Endogenous SiRNA Target Genes in Caenorhabditis Elegans. *BMC Genomics* **2008**, *9*, 1–10, doi:10.1186/1471-2164-9-270/FIGURES/5.
37. Elbashir, S.M.; Harborth, J.; Lendeckel, W.; Yalcin, A.; Weber, K.; Tuschl, T. Duplexes of 21-Nucleotide RNAs Mediate RNA Interference in Cultured Mammalian Cells. *Nature* **2001**, *411*, 494–498, doi:10.1038/35078107.
38. Lam, J.K.W.; Chow, M.Y.T.; Zhang, Y.; Leung, S.W.S. SiRNA versus MiRNA as Therapeutics for Gene Silencing. *Mol Ther Nucleic Acids* **2015**, *4*, e252, doi:10.1038/mtna.2015.23.
39. Rao, D.D.; Vorhies, J.S.; Senzer, N.; Nemunaitis, J. SiRNA vs. ShRNA: Similarities and Differences. *Adv Drug Deliv Rev* 2009, *61*, 746–759.
40. Paddison, P.J.; Caudy, A.A.; Bernstein, E.; Hannon, G.J.; Conklin, D.S. Short Hairpin RNAs (ShRNAs) Induce Sequence-Specific Silencing in Mammalian Cells. *Genes Dev* **2002**, *16*, 948–958, doi:10.1101/GAD.981002.
41. Bobbin, M.L.; Burnett, J.C.; Rossi, J.J. RNA Interference Approaches for Treatment of HIV-1 Infection. *Genome Med* **2015**, *7*, doi:10.1186/s13073-015-0174-y.
42. Carthew, R.W.; Sontheimer, E.J. Origins and Mechanisms of MiRNAs and SiRNAs. *Cell* **2009**, *136*, 642–655, doi:10.1016/j.cell.2009.01.035.
43. Yi, R.; Qin, Y.; Macara, I.G.; Cullen, B.R. Exportin-5 Mediates the Nuclear Export of Pre-MicroRNAs and Short Hairpin RNAs. *Genes Dev* **2003**, *17*, 3011–3016, doi:10.1101/GAD.1158803.
44. Kok, K.H.; Ng, M.H.J.; Ching, Y.P.; Jin, D.Y. Human TRBP and PACT Directly Interact with Each Other and Associate with Dicer to Facilitate the Production of Small Interfering RNA. *J Biol Chem* **2007**, *282*, 17649–17657, doi:10.1074/JBC.M611768200.

45. Haase, A.D.; Jaskiewicz, L.; Zhang, H.; Lainé, S.; Sack, R.; Gatignol, A.; Filipowicz, W. TRBP, a Regulator of Cellular PKR and HIV-1 Virus Expression, Interacts with Dicer and Functions in RNA Silencing. *EMBO Rep* **2005**, *6*, 961–967, doi:10.1038/SJ.EMBOR.7400509/SUPPL_FILE/EMBR7400509-SUP-0001.PDF.
46. Leuschner, P.J.F.; Ameres, S.L.; Kueng, S.; Martinez, J. Cleavage of the SiRNA Passenger Strand during RISC Assembly in Human Cells. *EMBO Rep* **2006**, *7*, 314–320, doi:10.1038/SJ.EMBOR.7400637/SUPPL_FILE/EMBR7400637-SUP-0001.PDF.
47. Song, E.; Lee, S.-K.; Wang, J.; Ince, N.; Ouyang, N.; Min, J.; Chen, J.; Shankar, P.; Lieberman, J. RNA Interference Targeting Fas Protects Mice from Fulminant Hepatitis. *Nat Med* **2003**, *9*, 347–351, doi:10.1038/nm828.
48. Ahn, I.; Kang, C.S.; Han, J. Where Should SiRNAs Go: Applicable Organs for SiRNA Drugs. *Experimental & Molecular Medicine 2023 55:7* **2023**, *55*, 1283–1292, doi:10.1038/s12276-023-00998-y.
49. Hu, B.; Zhong, L.; Weng, Y.; Peng, L.; Huang, Y.; Zhao, Y.; Liang, X.J. Therapeutic SiRNA: State of the Art. *Signal Transduct Target Ther* 2020, *5*.
50. Li, Z.; Rana, T.M. Molecular Mechanisms of RNA-Triggered Gene Silencing Machineries. *Acc Chem Res* **2012**, *45*, 1122–1131, doi:10.1021/AR200253U.
51. Morales-Becerril, A.; Aranda-Lara, L.; Isaac-Olivé, K.; Ocampo-García, B.E.; Morales-ávila, E. Nanocarriers for Delivery of SiRNA as Gene Silencing Mediator. *EXCLI J* **2022**, *21*, 1028, doi:10.17179/EXCLI2022-4975.
52. Ashique, S.; Almohaywi, B.; Haider, N.; Yasmin, S.; Hussain, A.; Mishra, N.; Garg, A. SiRNA-Based Nanocarriers for Targeted Drug Delivery to Control Breast Cancer. *Advances in Cancer Biology - Metastasis* **2022**, *4*, 100047, doi:10.1016/J.ADCANC.2022.100047.
53. Bramsen, J.B.; Laursen, M.B.; Nielsen, A.F.; Hansen, T.B.; Bus, C.; Langkjøør, N.; Babu, B.R.; Højland, T.; Abramov, M.; Van Aerschot, A.; et al. A Large-Scale Chemical Modification Screen Identifies Design Rules to Generate SiRNAs with High Activity, High Stability and Low Toxicity. *Nucleic Acids Res* **2009**, *37*, 2867–2881, doi:10.1093/nar/gkp106.
54. Lu, Y.; Huang, W.; Li, M.; Zheng, A. Exosome-Based Carrier for RNA Delivery: Progress and Challenges. *Pharmaceutics* **2023**, *15*, 598, doi:10.3390/PHARMACEUTICS15020598.
55. Moore, C.B.; Guthrie, E.H.; Huang, M.T.-H.; Taxman, D.J. Short Hairpin RNA (ShRNA): Design, Delivery, and Assessment of Gene Knockdown. *Methods Mol Biol* **2010**, *629*, 141–158, doi:10.1007/978-1-60761-657-3_10.
56. Bofill-De Ros, X.; Gu, S. Guidelines for the Optimal Design of MiRNA-Based ShRNAs. *Methods* **2016**, *103*, 157–166, doi:10.1016/j.ymeth.2016.04.003.
57. Brummelkamp, T.R.; Bernards, R.; Agami, R. A System for Stable Expression of Short Interfering RNAs in Mammalian Cells. *Science (1979)* **2002**, *296*, 550–553, doi:10.1126/science.1068999.

58. Paddison, P.J.; Silva, J.M.; Conklin, D.S.; Schlabach, M.; Li, M.; Aruleba, S.; Balija, V.; O'Shaughnessy, A.; Gnoj, L.; Scobie, K.; et al. A Resource for Large-Scale RNA-Interference-Based Screens in Mammals. *Nature* **2004**, *428*, 427–431, doi:10.1038/nature02370.

59. Rubinson, D.A.; Dillon, C.P.; Kwiatkowski, A. V; Sievers, C.; Yang, L.; Kopinja, J.; Rooney, D.L.; Zhang, M.; Ihrig, M.M.; McManus, M.T.; et al. A Lentivirus-Based System to Functionally Silence Genes in Primary Mammalian Cells, Stem Cells and Transgenic Mice by RNA Interference. *Nat Genet* **2003**, *33*, 401–406, doi:10.1038/ng1117.

60. Chu, L.; Gu, J.; Sun, L.; Qian, Q.; Qian, C.; Liu, X. Oncolytic Adenovirus-Mediated ShRNA against Apollon Inhibits Tumor Cell Growth and Enhances Antitumor Effect of 5-Fluorouracil. *Gene Ther* **2008**, *15*, 484–494, doi:10.1038/gt.2008.6.

61. Pinkenburg, O.; Platz, J.; Beisswenger, C.; Vogelmeier, C.; Bals, R. Inhibition of NF-KB Mediated Inflammation by SiRNA Expressed by Recombinant Adeno-Associated Virus. *J Virol Methods* **2004**, *120*, 119–122, doi:10.1016/J.JVIROMET.2004.04.007.

62. Hong, C.-S.; Goins, W.F.; Goss, J.R.; Burton, E.A.; Glorioso, J.C. Herpes Simplex Virus RNAi and Neprilysin Gene Transfer Vectors Reduce Accumulation of Alzheimer's Disease-Related Amyloid-β Peptide in Vivo. *Gene Ther* **2006**, *13*, 1068–1079, doi:10.1038/sj.gt.3302719.

63. Grimm, D.; Streetz, K.L.; Jopling, C.L.; Storm, T.A.; Pandey, K.; Davis, C.R.; Marion, P.; Salazar, F.; Kay, M.A. Fatality in Mice Due to Oversaturation of Cellular MicroRNA/Short Hairpin RNA Pathways. *Nature 2006 441:7092* **2006**, *441*, 537–541, doi:10.1038/nature04791.

64. Butt, M.H.; Zaman, M.; Ahmad, A.; Khan, R.; Mallhi, T.H.; Hasan, M.M.; Khan, Y.H.; Hafeez, S.; Massoud, E.E.S.; Rahman, M.H.; et al. Appraisal for the Potential of Viral and Nonviral Vectors in Gene Therapy: A Review. *Genes (Basel)* **2022**, *13*, doi:10.3390/GENES13081370.

65. Sun, A.; Tang, J.; Terranova, P.F.; Zhang, X.; Thrasher, J.B.; Li, B. Adeno-Associated Virus-Delivered Short Hairpin-Structured RNA for Androgen Receptor Gene Silencing Induces Tumor Eradication of Prostate Cancer Xenografts in Nude Mice: A Preclinical Study. *Int J Cancer* **2010**, *126*, 764–774, doi:10.1002/ijc.24778.

66. Hardee, C.L.; Arévalo-Soliz, L.M.; Hornstein, B.D.; Zechiedrich, L. Advances in Non-Viral DNA Vectors for Gene Therapy. *Genes (Basel)* **2017**, *8*, doi:10.3390/GENES8020065.

67. Qazi, Y.; Stagg, B.; Singh, N.; Singh, S.; Zhang, X.; Luo, L.; Simonis, J.; Kompella, U.B.; Ambati, B.K. Nanoparticle-Mediated Delivery of ShRNA.VEGF-A Plasmids Regresses Corneal Neovascularization. *Invest Ophthalmol Vis Sci* **2012**, *53*, 2837–2844, doi:10.1167/iovs.11-9139.

68. Li, D.-C.; Li, D.-C.; Zhao, H.; Li, Z.; Wang, J.-X.; Zhu, D.-M.; Zhou, J.; Cen, J.-N. A Study of the Suppressive Effect on Human Pancreatic Adenocarcinoma Cell Proliferation and Angiogenesis by Stable Plasmid-Based SiRNA Silencing of c-Src Gene Expression. *Oncol Rep* **2011**, *27*, 628–636, doi:10.3892/or.2011.1602.

69. Tang, Q.; Ma, X.; Zhang, Y.; Cai, X.; Xue, W.; Ma, D. Self-Sensibilized Polymeric Prodrug Co-Delivering MMP-9 ShRNA Plasmid for Combined Treatment of Tumors. *Acta Biomater* **2018**, *69*, 277–289, doi:10.1016/j.actbio.2018.01.014.
70. Zhang, Y.; Zhang, Y.-F.; Bryant, J.; Charles, A.; Boado, R.J.; Pardridge, W.M. Intravenous RNA Interference Gene Therapy Targeting the Human Epidermal Growth Factor Receptor Prolongs Survival in Intracranial Brain Cancer. *Clinical Cancer Research* **2004**, *10*, 3667–3677.
71. Giering, J.C.; Grimm, D.; Storm, T.A.; Kay, M.A. Expression of ShRNA From a Tissue-Specific Pol II Promoter Is an Effective and Safe RNAi Therapeutic. *Molecular Therapy* **2008**, *16*, 1630–1636, doi:10.1038/MT.2008.144.
72. Häcker, G.; Redecke, V.; Häcker, H. Activation of the Immune System by Bacterial CpG-DNA. *Immunology* **2002**, *105*, 245–251, doi:10.1046/J.0019-2805.2001.01350.X.
73. Walker, W.E.; Booth, C.J.; Goldstein, D.R. TLR9 and IRF3 Cooperate to Induce a Systemic Inflammatory Response in Mice Injected With Liposome:DNA. *Molecular Therapy* **2010**, *18*, 775–784, doi:10.1038/MT.2010.1.
74. Boura, J.S.; Vance, M.; Yin, W.; Madeira, C.; Lobato da Silva, C.; Porada, C.D.; Almeida-Porada, G. Evaluation of Gene Delivery Strategies to Efficiently Overexpress Functional HLA-G on Human Bone Marrow Stromal Cells. *Mol Ther Methods Clin Dev* **2014**, *1*, 14041, doi:10.1038/MTM.2014.41.
75. Yin, W.; Xiang, P.; Li, Q. Investigations of the Effect of DNA Size in Transient Transfection Assay Using Dual Luciferase System. *Anal Biochem* **2005**, *346*, 289–294, doi:10.1016/J.AB.2005.08.029.
76. Bandara, N.; Gurusinghe, S.; Chen, H.; Chen, S.; Wang, L.X.; Lim, S.Y.; Strappe, P. Minicircle DNA-Mediated Endothelial Nitric Oxide Synthase Gene Transfer Enhances Angiogenic Responses of Bone Marrow-Derived Mesenchymal Stem Cells. *Stem Cell Res Ther* **2016**, *7*, 1–15, doi:10.1186/S13287-016-0307-2/FIGURES/10.
77. Boye, C.; Arpag, S.; Francis, M.; DeClemente, S.; West, A.; Heller, R.; Bulysheva, A. Reduction of Plasmid Vector Backbone Length Enhances Reporter Gene Expression. *Bioelectrochemistry* **2022**, *144*, 107981, doi:10.1016/J.BIOELECHEM.2021.107981.
78. Mayrhofer, P.; Schleef, M.; Jechlinger, W. Use of Minicircle Plasmids for Gene Therapy. In *Methods in molecular biology (Clifton, N.J.)*; 2009; Vol. 542, pp. 87–104.
79. Miguel Prazeres, D.F.; Monteiro, G.A. Plasmid Biopharmaceuticals. *Microbiol Spectr* **2014**, *2*, doi:10.1128/microbiolspec.PLAS-0022-2014.
80. Ko, J.; Jun, H.; Chung, H.; Yoon, C.; Kim, T.; Kwon, M.; Lee, S.; Jung, S.; Kim, M.; Park, J.H. Comparison of EGF with VEGF Non-Viral Gene Therapy for Cutaneous Wound Healing of Streptozotocin Diabetic Mice. *Diabetes Metab J* **2011**, *35*, 226, doi:10.4093/DMJ.2011.35.3.226.
81. Munye, M.M.; Tagalakis, A.D.; Barnes, J.L.; Brown, R.E.; McAnulty, R.J.; Howe, S.J.; Hart, S.L. Minicircle DNA Provides Enhanced and Prolonged Transgene Expression Following Airway Gene Transfer. *Scientific Reports 2016 6:1* **2016**, *6*, 1–11, doi:10.1038/srep23125.

82. Bozza, M.; Green, E.W.; Espinet, E.; De Roia, A.; Klein, C.; Vogel, V.; Offringa, R.; Williams, J.A.; Sprick, M.; Harbottle, R.P. Novel Non-Integrating DNA Nano-S/MAR Vectors Restore Gene Function in Isogenic Patient-Derived Pancreatic Tumor Models. *Mol Ther Methods Clin Dev* **2020**, *17*, 957–968, doi:10.1016/j.omtm.2020.04.017.
83. Chen, G.; Zeng, L.; Bi, B.; Huang, X.; Qiu, M.; Chen, P.; Chen, Z.Y.; He, Y.; Pan, Y.; Chen, Y.; et al. Engineering Bifunctional Calcium Alendronate Gene-Delivery Nanoneedle for Synergistic Chemo/Immuno-Therapy Against HER2 Positive Ovarian Cancer. *Advanced Science* **2023**, *10*, 2204654, doi:10.1002/ADVS.202204654.
84. Borja-Cacho, D.; Matthews, J. MicroRNA-210 as a Novel Therapy for Treatment of Ischemic Heart Disease. *Circulation* **2008**, *6*, 2166–2171, doi:10.1021/nl061786n.Core-Shell.
85. Huang, M.; Nguyen, P.; Jia, F.; Hu, S. Double Knockdown of Prolyyl Hydroxylase and Factor Inhibiting HIF with Non-Viral Minicircle Gene Therapy Enhances Stem Cell Mobilization and Angiogenesis After Myocardial Infarction. *Circulation* **2011**, *124*, S46–S54, doi:10.1161/CIRCULATIONAHA.110.014019.Double.
86. Zhao, N.; Fogg, J.M.; Zechiedrich, L.; Zu, Y. Transfection of ShRNA-Encoding Minivector DNA of a Few Hundred Base Pairs to Regulate Gene Expression in Lymphoma Cells. *Gene Ther* **2011**, *18*, 220–224, doi:10.1038/gt.2010.123.
87. Izco, M.; Schleef, M.; Schmeer, M.; Carlos, E.; Verona, G.; Alvarez-Erviti, L. Targeted Extracellular Vesicle Gene Therapy for Modulating Alpha-Synuclein Expression in Gut and Spinal Cord. *Pharmaceutics 2023, Vol. 15, Page 1230* **2023**, *15*, 1230, doi:10.3390/PHARMACEUTICS15041230.
88. Lijkwan, M.A.; Hellingman, A.A.; Bos, E.J.; Van Der Bogt, K.E.A.; Huang, M.; Kooreman, N.G.; De Vries, M.R.; Peters, H.A.B.; Robbins, R.C.; Hamming, J.F.; et al. Short Hairpin RNA Gene Silencing of Prolyl Hydroxylase-2 with a Minicircle Vector Improves Neovascularization of Hindlimb Ischemia. *Hum Gene Ther* **2014**, *25*, 41, doi:10.1089/HUM.2013.110.
89. Ofek, P.; Tiram, G.; Satchi-Fainaro, R. Angiogenesis Regulation by Nanocarriers Bearing RNA Interference ☆. **2017**, doi:10.1016/j.addr.2017.01.008.
90. Pittella, F.; Miyata, K.; Maeda, Y.; Suma, T.; Watanabe, S.; Chen, Q.; Christie, R.J.; Osada, K.; Nishiyama, N.; Kataoka, K. Pancreatic Cancer Therapy by Systemic Administration of VEGF SiRNA Contained in Calcium Phosphate/Charge-Conversional Polymer Hybrid Nanoparticles. **2012**, doi:10.1016/j.jconrel.2012.05.005.
91. Şalva, E.; Kabasakal, L.; Eren, F.; Özkan, N.; Çakalağaoğlu, F.; Akbuğa, J. Local Delivery of Chitosan/VEGF SiRNA Nanoplexes Reduces Angiogenesis and Growth of Breast Cancer in Vivo. *Nucleic Acid Ther* **2012**, *22*, 40–48, doi:10.1089/nat.2011.0312.
92. Schiffelers, R.M.; Ansari, A.; Xu, J.; Zhou, Q.; Tang, Q.; Storm, G.; Molema, G.; Lu, P.Y.; Scaria, P. V; Woodle, M.C. Cancer SiRNA Therapy by Tumor Selective Delivery with Ligand-Targeted Sterically Stabilized Nanoparticle. *Nucleic Acids Res* **2004**, *32*, e149–e149, doi:10.1093/nar/gnh140.

93. Zuo, L.; Fan, Y.; Wang, F.; Gu, Q.; Xu, X. A SiRNA Targeting Vascular Endothelial Growth Factor-A Inhibiting Experimental Corneal Neovascularization. *Curr Eye Res* **2010**, *35*, 375–384, doi:10.3109/02713681003597230.
94. Shen, J.; Samul, R.; Silva, R.L.; Akiyama, H.; Liu, H.; Saishin, Y.; Hackett, S.F.; Zinnen, S.; Kossen, K.; Fosnaugh, K.; et al. Suppression of Ocular Neovascularization with SiRNA Targeting VEGF Receptor 1. *Gene Ther* **2006**, *13*, 225–234, doi:10.1038/sj.gt.3302641.
95. Zhao, X.; Zhu, D.-M.; Gan, W.-J.; Li, Z.; Zhang, J.-L.; Zhao, H.; Zhao, J.; Li, D.-C. Lentivirus-Mediated ShRNA Interference Targeting Vascular Endothelial Growth Factor Inhibits Angiogenesis and Progression of Human Pancreatic Carcinoma. *Oncol Rep* **2013**, *29*, 1019–1026, doi:10.3892/or.2012.2203.
96. Simmons, A.B.; Bretz, C.A.; Wang, H.; Kunz, E.; Hajj, K.; Kennedy, C.; Yang, Z.; Suwanmanee, T.; Kafri, · Tal; Hartnett, · M Elizabeth Gene Therapy Knockdown of VEGFR2 in Retinal Endothelial Cells to Treat Retinopathy. *Angiogenesis* **123AD**, *21*, 751–764, doi:10.1007/s10456-018-9618-5.
97. Che, J.; Tao, A.; Chen, S.; Li, X.; Zhao, Y.; Yuan, W. Biologically Responsive Carrier-Mediated Anti-Angiogenesis ShRNA Delivery for Tumor Treatment. *Sci Rep* **2016**, *6*, doi:10.1038/srep35661.
98. Liu, X.Q.; Xiong, M.H.; Shu, X.T.; Tang, R.Z.; Wang, J. Therapeutic Delivery of SiRNA Silencing HIF-1 Alpha with Micellar Nanoparticles Inhibits Hypoxic Tumor Growth. *Mol Pharm* **2012**, *9*, 2863–2874, doi:10.1021/MP300193F/ASSET/IMAGES/LARGE/MP-2012-00193F_0009.JPEG.
99. Araújo, R.S.; Silva, G.A. PlGF Silencing Combined with PEDF Overexpression: Modeling RPE Secretion as Potential Therapy for Retinal Neovascularization. *Mol Biol Rep* **2020**, *47*, 4413–4425, doi:10.1007/S11033-020-05496-2.
100. Li, X.; Yao, Q.Y.; Liu, H.C.; Jin, Q.W.; Xu, B.L.; Zhang, S.C.; Tu, C.T. Placental Growth Factor Silencing Ameliorates Liver Fibrosis and Angiogenesis and Inhibits Activation of Hepatic Stellate Cells in a Murine Model of Chronic Liver Disease. *J Cell Mol Med* **2017**, *21*, 2370–2385, doi:10.1111/jcmm.13158.
101. D'Souza, S.S.; Scherzinger-Laude, K.; Simon, M.; Salimath, B.P.; Rössler, J. Angiopoietin-2 Inhibition Using SiRNA or the Peptide Antagonist L1-10 Results in Antitumor Activity in Human Neuroblastoma. *J Cancer Res Clin Oncol* **2012**, *138*, 2017–2026, doi:10.1007/s00432-012-1282-3.
102. Zhang, Z.H.; Chen, Y.; Zhao, H.J.; Xie, C.Y.; Ding, J.; Hou, Y.T. Silencing of Heparanase by SiRNA Inhibits Tumor Metastasis and Angiogenesis of Human Breast Cancer in Vitro and in Vivo. *Cancer Biol Ther* **2007**, *6*, 587–595, doi:10.4161/cbt.6.4.3888.
103. Dolinsek, T.; Markelc, B.; Sersa, G.; Coer, A.; Stimac, M.; Lavrencak, J.; Brozic, A.; Kranjc, S.; Cemazar, M. Multiple Delivery of SiRNA against Endoglin into Murine Mammary Adenocarcinoma Prevents Angiogenesis and Delays Tumor Growth. *PLoS One* **2013**, *8*, doi:10.1371/journal.pone.0058723.

104. van Niel, G.; D'Angelo, G.; Raposo, G. Shedding Light on the Cell Biology of Extracellular Vesicles. *Nat Rev Mol Cell Biol* **2018**, *19*, 213–228, doi:10.1038/NRM.2017.125.
105. Elsharkasy, O.M.; Nordin, J.Z.; Hagey, D.W.; de Jong, O.G.; Schiffelers, R.M.; Andaloussi, S. el; Vader, P. Extracellular Vesicles as Drug Delivery Systems: Why and How? *Adv Drug Deliv Rev* **2020**, *159*, 332–343, doi:10.1016/J.ADDR.2020.04.004.
106. Harding, C.; Heuser, J.; Stahl, P. Receptor-Mediated Endocytosis of Transferrin and Recycling of the Transferrin Receptor in Rat Reticulocytes. *J Cell Biol* **1983**, *97*, 329–339, doi:10.1083/JCB.97.2.329.
107. Johnstone, R.M.; Adam, M.; Hammond, J.R.; Orr, L.; Turbide, C. Vesicle Formation during Reticulocyte Maturation. Association of Plasma Membrane Activities with Released Vesicles (Exosomes). *J Biol Chem* **1987**, *262*, 9412–9420.
108. Johnstone, R.M.; Mathew, A.; Mason, A.B.; Teng, K. Exosome Formation during Maturation of Mammalian and Avian Reticulocytes: Evidence That Exosome Release Is a Major Route for Externalization of Obsolete Membrane Proteins. *J Cell Physiol* **1991**, *147*, 27–36, doi:10.1002/JCP.1041470105.
109. Ulpiano, C.; da Silva, C.L.; Monteiro, G.A. Bioengineered Mesenchymal-Stromal-Cell-Derived Extracellular Vesicles as an Improved Drug Delivery System: Methods and Applications. *Biomedicines* 2023, *11*.
110. Roy, S.; Hochberg, F.H.; Jones, P.S. Extracellular Vesicles: The Growth as Diagnostics and Therapeutics; a Survey. *J Extracell Vesicles* **2018**, *7*, doi:10.1080/20013078.2018.1438720.
111. Alvarez-Erviti, L.; Seow, Y.; Yin, H.; Betts, C.; Lakhal, S.; Wood, M.J.A. Delivery of SiRNA to the Mouse Brain by Systemic Injection of Targeted Exosomes. *Nature Biotechnology 2011 29:4* **2011**, *29*, 341–345, doi:10.1038/nbt.1807.
112. Saleh, A.F.; Lázaro-Ibáñez, E.; Forsgard, M.A.M.; Shatnyeva, O.; Osteikoetxea, X.; Karlsson, F.; Heath, N.; Ingelsten, M.; Rose, J.; Harris, J.; et al. Extracellular Vesicles Induce Minimal Hepatotoxicity and Immunogenicity. *Nanoscale* **2019**, *11*, 6990–7001, doi:10.1039/C8NR08720B.
113. Millard, M.; Yakavetsa, I.; Piffoux, M.; Brun, A.; Gazeau, F.; Guigner, J.M.; Jasniewski, J.; Lassalle, H.P.; Wilhelm, C.; Bezdetnaya, L. MTHPC-Loaded Extracellular Vesicles Outperform Liposomal and Free MTHPC Formulations by an Increased Stability Drug Delivery Efficiency and Cytotoxic Effect in Tridimensional Model of Tumors. *Drug Deliv* **2018**, *25*, 1790–1801, doi:10.1080/10717544.2018.1513609.
114. Murphy, D.E.; de Jong, O.G.; Evers, M.J.W.; Nurazizah, M.; Schiffelers, R.M.; Vader, P. Natural or Synthetic RNA Delivery: A Stoichiometric Comparison of Extracellular Vesicles and Synthetic Nanoparticles. *Nano Lett* **2021**, *21*, 1888–1895, doi:10.1021/acs.nanolett.1c00094.
115. Teng, F.; Fussenegger, M. Shedding Light on Extracellular Vesicle Biogenesis and Bioengineering. *Advanced Science* **2020**, *8*, 2003505, doi:10.1002/ADVS.202003505.

116. Colombo, M.; Moita, C.; van Niel, G.; Kowal, J.; Vigneron, J.; Benaroch, P.; Manel, N.; Moita, L.F.; Théry, C.; Raposo, G. Analysis of ESCRT Functions in Exosome Biogenesis, Composition and Secretion Highlights the Heterogeneity of Extracellular Vesicles. *J Cell Sci* **2013**, *126*, 5553–5565, doi:10.1242/JCS.128868.
117. Trajkovic, K.; Hsu, C.; Chiantia, S.; Rajendran, L.; Wenzel, D.; Wieland, F.; Schwille, P.; Brügger, B.; Simons, M. Ceramide Triggers Budding of Exosome Vesicles into Multivesicular Endosomes. *Science* **2008**, *319*, 1244–1247, doi:10.1126/SCIENCE.1153124.
118. van Niel, G.; Charrin, S.; Simoes, S.; Romao, M.; Rochin, L.; Saftig, P.; Marks, M.S.; Rubinstein, E.; Raposo, G. The Tetraspanin CD63 Regulates ESCRT-Independent and -Dependent Endosomal Sorting during Melanogenesis. *Dev Cell* **2011**, *21*, 708–721, doi:10.1016/J.DEVCEL.2011.08.019.
119. Tricarico, C.; Clancy, J.; D'Souza-Schorey, C. Biology and Biogenesis of Shed Microvesicles. *Small GTPases* **2016**, *8*, 220–232, doi:10.1080/21541248.2016.1215283.
120. Cocucci, E.; Meldolesi, J. Ectosomes and Exosomes: Shedding the Confusion between Extracellular Vesicles. *Trends Cell Biol* **2015**, *25*, 364–372, doi:10.1016/J.TCB.2015.01.004.
121. Ni, K.; Wang, C.; Carnino, J.M.; Jin, Y. The Evolving Role of Caveolin-1: A Critical Regulator of Extracellular Vesicles. *Medical Sciences* **2020**, *8*, 46, doi:10.3390/medsci8040046.
122. Battistelli, M.; Falcieri, E. Apoptotic Bodies: Particular Extracellular Vesicles Involved in Intercellular Communication. *Biology (Basel)* **2020**, *9*, doi:10.3390/BIOLOGY9010021.
123. Villarroya-Beltri, C.; Gutiérrez-Vázquez, C.; Sánchez-Cabo, F.; Pérez-Hernández, D.; Vázquez, J.; Martin-Cofreces, N.; Martinez-Herrera, D.J.; Pascual-Montano, A.; Mittelbrunn, M.; Sánchez-Madrid, F. Sumoylated HnRNPA2B1 Controls the Sorting of MiRNAs into Exosomes through Binding to Specific Motifs. *Nat Commun* **2013**, *4*, doi:10.1038/NCOMMS3980.
124. Parchure, A.; Vyas, N.; Mayor, S. Wnt and Hedgehog: Secretion of Lipid-Modified. *Trends Cell Biol* **2018**, *28*, 157, doi:10.1016/J.TCB.2017.10.003.
125. Morelli, A.E.; Larregina, A.T.; Shufesky, W.J.; Sullivan, M.L.G.; Stolz, D.B.; Papworth, G.D.; Zahorchak, A.F.; Logar, A.J.; Wang, Z.; Watkins, S.C.; et al. Endocytosis, Intracellular Sorting, and Processing of Exosomes by Dendritic Cells. *Blood* **2004**, *104*, 3257–3266, doi:10.1182/BLOOD-2004-03-0824.
126. Théry, C.; Witwer, K.W.; Aikawa, E.; Alcaraz, M.J.; Anderson, J.D.; Andriantsitohaina, R.; Antoniou, A.; Arab, T.; Archer, F.; Atkin-Smith, G.K.; et al. Minimal Information for Studies of Extracellular Vesicles 2018 (MISEV2018): A Position Statement of the International Society for Extracellular Vesicles and Update of the MISEV2014 Guidelines. *J Extracell Vesicles* **2018**, *7*, doi:10.1080/20013078.2018.1535750.

127. Lotfy, A.; AboQuella, N.M.; Wang, H. Mesenchymal Stromal/Stem Cell (MSC)-Derived Exosomes in Clinical Trials. *Stem Cell Res Ther* **2023**, *14*, 66, doi:10.1186/S13287-023-03287-7.
128. Gupta, D.; Zickler, A.M.; El Andaloussi, S. Dosing Extracellular Vesicles. *Adv Drug Deliv Rev* **2021**, *178*, doi:10.1016/J.ADDR.2021.113961.
129. Lehrich, B.M.; Liang, Y.; Fiandaca, M.S. Foetal Bovine Serum Influence on in Vitro Extracellular Vesicle Analyses. *J Extracell Vesicles* **2021**, *10*, doi:10.1002/JEV2.12061.
130. Pincela Lins, P.M.; Pirlet, E.; Szymonik, M.; Bronckaers, A.; Nelissen, I. Manufacture of Extracellular Vesicles Derived from Mesenchymal Stromal Cells. *Trends Biotechnol* **2023**, *41*, 965–981, doi:10.1016/J.TIBTECH.2023.01.003.
131. Bahmani, L.; Ullah, M. Different Sourced Extracellular Vesicles and Their Potential Applications in Clinical Treatments. *Cells* **2022**, *11*, doi:10.3390/CELLS11131989.
132. Sanz-Ros, J.; Mas-Bargues, C.; Romero-García, N.; Huete-Acevedo, J.; Dromant, M.; Borrás, C. Extracellular Vesicles as Therapeutic Resources in the Clinical Environment. *Int J Mol Sci* **2023**, *24*, 24, doi:10.3390/IJMS24032344.
133. de Almeida Fuzeta, M.; Bernardes, N.; Oliveira, F.D.; Costa, A.C.; Fernandes-Platzgummer, A.; Farinha, J.P.; Rodrigues, C.A.V.; Jung, S.; Tseng, R.J.; Milligan, W.; et al. Scalable Production of Human Mesenchymal Stromal Cell-Derived Extracellular Vesicles Under Serum-/Xeno-Free Conditions in a Microcarrier-Based Bioreactor Culture System. *Front Cell Dev Biol* **2020**, *8*, doi:10.3389/fcell.2020.553444.
134. Haraszti, R.A.; Miller, R.; Stoppato, M.; Sere, Y.Y.; Coles, A.; Didiot, M.C.; Wollacott, R.; Sapp, E.; Dubuke, M.L.; Li, X.; et al. Exosomes Produced from 3D Cultures of MSCs by Tangential Flow Filtration Show Higher Yield and Improved Activity. *Molecular Therapy* **2018**, *26*, 2838–2847, doi:10.1016/j.ymthe.2018.09.015.
135. de Sousa Pinto, D.; Bandeiras, C.; de Almeida Fuzeta, M.; Rodrigues, C.A.V.; Jung, S.; Hashimura, Y.; Tseng, R.J.; Milligan, W.; Lee, B.; Ferreira, F.C.; et al. Scalable Manufacturing of Human Mesenchymal Stromal Cells in the Vertical-Wheel Bioreactor System: An Experimental and Economic Approach. *Biotechnol J* **2019**, *14*, doi:10.1002/biot.201800716.
136. Andriolo, G.; Provasi, E.; Lo Cicero, V.; Brambilla, A.; Soncin, S.; Torre, T.; Milano, G.; Biemmi, V.; Vassalli, G.; Turchetto, L.; et al. Exosomes From Human Cardiac Progenitor Cells for Therapeutic Applications: Development of a GMP-Grade Manufacturing Method. *Front Physiol* **2018**, *9*, doi:10.3389/FPHYS.2018.01169.
137. Lambrechts, T.; Papantoniou, I.; Viazzi, S.; Bovy, T.; Schrooten, J.; Luyten, F.P.; Aerts, J.M. Evaluation of a Monitored Multiplate Bioreactor for Large-Scale Expansion of Human Periosteum Derived Stem Cells for Bone Tissue Engineering Applications. *Biochem Eng J* **2016**, *108*, 58–68, doi:10.1016/J.BEJ.2015.07.015.
138. Mitchell, J.P.; Court, J.; Mason, M.D.; Tabi, Z.; Clayton, A. Increased Exosome Production from Tumour Cell Cultures Using the Integra CELLine Culture System. *J Immunol Methods* **2008**, *335*, 98–105, doi:10.1016/J.JIM.2008.03.001.

139. Jeppesen, D.K.; Nawrocki, A.; Jensen, S.G.; Thorsen, K.; Whitehead, B.; Howard, K.A.; Dyrskjøt, L.; Ørntoft, T.F.; Larsen, M.R.; Ostenfeld, M.S. Quantitative Proteomics of Fractionated Membrane and Lumen Exosome Proteins from Isogenic Metastatic and Nonmetastatic Bladder Cancer Cells Reveal Differential Expression of EMT Factors. *Proteomics* **2014**, *14*, 699–712, doi:10.1002/PMIC.201300452.
140. Grangier, A.; Branchu, J.; Volatron, J.; Piffoux, M.; Gazeau, F.; Wilhelm, C.; Silva, A.K.A. Technological Advances towards Extracellular Vesicles Mass Production. *Adv Drug Deliv Rev* **2021**, *176*, doi:10.1016/j.addr.2021.113843.
141. Gobin, J.; Muradia, G.; Mehic, J.; Westwood, C.; Couvrette, L.; Stalker, A.; Bigelow, S.; Luebbert, C.C.; Bissonnette, F.S.D.; Johnston, M.J.W.; et al. Hollow-Fiber Bioreactor Production of Extracellular Vesicles from Human Bone Marrow Mesenchymal Stromal Cells Yields Nanovesicles That Mirrors the Immuno-Modulatory Antigenic Signature of the Producer Cell. *Stem Cell Res Ther* **2021**, *12*, doi:10.1186/s13287-021-02190-3.
142. St-Denis-Bissonnette, F.; Cummings, S.E.; Qiu, S.; Stalker, A.; Muradia, G.; Mehic, J.; Mediratta, K.; Kaczmarek, S.; Burger, D.; Lee, S.H.; et al. A Clinically Relevant Large-Scale Biomanufacturing Workflow to Produce Natural Killer Cells and Natural Killer Cell-Derived Extracellular Vesicles for Cancer Immunotherapy. *J Extracell Vesicles* **2023**, *12*, e12387, doi:10.1002/jev2.12387.
143. Farid, S.S.; Jenkins, M.J. Bioprocesses for Cell Therapies. In *Biopharmaceutical Processing: Development, Design, and Implementation of Manufacturing Processes*; Elsevier, 2018; pp. 899–930 ISBN 9780128125526.
144. Haraszti, R.A.; Miller, R.; Stoppato, M.; Sere, Y.Y.; Coles, A.; Didiot, M.C.; Wollacott, R.; Sapp, E.; Dubuke, M.L.; Li, X.; et al. Exosomes Produced from 3D Cultures of MSCs by Tangential Flow Filtration Show Higher Yield and Improved Activity. *Molecular Therapy* **2018**, *26*, 2838, doi:10.1016/J.YMTHE.2018.09.015.
145. Xu, C.; Zhao, J.; Li, Q.; Hou, L.; Wang, Y.; Li, S.; Jiang, F.; Zhu, Z.; Tian, L. Exosomes Derived from Three-Dimensional Cultured Human Umbilical Cord Mesenchymal Stem Cells Ameliorate Pulmonary Fibrosis in a Mouse Silicosis Model. *Stem Cell Res Ther* **2020**, *11*, 1–12, doi:10.1186/S13287-020-02023-9/FIGURES/7.
146. Bandarra-Tavares, H.; Franchi-Mendes, T.; Ulpiano, C.; Morini, S.; Kaur, N.; Harris-Becker, A.; Vemuri, M.C.; Cabral, J.M.S.; Fernandes-Platzgummer, A.; da Silva, C.L. Dual Production of Human Mesenchymal Stromal Cells and Derived Extracellular Vesicles in a Dissolvable Microcarrier-Based Stirred Culture System. *Cytotherapy* **2024**, 1–8, doi:10.1016/j.jcyt.2024.03.001.
147. Jeske, R.; Liu, C.; Duke, L.; Canonicco Castro, M.L.; Muok, L.; Arthur, P.; Singh, M.; Jung, S.; Sun, L.; Li, Y. Upscaling Human Mesenchymal Stromal Cell Production in a Novel Vertical-Wheel Bioreactor Enhances Extracellular Vesicle Secretion and Cargo Profile. *Bioact Mater* **2023**, *25*, 732–747, doi:10.1016/j.bioactmat.2022.07.004.
148. Jalilian, E.; Massoumi, H.; Bigit, B.; Amin, S.; Katz, E.A.; Guaiquil, V.H.; Anwar, K.N.; Hematti, P.; Rosenblatt, M.I.; Djalilian, A.R. Bone Marrow Mesenchymal Stromal Cells in

a 3D System Produce Higher Concentration of Extracellular Vesicles (EVs) with Increased Complexity and Enhanced Neuronal Growth Properties. *Stem Cell Res Ther* **2022**, *13*, 1–13, doi:10.1186/S13287-022-03128-Z/FIGURES/5.

149. Fernandes-Platzgummer, A.; Cunha, R.; Morini, S.; Carvalho, M.; Moreno-Cid, J.; Cabral, J.; Lobato Da Silva, C.; Cabral, J.M.S.; Lobato Da Silva, C. Optimized Operation of a Controlled Stirred Tank Reactor System for the Production of Mesenchymal Stromal Cells and Their Extracellular. *Biotechnol Bioeng* **2023**, *120*, 2742–2755, doi:10.22541/au.167160787.74320022/v1.
150. Costa, M.H.G.; Costa, M.S.; Painho, B.; Sousa, C.D.; Carrondo, I.; Oltra, E.; Pelacho, B.; Prosper, F.; Isidro, I.A.; Alves, P.; et al. Enhanced Bioprocess Control to Advance the Manufacture of Mesenchymal Stromal Cell-Derived Extracellular Vesicles in Stirred-Tank Bioreactors. *Biotechnol Bioeng* **2023**, *120*, 2725–2741, doi:10.1002/bit.28378.
151. Barekzai, J.; Friedrich, J.; Okpara, M.; Refflinghaus, L.; Eckhardt, D.; Czermak, P.; Salzig, D. Dynamic Expansion of Mesenchymal Stem/Stromal Cells in a Stirred Tank Bioreactor Promotes the Release of Potent Extracellular Vesicles. *AIMS Bioeng* **2023**, *10*, 240–264, doi:10.3934/bioeng.2023016.
152. Thone, M.N.; Kwon, Y.J. Extracellular Blebs: Artificially-Induced Extracellular Vesicles for Facile Production and Clinical Translation. *Methods* **2020**, *177*, 135–145, doi:10.1016/j.ymeth.2019.11.007.
153. Dooley, K.; McConnell, R.E.; Xu, K.; Lewis, N.D.; Haupt, S.; Youniss, M.R.; Martin, S.; Sia, C.L.; McCoy, C.; Moniz, R.J.; et al. A Versatile Platform for Generating Engineered Extracellular Vesicles with Defined Therapeutic Properties. *Molecular Therapy* **2021**, *29*, 1729, doi:10.1016/J.YMTHE.2021.01.020.
154. Yuan, X.; Sun, L.; Jeske, R.; Nkosi, D.; York, S.B.; Liu, Y.; Grant, S.C.; Meckes, D.G.; Li, Y. Engineering Extracellular Vesicles by Three-Dimensional Dynamic Culture of Human Mesenchymal Stem Cells. *J Extracell Vesicles* **2022**, *11*, doi:10.1002/JEV2.12235.
155. Liu, W.; Li, L.; Rong, Y.; Qian, D.; Chen, J.; Zhou, Z.; Luo, Y.; Jiang, D.; Cheng, L.; Zhao, S.; et al. Hypoxic Mesenchymal Stem Cell-Derived Exosomes Promote Bone Fracture Healing by the Transfer of MiR-126. *Acta Biomater* **2020**, *103*, 196–212, doi:10.1016/J.ACTBIO.2019.12.020.
156. Tse, S.W.; Tan, C.F.; Park, J.E.; Gnanasekaran, J.; Gupta, N.; Low, J.K.; Yeoh, K.W.; Chng, W.J.; Tay, C.Y.; McCarthy, N.E.; et al. Microenvironmental Hypoxia Induces Dynamic Changes in Lung Cancer Synthesis and Secretion of Extracellular Vesicles. *Cancers 2020, Vol. 12, Page 2917* **2020**, *12*, 2917, doi:10.3390/CANCERS12102917.
157. Han, Y.; Ren, J.; Bai, Y.; Pei, X.; Han, Y. Exosomes from Hypoxia-Treated Human Adipose-Derived Mesenchymal Stem Cells Enhance Angiogenesis through VEGF/VEGF-R. *Int J Biochem Cell Biol* **2019**, *109*, 59–68, doi:10.1016/J.BIOCEL.2019.01.017.
158. Ban, J.J.; Lee, M.; Im, W.; Kim, M. Low PH Increases the Yield of Exosome Isolation. *Biochem Biophys Res Commun* **2015**, *461*, 76–79, doi:10.1016/J.BBRC.2015.03.172.

159. Gong, C.; Zhang, X.; Shi, M.; Li, F.; Wang, S.; Wang, Y.; Wang, Y.; Wei, W.; Ma, G.; Gong, C.; et al. Tumor Exosomes Reprogrammed by Low PH Are Efficient Targeting Vehicles for Smart Drug Delivery and Personalized Therapy against Their Homologous Tumor. *Advanced Science* **2021**, *8*, 2002787, doi:10.1002/ADVS.202002787.
160. Hedlund, M.; Nagaeva, O.; Kargl, D.; Baranov, V.; Mincheva-Nilsson, L. Thermal- and Oxidative Stress Causes Enhanced Release of NKG2D Ligand-Bearing Immunosuppressive Exosomes in Leukemia/Lymphoma T and B Cells. *PLoS One* **2011**, *6*, 16899, doi:10.1371/JOURNAL.PONE.0016899.
161. Nakamura, Y.; Kita, S.; Tanaka, Y.; Fukuda, S.; Obata, Y.; Okita, T.; Nishida, H.; Takahashi, Y.; Kawachi, Y.; Tsugawa-Shimizu, Y.; et al. Adiponectin Stimulates Exosome Release to Enhance Mesenchymal Stem-Cell-Driven Therapy of Heart Failure in Mice. *Molecular Therapy* **2020**, *28*, 2203–2219, doi:10.1016/J.YMTHE.2020.06.026.
162. Wang, J.; Bonacquisti, E.E.; Brown, A.D.; Nguyen, J. Boosting the Biogenesis and Secretion of Mesenchymal Stem Cell-Derived Exosomes. *Cells 2020, Vol. 9, Page 660* **2020**, *9*, 660, doi:10.3390/CELLS9030660.
163. Cheng, A.; Choi, D.; Lora, M.; Shum-Tim, D.; Rak, J.; Colmegna, I. Human Multipotent Mesenchymal Stromal Cells Cytokine Priming Promotes RAB27B-Regulated Secretion of Small Extracellular Vesicles with Immunomodulatory Cargo. *Stem Cell Res Ther* **2020**, *11*, doi:10.1186/S13287-020-02050-6.
164. Headland, S.E.; Jones, H.R.; D'Sa, A.S.V.; Perretti, M.; Norling, L. V. Cutting-Edge Analysis of Extracellular Microparticles Using Imagestreamx Imaging Flow Cytometry. *Sci Rep* **2014**, *4*, doi:10.1038/srep05237.
165. Momen-Heravi, F.; Bala, S.; Kodys, K.; Szabo, G. Exosomes Derived from Alcohol-Treated Hepatocytes Horizontally Transfer Liver Specific MiRNA-122 and Sensitize Monocytes to LPS. *Scientific Reports 2015 5:1* **2015**, *5*, 1–16, doi:10.1038/srep09991.
166. Adlerz, K.; Patel, D.; Rowley, J.; Ng, K.; Ahsan, T. Strategies for Scalable Manufacturing and Translation of MSC-Derived Extracellular Vesicles. *Stem Cell Res* **2020**, *48*, doi:10.1016/j.scr.2020.101978.
167. Liau, L.L.; Bin Hassan, M.N.F.; Tang, Y.L.; Ng, M.H.; Law, J.X. Feasibility of Human Platelet Lysate as an Alternative to Foetal Bovine Serum for in Vitro Expansion of Chondrocytes. *Int J Mol Sci* 2021, *22*, 1–17.
168. Shelke, G.V.; Lä Sser, C.; Gho, Y.S.; Lö Tvall, J.; Lö, J. Importance of Exosome Depletion Protocols to Eliminate Functional and RNA-Containing Extracellular Vesicles from Fetal Bovine Serum. *J Extracell Vesicles* **2014**, *3*, doi:10.3402/jev.v3.24783.
169. Lorenzini, B.; Peltzer, J.; Goulinet, S.; Rival, B.; Lataillade, J.J.; Uzan, G.; Banzet, S.; Mauduit, P. Producing Vesicle-Free Cell Culture Additive for Human Cells Extracellular Vesicles Manufacturing. *Journal of Controlled Release* **2023**, *355*, 501–514, doi:10.1016/j.jconrel.2023.01.073.
170. Zhu, D.; Fang, H.; Kusuma, G.D.; Schwab, R.; Barabadi, M.; Chan, S.T.; McDonald, H.; Leong, C.M.; Wallace, E.M.; Greening, D.W.; et al. Impact of Chemically Defined Culture

Media Formulations on Extracellular Vesicle Production by Amniotic Epithelial Cells. *Proteomics* **2021**, *21*, 2000080, doi:10.1002/PMIC.202000080.

171. Bost, J.P.; Saher, O.; Hagey, D.; Mamand, D.R.; Liang, X.; Zheng, W.; Corso, G.; Gustafsson, O.; Görgens, A.; Smith, C.E.; et al. Growth Media Conditions Influence the Secretion Route and Release Levels of Engineered Extracellular Vesicles. *Adv Healthc Mater* **2022**, *11*, 2101658, doi:10.1002/ADHM.202101658.
172. Patel, D.B.; Gray, K.M.; Santharam, Y.; Lamichhane, T.N.; Stroka, K.M.; Jay, S.M. Impact of Cell Culture Parameters on Production and Vascularization Bioactivity of Mesenchymal Stem Cell-Derived Extracellular Vesicles. *Bioeng Transl Med* **2017**, *2*, 170–179, doi:10.1002/btm2.10065.
173. Arteaga-Blanco, L.A.; Mojoli, A.; Monteiro, R.Q.; Sandim, V.; S Menna-Barreto, R.F.; Santos Pereira-Dutra, F.I.; Bozza, P.T.; de Oliveira Resende, R.; Chequer Bou-Habib, D.I. Characterization and Internalization of Small Extracellular Vesicles Released by Human Primary Macrophages Derived from Circulating Monocytes. *PLoS One* **2020**, *15*, doi:10.1371/journal.pone.0237795.
174. Kojima, R.; Bojar, D.; Rizzi, G.; Hamri, G.C. El; El-Baba, M.D.; Saxena, P.; Ausländer, S.; Tan, K.R.; Fussenegger, M. Designer Exosomes Produced by Implanted Cells Intracerebrally Deliver Therapeutic Cargo for Parkinson's Disease Treatment. *Nat Commun* **2018**, *9*, doi:10.1038/s41467-018-03733-8.
175. Jo, W.; Kim, J.; Yoon, J.; Jeong, D.; Cho, S.; Jeong, H.; Yoon, Y.J.; Kim, S.C.; Gho, Y.S.; Park, J. Large-Scale Generation of Cell-Derived Nanovesicles. *Nanoscale* **2014**, *6*, 12056–12064, doi:10.1039/C4NR02391A.
176. Wang, X.; Hu, S.; Li, J.; Zhu, D.; Wang, Z.; Cores, J.; Cheng, K.; Liu, G.; Huang, K. Extruded Mesenchymal Stem Cell Nanovesicles Are Equally Potent to Natural Extracellular Vesicles in Cardiac Repair. *ACS Appl Mater Interfaces* **2021**, *13*, 55767–55779, doi:10.1021/acsami.1c08044.
177. Staubach, S.; Bauer, F.N.; Tertel, T.; Börger, V.; Stambouli, O.; Salzig, D.; Giebel, B. Scaled Preparation of Extracellular Vesicles from Conditioned Media. *Adv Drug Deliv Rev* **2021**, *177*, 113940, doi:10.1016/J.ADDR.2021.113940.
178. Royo, F.; Théry, C.; Falcón-Pérez, J.M.; Nieuwland, R.; Witwer, K.W. Methods for Separation and Characterization of Extracellular Vesicles: Results of a Worldwide Survey Performed by the ISEV Rigor and Standardization Subcommittee. *Cells* **2020**, *9*, doi:10.3390/CELLS9091955.
179. Otsuru, S.; Desbourdes, L.; Guess, A.J.; Hofmann, T.J.; Relation, T.; Kaito, T.; Dominici, M.; Iwamoto, M.; Horwitz, E.M. Extracellular Vesicles Released from Mesenchymal Stromal Cells Stimulate Bone Growth in Osteogenesis Imperfecta. *Cytotherapy* **2018**, *20*, 62–73, doi:10.1016/j.jcyt.2017.09.012.
180. Han, T.; Song, P.; Wu, Z.; Xiang, X.; Liu, Y.; Wang, Y.; Fang, H.; Niu, Y.; Shen, C. MSC Secreted Extracellular Vesicles Carrying TGF-Beta Upregulate Smad 6 Expression and

Promote the Regrowth of Neurons in Spinal Cord Injured Rats. *Stem Cell Rev Rep* **2022**, *18*, 1078–1096, doi:10.1007/s12015-021-10219-6.

181. Webber, J.; Clayton, A. How Pure Are Your Vesicles? *J Extracell Vesicles* **2013**, *2*, doi:10.3402/JEV.V2I0.19861.
182. Williams, S.; Jalal, A.R.; Lewis, M.P.; Davies, O.G. A Survey to Evaluate Parameters Governing the Selection and Application of Extracellular Vesicle Isolation Methods. *J Tissue Eng* **2023**, *14*, doi:10.1177/20417314231155114.
183. Ludwig, A.K.; De Miroschedji, K.; Doeppner, T.R.; Börger, V.; Ruesing, J.; Rebmann, V.; Durst, S.; Jansen, S.; Bremer, M.; Behrmann, E.; et al. Precipitation with Polyethylene Glycol Followed by Washing and Pelleting by Ultracentrifugation Enriches Extracellular Vesicles from Tissue Culture Supernatants in Small and Large Scales. *J Extracell Vesicles* **2018**, *7*, doi:10.1080/20013078.2018.1528109.
184. Paolini, L.; Zendrini, A.; Noto, G. Di; Busatto, S.; Lottini, E.; Radeghieri, A.; Dossi, A.; Caneschi, A.; Ricotta, D.; Bergese, P. Residual Matrix from Different Separation Techniques Impacts Exosome Biological Activity. *Sci Rep* **2016**, *6*, doi:10.1038/SREP23550.
185. Kordelas, L.; Rebmann, V.; Ludwig, A.K.; Radtke, S.; Ruesing, J.; Doeppner, T.R.; Epple, M.; Horn, P.A.; Beelen, D.W.; Giebel, B. MSC-Derived Exosomes: A Novel Tool to Treat Therapy-Refractory Graft-versus-Host Disease. *Leukemia 2014 28:4* **2014**, *28*, 970–973, doi:10.1038/leu.2014.41.
186. Doeppner, T.R.; Herz, J.; Görgens, A.; Schlechter, J.; Ludwig, A.-K.; Radtke, S.; de Miroschedji, K.; Horn, P.A.; Giebel, B.; Hermann, D.M. Extracellular Vesicles Improve Post-Stroke Neuroregeneration and Prevent Postischemic Immunosuppression. *Stem Cells Transl Med* **2015**, *4*, 1131–1143, doi:10.5966/sctm.2015-0078.
187. Liangsupree, T.; Multia, E.; Riekkola, M.L. Modern Isolation and Separation Techniques for Extracellular Vesicles. *J Chromatogr A* **2021**, *1636*, doi:10.1016/j.chroma.2020.461773.
188. Busatto, S.; Vilanilam, G.; Ticer, T.; Lin, W.L.; Dickson, D.W.; Shapiro, S.; Bergese, P.; Wolfram, J. Tangential Flow Filtration for Highly Efficient Concentration of Extracellular Vesicles from Large Volumes of Fluid. *Cells* **2018**, *7*, 273, doi:10.3390/CELLS7120273.
189. Benedikter, B.J.; Bouwman, F.G.; Vajen, T.; Heinzmann, A.C.A.; Grauls, G.; Mariman, E.C.; Wouters, E.F.M.; Savelkoul, P.H.; Lopez-Iglesias, C.; Koenen, R.R.; et al. Ultrafiltration Combined with Size Exclusion Chromatography Efficiently Isolates Extracellular Vesicles from Cell Culture Media for Compositional and Functional Studies. *Sci Rep* **2017**, *7*, doi:10.1038/s41598-017-15717-7.
190. Cardoso, R.M.S.; Rodrigues, S.C.; Gomes, C.F.; Duarte, F. V.; Romao, M.; Leal, E.C.; Freire, P.C.; Neves, R.; Simões-Correia, J. Development of an Optimized and Scalable Method for Isolation of Umbilical Cord Blood-derived Small Extracellular Vesicles for Future Clinical Use. *Stem Cells Transl Med* **2021**, *10*, 910, doi:10.1002/SCTM.20-0376.

191. Monguió-Tortajada, M.; Roura, S.; Gálvez-Montón, C.; Pujal, J.M.; Aran, G.; Sanjurjo, L.; Franquesa, M.; Sarrias, M.R.; Bayes-Genis, A.; Borràs, F.E. Nanosized UCMSC-Derived Extracellular Vesicles but Not Conditioned Medium Exclusively Inhibit the Inflammatory Response of Stimulated T Cells: Implications for Nanomedicine. *Theranostics* **2017**, *7*, 270–284, doi:10.7150/THNO.16154.

192. Shigemoto-Kuroda, T.; Oh, J.Y.; Kim, D. ki; Jeong, H.J.; Park, S.Y.; Lee, H.J.; Park, J.W.; Kim, T.W.; An, S.Y.; Prockop, D.J.; et al. MSC-Derived Extracellular Vesicles Attenuate Immune Responses in Two Autoimmune Murine Models: Type 1 Diabetes and Uveoretinitis. *Stem Cell Reports* **2017**, *8*, 1214–1225, doi:10.1016/J.STEMCR.2017.04.008.

193. Kim, D.K.; Nishida, H.; An, S.Y.; Shetty, A.K.; Bartosh, T.J.; Prockop, D.J. Chromatographically Isolated CD63+CD81+ Extracellular Vesicles from Mesenchymal Stromal Cells Rescue Cognitive Impairments after TBI. *Proc Natl Acad Sci U S A* **2015**, *113*, 170–175, doi:10.1073/PNAS.1522297113/SUPPL_FILE/PNAS.201522297SI.PDF.

194. Pacienza, N.; Lee, R.H.; Bae, E.H.; Kim, D. ki; Liu, Q.; Prockop, D.J.; Yannarelli, G. In Vitro Macrophage Assay Predicts the In Vivo Anti-Inflammatory Potential of Exosomes from Human Mesenchymal Stromal Cells. *Mol Ther Methods Clin Dev* **2019**, *13*, 67–76, doi:10.1016/J.OMTM.2018.12.003.

195. Heath, N.; Grant, L.; De Oliveira, T.M.; Rowlinson, R.; Osteikoetxea, X.; Dekker, N.; Overman, R. Rapid Isolation and Enrichment of Extracellular Vesicle Preparations Using Anion Exchange Chromatography. *Scientific Reports 2018 8:1* **2018**, *8*, 1–12, doi:10.1038/s41598-018-24163-y.

196. Seo, N.; Nakamura, J.; Kaneda, T.; Tateno, H.; Shimoda, A.; Ichiki, T.; Furukawa, K.; Hirabayashi, J.; Akiyoshi, K.; Shiku, H. Distinguishing Functional Exosomes and Other Extracellular Vesicles as a Nucleic Acid Cargo by the Anion-Exchange Method. *J Extracell Vesicles* **2022**, *11*, doi:10.1002/JEV2.12205.

197. Heath, N.; Grant, L.; De Oliveira, T.M.; Rowlinson, R.; Osteikoetxea, X.; Dekker, N.; Overman, R. Rapid Isolation and Enrichment of Extracellular Vesicle Preparations Using Anion Exchange Chromatography. *Sci Rep* **2018**, *8*, 1–12, doi:10.1038/s41598-018-24163-y.

198. Barnes, B.; Caws, T.; Thomas, S.; Shephard, A.P.; Corteling, R.; Hole, P.; Bracewell, D.G. Investigating Heparin Affinity Chromatography for Extracellular Vesicle Purification and Fractionation. *J Chromatogr A* **2022**, *1670*, 462987, doi:10.1016/J.CHROMA.2022.462987.

199. Filipović, L.; Spasojević, M.; Prodanović, R.; Korać, A.; Matijaševic, S.; Brajušković, G.; de Marco, A.; Popović, M. Affinity-Based Isolation of Extracellular Vesicles by Means of Single-Domain Antibodies Bound to Macroporous Methacrylate-Based Copolymer. *N Biotechnol* **2022**, *69*, 36–48, doi:10.1016/J.NBT.2022.03.001.

200. Popovic, M.; Mazzega, E.; Toffoletto, B.; de Marco, A. Isolation of Anti-Extra-Cellular Vesicle Single-Domain Antibodies by Direct Panning on Vesicle-Enriched Fractions. *Microb Cell Fact* **2018**, *17*, 6, doi:10.1186/S12934-017-0856-9.

201. Multia, E.; Tear, C.J.Y.; Palviainen, M.; Siljander, P.; Riekkola, M.L. Fast Isolation of Highly Specific Population of Platelet-Derived Extracellular Vesicles from Blood Plasma by Affinity Monolithic Column, Immobilized with Anti-Human CD61 Antibody. *Anal Chim Acta* **2019**, *1091*, 160–168, doi:10.1016/J.ACA.2019.09.022.

202. Sun, D.; Zhuang, X.; Xiang, X.; Liu, Y.; Zhang, S.; Liu, C.; Barnes, S.; Grizzle, W.; Miller, D.; Zhang, H.G. A Novel Nanoparticle Drug Delivery System: The Anti-Inflammatory Activity of Curcumin Is Enhanced When Encapsulated in Exosomes. *Mol Ther* **2010**, *18*, 1606–1614, doi:10.1038/MT.2010.105.

203. Didiot, M.C.; Hall, L.M.; Coles, A.H.; Haraszti, R.A.; Godinho, B.M.D.C.; Chase, K.; Sapp, E.; Ly, S.; Alterman, J.F.; Hassler, M.R.; et al. Exosome-Mediated Delivery of Hydrophobically Modified SiRNA for Huntingtin MRNA Silencing. *Molecular Therapy* **2016**, *24*, 1836–1847, doi:10.1038/mt.2016.126.

204. Goh, W.J.; Lee, C.K.; Zou, S.; Woon, E.C.Y.; Czarny, B.; Pastorin, G. Doxorubicin-Loaded Cell-Derived Nanovesicles: An Alternative Targeted Approach for Anti-Tumor Therapy. *Int J Nanomedicine* **2017**, *12*, 2759, doi:10.2147/IJN.S131786.

205. Kim, M.S.; Haney, M.J.; Zhao, Y.; Mahajan, V.; Deygen, I.; Klyachko, N.L.; Inskoe, E.; Piroyan, A.; Sokolsky, M.; Okolie, O.; et al. Development of Exosome-Encapsulated Paclitaxel to Overcome MDR in Cancer Cells. *Nanomedicine* **2016**, *12*, 655–664, doi:10.1016/J.NANO.2015.10.012.

206. Shtam, T.A.; Kovalev, R.A.; Varfolomeeva, E.Y.; Makarov, E.M.; Kil, Y. v.; Filatov, M. v. Exosomes Are Natural Carriers of Exogenous SiRNA to Human Cells in Vitro. *Cell Commun Signal* **2013**, *11*, doi:10.1186/1478-811X-11-88.

207. Bala, S.; Csak, T.; Momen-Heravi, F.; Lippai, D.; Kodys, K.; Catalano, D.; Satishchandran, A.; Ambros, V.; Szabo, G. Biodistribution and Function of Extracellular MiRNA-155 in Mice. *Scientific Reports 2015 5:1* **2015**, *5*, 1–12, doi:10.1038/srep10721.

208. Tian, Y.; Li, S.; Song, J.; Ji, T.; Zhu, M.; Anderson, G.J.; Wei, J.; Nie, G. A Doxorubicin Delivery Platform Using Engineered Natural Membrane Vesicle Exosomes for Targeted Tumor Therapy. *Biomaterials* **2014**, *35*, 2383–2390, doi:10.1016/J.BIOMATERIALS.2013.11.083.

209. Usman, W.M.; Pham, T.C.; Kwok, Y.Y.; Vu, L.T.; Ma, V.; Peng, B.; Chan, Y.S.; Wei, L.; Chin, S.M.; Azad, A.; et al. Efficient RNA Drug Delivery Using Red Blood Cell Extracellular Vesicles. *Nat Commun* **2018**, *9*, doi:10.1038/S41467-018-04791-8.

210. Lamichhane, T.N.; Jeyaram, A.; Patel, D.B.; Parajuli, B.; Livingston, N.K.; Arumugasaamy, N.; Schardt, J.S.; Jay, S.M. Oncogene Knockdown via Active Loading of Small RNAs into Extracellular Vesicles by Sonication. *Cell Mol Bioeng* **2016**, *9*, 315–324, doi:10.1007/S12195-016-0457-4.

211. Haney, M.J.; Klyachko, N.L.; Zhao, Y.; Gupta, R.; Plotnikova, E.G.; He, Z.; Patel, T.; Piroyan, A.; Sokolsky, M.; Kabanov, A. v.; et al. Exosomes as Drug Delivery Vehicles for Parkinson's Disease Therapy. *J Control Release* **2015**, *207*, 18, doi:10.1016/J.JCONREL.2015.03.033.
212. Jang, S.C.; Kim, O.Y.; Yoon, C.M.; Choi, D.S.; Roh, T.Y.; Park, J.; Nilsson, J.; Lötvall, J.; Kim, Y.K.; Gho, Y.S. Bioinspired Exosome-Mimetic Nanovesicles for Targeted Delivery of Chemotherapeutics to Malignant Tumors. *ACS Nano* **2013**, *7*, 7698–7710, doi:10.1021/NN402232G.
213. Ramanathan, S.; Shenoda, B.B.; Lin, Z.; Alexander, G.M.; Huppert, A.; Sacan, A.; Ajit, S.K. Inflammation Potentiates MiR-939 Expression and Packaging into Small Extracellular Vesicles. *J Extracell Vesicles* **2019**, *8*, doi:10.1080/20013078.2019.1650595.
214. Liang, G.; Kan, S.; Zhu, Y.; Feng, S.; Feng, W.; Gao, S. Engineered Exosome-Mediated Delivery of Functionally Active MiR-26a and Its Enhanced Suppression Effect in HepG2 Cells. *Int J Nanomedicine* **2018**, *13*, 585, doi:10.2147/IJN.S154458.
215. Lamichhane, T.N.; Raiker, R.S.; Jay, S.M. Exogenous DNA Loading into Extracellular Vesicles via Electroporation Is Size-Dependent and Enables Limited Gene Delivery. *Mol Pharm* **2015**, *12*, 3650–3657, doi:10.1021/acs.molpharmaceut.5b00364.
216. Izco, M.; Blesa, J.; Schleef, M.; Schmeer, M.; Porcari, R.; Al-Shawi, R.; Ellmerich, S.; de Toro, M.; Gardiner, C.; Seow, Y.; et al. Systemic Exosomal Delivery of ShRNA Minicircles Prevents Parkinsonian Pathology. *Molecular Therapy* **2019**, *27*, 2111–2122, doi:10.1016/j.ymthe.2019.08.010.
217. Sato, Y.T.; Umezaki, K.; Sawada, S.; Mukai, S.A.; Sasaki, Y.; Harada, N.; Shiku, H.; Akiyoshi, K. Engineering Hybrid Exosomes by Membrane Fusion with Liposomes. *Sci Rep* **2016**, *6*, doi:10.1038/SREP21933.
218. Hettich, B.F.; Bader, J.J.; Leroux, J.C. Encapsulation of Hydrophilic Compounds in Small Extracellular Vesicles: Loading Capacity and Impact on Vesicle Functions. *Adv Healthc Mater* **2021**, 2100047, doi:10.1002/ADHM.202100047.
219. Johnsen, K.B.; Gudbergsson, J.M.; Skov, M.N.; Christiansen, G.; Gurevich, L.; Moos, T.; Duroux, M. Evaluation of Electroporation-Induced Adverse Effects on Adipose-Derived Stem Cell Exosomes. *Cytotechnology* **2016**, *68*, 2125–2138, doi:10.1007/s10616-016-9952-7.
220. Man, K.; Brunet, M.Y.; Jones, M.C.; Cox, S.C. Engineered Extracellular Vesicles: Tailored-Made Nanomaterials for Medical Applications. *Nanomaterials (Basel)* **2020**, *10*, 1–30, doi:10.3390/NANO10091838.
221. Herrmann, I.K.; Wood, M.J.A.; Fuhrmann, G. Extracellular Vesicles as a Next-Generation Drug Delivery Platform. *Nat Nanotechnol* **2021**, *16*, 748–759, doi:10.1038/s41565-021-00931-2.
222. Farhat, W.; Yeung, V.; Kahale, F.; Parekh, M.; Cortinas, J.; Chen, L.; Ross, A.E.; Ciolino, J.B. Doxorubicin-Loaded Extracellular Vesicles Enhance Tumor Cell Death in Retinoblastoma. *Bioengineering* **2022**, *9*, 671, doi:10.3390/bioengineering9110671.

223. Pascucci, L.; Coccè, V.; Bonomi, A.; Ami, D.; Ceccarelli, P.; Ciusani, E.; Viganò, L.; Locatelli, A.; Sisto, F.; Doglia, S.M.; et al. Paclitaxel Is Incorporated by Mesenchymal Stromal Cells and Released in Exosomes That Inhibit in Vitro Tumor Growth: A New Approach for Drug Delivery. *Journal of Controlled Release* **2014**, *192*, 262–270, doi:10.1016/J.JCONREL.2014.07.042.

224. Lee, S.-T.; Im, W.; Ban, J.-J.; Lee, M.; Jung, K.-H.; Lee, S.K.; Chu, K.; Kim, M. Exosome-Based Delivery of MiR-124 in a Huntington's Disease Model. *J Mov Disord* **2017**, *10*, 45, doi:10.14802/JMD.16054.

225. Hung, M.E.; Leonard, J.N. A Platform for Actively Loading Cargo RNA to Elucidate Limiting Steps in EV-Mediated Delivery. *J Extracell Vesicles* **2016**, *5*, doi:10.3402/JEV.V5.31027.

226. Li, Z.; Zhou, X.; Wei, M.; Gao, X.; Zhao, L.; Shi, R.; Sun, W.; Duan, Y.; Yang, G.; Yuan, L. In Vitro and in Vivo RNA Inhibition by CD9-HuR Functionalized Exosomes Encapsulated with MiRNA or CRISPR/DCas9. *Nano Lett* **2019**, *19*, 19–28, doi:10.1021/ACS.NANOLETT.8B02689.

227. Mizrak, A.; Bolukbasi, M.F.; Ozdener, G.B.; Brenner, G.J.; Madlener, S.; Erkan, E.P.; Ströbel, T.; Breakefield, X.O.; Saydam, O. Genetically Engineered Microvesicles Carrying Suicide MRNA/Protein Inhibit Schwannoma Tumor Growth. *Molecular Therapy* **2013**, *21*, 101, doi:10.1038/MT.2012.161.

228. Vituret, C.; Gallay, K.; Confort, M.P.; Ftaich, N.; Matei, C.I.; Archer, F.; Ronfort, C.; Mornex, J.F.; Chanson, M.; di Pietro, A.; et al. Transfer of the Cystic Fibrosis Transmembrane Conductance Regulator to Human Cystic Fibrosis Cells Mediated by Extracellular Vesicles. *Hum Gene Ther* **2016**, *27*, 166–183, doi:10.1089/HUM.2015.144.

229. Zhang, H.; Wang, Y.; Bai, M.; Wang, J.; Zhu, K.; Liu, R.; Ge, S.; Li, J.L.; Ning, T.; Deng, T.; et al. Exosomes Serve as Nanoparticles to Suppress Tumor Growth and Angiogenesis in Gastric Cancer by Delivering Hepatocyte Growth Factor SiRNA. *Cancer Sci* **2018**, *109*, 629, doi:10.1111/CAS.13488.

230. Wiklander, O.P.B.; Nordin, J.Z.; O'Loughlin, A.; Gustafsson, Y.; Corso, G.; Mäger, I.; Vader, P.; Lee, Y.; Sork, H.; Seow, Y.; et al. Extracellular Vesicle in Vivo Biodistribution Is Determined by Cell Source, Route of Administration and Targeting. *J Extracell Vesicles* **2015**, *4*, 1–13, doi:10.3402/JEV.V4.26316.

231. Sato, Y.T.; Umezaki, K.; Sawada, S.; Mukai, S.A.; Sasaki, Y.; Harada, N.; Shiku, H.; Akiyoshi, K. Engineering Hybrid Exosomes by Membrane Fusion with Liposomes. *Scientific Reports 2016 6:1* **2016**, *6*, 1–11, doi:10.1038/srep21933.

232. Jia, G.; Han, Y.; An, Y.; Ding, Y.; He, C.; Wang, X.; Tang, Q. NRP-1 Targeted and Cargo-Loaded Exosomes Facilitate Simultaneous Imaging and Therapy of Glioma in Vitro and in Vivo. *Biomaterials* **2018**, *178*, 302–316, doi:10.1016/J.BIOMATERIALS.2018.06.029.

233. Kamerkar, S.; Lebleu, V.S.; Sugimoto, H.; Yang, S.; Ruivo, C.F.; Melo, S.A.; Lee, J.J.; Kalluri, R. Exosomes Facilitate Therapeutic Targeting of Oncogenic Kras in Pancreatic Cancer. *Nature* **2017**, *546*, 498, doi:10.1038/NATURE22341.

234. Liang, G.; Zhu, Y.; Ali, D.J.; Tian, T.; Xu, H.; Si, K.; Sun, B.; Chen, B.; Xiao, Z. Engineered Exosomes for Targeted Co-Delivery of MiR-21 Inhibitor and Chemotherapeutics to Reverse Drug Resistance in Colon Cancer. *J Nanobiotechnology* **2020**, *18*, 1–15, doi:10.1186/s12951-019-0563-2.
235. Hartman, Z.C.; Wei, J.; Glass, O.K.; Guo, H.; Lei, G.; Yang, X.Y.; Osada, T.; Hobeika, A.; Delcayre, A.; le Pecq, J.B.; et al. Increasing Vaccine Potency through Exosome Antigen Targeting. *Vaccine* **2011**, *29*, 9361–9367, doi:10.1016/J.VACCINE.2011.09.133.
236. Kooijmans, S.A.A.; Aleza, C.G.; Roffler, S.R.; van Solinge, W.W.; Vader, P.; Schiffelers, R.M. Display of GPI-Anchored Anti-EGFR Nanobodies on Extracellular Vesicles Promotes Tumour Cell Targeting. *J Extracell Vesicles* **2016**, *5*, doi:10.3402/JEV.V5.31053.
237. Kim, M.S.; Haney, M.J.; Zhao, Y.; Yuan, D.; Deygen, I.; Klyachko, N.L.; Kabanov, A. v.; Batrakova, E. v. Engineering Macrophage-Derived Exosomes for Targeted Paclitaxel Delivery to Pulmonary Metastases: In Vitro and in Vivo Evaluations. *Nanomedicine* **2018**, *14*, 195–204, doi:10.1016/J.NANO.2017.09.011.
238. Kooijmans, S.A.A.; Fliervoet, L.A.L.; van der Meel, R.; Fens, M.H.A.M.; Heijnen, H.F.G.; van Bergen En Henegouwen, P.M.P.; Vader, P.; Schiffelers, R.M. PEGylated and Targeted Extracellular Vesicles Display Enhanced Cell Specificity and Circulation Time. *Journal of Controlled Release* **2016**, *224*, 77–85, doi:10.1016/J.JCONREL.2016.01.009.
239. Huang, L.; Gu, N.; Zhang, X.E.; Wang, D.B. Light-Inducible Exosome-Based Vehicle for Endogenous RNA Loading and Delivery to Leukemia Cells. *Adv Funct Mater* **2019**, *29*, doi:10.1002/ADFM.201807189.
240. Pi, F.; Binzel, D.W.; Lee, T.J.; Li, Z.; Sun, M.; Rychahou, P.; Li, H.; Haque, F.; Wang, S.; Croce, C.M.; et al. Nanoparticle Orientation to Control RNA Loading and Ligand Display on Extracellular Vesicles for Cancer Regression. *Nat Nanotechnol* **2018**, *13*, 82, doi:10.1038/S41565-017-0012-Z.
241. Smyth, T.; Petrova, K.; Payton, N.M.; Persaud, I.; Redzic, J.S.; Graner, M.W.; Smith-Jones, P.; Anchordoquy, T.J. Surface Functionalization of Exosomes Using Click. *Bioconjug Chem* **2014**, *25*, 1777, doi:10.1021/BC500291R.
242. Lee, J.; Lee, H.; Goh, U.; Kim, J.; Jeong, M.; Lee, J.; Park, J.H. Cellular Engineering with Membrane Fusogenic Liposomes to Produce Functionalized Extracellular Vesicles. *ACS Appl Mater Interfaces* **2016**, *8*, 6790–6795, doi:10.1021/acsami.6b01315.
243. Qi, H.; Liu, C.; Long, L.; Ren, Y.; Zhang, S.; Chang, X.; Qian, X.; Jia, H.; Zhao, J.; Sun, J.; et al. Blood Exosomes Endowed with Magnetic and Targeting Properties for Cancer Therapy. *ACS Nano* **2016**, *10*, 3323–3333, doi:10.1021/ACSNANO.5B06939.
244. Nakase, I.; Futaki, S. Combined Treatment with a PH-Sensitive Fusogenic Peptide and Cationic Lipids Achieves Enhanced Cytosolic Delivery of Exosomes. *Scientific Reports 2015 5:1* **2015**, *5*, 1–13, doi:10.1038/srep10112.
245. Li, L.; He, D.; Guo, Q.; Zhang, Z.; Ru, D.; Wang, L.; Gong, K.; Liu, F.; Duan, Y.; Li, H. Exosome-Liposome Hybrid Nanoparticle Codelivery of TP and MiR497 Conspicuously

Overcomes Chemoresistant Ovarian Cancer. *J Nanobiotechnology* **2022**, *20*, doi:10.1186/S12951-022-01264-5.

246. Piffoux, M.; Silva, A.K.A.; Wilhelm, C.; Gazeau, F.; Tareste, D. Modification of Extracellular Vesicles by Fusion with Liposomes for the Design of Personalized Biogenic Drug Delivery Systems. *ACS Nano* **2018**, *12*, 6830–6842, doi:10.1021/acsnano.8b02053.
247. Lin, Y.; Wu, J.; Gu, W.; Huang, Y.; Tong, Z.; Huang, L.; Tan, J. Exosome-Liposome Hybrid Nanoparticles Deliver CRISPR/Cas9 System in MSCs. *Adv Sci (Weinh)* **2018**, *5*, doi:10.1002/ADVS.201700611.
248. Jhan, Y.Y.; Prasca-Chamorro, D.; Palou Zuniga, G.; Moore, D.M.; Arun Kumar, S.; Gaharwar, A.K.; Bishop, C.J. Engineered Extracellular Vesicles with Synthetic Lipids via Membrane Fusion to Establish Efficient Gene Delivery. *Int J Pharm* **2020**, *573*, doi:10.1016/J.IJPHARM.2019.118802.
249. Zhang, K.L.; Wang, Y.J.; Sun, J.; Zhou, J.; Xing, C.; Huang, G.; Li, J.; Yang, H. Artificial Chimeric Exosomes for Anti-Phagocytosis and Targeted Cancer Therapy. *Chem Sci* **2019**, *10*, 1555, doi:10.1039/C8SC03224F.
250. Munagala, R.; Aqil, F.; Jeyabalan, J.; Kandimalla, R.; Wallen, M.; Tyagi, N.; Wilcher, S.; Yan, J.; Schultz, D.J.; Spencer, W.; et al. Exosome-Mediated Delivery of RNA and DNA for Gene Therapy. *Cancer Lett* **2021**, *505*, 58–72, doi:10.1016/J.CANLET.2021.02.011.
251. Pittenger, M.F.; Mackay, A.M.; Beck, S.C.; Jaiswal, R.K.; Douglas, R.; Mosca, J.D.; Moorman, M.A.; Simonetti, D.W.; Craig, S.; Marshak, D.R. Multilineage Potential of Adult Human Mesenchymal Stem Cells. *Science* **1999**, *284*, 143–147.
252. Crisan, M.; Yap, S.; Casteilla, L.; Chen, C.-W.; Corselli, M.; Park, T.S.; Andriolo, G.; Sun, B.; Zheng, B.; Zhang, L.; et al. A Perivascular Origin for Mesenchymal Stem Cells in Multiple Human Organs. *Cell Stem Cell* **2008**, *3*, 301–313, doi:10.1016/j.stem.2008.07.003.
253. Caplan, A.I.; Correa, D. The MSC: An Injury Drugstore. *Cell Stem Cell* 2011, *9*, 11–15.
254. Friedenstein, A.F.; Chailakhjan, R.H.; Lalykina, K.S. The Development of Fibroblast Colonies in Marrow and Spleen Cells Monolayer Cultures of Guinea-Pig Bone. *Development* **1970**, *38*, 1–6, doi:10.2466/pr0.102.3.855-860.
255. Yu. F. Gorskaya, A.Ya.F.; Kulagina, and N.N. Precursor Cells of Fibroblasts Detected by in Vitro Cloning of Cells from Hematopoietic Organs of Normal and Irradiated Mice. *Bull Exp Biol Med* **1976**, *81*, 195–198.
256. Murray, I.R.; West, C.C.; Hardy, W.R.; James, A.W.; Park, T.S.; Nguyen, A.; Tawonsawatruk, T.; Lazzari, L.; Soo, C.; Péault, B. Natural History of Mesenchymal Stem Cells, from Vessel Walls to Culture Vessels. *Cellular and Molecular Life Sciences* **2014**, *71*, 1353–1374, doi:10.1007/s00018-013-1462-6.
257. Hass, R.; Kasper, C.; Böhm, S.; Jacobs, R. Different Populations and Sources of Human Mesenchymal Stem Cells (MSC): A Comparison of Adult and Neonatal Tissue-Derived MSC. *Cell Communication and Signaling* **2011**, *9*, 1–14, doi:10.1186/1478-811X-9-12.

258. Tsvetkova, A. v.; Vakhrushev, I. v.; Basok, Y.B.; Grigor'ev, A.M.; Kirsanova, L.A.; Lupatov, A.Y.; Sevastianov, V.I.; Yarygin, K.N. Chondrogeneic Potential of MSC from Different Sources in Spheroid Culture. *Bull Exp Biol Med* **2021**, *170*, 528–536, doi:10.1007/s10517-021-05101-x.

259. Dominici, M.; Le Blanc, K.; Mueller, I.; Slaper-Cortenbach, I.; Marini, F.C.; Krause, D.S.; Deans, R.J.; Keating, A.; Prockop, D.J.; Horwitz, E.M. Minimal Criteria for Defining Multipotent Mesenchymal Stromal Cells. The International Society for Cellular Therapy Position Statement. *Cytotherapy* **2006**, *8*, 315–317, doi:10.1080/14653240600855905.

260. Viswanathan, S.; Shi, Y.; Galipeau, J.; Krampera, M.; Leblanc, K.; Martin, I.; Nolta, J.; Phinney, D.G.; Sensebe, L. Mesenchymal Stem versus Stromal Cells: International Society for Cell & Gene Therapy (ISCT®) Mesenchymal Stromal Cell Committee Position Statement on Nomenclature. *Cytotherapy* **2019**, *21*, 1019–1024, doi:10.1016/j.jcyt.2019.08.002.

261. Meirelles, L. da S.; Fontes, A.M.; Covas, D.T.; Caplan, A.I. Mechanisms Involved in the Therapeutic Properties of Mesenchymal Stem Cells. *Cytokine Growth Factor Rev* **2009**, *20*, 419–427, doi:10.1016/j.cytogfr.2009.10.002.

262. Zachar, L.; Bačenková, D.; Rosocha, J. Activation, Homing, and Role of the Mesenchymal Stem Cells in the Inflammatory Environment. *J Inflamm Res* **2016**, *9*, 231–240, doi:10.2147/JIR.S121994.

263. Gao, F.; Chiu, S.M.; Motan, D.A.L.; Zhang, Z.; Chen, L.; Ji, H.-L.; Tse, H.-F.; Fu, Q.-L.; Lian, Q. Mesenchymal Stem Cells and Immunomodulation: Current Status and Future Prospects. *Cell Death Dis* **2016**, *7*, e2062, doi:10.1038/cddis.2015.327.

264. Hiwatashi, N.; Bing, R.; Kraja, I.; Branski, R.C. Mesenchymal Stem Cells Have Anti-Fibrotic Effects on Transforming Growth Factor-B1-Stimulated Vocal Fold Fibroblasts. *Laryngoscope* **2017**, *127*, 35–41, doi:10.1002/cncr.27633.Percutaneous.

265. Ulpiano, C.; da Silva, C.L.; Monteiro, G.A. Mesenchymal Stromal Cells (MSCs): A Promising Tool for Cell-Based Angiogenic Therapy. *Curr Gene Ther* **2021**, *21*, 382–405, doi:10.2174/1566523221666210917114353.

266. Hou, J.; Peng, X.; Wang, J.; Zhang, H.; Xia, J.; Ge, Q.; Wang, X.; Chen, X.; Wu, X. Mesenchymal Stem Cells Promote Endothelial Progenitor Cell Proliferation by Secreting Insulin-like Growth Factor-1. *Mol Med Rep* **2017**, *16*, 1502–1508, doi:10.3892/mmr.2017.6741.

267. Bao, X.; Feng, M.; Wei, J.; Han, Q.; Zhao, H.; Li, G.; Zhu, Z.; Xing, H.; An, Y.; Qin, C.; et al. Transplantation of Flk-1+ Human Bone Marrow-Derived Mesenchymal Stem Cells Promotes Angiogenesis and Neurogenesis after Cerebral Ischemia in Rats. *European Journal of Neuroscience* **2011**, *34*, 87–98, doi:10.1111/j.1460-9568.2011.07733.x.

268. Guillamat-Prats, R. The Role of MSC in Wound Healing, Scarring and Regeneration. *Cells* **2021**, *10*, doi:10.3390/cells10071729.

269. Li, M.; Chen, H.; Zhu, M. Mesenchymal Stem Cells for Regenerative Medicine in Central Nervous System. *Front Neurosci* **2022**, *16*, 2147, doi:10.3389/FNINS.2022.1068114/BIBTEX.
270. Lazarus, H.M.; Haynesworth, S.E.; Gerson, S.L.; Rosenthal, N.S.; Caplan, A.I. Ex Vivo Expansion and Subsequent Infusion of Human Bone Marrow-Derived Stromal Progenitor Cells (Mesenchymal Progenitor Cells): Implications for Therapeutic Use - PubMed. *Bone Marrow Transplant* **1995**, *16*, 557–564.
271. Maldonado, V. V.; Patel, N.H.; Smith, E.E.; Barnes, C.L.; Gustafson, M.P.; Rao, R.R.; Samsonraj, R.M. Clinical Utility of Mesenchymal Stem/Stromal Cells in Regenerative Medicine and Cellular Therapy. *J Biol Eng* 2023, *17*.
272. Levy, O.; Kuai, R.; Siren, E.M.J.; Bhere, D.; Milton, Y.; Nissar, N.; de Biasio, M.; Heinelt, M.; Reeve, B.; Abdi, R.; et al. Shattering Barriers toward Clinically Meaningful MSC Therapies. *Sci Adv* **2020**, *6*, doi:10.1126/sciadv.aba6884.
273. Alofisel | European Medicines Agency Available online: https://www.ema.europa.eu/en/medicines/human/EPAR/alofisel (accessed on 12 February 2023).
274. Sarvar, D.P.; Shamsasenjan, K.; Akbarzadehlaleh, P. Mesenchymal Stem Cell-Derived Exosomes: New Opportunity in Cell-Free Therapy. *Adv Pharm Bull* **2016**, *6*, 293–299, doi:10.15171/apb.2016.041.
275. Baek, G.; Choi, H.; Kim, Y.; Lee, H.C.; Choi, C. Mesenchymal Stem Cell-Derived Extracellular Vesicles as Therapeutics and as a Drug Delivery Platform. *Stem Cells Transl Med* **2019**, *8*, 880–886, doi:10.1002/SCTM.18-0226.
276. Doeppner, T.R.; Herz, J.; Görgens, A.; Schlechter, J.; Ludwig, A.-K.; Radtke, S.; de Miroschedji, K.; Horn, P.A.; Giebel, B.; Hermann, D.M. Extracellular Vesicles Improve Post-Stroke Neuroregeneration and Prevent Postischemic Immunosuppression. *Stem Cells Transl Med* **2015**, *4*, 1131–1143, doi:10.5966/SCTM.2015-0078/-/DC1.
277. Jeong, J.O.; Han, J.W.; Kim, J.M.; Cho, H.J.; Park, C.; Lee, N.; Kim, D.W.; Yoon, Y.S. Malignant Tumor Formation after Transplantation of Short-Term Cultured Bone Marrow Mesenchymal Stem Cells in Experimental Myocardial Infarction and Diabetic Neuropathy. *Circ Res* **2011**, *108*, 1340–1347, doi:10.1161/CIRCRESAHA.110.239848.
278. Wang, S.; Guo, L.; Ge, J.; Yu, L.; Cai, T.; Tian, R.; Jiang, Y.; Zhao, R.C.H.; Wu, Y. Excess Integrins Cause Lung Entrapment of Mesenchymal Stem Cells. *Stem Cells* **2015**, *33*, 3315–3326, doi:10.1002/STEM.2087.
279. Bahr, M.M.; Amer, M.S.; Abo-El-Sooud, K.; Abdallah, A.N.; El-Tookhy, O.S. Preservation Techniques of Stem Cells Extracellular Vesicles: A Gate for Manufacturing of Clinical Grade Therapeutic Extracellular Vesicles and Long-Term Clinical Trials. *Int J Vet Sci Med* 2020, *8*, 1–8.
280. Kou, M.; Huang, L.; Yang, J.; Chiang, Z.; Chen, S.; Liu, J.; Guo, L.; Zhang, X.; Zhou, X.; Xu, X.; et al. Mesenchymal Stem Cell-Derived Extracellular Vesicles for

Immunomodulation and Regeneration: A next Generation Therapeutic Tool? *Cell Death & Disease 2022 13:7* **2022**, *13*, 1–16, doi:10.1038/s41419-022-05034-x.

281. Cosenza, S.; Ruiz, M.; Toupet, K.; Jorgensen, C.; Noël, D. Mesenchymal Stem Cells Derived Exosomes and Microparticles Protect Cartilage and Bone from Degradation in Osteoarthritis. *Sci Rep* **2017**, *7*, doi:10.1038/S41598-017-15376-8.
282. Cheng, S.; Xi, Z.; Chen, G.; Liu, K.; Ma, R.; Zhou, C. Extracellular Vesicle-Carried MicroRNA-27b Derived from Mesenchymal Stem Cells Accelerates Cutaneous Wound Healing via E3 Ubiquitin Ligase ITCH. *J Cell Mol Med* **2020**, *24*, 11254–11271, doi:10.1111/JCMM.15692.
283. Han, T.; Song, P.; Wu, Z.; Xiang, X.; Liu, Y.; Wang, Y.; Fang, H.; Niu, Y.; Shen, C. MSC Secreted Extracellular Vesicles Carrying TGF-Beta Upregulate Smad 6 Expression and Promote the Regrowth of Neurons in Spinal Cord Injured Rats. *Stem Cell Rev Rep* **2022**, *18*, 1078–1096, doi:10.1007/S12015-021-10219-6.
284. Yeo, R.W.Y.; Lai, R.C.; Zhang, B.; Tan, S.S.; Yin, Y.; Teh, B.J.; Lim, S.K. Mesenchymal Stem Cell: An Efficient Mass Producer of Exosomes for Drug Delivery. *Adv Drug Deliv Rev* **2013**, *65*, 336–341, doi:10.1016/J.ADDR.2012.07.001.
285. Lang, F.M.; Hossain, A.; Gumin, J.; Momin, E.N.; Shimizu, Y.; Ledbetter, D.; Shahar, T.; Yamashita, S.; Parker Kerrigan, B.; Fueyo, J.; et al. Mesenchymal Stem Cells as Natural Biofactories for Exosomes Carrying MiR-124a in the Treatment of Gliomas. *Neuro Oncol* **2018**, *20*, 380, doi:10.1093/NEUONC/NOX152.
286. O'Brien, K.P.; Khan, S.; Gilligan, K.E.; Zafar, H.; Lalor, P.; Glynn, C.; O'Flatharta, C.; Ingoldsby, H.; Dockery, P.; de Bhulbh, A.; et al. Employing Mesenchymal Stem Cells to Support Tumor-Targeted Delivery of Extracellular Vesicle (EV)-Encapsulated MicroRNA-379. *Oncogene* **2018**, *37*, 2137–2149, doi:10.1038/S41388-017-0116-9.
287. Xu, Y.; Shen, L.; Li, F.; Yang, J.; Wan, X.; Ouyang, M. MicroRNA-16-5p-Containing Exosomes Derived from Bone Marrow-Derived Mesenchymal Stem Cells Inhibit Proliferation, Migration, and Invasion, While Promoting Apoptosis of Colorectal Cancer Cells by Downregulating ITGA2. *J Cell Physiol* **2019**, *234*, 21380–21394, doi:10.1002/JCP.28747.
288. Li, P.; Xin, H.; Lu, L. Extracellular Vesicle-Encapsulated MicroRNA-424 Exerts Inhibitory Function in Ovarian Cancer by Targeting MYB. *J Transl Med* **2021**, *19*, 1–17, doi:10.1186/s12967-020-02652-x.
289. Lou, G.; Yang, Y.; Liu, F.; Ye, B.; Chen, Z.; Zheng, M.; Liu, Y. MiR-122 Modification Enhances the Therapeutic Efficacy of Adipose Tissue-derived Mesenchymal Stem Cells against Liver Fibrosis. *J Cell Mol Med* **2017**, *21*, 2963, doi:10.1111/JCMM.13208.
290. Tao, S.-C.; Guo, S.-C.; Li, M.; Ke, Q.-F.; Guo, Y.-P.; Zhang, C.-Q. Chitosan Wound Dressings Incorporating Exosomes Derived from MicroRNA-126-Overexpressing Synovium Mesenchymal Stem Cells Provide Sustained Release of Exosomes and Heal Full-Thickness Skin Defects in a Diabetic Rat Model. *Stem Cells Transl Med* **2017**, *6*, 736–747, doi:10.5966/SCTM.2016-0275.

291. Xin, H.; Liu, Z.; Buller, B.; Li, Y.; Golembieski, W.; Gan, X.; Wang, F.; Lu, M.; Ali, M.M.; Zhang, Z.G.; et al. MiR-17-92 Enriched Exosomes Derived from Multipotent Mesenchymal Stromal Cells Enhance Axon-Myelin Remodeling and Motor Electrophysiological Recovery after Stroke. *Journal of Cerebral Blood Flow & Metabolism* **2021**, *41*, 1131, doi:10.1177/0271678X20950489.
292. Wang, B.; Yao, K.; Huuskes, B.M.; Shen, H.H.; Zhuang, J.; Godson, C.; Brennan, E.P.; Wilkinson-Berka, J.L.; Wise, A.F.; Ricardo, S.D. Mesenchymal Stem Cells Deliver Exogenous MicroRNA-Let7c via Exosomes to Attenuate Renal Fibrosis. *Mol Ther* **2016**, *24*, 1290–1301, doi:10.1038/MT.2016.90.
293. Altanerova, U.; Jakubechova, J.; Benejova, K.; Priscakova, P.; Pesta, M.; Pitule, P.; Topolcan, O.; Kausitz, J.; Zduriencikova, M.; Repiska, V.; et al. Prodrug Suicide Gene Therapy for Cancer Targeted Intracellular by Mesenchymal Stem Cell Exosomes. *Int J Cancer* **2019**, *144*, 897–908, doi:10.1002/IJC.31792.
294. Geng, W.; Tang, H.; Luo, S.; Lv, Y.; Liang, D.; Kang, X.; Hong, W. Exosomes from MiRNA-126-Modified ADSCs Promotes Functional Recovery after Stroke in Rats by Improving Neurogenesis and Suppressing Microglia Activation. *Am J Transl Res* **2019**, *11*, 780.
295. Li, D.; Zhang, P.; Yao, X.; Li, H.; Shen, H.; Li, X.; Wu, J.; Lu, X. Exosomes Derived From MiR-133b-Modified Mesenchymal Stem Cells Promote Recovery After Spinal Cord Injury. *Front Neurosci* **2018**, *12*, doi:10.3389/FNINS.2018.00845.
296. Chen, Z.; Wang, H.; Xia, Y.; Yan, F.; Lu, Y. Therapeutic Potential of Mesenchymal Cell–Derived MiRNA-150-5p–Expressing Exosomes in Rheumatoid Arthritis Mediated by the Modulation of MMP14 and VEGF. *The Journal of Immunology* **2018**, *201*, 2472–2482, doi:10.4049/jimmunol.1800304.
297. Wang, Z.; Yan, K.; Ge, G.; Zhang, D.; Bai, J.; Guo, X.; Zhou, J.; Xu, T.; Xu, M.; Long, X.; et al. Exosomes Derived from MiR-155-5p-Overexpressing Synovial Mesenchymal Stem Cells Prevent Osteoarthritis via Enhancing Proliferation and Migration, Attenuating Apoptosis, and Modulating Extracellular Matrix Secretion in Chondrocytes. *Cell Biol Toxicol* **2021**, *37*, 85–96, doi:10.1007/S10565-020-09559-9.
298. Li, X.; Liu, L.; Yang, J.; Yu, Y.; Chai, J.; Wang, L.; Ma, L.; Yin, H. Exosome Derived From Human Umbilical Cord Mesenchymal Stem Cell Mediates MiR-181c Attenuating Burn-Induced Excessive Inflammation. *EBioMedicine* **2016**, *8*, 72, doi:10.1016/J.EBIOM.2016.04.030.
299. Sheng, Y.; Zhou, X.; Wang, J.; Shen, H.; Wu, S.; Guo, W.; Yang, Y. MSC Derived EV Loaded with MiRNA-22 Inhibits the Inflammatory Response and Nerve Function Recovery after Spinal Cord Injury in Rats. *J Cell Mol Med* **2021**, *25*, 10268–10278, doi:10.1111/JCMM.16965.
300. Chen, Y.; Tian, Z.; He, L.; Liu, C.; Wang, N.; Rong, L.; Liu, B. Exosomes Derived from MiR-26a-Modified MSCs Promote Axonal Regeneration via the PTEN/AKT/MTOR Pathway Following Spinal Cord Injury. *Stem Cell Res Ther* **2021**, *12*, doi:10.1186/S13287-021-02282-0.

301. Jahangard, Y.; Monfared, H.; Moradi, A.; Zare, M.; Mirnajafi-Zadeh, J.; Mowla, S.J. Therapeutic Effects of Transplanted Exosomes Containing MiR-29b to a Rat Model of Alzheimer's Disease. *Front Neurosci* **2020**, *14*, 564, doi:10.3389/FNINS.2020.00564/BIBTEX.
302. Mao, G.; Zhang, Z.; Hu, S.; Zhang, Z.; Chang, Z.; Huang, Z.; Liao, W.; Kang, Y. Exosomes Derived from MiR-92a-3p-Overexpressing Human Mesenchymal Stem Cells Enhance Chondrogenesis and Suppress Cartilage Degradation via Targeting WNT5A. *Stem Cell Res Ther* **2018**, *9*, doi:10.1186/S13287-018-1004-0.
303. Yang, J.; Zhang, X.; Chen, X.; Wang, L.; Yang, G. Exosome Mediated Delivery of MiR-124 Promotes Neurogenesis after Ischemia. *Mol Ther Nucleic Acids* **2017**, *7*, 278–287, doi:10.1016/j.omtn.2017.04.010.
304. Ma, T.; Chen, Y.; Chen, Y.; Meng, Q.; Sun, J.; Shao, L.; Yu, Y.; Huang, H.; Hu, Y.; Yang, Z.; et al. MicroRNA-132, Delivered by Mesenchymal Stem Cell-Derived Exosomes, Promote Angiogenesis in Myocardial Infarction. *Stem Cells Int* **2018**, *2018*, doi:10.1155/2018/3290372.
305. Jing, L.; Hua, X.; Yuanna, D.; Rukun, Z.; Junjun, M. Exosomal MiR-499a-5p Inhibits Endometrial Cancer Growth and Metastasis via Targeting VAV3. *Cancer Manag Res* **2020**, *12*, 13541–13552, doi:10.2147/CMAR.S283747.
306. Wang, Y.; Ding, N.; Guan, G.; Liu, G.; Huo, D.; Li, Y.; Wei, K.; Yang, J.; Cheng, P.; Zhu, C. Rapid Delivery of Hsa-MiR-590-3p Using Targeted Exosomes to Treat Acute Myocardial Infarction Through Regulation of the Cell Cycle. *J Biomed Nanotechnol* **2018**, *14*, 968–977, doi:10.1166/JBN.2018.2493.
307. Huang, W.; Qu, M.; Li, L.; Liu, T.; Lin, M.; Yu, X. SiRNA in MSC-Derived Exosomes Silences CTGF Gene for Locomotor Recovery in Spinal Cord Injury Rats. *Stem Cell Res Ther* **2021**, *12*, 1–14, doi:10.1186/s13287-021-02401-x.
308. Zhou, W.; Zhou, Y.; Chen, X.; Ning, T.; Chen, H.; Guo, Q.; Zhang, Y.; Liu, P.; Zhang, Y.; Li, C.; et al. Pancreatic Cancer-Targeting Exosomes for Enhancing Immunotherapy and Reprogramming Tumor Microenvironment. *Biomaterials* **2021**, *268*, 120546, doi:10.1016/J.BIOMATERIALS.2020.120546.
309. Mendt, M.; Kamerkar, S.; Sugimoto, H.; McAndrews, K.M.; Wu, C.-C.; Gagea, M.; Yang, S.; Blanko, E.V.R.; Peng, Q.; Ma, X.; et al. Generation and Testing of Clinical-Grade Exosomes for Pancreatic Cancer. *JCI Insight* **2018**, *3*, doi:10.1172/jci.insight.99263.
310. Greco, K.A.; Franzen, C.A.; Foreman, K.E.; Flanigan, R.C.; Kuo, P.C.; Gupta, G.N. PLK-1 Silencing in Bladder Cancer by SiRNA Delivered With Exosomes. *Urology* **2016**, *91*, 241.e1-241.e7, doi:10.1016/J.UROLOGY.2016.01.028.
311. Cui, Y.; Guo, Y.; Kong, L.; Shi, J.; Liu, P.; Li, R.; Geng, Y.; Gao, W.; Zhang, Z.; Fu, D. A Bone-Targeted Engineered Exosome Platform Delivering SiRNA to Treat Osteoporosis. *Bioact Mater* **2022**, *10*, 207–221, doi:10.1016/J.BIOACTMAT.2021.09.015.
312. Zhang, H.; Wu, J.; Wu, J.; Fan, Q.; Zhou, J.; Wu, J.; Liu, S.; Zang, J.; Ye, J.; Xiao, M.; et al. Exosome-Mediated Targeted Delivery of MiR-210 for Angiogenic Therapy after

Cerebral Ischemia in Mice. *J Nanobiotechnology* **2019**, *17*, 1–13, doi:10.1186/s12951-019-0461-7.

313. Guo, S.; Perets, N.; Betzer, O.; Ben-Shaul, S.; Sheinin, A.; Michaelevski, I.; Popovtzer, R.; Offen, D.; Levenberg, S. Intranasal Delivery of Mesenchymal Stem Cell Derived Exosomes Loaded with Phosphatase and Tensin Homolog SiRNA Repairs Complete Spinal Cord Injury. *ACS Nano* **2019**, *13*, 10015–10028, doi:10.1021/ACSNANO.9B01892.
314. Wang, G.; Yuan, J.; Cai, X.; Xu, Z.; Wang, J.; Ocansey, D.K.W.; Yan, Y.; Qian, H.; Zhang, X.; Xu, W.; et al. HucMSC-exosomes Carrying MiR-326 Inhibit Neddylation to Relieve Inflammatory Bowel Disease in Mice. *Clin Transl Med* **2020**, *10*, doi:10.1002/CTM2.113.
315. Ma, J.; Zhao, Y.; Sun, L.; Sun, X.; Zhao, X.; Sun, X.; Qian, H.; Xu, W.; Zhu, W. Exosomes Derived from Akt-Modified Human Umbilical Cord Mesenchymal Stem Cells Improve Cardiac Regeneration and Promote Angiogenesis via Activating Platelet-Derived Growth Factor D. *Stem Cells Transl Med* **2017**, *6*, 51, doi:10.5966/SCTM.2016-0038.
316. Liu, J.; Yan, Z.; Yang, F.; Huang, Y.; Yu, Y.; Zhou, L.; Sun, Z.; Cui, D.; Yan, Y. Exosomes Derived from Human Umbilical Cord Mesenchymal Stem Cells Accelerate Cutaneous Wound Healing by Enhancing Angiogenesis through Delivering Angiopoietin-2. *Stem Cell Rev Rep* **2021**, *17*, 305–317, doi:10.1007/s12015-020-09992-7.
317. Huang, B.; Su, Y.; Shen, E.; Song, M.; Liu, D.; Qi, H. Extracellular Vesicles from GPNMB-Modified Bone Marrow Mesenchymal Stem Cells Attenuate Bone Loss in an Ovariectomized Rat Model. *Life Sci* **2021**, *272*, 119208, doi:10.1016/J.LFS.2021.119208.
318. Huang, X.; Ding, J.; Li, Y.; Liu, W.; Ji, J.; Wang, H.; Wang, X. Exosomes Derived from PEDF Modified Adipose-Derived Mesenchymal Stem Cells Ameliorate Cerebral Ischemia-Reperfusion Injury by Regulation of Autophagy and Apoptosis. *Exp Cell Res* **2018**, *371*, 269–277, doi:10.1016/J.YEXCR.2018.08.021.
319. Li, X.; Wang, Y.; Shi, L.; Li, B.; Li, J.; Wei, Z.; Lv, H.; Wu, L.; Zhang, H.; Yang, B.; et al. Magnetic Targeting Enhances the Cutaneous Wound Healing Effects of Human Mesenchymal Stem Cell-Derived Iron Oxide Exosomes. *J Nanobiotechnology* **2020**, *18*, 113, doi:10.1186/S12951-020-00670-X.
320. Melzer, C.; Rehn, V.; Yang, Y.; Bähre, H.; von der Ohe, J.; Hass, R. Taxol-Loaded MSC-Derived Exosomes Provide a Therapeutic Vehicle to Target Metastatic Breast Cancer and Other Carcinoma Cells. *Cancers 2019, Vol. 11, Page 798* **2019**, *11*, 798, doi:10.3390/CANCERS11060798.
321. Altanerova, U.; Babincova, M.; Babinec, P.; Benejova, K.; Jakubechova, J.; Altanerova, V.; Zduriencikova, M.; Repiska, V.; Altaner, C. Human Mesenchymal Stem Cell-Derived Iron Oxide Exosomes Allow Targeted Ablation of Tumor Cells via Magnetic Hyperthermia. *Int J Nanomedicine* **2017**, *12*, 7923, doi:10.2147/IJN.S145096.
322. Wei, H.; Chen, J.; Wang, S.; Fu, F.; Zhu, X.; Wu, C.; Liu, Z.; Zhong, G.; Lin, J. A Nanodrug Consisting Of Doxorubicin And Exosome Derived From Mesenchymal Stem Cells For Osteosarcoma Treatment In Vitro. *Int J Nanomedicine* **2019**, *14*, 8603, doi:10.2147/IJN.S218988.

323. Bagheri, E.; Abnous, K.; Farzad, S.A.; Taghdisi, S.M.; Ramezani, M.; Alibolandi, M. Targeted Doxorubicin-Loaded Mesenchymal Stem Cells-Derived Exosomes as a Versatile Platform for Fighting against Colorectal Cancer. *Life Sci* **2020**, *261*, 118369, doi:10.1016/J.LFS.2020.118369.

324. Liang, L.; Zhao, L.; Wang, Y.; Wang, Y. Treatment for Hepatocellular Carcinoma Is Enhanced When Norcantharidin Is Encapsulated in Exosomes Derived from Bone Marrow Mesenchymal Stem Cells. *Mol Pharm* **2021**, *18*, 1003–1013, doi:10.1021/ACS.MOLPHARMACEUT.0C00976.

325. Zhou, Y.; Zhou, W.; Chen, X.; Wang, Q.; Li, C.; Chen, Q.; Zhang, Y.; Lu, Y.; Ding, X.; Jiang, C. Bone Marrow Mesenchymal Stem Cells-Derived Exosomes for Penetrating and Targeted Chemotherapy of Pancreatic Cancer. *Acta Pharm Sin B* **2020**, *10*, 1563–1575, doi:10.1016/J.APSB.2019.11.013.

326. Kalimuthu, S.; Gangadaran, P.; Rajendran, R.L.; Zhu, L.; Oh, J.M.; Lee, H.W.; Gopal, A.; Baek, S.H.; Jeong, S.Y.; Lee, S.W.; et al. A New Approach for Loading Anticancer Drugs into Mesenchymal Stem Cell-Derived Exosome Mimetics for Cancer Therapy. *Front Pharmacol* **2018**, *9*, 1116, doi:10.3389/FPHAR.2018.01116/BIBTEX.

327. Singh, A.; Raghav, A.; Shiekh, P.A.; Kumar, A. Transplantation of Engineered Exosomes Derived from Bone Marrow Mesenchymal Stromal Cells Ameliorate Diabetic Peripheral Neuropathy under Electrical Stimulation. *Bioact Mater* **2021**, *6*, 2231–2249, doi:10.1016/J.BIOACTMAT.2021.01.008.

328. Tian, T.; Zhang, H.X.; He, C.P.; Fan, S.; Zhu, Y.L.; Qi, C.; Huang, N.P.; Xiao, Z.D.; Lu, Z.H.; Tannous, B.A.; et al. Surface Functionalized Exosomes as Targeted Drug Delivery Vehicles for Cerebral Ischemia Therapy. *Biomaterials* **2018**, *150*, 137–149, doi:10.1016/J.BIOMATERIALS.2017.10.012.

329. Rajendran, R.L.; Paudel, S.; Gangadaran, P.; Oh, J.M.; Oh, E.J.; Hong, C.M.; Lee, S.; Chung, H.Y.; Lee, J.; Ahn, B.C. Extracellular Vesicles Act as Nano-Transporters of Tyrosine Kinase Inhibitors to Revert Iodine Avidity in Thyroid Cancer. *Pharmaceutics* **2021**, *13*, 1–17, doi:10.3390/PHARMACEUTICS13020248.

330. Gomari, H.; Moghadam, M.F.; Soleimani, M. Targeted Cancer Therapy Using Engineered Exosome as a Natural Drug Delivery Vehicle. *Onco Targets Ther* **2018**, *11*, 5753–5762, doi:10.2147/OTT.S173110.

331. Chulpanova, D.S.; Gilazieva, Z.E.; Kletukhina, S.K.; Aimaletdinov, A.M.; Garanina, E.E.; James, V.; Rizvanov, A.A.; Solovyeva, V. v. Cytochalasin B-Induced Membrane Vesicles from Human Mesenchymal Stem Cells Overexpressing IL2 Are Able to Stimulate CD8+ T-Killers to Kill Human Triple Negative Breast Cancer Cells. *Biology 2021, Vol. 10, Page 141* **2021**, *10*, 141, doi:10.3390/BIOLOGY10020141.

332. Conceição, M.; Forcina, L.; Wiklander, O.P.B.; Gupta, D.; Nordin, J.Z.; Vrellaku, B.; McClorey, G.; Mäger, I.; Görgens, A.; Lundin, P.; et al. Engineered Extracellular Vesicle Decoy Receptor-Mediated Modulation of the IL6 Trans-Signalling Pathway in Muscle. *Biomaterials* **2021**, *266*, doi:10.1016/J.BIOMATERIALS.2020.120435.

333. Wang, X.; Chen, Y.; Zhao, Z.; Meng, Q.; Yu, Y.; Sun, J.; Yang, Z.; Chen, Y.; Li, J.; Ma, T.; et al. Engineered Exosomes with Ischemic Myocardium-Targeting Peptide for Targeted Therapy in Myocardial Infarction. *J Am Heart Assoc* **2018**, *7*, doi:10.1161/JAHA.118.008737.
334. Xu, F.; Fei, Z.; Dai, H.; Xu, J.; Fan, Q.; Shen, S.; Zhang, Y.; Ma, Q.; Chu, J.; Peng, F.; et al. Mesenchymal Stem Cell-Derived Extracellular Vesicles with High PD-L1 Expression for Autoimmune Diseases Treatment. *Advanced Materials* **2022**, *34*, doi:10.1002/ADMA.202106265.
335. Zhuang, M.; Chen, X.; Du, D.; Shi, J.; Deng, M.; Long, Q.; Yin, X.; Wang, Y.; Rao, L. SPION Decorated Exosome Delivery of TNF-α to Cancer Cell Membranes through Magnetism. *Nanoscale* **2019**, *12*, 173–188, doi:10.1039/C9NR05865F.
336. Yuan, Z.Q.; Kolluri, K.K.; Gowers, K.H.C.; Janes, S.M. TRAIL Delivery by MSC-Derived Extracellular Vesicles Is an Effective Anticancer Therapy. *J Extracell Vesicles* **2017**, *6*, doi:10.1080/20013078.2017.1265291.
337. Luo, Z.W.; Li, F.X.Z.; Liu, Y.W.; Rao, S.S.; Yin, H.; Huang, J.; Chen, C.Y.; Hu, Y.; Zhang, Y.; Tan, Y.J.; et al. Aptamer-Functionalized Exosomes from Bone Marrow Stromal Cells Target Bone to Promote Bone Regeneration. *Nanoscale* **2019**, *11*, 20884–20892, doi:10.1039/C9NR02791B.
338. Gangadaran, P.; Gunassekaran, G.R.; Rajendran, R.L.; Oh, J.M.; Vadevoo, S.M.P.; Lee, H.W.; Hong, C.M.; Lee, B.; Lee, J.; Ahn, B.C. Interleukin-4 Receptor Targeting Peptide Decorated Extracellular Vesicles as a Platform for In Vivo Drug Delivery to Thyroid Cancer. *Biomedicines* **2022**, *10*, 1978, doi:10.3390/BIOMEDICINES10081978/S1.
339. Hosseini Shamili, F.; Alibolandi, M.; Rafatpanah, H.; Abnous, K.; Mahmoudi, M.; Kalantari, M.; Taghdisi, S.M.; Ramezani, M. Immunomodulatory Properties of MSC-Derived Exosomes Armed with High Affinity Aptamer toward Mylein as a Platform for Reducing Multiple Sclerosis Clinical Score. *Journal of Controlled Release* **2019**, *299*, 149–164, doi:10.1016/J.JCONREL.2019.02.032.
340. Cui, G.H.; Guo, H.D.; Li, H.; Zhai, Y.; Gong, Z. bin; Wu, J.; Liu, J.S.; Dong, Y.R.; Hou, S.X.; Liu, J.R. RVG-Modified Exosomes Derived from Mesenchymal Stem Cells Rescue Memory Deficits by Regulating Inflammatory Responses in a Mouse Model of Alzheimer's Disease. *Immun Ageing* **2019**, *16*, doi:10.1186/S12979-019-0150-2.
341. Feng, K.; Xie, X.; Yuan, J.; Gong, L.; Zhu, Z.; Zhang, J.; Li, H.; Yang, Y.; Wang, Y. Reversing the Surface Charge of MSC-derived Small Extracellular Vesicles by EPL-PEG-DSPE for Enhanced Osteoarthritis Treatment. *J Extracell Vesicles* **2021**, *10*, doi:10.1002/JEV2.12160.
342. Lee, J.R.; Kyung, J.W.; Kumar, H.; Kwon, S.P.; Song, S.Y.; Han, I.B.; Kim, B.S. Targeted Delivery of Mesenchymal Stem Cell-Derived Nanovesicles for Spinal Cord Injury Treatment. *Int J Mol Sci* **2020**, *21*, 1–20, doi:10.3390/ijms21114185.
343. Zhang, N.; Song, Y.; Huang, Z.; Chen, J.; Tan, H.; Yang, H.; Fan, M.; Li, Q.; Wang, Q.; Gao, J.; et al. Monocyte Mimics Improve Mesenchymal Stem Cell-Derived Extracellular

Vesicle Homing in a Mouse MI/RI Model. *Biomaterials* **2020**, *255*, 120168, doi:10.1016/J.BIOMATERIALS.2020.120168.

344. Hu, S.; Wang, X.; Li, Z.; Zhu, D.; Cores, J.; Wang, Z.; Li, J.; Mei, X.; Cheng, X.; Su, T.; et al. Platelet Membrane and Stem Cell Exosome Hybrids Enhance Cellular Uptake and Targeting to Heart Injury. *Nano Today* **2021**, *39*, 101210, doi:10.1016/J.NANTOD.2021.101210.
345. Snajdauf, M.; Havlova, K.; Vachtenheim, J.; Ozaniak, A.; Lischke, R.; Bartunkova, J.; Smrz, D.; Strizova, Z. The TRAIL in the Treatment of Human Cancer: An Update on Clinical Trials. *Front Mol Biosci* **2021**, *8*, 87, doi:10.3389/FMOLB.2021.628332/BIBTEX.
346. Li, Z.; Zhao, P.; Zhang, Y.; Wang, J.; Wang, C.; Liu, Y.; Yang, G.; Yuan, L. Exosome-Based Ldlr Gene Therapy for Familial Hypercholesterolemia in a Mouse Model. *Theranostics* **2021**, *11*, 2953, doi:10.7150/THNO.49874.
347. Fuzeta, M. de A.; Gonçalves, P.P.; Fernandes-Platzgummer, A.; Cabral, J.M.S.; Bernardes, N.; Silva, C.L. da From Promise to Reality: Bioengineering Strategies to Enhance the Therapeutic Potential of Extracellular Vesicles. *Bioengineering 2022, Vol. 9, Page 675* **2022**, *9*, 675, doi:10.3390/BIOENGINEERING9110675.
348. Johnson, J.; Shojaee, M.; Mitchell Crow, J.; Khanabdali, R. From Mesenchymal Stromal Cells to Engineered Extracellular Vesicles: A New Therapeutic Paradigm. *Front Cell Dev Biol* **2021**, *9*, doi:10.3389/fcell.2021.705676.
349. Tan, T.T.; Lai, R.C.; Padmanabhan, J.; Sim, W.K.; Choo, A.B.H.; Lim, S.K. Assessment of Tumorigenic Potential in Mesenchymal-Stem/Stromal-Cell-Derived Small Extracellular Vesicles (MSC-SEV). *Pharmaceuticals* **2021**, *14*, doi:10.3390/PH14040345.
350. Yang, Z.; Shi, J.; Xie, J.; Wang, Y.; Sun, J.; Liu, T.; Zhao, Y.; Zhao, X.; Wang, X.; Ma, Y.; et al. Large-Scale Generation of Functional MRNA-Encapsulating Exosomes via Cellular Nanoporation. *Nat Biomed Eng* **2020**, *4*, 69, doi:10.1038/S41551-019-0485-1.
351. Karagiannis, T.C.; El-Osta, A. RNA Interference and Potential Therapeutic Applications of Short Interfering RNAs. *Cancer Gene Ther* **2005**, *12*, 787–795, doi:10.1038/sj.cgt.7700857.
352. Thomas, C.E.; Ehrhardt, A.; Kay, M.A. Progress and Problems with the Use of Viral Vectors for Gene Therapy. *Nat Rev Genet* **2003**, *4*, 346–358, doi:10.1038/nrg1066.
353. Alves, C.P.A.; Šimčíková, M.; Brito, L.; Monteiro, G.A.; Prazeres, D.M.F. Development of a Nicking Endonuclease-Assisted Method for the Purification of Minicircles. *J Chromatogr A* **2016**, *1443*, 136–144, doi:10.1016/j.chroma.2016.03.035.
354. Brito, L. *Minicircle Production and Delivery to Human Mesenchymal Stem/Stromal Cells for Angiogenesis Stimulation*; Lisboa, 2014;
355. Bofill-De Ros, X.; Gu, S. Guidelines for the Optimal Design of MiRNA-Based ShRNAs. *Methods* **2016**, *103*, 157–166, doi:10.1016/j.ymeth.2016.04.003.
356. Moore, C.B.; Guthrie, E.H.; Huang, M.T.; Taxman, D.J. Short Hairpin RNA (ShRNA): Design, Delivery, and Assessment of Gene Knockdown. *Methods Mol Biol* **2013**, 1–15, doi:10.1007/978-1-60761-657-3.

357. Brummelkamp, T.R. A System for Stable Expression of Short Interfering RNAs in Mammalian Cells. *Science (1979)* **2002**, *296*, 550–553, doi:10.1126/science.1068999.
358. Park, J.H.; Hong, S.W.; Yun, S.; Lee, D.; Shin, C. Effect of SiRNA with an Asymmetric RNA/DTdT Overhang on RNA Interference Activity. *Nucleic Acid Ther* **2014**, *24*, 364–371, doi:10.1089/nat.2014.0494.
359. Zuo, L.; Fan, Y.; Wang, F.; Gu, Q.; Xu, X. A SiRNA Targeting Vascular Endothelial Growth Factor-A Inhibiting Experimental Corneal Neovascularization. *Curr Eye Res* **2010**, *35*, 375–384, doi:10.3109/02713681003597230.
360. Feng, W.; Li, H.M.; Wang, H.P.; Ma, J.L.; Chen, X.F.; Wei, F.; Yi, M.Y.; Huang, Q. SiRNA-Mediated Knockdown of VEGF-A, VEGF-C and VEGFR-3 Suppresses the Growth and Metastasis of Mouse Bladder Carcinoma in Vivo. *Exp Ther Med* **2010**, *1*, 899–904, doi:10.3892/etm.2010.113.
361. Eswarappa, S.M.; Potdar, A.A.; Koch, W.J.; Fan, Y.; Vasu, K.; Lindner, D.; Willard, B.; Graham, L.M.; Dicorleto, P.E.; Fox, P.L. Programmed Translational Readthrough Generates Antiangiogenic VEGF-Ax. *Cell* **2014**, *157*, 1605–1618, doi:10.1016/j.cell.2014.04.033.
362. Wang, F.-Q.; Barfield, E.; Dutta, S.; Pua, T.; Fishman, D.A. VEGFR-2 Silencing by Small Interference RNA (SiRNA) Suppresses LPA-Induced Epithelial Ovarian Cancer (EOC) Invasion. *Gynecol Oncol* **2009**, *115*, 414–423, doi:10.1016/j.ygyno.2009.08.019.
363. Matsushima, S.; Shimizu, A.; Kondo, M.; Asano, H.; Ueno, N.; Nakayama, H.; Sato, N.; Komeno, M.; Ogita, H.; Kurokawa-Seo, M. Anosmin-1 Activates Vascular Endothelial Growth Factor Receptor and Its Related Signaling Pathway for Olfactory Bulb Angiogenesis. *Scientific Reports 2020 10:1* **2020**, *10*, 1–15, doi:10.1038/s41598-019-57040-3.
364. Jin, C.; Ding, P.; Wang, Y.; Ma, D. Regulation of EGF Receptor Signaling by the MARVEL Domain-Containing Protein CKLFSF8. *FEBS Lett* **2005**, *579*, 6375–6382, doi:10.1016/j.febslet.2005.10.021.
365. Chan, C.H.; Li, C.F.; Yang, W.L.; Gao, Y.; Lee, S.W.; Feng, Z.; Huang, H.Y.; Tsai, K.K.C.; Flores, L.G.; Shao, Y.; et al. The Skp2-SCF E3 Ligase Regulates Akt Ubiquitination, Glycolysis, Herceptin Sensitivity, and Tumorigenesis. *Cell* **2012**, *149*, 1098–1111, doi:10.1016/j.cell.2012.02.065.
366. Michaela Simcikova Development of a Process for the Production and Purification of Minicircles for Biopharmaceutical Applications., Instituto Superior Técnico, Universidade de Lisboa, 2013.
367. Silva-Santos, A.R.; Alves, C.P.A.; Monteiro, G.; Azevedo, A.M.; Prazeres, D.M.F. Multimodal Chromatography of Supercoiled Minicircles: A Closer Look into DNA-Ligand Interactions. *Sep Purif Technol* **2019**, *212*, 161–170, doi:10.1016/j.seppur.2018.11.015.
368. Madeira, C.; Ribeiro, S.C.; Pinheiro, I.S.M.; Martins, S.A.M.; Andrade, P.Z.; da Silva, C.L.; Cabral, J.M.S. Gene Delivery to Human Bone Marrow Mesenchymal Stem Cells by Microporation. *J Biotechnol* **2011**, *151*, 130–136, doi:10.1016/j.jbiotec.2010.11.002.

369. Serra, J.; Alves, C.P.A.; Brito, L.; Monteiro, G.A.; Cabral, J.M.S.; Prazeres, D.M.F.; da Silva, C.L. Engineering of Human Mesenchymal Stem/Stromal Cells (MSC) with VEGF-Encoding Minicircles for Angiogenic Gene Therapy. *Hum Gene Ther* **2018**, *30*, 316–329, doi:10.1089/hum.2018.154.
370. Silva, M.; Monteiro, G.A.; Fialho, A.M.; Bernardes, N.; da Silva, C.L. Conditioned Medium From Azurin-Expressing Human Mesenchymal Stromal Cells Demonstrates Antitumor Activity Against Breast and Lung Cancer Cell Lines. *Front Cell Dev Biol* **2020**, *8*, 471, doi:10.3389/FCELL.2020.00471/BIBTEX.
371. Livak, K.J.; Schmittgen, T.D. Analysis of Relative Gene Expression Data Using Real-Time Quantitative PCR and the 2−ΔΔCT Method. *Methods* **2001**, *25*, 402–408, doi:10.1006/METH.2001.1262.
372. Haimes, J.; Kelley, M. Demonstration of a ΔΔCq Calculation Method to Compute Relative Gene Expression from QPCR Data. *Dharmacon Tecn Note* **2015**.
373. Adair, T.H.; Montani, J.-P. Angiogenesis Assays. In *Angiogenesis*; Morgan & Claypool Life Sciences: San Rafael (CA), 2010.
374. Carpentier, G.; Berndt, S.; Ferratge, S.; Rasband, W.; Cuendet, M.; Uzan, G.; Albanese, P. Angiogenesis Analyzer for ImageJ — A Comparative Morphometric Analysis of "Endothelial Tube Formation Assay" and "Fibrin Bead Assay." *Scientific Reports 2020 10:1* **2020**, *10*, 1–13, doi:10.1038/s41598-020-67289-8.
375. Lee, H.; Kang, K.T. Advanced Tube Formation Assay Using Human Endothelial Colony Forming Cells for in Vitro Evaluation of Angiogenesis. *Korean J Physiol Pharmacol* **2018**, *22*, 705, doi:10.4196/KJPP.2018.22.6.705.
376. Simcikova, M.; Prather, K.L.J.; Prazeres, D.M.F.; Monteiro, G.A. On the Dual Effect of Glucose during Production of PBAD/AraC-Based Minicircles. *Vaccine* **2014**, *32*, 2843–2846, doi:10.1016/j.vaccine.2014.02.035.
377. Folsom, J.P.; Parker, A.E.; Carlson, R.P. Physiological and Proteomic Analysis of Escherichia Coli Iron-Limited Chemostat Growth. *J Bacteriol* **2014**, *196*, 2748–2761, doi:10.1128/JB.01606-14.
378. Cai-juan, L.; Su-fen, G.; Tie-mei, S. Culture Supernatants of Breast Cancer Cell Line MDA-MB-231 Treated with Parthenolide Inhibit the Proliferation, Migration, and Lumen Formation Capacity of Human Umbilical Vein Endothelial Cells. *Chin Med J (Engl)* **2012**, *125*, 2195–2199, doi:10.3760/cma.j.issn.0366-6999.2012.12.020.
379. Imoukhuede, P.I.; Popel, A.S. Quantification and Cell-to-Cell Variation of Vascular Endothelial Growth Factor Receptors. *Exp Cell Res* **2011**, *317*, 955–965, doi:10.1016/J.YEXCR.2010.12.014.
380. Serra, J.; Alves, C.P.A.; Cabral, J.M.S.; Monteiro, G.A.; da Silva, C.L.; Prazeres, D.M.F. Minicircle-Based Expression of Vascular Endothelial Growth Factor in Mesenchymal Stromal Cells from Diverse Human Tissues. *Journal of Gene Medicine* **2021**, *23*, doi:10.1002/jgm.3342.

381. Darquet, A.M.; Cameron, B.; Wils, P.; Scherman, D.; Crouzet, J. A New DNA Vehicle for Nonviral Gene Delivery: Supercoiled Minicircle. *Gene Ther* **1997**, *4*, 1341–1349, doi:10.1038/sj.gt.3300540.
382. Bigger, B.W.; Tolmachov, O.; Collombet, J.M.; Fragkos, M.; Palaszewski, I.; Coutelle, C. An AraC-Controlled Bacterialcre Expression System to Produce DNA Minicircle Vectors for Nuclear and Mitochondrial Gene Therapy. *Journal of Biological Chemistry* **2001**, *276*, 23018–23027, doi:10.1074/JBC.M010873200.
383. Nehlsen, K.; Broll, S.; Bode, J.; Article Kristina Nehlsen, R. Replicating Minicircles: Generation of Nonviral Episomes for the Efficient Modification of Dividing Cells. *Gene Ther Mol Biol* **2006**, *10*, 233–244.
384. Chen, Z.-Y.; He, C.-Y.; Ehrhardt, A.; Kay, M.A. Minicircle DNA Vectors Devoid of Bacterial DNA Result in Persistent and High-Level Transgene Expression in Vivo. *Molecular Therapy* **2003**, *8*, doi:10.1016/S1525-0016(03)00168-0.
385. Jechlinger, W.; Tabrizi, C.A.; Lubitz, W.; Mayrhofer, P. Minicircle DNA Immobilized in Bacterial Ghosts: In Vivo Production of Safe Non-Viral DNA Delivery Vehicles. *J Mol Microbiol Biotechnol* **2004**, *8*, 222–231, doi:10.1159/000086703.
386. Alves, C.P.A.; Prazeres, D.M.F.; Monteiro, G.A. Minicircle Biopharmaceuticals–An Overview of Purification Strategies. *Frontiers in Chemical Engineering* **2021**, *2*, 612594, doi:10.3389/FCENG.2020.612594/BIBTEX.
387. Kay, M.A.; He, C.Y.; Chen, Z.Y. A Robust System for Production of Minicircle DNA Vectors. *Nat Biotechnol* **2010**, *28*, 1287–1289, doi:10.1038/nbt.1708.
388. Sousa, F.; Prazeres, D.M.F.; Queiroz, J.A. Improvement of Transfection Efficiency by Using Supercoiled Plasmid DNA Purified with Arginine Affinity Chromatography. *J Gene Med* **2009**, *11*, 79–88, doi:10.1002/JGM.1272.
389. Dhanoya, A.; Chain, B.M.; Keshavarz-Moore, E. The Impact of DNA Topology on Polyplex Uptake and Transfection Efficiency in Mammalian Cells. *J Biotechnol* **2011**, *155*, 377–386, doi:10.1016/J.JBIOTEC.2011.07.023.
390. Kreiss, P.; Cameron, B.; Darquet, A.M.; Scherman, D.; Crouzet, J. Production of a New DNA Vehicle for Gene Transfer Using Site-Specific Recombination. *Applied Microbiology and Biotechnology* **1998**, *49*.
391. Bigger, B.W.; Tolmachov, O.; Collombet, J.M.; Fragkos, M.; Palaszewski, I.; Coutelle, C. An AraC-Controlled Bacterialcre Expression System to Produce DNA Minicircle Vectors for Nuclear and Mitochondrial Gene Therapy. *Journal of Biological Chemistry* **2001**, *276*, 23018–23027, doi:10.1074/JBC.M010873200.
392. Chen, Z.Y.; He, C.Y.; Ehrhardt, A.; Kay, M.A. Minicircle DNA Vectors Devoid of Bacterial DNA Result in Persistent and High-Level Transgene Expression in Vivo. *Molecular Therapy* **2003**, *8*, 495–500, doi:10.1016/S1525-0016(03)00168-0.
393. Kay, M.A.; He, C.Y.; Chen, Z.Y. A Simple And Rapid Minicircle DNA Vector Manufacturing System. *Nat Biotechnol* **2010**, *28*, 1287, doi:10.1038/NBT.1708.

394. Escoffre, J.M.; Debin, A.; Reynes, J.P.; Drocourt, D.; Tiraby, G.; Hellaudais, L.; Teissie, J.; Golzio, M. Long-Lasting in Vivo Gene Silencing by Electrotransfer of ShRNA Expressing Plasmid. *Technol Cancer Res Treat* **2008**, *7*, 109–116, doi:10.1177/153303460800700203.

395. Stimac, M.; Dolinsek, T.; Lampreht, U.; Cemazar, M.; Sersa, G. Gene Electrotransfer of Plasmid with Tissue Specific Promoter Encoding ShRNA against Endoglin Exerts Antitumor Efficacy against Murine TS/A Tumors by Vascular Targeted Effects. *PLoS One* **2015**, *10*, e0124913, doi:10.1371/JOURNAL.PONE.0124913.

396. Kim, H.A.; Nam, K.; Kim, S.W. Tumor Targeting RGD Conjugated Bio-Reducible Polymer for VEGF SiRNA Expressing Plasmid Delivery. *Biomaterials* **2014**, *35*, 7543–7552, doi:10.1016/J.BIOMATERIALS.2014.05.021.

397. Hunt, M.A.; Currie, M.J.; Robinson, B.A.; Dachs, G.U. Optimizing Transfection of Primary Human Umbilical Vein Endothelial Cells Using Commercially Available Chemical Transfection Reagents. *Journal of Biomolecular Techniques* **2010**, *21*, 66–72.

398. Lee, H.; Kang, K.T. Differential Angiogenic Responses of Human Endothelial Colony-Forming Cells to Different Molecular Subtypes of Breast Cancer Cells. *J Lipid Atheroscler* **2021**, *10*.

399. Yoo, J.Y.; Kim, J.-H.; Kwon, Y.-G.; Kim, E.-C.; Kim, N.K.; Choi, H.J.; Yun, C.-O. VEGF-Specific Short Hairpin RNA-Expressing Oncolytic Adenovirus Elicits Potent Inhibition of Angiogenesis and Tumor Growth. *Molecular Therapy* **2007**, *15*, 295–302, doi:10.1038/sj.mt.6300023.

400. Yadav, U.C.S.; Srivastava, S.K.; Ramana, K. V. Prevention of VEGF-Induced Growth and Tube Formation in Human Retinal Endothelial Cell by Aldose Reductase Inhibition. *J Diabetes Complications* **2012**, *26*, 369, doi:10.1016/J.JDIACOMP.2012.04.017.

401. Yang, W.J.; Yang, Y.N.; Cao, J.; Man, Z.H.; Li, Y.; Xing, Y.Q. Paxillin Regulates Vascular Endothelial Growth Factor A-Induced in Vitro Angiogenesis of Human Umbilical Vein Endothelial Cells. *Mol Med Rep* **2015**, *11*, 1784, doi:10.3892/MMR.2014.2961.

402. Phinney, D.G.; Pittenger, M.F. Concise Review: MSC-Derived Exosomes for Cell-Free Therapy. *Stem Cells* **2017**, *35*, 851–858, doi:10.1002/stem.2575.

403. Gatti, S.; Bruno, S.; Deregibus, M.C.; Sordi, A.; Cantaluppi, V.; Tetta, C.; Camussi, G. Microvesicles Derived from Human Adult Mesenchymal Stem Cells Protect against Ischaemia-Reperfusion-Induced Acute and Chronic Kidney Injury. *Nephrology Dialysis Transplantation* **2011**, *26*, 1474–1483, doi:10.1093/ndt/gfr015.

404. Viswanathan, S.; Ciccocioppo, R.; Galipeau, J.; Krampera, M.; Le Blanc, K.; Martin, I.; Moniz, K.; Nolta, J.; Phinney, D.G.; Shi, Y.; et al. Consensus International Council for Commonality in Blood Banking Automation–International Society for Cell & Gene Therapy Statement on Standard Nomenclature Abbreviations for the Tissue of Origin of Mesenchymal Stromal Cells. *Cytotherapy* **2021**, *23*, 1060–1063, doi:10.1016/J.JCYT.2021.04.009.

405. Ridzuan, N.; Zakaria, N.; Widera, D.; Sheard, J.; Morimoto, M.; Kiyokawa, H.; Azmel, S.; Isa, M.; Kaur, G.; Singh, C.; et al. Human Umbilical Cord Mesenchymal Stem Cell-Derived Extracellular Vesicles Ameliorate Airway Inflammation in a Rat Model of Chronic Obstructive Pulmonary Disease (COPD). *Stem Cell Res Ther* **2021**, *12*, doi:10.1186/s13287-020-02088-6.

406. Doeppner, T.R.; Herz, J.; Görgens, A.; Schlechter, J.; Ludwig, A.-K.; Radtke, S.; de Miroschedji, K.; Horn, P.A.; Giebel, B.; Hermann, D.M. Extracellular Vesicles Improve Post-Stroke Neuroregeneration and Prevent Postischemic Immunosuppression. *Stem Cells Transl Med* **2015**, *4*, 1131–1143, doi:10.5966/sctm.2015-0078.

407. Mendt, M.; Kamerkar, S.; Sugimoto, H.; McAndrews, K.M.; Wu, C.C.; Gagea, M.; Yang, S.; Blanko, E.V.R.; Peng, Q.; Ma, X.; et al. Generation and Testing of Clinical-Grade Exosomes for Pancreatic Cancer. *JCI Insight* **2018**, *3*, doi:10.1172/jci.insight.99263.

408. Silva, R.M.; Rosa, S.S.; Cunha, R.; L. da Silva, C.; Azevedo, A.M.; Fernandes-Platzgummer, A. Anion Exchange Chromatography-Based Platform for the Scalable Purification of Extracellular Vesicles Derived from Human Mesenchymal Stromal Cells. *Sep Purif Technol* **2023**, *310*, doi:10.1016/j.seppur.2023.123238.

409. de Soure, A.M.; Fernandes-Platzgummer, A.; Moreira, F.; Lilaia, C.; Liu, S.H.; Ku, C.P.; Huang, Y.F.; Milligan, W.; Cabral, J.M.S.; da Silva, C.L. Integrated Culture Platform Based on a Human Platelet Lysate Supplement for the Isolation and Scalable Manufacturing of Umbilical Cord Matrix-Derived Mesenchymal Stem/Stromal Cells. *J Tissue Eng Regen Med* **2017**, *11*, 1630–1640, doi:10.1002/TERM.2200.

410. Santos, F. Dos; Andrade, P.Z.; Abecasis, M.M.; Gimble, J.M.; Chase, L.G.; Campbell, A.M.; Boucher, S.; Vemuri, M.C.; Silva, C.L. Da; Cabral, J.M.S. Toward a Clinical-Grade Expansion of Mesenchymal Stem Cells from Human Sources: A Microcarrier-Based Culture System under Xeno-Free Conditions. *Tissue Eng Part C Methods* **2011**, *17*, 1201–1210, doi:10.1089/ten.tec.2011.0255.

411. van Balkom, B.W.M.; Gremmels, H.; Giebel, B.; Lim, S.K. Proteomic Signature of Mesenchymal Stromal Cell-Derived Small Extracellular Vesicles. *Proteomics* **2019**, *19*, 1800163, doi:10.1002/PMIC.201800163.

412. Théry, C.; Witwer, K.W.; Aikawa, E.; Alcaraz, M.J.; Anderson, J.D.; Andriantsitohaina, R.; Antoniou, A.; Arab, T.; Archer, F.; Atkin-Smith, G.K.; et al. Minimal Information for Studies of Extracellular Vesicles 2018 (MISEV2018): A Position Statement of the International Society for Extracellular Vesicles and Update of the MISEV2014 Guidelines. *J Extracell Vesicles* **2018**, *7*, doi:10.1080/20013078.2018.1535750.

413. Chuo, S.T.Y.; Chien, J.C.Y.; Lai, C.P.K. Imaging Extracellular Vesicles: Current and Emerging Methods. *J Biomed Sci* **2018**, *25*, doi:10.1186/S12929-018-0494-5.

414. Schop, D.; Janssen, F.W.; Van Rijn, L.D.S.; Fernandes, H.; Bloem, R.M.; De Bruijn, J.D.; Van Dijkhuizen-Radersma, R. Growth, Metabolism, and Growth Inhibitors of Mesenchymal Stem Cells. *Tissue Eng Part A* **2009**, *15*, 1877–1886, doi:10.1089/TEN.TEA.2008.0345.

415. Dos Santos, F.; Campbell, A.; Fernandes-Platzgummer, A.; Andrade, P.Z.; Gimble, J.M.; Wen, Y.; Boucher, S.; Vemuri, M.C.; Da Silva, C.L.; Cabral, J.M.S. A Xenogeneic-Free Bioreactor System for the Clinical-Scale Expansion of Human Mesenchymal Stem/Stromal Cells. *Biotechnol Bioeng* **2014**, *111*, 1116–1127, doi:10.1002/bit.25187.

416. Andriolo, G.; Provasi, E.; Lo Cicero, V.; Brambilla, A.; Soncin, S.; Torre, T.; Milano, G.; Biemmi, V.; Vassalli, G.; Turchetto, L.; et al. Exosomes from Human Cardiac Progenitor Cells for Therapeutic Applications: Development of a GMP-Grade Manufacturing Method. *Front Physiol* **2018**, *9*, doi:10.3389/FPHYS.2018.01169/FULL.

417. Kim, M.; Yun, H.-W.; Do, •; Park, Y.; Byung, •; Choi, H.; Min, B.-H. Three-Dimensional Spheroid Culture Increases Exosome Secretion from Mesenchymal Stem Cells. *Tissue Eng Regen Med* **2018**, *15*, doi:10.1007/s13770-018-0139-5.

418. Mizukami, A.; Fernandes-Platzgummer, A.; Carmelo, J.G.; Swiech, K.; Covas, D.T.; Cabral, J.M.S.; da Silva, C.L. Stirred Tank Bioreactor Culture Combined with Serum-/Xenogeneic-Free Culture Medium Enables an Efficient Expansion of Umbilical Cord-Derived Mesenchymal Stem/Stromal Cells. *Biotechnol J* **2016**, *11*, 1048–1059, doi:10.1002/biot.201500532.

419. Cunha, B.; Aguiar, T.; Silva, M.M.; Silva, R.J.S.; Sousa, M.F.Q.; Pineda, E.; Peixoto, C.; Carrondo, M.J.T.; Serra, M.; Alves, P.M. Exploring Continuous and Integrated Strategies for the Up- and Downstream Processing of Human Mesenchymal Stem Cells. *J Biotechnol* **2015**, *213*, 97–108, doi:10.1016/J.JBIOTEC.2015.02.023.

420. Heathman, T.R.J.; Nienow, A.W.; Rafiq, Q.A.; Coopman, K.; Kara, B.; Hewitt, C.J. Agitation and Aeration of Stirred-Bioreactors for the Microcarrier Culture of Human Mesenchymal Stem Cells and Potential Implications for Large-Scale Bioprocess Development. *Biochem Eng J* **2018**, *136*, 9–17, doi:10.1016/j.bej.2018.04.011.

421. Kuan-liang Chen, A.; Kong Chew, Y.; Tan, H.Y.; Reuveny, S.; Kah Weng, S.O. Increasing Efficiency of Human Mesenchymal Stromal Cell Culture by Optimization of Microcarrier Concentration and Design of Medium Feed. *Cytotherapy* **2015**, *17*, doi:10.1016/j.jcyt.2014.08.011.

422. Mastrogiacomo, M.; Brini, A.T.; Visai, L.; De Girolamo, L.; Swiech, K. Successful Use of Human AB Serum to Support the Expansion of Adipose Tissue-Derived Mesenchymal Stem/Stromal Cell in a Microcarrier-Based Platform. *Front. Bioeng. Biotechnol.* **2020**, *8*, doi:10.3389/fbioe.2020.00307.

423. Tozetti, P.A.; Caruso, S.R.; Mizukami, A.; Fernandes, T.R.; da Silva, F.B.; Traina, F.; Covas, D.T.; Orellana, M.D.; Swiech, K. Expansion Strategies for Human Mesenchymal Stromal Cells Culture under Xeno-Free Conditions. *Biotechnol Prog* **2017**, *33*, 1358–1367, doi:10.1002/BTPR.2494.

424. Bieback, K.; Fernandez-Muñoz, B.; Pati, S.; Schäfer, R. Gaps in the Knowledge of Human Platelet Lysate as a Cell Culture Supplement for Cell Therapy: A Joint Publication from the AABB and the International Society for Cell & Gene Therapy. *Cytotherapy* **2019**, *21*, 911–924, doi:10.1016/j.jcyt.2019.06.006.

425. Sion, C.; Loubière, C.; Wlodarczyk-Biegun, M.K.; Davoudi, N.; Müller-Renno, C.; Guedon, E.; Chevalot, I.; Olmos, E. Effects of Microcarriers Addition and Mixing on WJ-MSC Culture in Bioreactors. *Biochem Eng J* **2020**, *157*, doi:10.1016/j.bej.2020.107521.
426. de Soure, A.M.; Fernandes-Platzgummer, A.; Moreira, F.; Lilaia, C.; Liu, S.-H.; Ku, C.-P.; Huang, Y.-F.; Milligan, W.; Cabral, J.M.S.; da Silva, C.L. Integrated Culture Platform Based on a Human Platelet Lysate Supplement for the Isolation and Scalable Manufacturing of Umbilical Cord Matrix-Derived Mesenchymal Stem/Stromal Cells. *J Tissue Eng Regen Med* **2017**, *11*, 1630–1640, doi:10.1002/term.2200.
427. Petry, F.; Smith, J.R.; Leber, J.; Salzig, D.; Czermak, P.; Weiss, M.L. Manufacturing of Human Umbilical Cord Mesenchymal Stromal Cells on Microcarriers in a Dynamic System for Clinical Use. *Stem Cells Int* **2016**, doi:10.1155/2016/4834616.
428. Ferrari, C.; Balandras, F.; Guedon, E.; Olmos, E.; Chevalot, I.; Marc, A. Limiting Cell Aggregation during Mesenchymal Stem Cell Expansion on Microcarriers. *Biotechnol Prog* **2012**, *28*, 780–787, doi:10.1002/btpr.1527.
429. Chen, S.; Sato, Y.; Tada, Y.; Suzuki, Y.; Takahashi, R.; Okanojo, M.; Nakashima, K. Facile Bead-to-Bead Cell-Transfer Method for Serial Subculture and Large-Scale Expansion of Human Mesenchymal Stem Cells in Bioreactors. *Stem Cells Transl Med* **2021**, *10*, 1329–1342, doi:10.1002/sctm.20-0501.
430. Schnitzler, A.C.; Verma, A.; Kehoe, D.E.; Jing, D.; Murrell, J.R.; Der, K.A.; Aysola, M.; Rapiejko, P.J.; Punreddy, S.; Rook, M.S. Bioprocessing of Human Mesenchymal Stem/Stromal Cells for Therapeutic Use: Current Technologies and Challenges. *Biochem Eng J* **2016**, *108*, 3–13, doi:10.1016/J.BEJ.2015.08.014.
431. Jossen, V.; Schirmer, C.; Mostafa Sindi, D.; Eibl, R.; Kraume, M.; Pörtner, R.; Eibl, D. Theoretical and Practical Issues That Are Relevant When Scaling Up HMSC Microcarrier Production Processes. *Stem Cells Int* **2016**, *2016*, doi:10.1155/2016/4760414.
432. Zhu, J.; Lu, K.; Zhang, N.; Zhao, Y.; Ma, Q.; Shen, J.; Lin, Y.; Xiang, P.; Tang, Y.; Hu, X.; et al. Myocardial Reparative Functions of Exosomes from Mesenchymal Stem Cells Are Enhanced by Hypoxia Treatment of the Cells via Transferring MicroRNA-210 in an NSMase2-Dependent Way. *Artif Cells Nanomed Biotechnol* **2018**, *46*, 1659–1670, doi:10.1080/21691401.2017.1388249.
433. Wright, A.; Snyder, O.; He, H.; Christenson, L.K.; Fleming, S.; Weiss, M.L. Procoagulant Activity of Umbilical Cord-Derived Mesenchymal Stromal Cells' Extracellular Vesicles (MSC-EVs). *Int J Mol Sci* **2023**, *24*, 9216, doi:10.3390/IJMS24119216/S1.
434. Görgens, A.; Corso, G.; Hagey, D.W.; Jawad Wiklander, R.; Gustafsson, M.O.; Felldin, U.; Lee, Y.; Bostancioglu, R.B.; Sork, H.; Liang, X.; et al. Identification of Storage Conditions Stabilizing Extracellular Vesicles Preparations. *J Extracell Vesicles* **2022**, *11*, doi:10.1002/JEV2.12238.
435. Yáñez-Mó, M.; Siljander, P.R.M.; Andreu, Z.; Zavec, A.B.; Borràs, F.E.; Buzas, E.I.; Buzas, K.; Casal, E.; Cappello, F.; Carvalho, J.; et al. Biological Properties of Extracellular

Vesicles and Their Physiological Functions. *J Extracell Vesicles* **2015**, *4*, 1–60, doi:10.3402/JEV.V4.27066.

436. Yu, D.; Mei, Y.; Wang, L.; Zhao, Y.; Fan, X.; Liang, D.; Li, L.; Zhu, J.; Bi, S.; Wang, X.; et al. Nano-Seq Analysis Reveals Different Functional Tendency between Exosomes and Microvesicles Derived from HUMSC. *Stem Cell Res Ther* **2023**, *14*, doi:10.1186/s13287-023-03491-5.
437. Wang, Z. gang; He, Z. yi; Liang, S.; Yang, Q.; Cheng, P.; Chen, A. min Comprehensive Proteomic Analysis of Exosomes Derived from Human Bone Marrow, Adipose Tissue, and Umbilical Cord Mesenchymal Stem Cells. *Stem Cell Res Ther* **2020**, *11*, doi:10.1186/s13287-020-02032-8.
438. Nguyen, V.V.T.; Witwer, K.W.; Verhaar, M.C.; Strunk, D.; Bas, □; Van Balkom, W.M.; Van Balkom, B.W.M. Functional Assays to Assess the Therapeutic Potential of Extracellular Vesicles. **2020**, doi:10.1002/jev2.12033.
439. Bucar, S.; Branco, A.D. de M.; Mata, M.F.; Milhano, J.C.; Caramalho, Í.; Cabral, J.M.S.; Fernandes-Platzgummer, A.; da Silva, C.L. Influence of the Mesenchymal Stromal Cell Source on the Hematopoietic Supportive Capacity of Umbilical Cord Blood-Derived CD34+-Enriched Cells. *Stem Cell Res Ther* **2021**, *12*, 1–16, doi:10.1186/S13287-021-02474-8/FIGURES/6.
440. Budgude, P.; Kale, V.; Vaidya, A. Cryopreservation of Mesenchymal Stromal Cell-Derived Extracellular Vesicles Using Trehalose Maintains Their Ability to Expand Hematopoietic Stem Cells in Vitro. *Cryobiology* **2021**, *98*, 152–163, doi:10.1016/J.CRYOBIOL.2020.11.009.
441. Blazquez, R.; Miguel Sanchez-Margallo, F.; de la Rosa, O.; Dalemans, W.; Álvarez, V.; Tarazona, R.; Casado, J.G.; Maria Merino, A. Immunomodulatory Potential of Human Adipose Mesenchymal Stem Cells Derived Exosomes on in Vitro Stimulated T Cells. *Front Immunol* **2014**, *5*, doi:10.3389/fimmu.2014.00556.
442. Guo, L.; Lai, P.; Wang, Y.; Huang, T.; Chen, X.; Geng, S.; Huang, X.; Luo, C.; Wu, S.; Ling, W.; et al. Extracellular Vesicles Derived from Mesenchymal Stem Cells Prevent Skin Fibrosis in the CGVHD Mouse Model by Suppressing the Activation of Macrophages and B Cells Immune Response. *Int Immunopharmacol* **2020**, *84*, 106541, doi:10.1016/J.INTIMP.2020.106541.
443. Pinto, D.S.; Ahsan, T.; Serra, J.; Fernandes-Platzgummer, A.; Cabral, J.M.S.; Silva, C.L. Modulation of the in Vitro Angiogenic Potential of Human Mesenchymal Stromal Cells from Different Tissue Sources. *J Cell Physiol* **2020**, *235*, 7224–7238, doi:10.1002/jcp.29622.
444. Arabi, F.; Mansouri, V.; Ahmadbeigi, N. Gene Therapy Clinical Trials, Where Do We Go? An Overview. *Biomedicine & Pharmacotherapy* **2022**, *153*, 113324, doi:10.1016/J.BIOPHA.2022.113324.
445. Ibraheem, D.; Elaissari, A.; Fessi, H. Gene Therapy and DNA Delivery Systems. *Int J Pharm* **2014**, *459*, 70–83, doi:10.1016/J.IJPHARM.2013.11.041.

446. Sharma, S.; Parveen, R.; Biswa, ·; Chatterji, P. Toxicology of Nanoparticles in Drug Delivery. *Curr Pathobiol Rep* **2021**, *3*, 133–144, doi:10.1007/s40139-021-00227-z.

447. Evers, M.J.W.; Van De Wakker, S.I.; De Groot, E.M.; De Jong, O.G.; Gitz-François, J.J.J.; Seinen, C.S.; Sluijter, J.P.G.; Schiffelers, R.M.; Vader, P. Functional SiRNA Delivery by Extracellular Vesicle-Liposome Hybrid Nanoparticles. *Adv Healthc Mater* **2021**, *11*, doi:10.1002/adhm.202101202.

448. Kao, C.Y.; Papoutsakis, E.T. Engineering Human Megakaryocytic Microparticles for Targeted Delivery of Nucleic Acids to Hematopoietic Stem and Progenitor Cells. *Sci Adv* **2018**, *4*, doi:10.1126/SCIADV.AAU6762.

449. Pomatto, M.A.C.; Bussolati, B.; D'Antico, S.; Ghiotto, S.; Tetta, C.; Brizzi, M.F.; Camussi, G. Improved Loading of Plasma-Derived Extracellular Vesicles to Encapsulate Antitumor MiRNAs. *Mol Ther Methods Clin Dev* **2019**, *13*, 133–144, doi:10.1016/j.omtm.2019.01.001.

450. Zhang, D.; Lee, H.; Zhu, Z.; Minhas, J.K.; Jin, Y. Enrichment of Selective MiRNAs in Exosomes and Delivery of Exosomal MiRNAs in Vitro and in Vivo. *Am J Physiol Lung Cell Mol Physiol* **2017**, *312*, 110–121, doi:10.1152/ajplung.00423.2016.-Exosomes.

451. Kim, S.M.; Yang, Y.; Oh, S.J.; Hong, Y.; Seo, M.; Jang, M. Cancer-Derived Exosomes as a Delivery Platform of CRISPR/Cas9 Confer Cancer Cell Tropism-Dependent Targeting. *Journal of Controlled Release* **2017**, *266*, 8–16, doi:10.1016/j.jconrel.2017.09.013.

452. Zhao, Z.-L.; Liu, C.; Wang, Q.-Z.; Wu, H.-W.; Zheng, J.-W. Engineered Exosomes for Targeted Delivery of MiR-187-3p Suppress the Viability of Hemangioma Stem Cells by Targeting Notch Signaling. *Ann Transl Med* **2022**, *10*, 621–621, doi:10.21037/atm-21-4138.

453. de Abreu, R.C.; Ramos, C. V.; Becher, C.; Lino, M.; Jesus, C.; da Costa Martins, P.A.; Martins, P.A.T.; Moreno, M.J.; Fernandes, H.; Ferreira, L. Exogenous Loading of MiRNAs into Small Extracellular Vesicles. *J Extracell Vesicles* **2021**, *10*, doi:10.1002/jev2.12111.

454. Kang, M.; Hisey, C.; Tsai, B.; Nursalim, Y.; Blenkiron, C.; Chamley, L.W. Placental Extracellular Vesicles Can Be Loaded with Plasmid DNA. *Mol Pharm* **2023**, *20*, 1898–1913, doi:10.1021/acs.molpharmaceut.2c00533.

455. Aqil, F.; Munagala, R.; Jeyabalan, J.; Agrawal, A.K.; Kyakulaga, A.-H.; Wilcher, S.A.; Gupta, R.C. Milk Exosomes-Natural Nanoparticles for SiRNA Delivery. *Cancer Lett* **2019**, *449*, 186–195, doi:10.1016/j.canlet.2019.02.011.

456. Wang, B.; Han, S. Modified Exosomes Reduce Apoptosis and Ameliorate Neural Deficits Induced by Traumatic Brain Injury. *ASAIO Journal* **2019**, *65*, 285–292, doi:10.1097/MAT.0000000000000810.

457. Piffoux, M.; Volatron, J.; Cherukula, K.; Aubertin, K.; Wilhelm, C.; Silva, A.K.A.; Gazeau, F. Engineering and Loading Therapeutic Extracellular Vesicles for Clinical Translation: A Data Reporting Frame for Comparability. *Adv Drug Deliv Rev* **2021**, *178*, doi:10.1016/j.addr.2021.113972.

458. Rankin-Turner, S.; Vader, P.; O'driscoll, L.; Giebel, B.; Heaney, L.M.; Davies, O.G. A Call for the Standardised Reporting of Factors Affecting the Exogenous Loading of Extracellular Vesicles with Therapeutic Cargos. *Adv Drug Deliv Rev* **2021**, *173*, 479–491, doi:10.1016/j.addr.2021.04.012.

459. Yang, Z.; Xie, J.; Zhu, J.; Kang, C.; Chiang, C.; Wang, X.; Wang, X.; Kuang, T.; Chen, F.; Chen, Z.; et al. Functional Exosome-Mimic for Delivery of SiRNA to Cancer: In Vitro and in Vivo Evaluation. *Journal of Controlled Release* **2016**, *243*, 160–171, doi:10.1016/J.JCONREL.2016.10.008.

460. Kooijmans, S.A.A.; Stremersch, S.; Braeckmans, K.; De Smedt, S.C.; Hendrix, A.; Wood, M.J.A.; Schiffelers, R.M.; Raemdonck, K.; Vader, P. Electroporation-Induced SiRNA Precipitation Obscures the Efficiency of SiRNA Loading into Extracellular Vesicles. *Journal of Controlled Release* **2013**, *172*, 229–238, doi:10.1016/J.JCONREL.2013.08.014.

461. Fuhrmann, G.; Serio, A.; Mazo, M.; Nair, R.; Stevens, M.M. Active Loading into Extracellular Vesicles Significantly Improves the Cellular Uptake and Photodynamic Effect of Porphyrins. *Journal of Controlled Release* **2015**, *205*, 35–44, doi:10.1016/J.JCONREL.2014.11.029.

462. Nordin, J.Z.; Lee, Y.; Vader, P.; Mäger, I.; Johansson, H.J.; Heusermann, W.; Wiklander, O.P.B.; Hällbrink, M.; Seow, Y.; Bultema, J.J.; et al. Ultrafiltration with Size-Exclusion Liquid Chromatography for High Yield Isolation of Extracellular Vesicles Preserving Intact Biophysical and Functional Properties. *Nanomedicine* **2015**, *11*, 879–883, doi:10.1016/J.NANO.2015.01.003.

463. Heusermann, W.; Hean, J.; Trojer, D.; Steib, E.; von Bueren, S.; Graff-Meyer, A.; Genoud, C.; Martin, K.; Pizzato, N.; Voshol, J.; et al. Exosomes Surf on Filopodia to Enter Cells at Endocytic Hot Spots, Traffic within Endosomes, and Are Targeted to the ER. *Journal of Cell Biology* **2016**, *213*, 173–184, doi:10.1083/jcb.201506084.

464. Joshi, B.S.; de Beer, M.A.; Giepmans, B.N.G.; Zuhorn, I.S. Endocytosis of Extracellular Vesicles and Release of Their Cargo from Endosomes. *ACS Nano* **2020**, *14*, 4444–4455, doi:10.1021/acsnano.9b10033.

465. Lennaárd, A.J.; Mamand, D.R.; Wiklander, R.J.; Andaloussi, S.E.L.; Wiklander, O.P.B. Optimised Electroporation for Loading of Extracellular Vesicles with Doxorubicin. *Pharmaceutics* **2022**, *14*, doi:10.3390/pharmaceutics14010038.

466. Rodríguez, D.A.; Vader, P. Extracellular Vesicle-Based Hybrid Systems for Advanced Drug Delivery. *Pharmaceutics* **2022**, *14*, doi:10.3390/PHARMACEUTICS14020267.

467. Liu, Q.; Adah, D.; Yao, Y.; Zhao, S.; Qin, L.; Yang, Y.; Lu, J.; Yu, S.; Chen, X. Exosomes from Plasmodium-Infected Hosts Inhibit Tumor Angiogenesis in a Murine Lewis Lung Cancer Model. *Oncogenesis* **2017**, *6*, e351, doi:10.1038/oncsis.2017.52.

468. Araújo, R.S.; Silva, M.S.; Santos, D.F.; Silva, G.A. Dysregulation of Trophic Factors Contributes to Diabetic Retinopathy in the Ins2Akita Mouse. *Exp Eye Res* **2020**, *194*, 1–6, doi:10.1016/j.exer.2020.108027.

469. Mcintyre, G.J.; Arndt, A.J.; Gillespie, K.M.; Mak, W.M.; Fanning, G.C. A Comparison of Multiple ShRNA Expression Methods for Combinatorial RNAi. *Genet Vaccines Ther* **2011**, *9*, 9, doi:10.1186/1479-0556-9-9.

470. Araújo, R.S.; Bitoque, D.B.; Silva, G.A. Development of Strategies to Modulate Gene Expression of Angiogenesis-Related Molecules in the Retina. *Gene* **2021**, *791*, 145724, doi:10.1016/J.GENE.2021.145724.

471. Bian, S.; Zhang, L.; Duan, L.; Wang, X.; Min, Y.; Yu, H. Extracellular Vesicles Derived from Human Bone Marrow Mesenchymal Stem Cells Promote Angiogenesis in a Rat Myocardial Infarction Model. *J Mol Med* **2014**, *92*, 387–397, doi:10.1007/s00109-013-1110-5.

472. Zhang, L.; Zhao, R.C.; Liang, X.; Han, Q.; Wang, S. Exosomes Secreted by Mesenchymal Stem Cells Promote Endothelial Cell Angiogenesis by Transferring MiR-125a. *J Cell Sci* **2016**, *129*, 2182–2189, doi:10.1242/jcs.170373.

473. Pakravan, K.; Babashah, S.; Sadeghizadeh, M.; Mowla, S.J.; Mossahebi-Mohammadi, M.; Ataei, F.; Dana, N.; Javan, M. MicroRNA-100 Shuttled by Mesenchymal Stem Cell-Derived Exosomes Suppresses in Vitro Angiogenesis through Modulating the MTOR/HIF-1α/VEGF Signaling Axis in Breast Cancer Cells. *Cellular oncology* **2017**, *40*, 457–470, doi:10.1007/S13402-017-0335-7.

474. Lee, J.-K.; Park, S.-R.; Jung, B.-K.; Jeon, Y.-K.; Lee, Y.-S.; Kim, M.-K.; Kim, Y.-G.; Jang, J.-Y.; Kim, C.-W. Exosomes Derived from Mesenchymal Stem Cells Suppress Angiogenesis by Down-Regulating VEGF Expression in Breast Cancer Cells. *PLoS One* **2013**, *8*, e84256, doi:10.1371/journal.pone.0084256.

475. Rosenberger, L.; Ezquer, M.; Lillo-Vera, F.; Pedraza, P.L.; Ortúzar, M.I.; González, P.L.; Figueroa-Valdés, A.I.; Cuenca, J.; Ezquer, F.; Khoury, M.; et al. Stem Cell Exosomes Inhibit Angiogenesis and Tumor Growth of Oral Squamous Cell Carcinoma. *Scientific Reports 2019 9:1* **2019**, *9*, 1–12, doi:10.1038/s41598-018-36855-6.

476. Alcayaga-Miranda, F.; González, P.L.; Lopez-Verrilli, A.; Varas-Godoy, M.; Aguila-Díaz, C.; Contreras, L.; Khoury, M. Prostate Tumor-Induced Angiogenesis Is Blocked by Exosomes Derived from Menstrual Stem Cells through the Inhibition of Reactive Oxygen Species. *Oncotarget* **2016**, *7*, 44462, doi:10.18632/ONCOTARGET.9852.

477. Gu, C.; Zhang, H.; Gao, Y. Adipose Mesenchymal Stem Cells-secreted Extracellular Vesicles Containing MicroRNA-192 Delays Diabetic Retinopathy by Targeting ITGA1. *J Cell Physiol* **2020**, 1–16, doi:10.1002/jcp.30213.

478. Safwat, A.; Sabry, D.; Ragiae, A.; Amer, E.; Mahmoud, R.H.; Shamardan, R.M. Adipose Mesenchymal Stem Cells–Derived Exosomes Attenuate Retina Degeneration of Streptozotocin-Induced Diabetes in Rabbits. *J Circ Biomark* **2018**, *7*, 1–10, doi:10.1177/1849454418807827.

479. Gutiérrez-Granados, S.; Cervera, L.; Kamen, A.A.; Gòdia, F. Advancements in Mammalian Cell Transient Gene Expression (TGE) Technology for Accelerated Production of Biologics. *Crit Rev Biotechnol* 2018, *38*, 918–940.

480. Ramos-Murillo, A.I.; Rodríguez, E.; Beltrán, K.; Ricaurte, C.; Camacho, B.; Salguero, G.; Godoy-Silva, R.D. Efficient Non-Viral Gene Modification of Mesenchymal Stromal Cells from Umbilical Cord Wharton's Jelly with Polyethylenimine. *Pharmaceutics* **2020**, *12*, 1–19, doi:10.3390/PHARMACEUTICS12090896.
481. Rankin-Turner, S.; Vader, P.; O'Driscoll, L.; Giebel, B.; Heaney, L.M.; Davies, O.G. A Call for the Standardised Reporting of Factors Affecting the Exogenous Loading of Extracellular Vesicles with Therapeutic Cargos. *Adv Drug Deliv Rev* **2021**, *173*, 479–491, doi:10.1016/J.ADDR.2021.04.012.
482. Cui, Y.; Guo, Y.; Kong, L.; Shi, J.; Liu, P.; Li, R.; Geng, Y.; Gao, W.; Zhang, Z.; Fu, D. A Bone-Targeted Engineered Exosome Platform Delivering SiRNA to Treat Osteoporosis. *Bioact Mater* **2022**, *10*, 207–221, doi:10.1016/J.BIOACTMAT.2021.09.015.
483. Tian, T.; Zhang, H.X.; He, C.P.; Fan, S.; Zhu, Y.L.; Qi, C.; Huang, N.P.; Xiao, Z.D.; Lu, Z.H.; Tannous, B.A.; et al. Surface Functionalized Exosomes as Targeted Drug Delivery Vehicles for Cerebral Ischemia Therapy. *Biomaterials* **2018**, *150*, 137–149, doi:10.1016/J.BIOMATERIALS.2017.10.012.